



Pacific Northwest
NATIONAL LABORATORY

*Proudly Operated by **Battelle** Since 1965*

Analysis of How Environmental Conditions Affect Dispersant Performance during Deep Ocean Application

Final Report

August 2017

GT Bonheyo

K Rose

A Bunn

A Avila

T Bays

V Cullinan

R Duran

R Jeters

L-J Kuo

J Park

J Velma

E Winder

P Wingo



Prepared for the U.S. Department of the Interior,
Bureau of Safety and Environmental Enforcement (BSEE)
under Contract Number E14PG00043 and E15PS00027

U.S. DEPARTMENT OF
ENERGY

Disclaimer

This report has been reviewed by the Bureau of Safety and Environmental Enforcement (BSEE). Review does not signify that the contents necessarily reflect the views and policies of the Bureau, nor does mention of the trade names or commercial products constitute endorsement or recommendation for use.

Analysis of How Environmental Conditions Affect Dispersant Performance during Deep Ocean Application

Final Report

August 2017

GT Bonheyo^{1,2}
K Rose³
A Bunn⁴
A Avila¹
T Bays⁴
V Cullinan¹
R Duran³

R Jeters¹
L-J Kuo¹
J Park¹
J Velma³
E Winder¹
P Wingo³

Prepared for
the U.S. Department of Energy
under Contract DE-AC05-76RL01830

Pacific Northwest National Laboratory
Richland, Washington 99352

¹ Pacific Northwest National Laboratory- Marine Science Laboratory, Sequim, WA

² Washington State University, Pullman, WA

³ National Energy Technology Laboratory, Albany, OR

⁴ Pacific Northwest National Laboratory, Richland, WA

Preface

The study reported herein was funded by the U.S. Department of the Interior, Bureau of Safety and Environmental Enforcement (BSEE) through an Interagency Agreement, BSEE Contracts E14PG00043, “Biodegradation and Toxicity Following Dispersant Usage in a Cold, Stratified, Deep Sea Setting,” and E15PS00027, “Analysis of How Environmental Conditions Affect Dispersant Performance During Deep Ocean Application,” with the U.S. Department of Energy, Pacific Northwest National Laboratory. This report describes Pacific Northwest National Laboratory researchers’ experiments conducted to assess the behavior of oil, with and without dispersants, under pressure and the development of methods to conduct high-pressure studies.

Point of Contact

George Bonheyo, Ph.D. George.bonheyo@pnl.gov

Executive Summary

Oil exploration in the deep waters of the Outer Continental Shelf creates a need for adequate spill response tools that can meet the unique conditions presented by deep ocean blowouts. This study entailed the design and execution of basic and applied research to 1) better understand the behavior of oil, dispersants, and microorganisms under relevant conditions; 2) identify tools for conducting high-pressure oil research; and 3) apply the data and insights to improve how models, such as the Blowout and Spill Occurrence Model (BLOSOM) predict the movement of oil with and without dispersant.

The ability to conduct high-pressure studies and to examine pressurized fluids (including oil) without depressurizing and thus physically altering the sample remains challenging. A wide range of analytical methods were evaluated and all were hampered by factors such as difficulty taking measurements through the thick steel walls of a pressure vessel, the tendency of oil to adhere to chamber or tubing surfaces; the often rapid movement of oil up to the surface of a fluid; and difficulties holding oil droplets within a zone of interrogation long enough for measurements to be completed.

Experiments conducted to examine the effect of a dispersant on the bacterial and fungal metabolism of oil and on the influence of oil droplet size on the rate of biodegradation yielded inconsistent results. Although the dispersant Corexit 9500 was not toxic to a set of model oil-degrading organisms, its use had very inconsistent effects on the degradation of a large panel of hydrocarbons that were tested. Droplet size studies were also inconsistent; no clear pattern was observed based upon initial conditions.

Another set of experiments sought to examine how pressure and/or temperature affect microbial growth, and the metabolism of high concentrations of oil. Cold temperatures, and nutrient or oxygen depletion were found to have the most significant impact. Pressure also negatively affected the growth of marine species collected in surface water.

Blowout simulation experiments involving the rapid depressurization of oil found the following:

- Depressurization leads to the atomization and emulsification of a fraction of the oil without the use of dispersants.
- The addition of a dispersant resulted in a greater volume fraction of the oil having smaller droplet sizes.
- Matching the temperature of the dispersant to the oil did not appear to affect the outcome.
- Premixing dispersant with the oil (optimal mixing) rather than injecting the oil into the plume did not appear to affect the oil droplet size distribution.
- The droplet sizes produced by the experimentally derived PNNL distributions differed in size from the size range used for the Johansen et al. 2013 distribution by roughly an order of magnitude. Although the method of measurement used in this study did provide a wider dynamic range of measurement, it appears that the experimental design (e.g., orifice diameter, discharge rate, GOR) also impacted the distributions.

The presence of a sediment in the oil was found to reduce median droplet sizes by >60% compared to an identical oil containing little or no sediment. The effect was also observed when a dispersant was used in different concentrations.

The BLOSOM has been updated to include the droplet size distribution provided in Johansen et al. (2013) to simulate the presence of dispersant.

The droplet size distributions derived from the experiments have been implemented in BLOSOM. The newly implemented distributions produced droplet size distributions under simulated conditions that were consistent with those provided in literature.

Using realistic hydrodynamic conditions and either the Johansen et al. 2013 or PNNL experimentally derived size distributions, BLOSOM simulations resulted in a greater amount of oil remaining at depth when the application of dispersant was included at the blowout as part of the simulation. This is consistent with observations from the Deepwater Horizon accident.

A strong correlation between crude oil viscosity and dispersant effectiveness was identified through the literature review process, and was implemented in BLOSOM as an additional option.

Acknowledgments

The authors wish to thank John Linehan, and Molly O'Hagan for their efforts testing high-pressure nuclear magnetic resonance spectroscopy as a means of monitoring water + oil + dispersant mixtures under pressure.

Acronyms and Abbreviations

3D	three-dimensional
ABW	UltraSeal ABW (a coating from Nanofilm Ltd)
ADC	analog-to-digital converter
AFT	Anti-Fouling Treatment
ANS	Alaskan North Slope (crude oil)
ATCC	American Type Culture Collection
atm	standard atmosphere (unit of pressure)
BSEE	Bureau of Safety and Environmental Enforcement
BLOSOM	Blowout and Spill Occurrence Model
°C	degree(s) Celsius
cm	centimeter(s)
cP	centipoise
CV	coefficient of variation
DOF	depth of field
DOSS	dioctyl sodium sulfosuccinate
DOSY	diffusion ordered spectroscopy
DOR	dispersant oil ratio
DSD	droplet size distribution
DWR	dispersant water ratio
EC ₅₀	effective concentration that reduces bioluminescence to ≤50% of the control
EPA	U.S. Environmental Protection Agency
FOV	field of view
g	gram(s)
GC-MS	gas chromatography-mass spectrometry
¹ H-DOSY	diffusion ordered spectroscopy
¹ H-NMR	proton nuclear magnetic resonance
hr	hour(s)
HyCOM	Hybrid Coordinate Ocean Model
ID	inside diameter
IFP	Institute Francais du Pétrole
in.	inch(es)
J2013	DSD in Johansen et al. (2013)
K	degree(s) Kelvin
km	kilometer(s)
μL	microliter(s)
L	liter(s)

LED	light-emitting diode
μm	micron(s)
m	meter(s)
MΩ	megaohm(s)
MC 252	Mississippi Canyon Block 252 well
MDL	method detection limit
mg	milligram(s)
MHz	megahertz
mL	milliliter(s)
mm	millimeter(s)
mN/m	millinewton(s) per meter
mPa	millipascal
mPa-s	millipascal-second
MNS	Mackay-Nadau-Steelman
MSL	Marine Science Laboratory
NCOM	Navy Coastal Ocean Model
NETL	National Energy Technology Laboratory
nm	nanometer
NMR	nuclear magnetic resonance (spectroscopy)
OD	outside diameter
O.D.	optical density (absorbance)
O.D. ₅₉₀	optical density of a sample measured at a wavelength of 590 nanometers
OPA	oil-particle-aggregate
PAH	polycyclic aromatic hydrocarbon
PCR	polymerase chain reaction
PNNL	Pacific Northwest National Laboratory
PNNL2017	DSD obtained experimentally by PNNL
ppm	parts per million
ppt	parts per thousand
psi	pound(s) per square inch (unit of pressure)
PSU	practical salinity unit(s)
PTFE	polytetrafluoroethylene
rpm	rotations per minute
s	second(s)
SCFM	standard cubic feet per minute
WTI	West Texas Intermediate (crude oil)

Contents

Preface	iii
Executive Summary	5
Acknowledgments.....	vii
Acronyms and Abbreviations	ix
1.0 Introduction	1.1
2.0 Background.....	2.1
3.0 Study Methods.....	3.1
3.1 Marine Laboratory Facilities.....	3.1
3.2 Droplet Size Determination.....	3.2
4.0 Project Tasks, Experimental Design, and Findings	4.1
4.1 Characterize the Physical State of Oil after Treatment with a Dispersant in a Cold, Deep, Low Turbulence Setting	4.1
4.1.1 Oil and Dispersant Samples	4.2
4.1.2 Pressure Systems	4.2
4.1.3 Oleophobic Coatings	4.3
4.1.4 View Cells.....	4.8
4.1.5 Interfacial Tension.....	4.10
4.1.6 Visualization of the Effect of Pressure on Droplet Size.....	4.14
4.2 Examine the Influence of Droplet Size on Biodegradation.....	4.16
4.2.1 Means of Creating and Maintaining Droplet Suspensions	4.16
4.2.2 Microorganisms Used in the Experiments	4.16
4.2.3 Experimental Setup to Examine the Effect of Droplet Size on Biodegradation	4.26
4.2.4 Results of the Droplet Study	4.28
4.3 Explore Novel, Noninvasive Approaches to Characterizing Emulsions and Oil Degradation in Pressure Chambers	4.35
4.3.1 Nuclear Magnetic Resonance Spectroscopy	4.35
4.3.2 Investigation of Other Spectroscopic Approaches	4.40
4.4 Examine the Effect of Deep Water Conditions on Cell Growth and the Biodegradation of High Concentrations of Oil	4.42
4.4.1 Microbiology: Strain Selection	4.42
4.5 Characterize the Effects of Pressure, Time, DOR, and Oil:Water Ratio on Droplet Size.....	4.44
4.5.1 Oil and Dispersant Physical Characteristics: Rheometrics	4.44
4.6 Characterize the Effect of Pressure Drop and Temperature on Oil Droplet Size.....	4.48
4.6.1 Sensor Array Development	4.50
4.6.2 Results from the Thermal Array.....	4.50
4.6.3 Blowout Testing: Particle Size Analysis.....	4.51
4.6.4 Dispersant Injection.....	4.53

4.6.5	The Tests	4.54
4.6.6	Test Results	4.54
4.7	Explore the Effect of Sediments on Droplet Size.....	4.66
4.8	Update BLOSOM (Blowout and Spill Occurrence Model) to Incorporate Dispersant Effects on Droplet Size Distributions	4.72
4.8.1	Results: Numerical Simulations	4.78
4.8.2	Future Enhancements: BLOSOM	4.85
5.0	Conclusions and Next Steps	5.86
6.0	References	6.1
	Appendix A – Interfacial Tension Data	A.1
	Appendix B – PAH Analysis Following Biodegradation	B.1
	Appendix C – Droplet Size Distribution.....	C.1
	Appendix D – Determination of Oil, Dispersant, and Seawater Fluorescent Spectra.....	D.1
	Appendix E – Determination of Oil, Dispersant, and Seawater Ratios Using Fluorescence.....	E.1

Figures

3.1. Location of the PNNL-Marine Science Laboratory on Sequim Bay in northwest Washington	3.1
3.2. Example of particle (droplet) identification in a challenging blowout test image with larger droplets and a large cloud of atomized droplets	3.2
3.3. A) The original photo with ruler for scale; B) the cropped subsection of the photo used for particle size determination; C) a mask of the cropped image with a 10 mm scale bar; and D) a second mask with a 1 mm scale bar	3.4
4.1. Examples of a non-mixing and mixing reactorfitted with the ethylene glycol cooling systems.....	4.3
4.2. Photo of the sampling tubes and mixer assembly with the reactor vessel removed and the reactor head to show the arrangement of access ports.....	4.3
4.3. A ramé-hart 590-U1 Advanced Automated Goniometer/Tensiometer used to measure contact angle of oil on surfaces to determine the oleophobicity of a surface and to measure the interfacial tension between fluids.....	4.5
4.4. Left panel: Positive control test with Islands 77 showing >99% reduction in luminescence compared with the stainless steel negative control blank. Right panel: Aculon Glass Repellency coated glass coupon compared with uncoated glass negative control blank.....	4.7
4.5. Coatings used on stainless steel coatings showed no toxic effects	4.8
4.6. View cells disconnected from the Teledyne pump and Parr reactor	4.9
4.7. Effect of dispersant concentration and temperature on the interfacial tension between oil and water	4.12
4.8. Effect of dispersant concentration and temperature on the interfacial tension between oil and water. *Approximation: the droplet would not remain formed long enough to test	4.13
4.9. Original and cropped images taken of 400 µL oil with 16 µL Corexit in 200 mL seawater at 17.8°C	4.15
4.10. Left to right: <i>Hormoconis resinae</i> , <i>Alkanivorax borkumensis</i> , and <i>Pseudomonas putida</i> grown on agar media.	4.17
4.11. Preliminary glucose assays	4.18
4.12. Preliminary protein assays	4.19
4.13. Glucose assays	4.20
4.14. Protein assays	4.21
4.15. Protein assays	4.22
4.16. Glucose assays	4.23
4.17. Experimental setup for testing the effect of dispersant/emulsifier on cell growth.....	4.24
4.18. Impact of dispersant/emulsifier on <i>A. borkumensi</i>	4.24
4.19. Impact of dispersant/emulsifier on seawater microorganism mix.....	4.25
4.20. Microtox [®] assay results.....	4.26
4.21. Diffusion ordered spectrum of Finasol OSR 52 in deuterium oxide.....	4.36
4.22. ¹ H-NMR spectrum of 1 micron diameter polystyrene beads.....	4.37
4.23. Three spectra aligned vertically obtained by ¹ H-NMR spectroscopy for Finasol OSR 52, DOSS, and Corexit EC9500A.....	4.37

4.24. ¹ H-DOSY spectra of A) 1:50 Finasol OSR 52: D ₂ O ratio and B) 1:1 ODR in a 1:50 analyte mixture:D ₂ O	4.39
4.25. Absorption spectra of water.	4.40
4.26. Non-Newtonian shear-thinning behavior exhibited by Corexit EC9500 during a viscosity vs. shear rate sweep.....	4.45
4.27. Finasol OSR 52 viscosity vs. temperature curve. Testing performed by SwRI.....	4.46
4.28. Corexit EC9500 viscosity vs. temperature curve. Testing performed by SwRI	4.46
4.29. Alaska North Slope crude oil viscosity vs. temperature curve.....	4.47
4.30. Macondo crude oil viscosity vs temperature curve	4.47
4.31. Graph illustrating the increase in density of Macondo crude oil while cooling from 52.5°C to 19.5°C	4.48
4.32. Test tank showing a 4×3 thermal probe array	4.49
4.33. Laboratory setup for the blowout tank.....	4.50
4.34. Sample data from the thermal array indicating the temperature of the surrounding water	4.51
4.35. Image acquired at 10 min after blowout.....	4.52
4.36. A subsection of the camera field of view imaged at 5 s post-blowout and a subsection of the camera field of view imaged at 10 min post-blowout.....	4.53
4.37. Time series of images during a Macondo crude oil blowoutwith coinjection of 1.0 g of Corexit EC9500 into raw seawater	4.54
4.38. Droplet size distributions for blowout #2 at approximately 5 s after the start of the blowout and again after 10 min after blowout start.....	4.57
4.39. Droplet size distributions for blowout #2-2 at approximately 5 s after the start of the blowout and again after 10 min after blowout start.....	4.58
4.40. Droplet size distributions for blowout #3 at approximately 5 s after the start of the blowout and again after 10 min after blowout start.....	4.59
4.41. Droplet size distributions for blowout #3-2 at approximately 5 s after the start of the blowout and again after 10 min after blowout start.....	4.60
4.42. Droplet size distributions for blowout #3-3 at approximately 5 s after the start of the blowout and again after 10 min after blowout start.....	4.61
4.43. Droplet size distributions for blowout #4 at approximately 5 s after the start of the blowout and again after 10 min after blowout start.....	4.62
4.44. Droplet size distributions for blowout #4-2 at approximately 5 s after the start of the blowout and again after 10 min after blowout start.....	4.63
4.45. Droplet size distributions for blowout #5 at approximately 5 s after the start of the blowout and again after 10 min after blowout start.....	4.64
4.46. Droplet size distributions for blowout #6 at approximately 5 s after the start of the blowout and again after 10 min after blowout start.....	4.65
4.47. Size distributions for samples with and without sediment and no dispersant	4.68
4.48. Size distributions for samples with and without sediment and a DOR of 1:50.....	4.69
4.49. Size distributions for samples with and without sediment and a DOR of 1:25.....	4.70
4.50. Oil suspensions without sediment and with sediment after mixing but prior to the addition of Corexit	4.71

4.51. Surface expression of oil without sediment and with sediment after the addition of dispersant	4.72
4.52. Johansen et al. (2013) distributions for oil droplet size as a function of droplet size as computed by BLOSOM internally	4.73
4.53. Droplet size distributions as a function of droplet size for experiments using oil at 16.8°C with application of dispersant and without dispersant	4.75
4.54. Droplet size distributions for blowouts with oil at 60°C as a function of droplet size.....	4.75
4.55. Normalized droplet size distribution as a function of droplet size for two experiments without any dispersant applied. Gray indicates the intersection of the two distributions.	4.76
4.56. Normalized droplet size distribution as a function of droplet size for two experiments with dispersant applied.....	4.77
4.57. Droplet size distribution as a function of droplet size for the blowout without dispersant and the blowout with dispersant used for BLOSOM simulations.....	4.77
4.58. Droplet size distributions from Johansen et al. (2013) as implemented in BLOSOM for both dispersant-treated and untreated oil.	4.78
4.59. The droplet size distributions from the experimentally derived observations, as implemented in BLOSOM.....	4.79
4.60. Oil blowout as simulated with BLOSOM after a 30-day simulation using the distribution from Johansen et al. (2013) for untreated droplet sizes	4.80
4.61. Oil blowout as a function of longitude, latitude, and depth, after a 30-day simulation with BLOSOM, using the distribution from Johansen et al. (2013) for treated droplet sizes	4.81
4.62. Oil blowout as simulated with BLOSOM after a 30-day simulation using the distribution from PNNL for untreated droplet sizes	4.82
4.63. Oil blowout as simulated with BLOSOM after a 30-day simulation using the distribution from PNNL for treated droplet sizes	4.83
4.64. Curve fit for dispersant effectiveness as a function of oil viscosity.....	4.85

Tables

3.1. Comparison of water properties: Sequim Bay, WA and Gulf of Mexico.	3.1
3.2. Particle size determination using a polystyrene bead standard.	3.4
3.3. Example of raw data obtained from Fuji particle size analysis.....	3.5
3.4. Sequoia LISST bins and digital floc camera bins used in particle size analysis research.....	3.6
4.1. Contact angles using crude oil.	4.6
4.2. Contact angles using decane.	4.6
4.3. Composition of samples used to study the effect of droplet size on biodegradation	4.28
4.4. Summary of the droplet size data for the <i>Alcanivorax borkumensis</i> and <i>Pseudomonas putida</i> samples	4.30
4.5. Summary of the droplet size data for the <i>Hormiconis resiniae</i> samples.....	4.31
4.6. Percent loss of hydrocarbon compared to Sample O; bacterial exposures	4.32
4.7. Percent loss of hydrocarbon compared to Sample O; fungal exposures. ^(a)	4.33
4.8. Tests performed on the ¹ H-NMR spectrometer for <i>in situ</i> particle size determination and micelle diffusion analysis	4.38
4.9. Samples and ratios used to try and force micelle formation for particle size determination and diffusion analysis	4.39
4.10. Density measurements of Finasol OSR 52, Corexit EC9500, Alaska North Slope crude oil, and Macondo crude oil obtained at 20°C and at 70°C.....	4.48
4.11. Cross-sectional area of oil particles at 5 s and 10 min after a test blowout with no dispersant.	4.53
4.12. Test parameters used for the simulated blowouts	4.56
4.13. Summary of droplet size data (mm).....	4.67
4.14. Experimental setup for each blowout.....	4.76
4.15. Percent of oil mass by depth for each of the four BLOSOM simulations	4.84
4.16. Values for parameters A, B, and C used to determine dispersant effectiveness as a function of viscosity values obtained using either the IFP or MNS test protocol.....	4.85

1.0 Introduction

This report covers two projects conducted under BSEE Contracts E14PG00043, “Biodegradation and Toxicity Following Dispersant Usage in a Cold, Stratified, Deep Sea Setting,” and E15PS00027, “Analysis of How Environmental Conditions Affect Dispersant Performance During Deep Ocean Application,” with the U.S. Department of Energy, Pacific Northwest National Laboratory. The primary objective of these projects was to examine how deep subsea conditions such as pressure, pressure drop, and temperature combine with other aspects, such as dispersant-to-oil ratio (DOR), degassing, and sediment to affect the effectiveness of dispersants. The principal means of evaluating *dispersant effectiveness* in this effort was to examine oil droplet size, including changes in droplet size over time. Additional studies explored noninvasive methods for measuring pressurized fluids in closed laboratory systems (pressure vessels) to monitor droplet size, oil and dispersant mixing, and oil chemistry. A second set of studies examined the potential effect of dispersant use and droplet size on microbial biodegradation of oil. Finally, results of the study were provided to the National Energy Technology Laboratory to strengthen the Blowout and Spill Occurrence Model (BLOSOM) for deep ocean scenarios.

The overall study was organized as a set of eight research tasks, which are used as the basis for organizing the remainder of this report. Chapter 2.0, Background, provides context for the study. Chapter 3.0, Study Methods, describes some of the general methods used throughout the study. Chapter 4.0, Project Tasks, Experimental Design, and Findings, describes each of the eight study tasks, including the rationale, experimental design, findings, and conclusions. The tasks in Chapter 4.0 include the following:

1. Characterize the physical state of oil after treatment with a dispersant in a cold, deep, low turbulence setting.
2. Examine the influence of droplet size on biodegradation.
3. Explore novel, noninvasive approaches to characterize emulsions and oil degradation in pressure chambers.
4. Examine the effect of deep water conditions on cell growth and the biodegradation of high concentrations of oil.
5. Characterize the effects of pressure, time, DOR, and oil:water ratio on droplet size.
6. Characterize the effect of pressure drop and temperature on oil droplet size.
7. Explore the effect of sediments on droplet size.
8. Update BLOSOM (Blowout and Spill Occurrence Model) to incorporate dispersant effects on droplet size distributions.

2.0 Background

Oil production in waters of the U.S. Outer Continental Shelf is likely to increase in the foreseeable future. In 2012, U.S. crude oil production was 6.5 million barrels per day, of which 20% came from federal offshore sources and 19% from Gulf of Mexico federal offshore sources in particular (US-EIA 2013). After a temporary drilling moratorium (imposed after the Deepwater Horizon spill) was lifted in October 2010, the Gulf of Mexico yielded total discoveries of 411 million barrels in 2011—a 90% increase over 2010 discoveries—which placed it among the top three geographical regions of the U.S. for new discoveries (US-EIA 2011). Production in waters deeper than 1300 ft in the Gulf was forecasted to be 1.5 million barrels per day in 2014, and some analysts are forecasting that the deep waters of the Gulf of Mexico will produce 1.9 million barrels per day in 2020 (Klump 2013). In 2016, there were eight new field starts in water between 3700 ft and 9556 ft and there are 7 anticipated starts for 2017-2018 ranging from depths of 1200 ft to 7128 ft (US-EIA 2017).

While deep ocean exploration represents an important resource for growing U.S. energy demands, the Deepwater Horizon blowout of 2010 highlights the many uncertainties about spill remediation, and in particular the interplay of oil leaks, dispersants, and biodegradation in the cold and high-pressure environment of the Outer Continental Shelf. Oil breaks down due to physical, chemical, and biological (metabolic) effects, and the rate of each effect is affected by the environmental conditions that are present. Oil spill dynamics and cleanup are much better studied in the surface environment than in the deep ocean, because of the more recent onset of deep ocean drilling and the challenges of conducting studies in the deep ocean or under simulated conditions. Some of these challenges are noted below and motivated the studies outlined in this report.

Dispersant use in surface and deepwater conditions. During the Deepwater Horizon incident, a total of 771,000 gallons of Corexit 9500A was injected subsurface, representing 42% of the 1.84 million total gallons of dispersant used during the response (USCG 2011). This represented the first deep ocean use of dispersant and only six shallow subsurface tests had been previously performed (USCG 2011).⁴ Dispersants are added to released crude oil to break its physical form into small droplets, thereby increasing its surface area to provide greater accessibility to water and microorganisms to facilitate biodegradation (National Research Council 1989). The resulting small droplets may disperse and spread throughout the water column, thereby diluting the amount of suspended oil per unit volume of seawater and enhancing biodegradation by enabling the natural concentration in seawater of available nitrogen, phosphorous, oxygen, and other essential elements for microbial growth to remain sufficiently high. Desired outcomes of dispersant use are to enhance biodegradation and ultimately to restore an environment to one in which there is no measurable toxicity. Dispersants are most effective when used on freshly ejected, non-weathered oil, which is one motivation for applying dispersants at the source of a leak. However, while dispersant activity has been fairly well characterized for surface environments that have a relatively high degree of mixing (by waves), oxygenation (which promotes aerobic metabolism), light (photo-oxidation), atmospheric pressure, and warmer temperatures, few controlled studies have been performed to examine the effectiveness of dispersants in dark, high-pressure, low-temperature environments, and where mixing is greatly reduced short distances from the point of blowout and the initial injection of dispersant (GAO 2012; National Research Council 2005).

The ability of microorganisms to biodegrade dispersants (e.g., Corexit 9500) and dispersant-treated oil have been the subject of a number of studies (see for example, Mulkins-Philips and Stewart 1974; Lindstrom and Braddock 1999, 2002; Venosa and Holder 2007; Campo et al. 2013; Prince et al. 2013; McFarlin et al. 2014; and Kleindienst et al. 2015). While it is clear from these studies that some microorganisms are capable of degrading oil, dispersants, and dispersant:oil mixtures, some discrepancy exists about whether dispersants promote or slow down the process of biodegradation (Prince et al. 2013;

Kleindienst et al. 2015). Conflicting test results may stem from differences in the experimental design and methods of analysis, the test conditions (e.g., volume, temperature, mixing, oxygenation), and the microorganisms, oil, and dispersant used in the tests.

Effects of pressure and pressure drop on oil droplet size and dispersant use. Even though the hydrostatic pressure found at a 2 km deep wellhead is approximately 2900 psi, the pressure of oil at a blowout may be even higher—10,000 to 15,000 psi—resulting in a relative drop in pressure of over 7000 psi. The pressure drop, the size of the leak orifice, and viscosity of the oil will influence the velocity of the escaping oil and initial mixing. As oil leaves the wellhead and drops in pressure, the liquid oil expands slightly, but any undissolved gas portion rapidly expands in volume and a significant portion of the dissolved gas will escape initially. The initial expansion of gas contributes to turbulent mixing, which promotes oil and water mixing, and it may support dispersant and oil mixing when a dispersant is injected at the leak site, or it may lead to some phase separation of the oil and dispersant. Oil will also increase in viscosity due to the loss of gas and the drop in temperature, which will interfere with the ability of dispersants to penetrate the oil (US-EIS 2013; Becker and Lindblom 1983). The dispersants may also affect the solubility of gas in the oil and mixing of oil with water, which in turn could affect how much and how quickly the released gas is dissolved into the surrounding water. Shortly after the initial ejection from the well, high ambient pressure will impede the release and expansion of any remaining dissolved gas from oil, thereby reducing the buoyancy of oil plume (Johansen et al. 2013). It is unclear how all of these effects balance out and ultimately affect dispersant effectiveness.

Effects of temperature on oil droplet size and dispersant use. While the ambient seawater temperature on the deep ocean seafloor may be less than 4°C, the temperature of the oil at the wellhead may exceed 100°C. Temperature directly contributes to the viscosity of oil, which increases with colder temperatures. Dispersants are less effective at penetrating and emulsifying viscous oil, and temperature also affects the solubility of the dispersant (US-EIS 2013; Becker and Lindblom 1983). Unless a means of temperature control is provided, upon reaching the location of a deep ocean blowout, the temperature of the dispersants are likely to be close to the ambient water temperature. Whether dispersants are injected down into the wellhead, providing some opportunity for mixing and heating prior to mixing with cold ocean water, or are injected at the site of the blowout as the oil meets the cold water may have an impact on their effectiveness.

3.0 Study Methods

3.1 Marine Laboratory Facilities

The majority of the tests were conducted at the Pacific Northwest National Laboratory’s Marine Science Laboratory located in Sequim, Washington (Figure 3.1), while the high-pressure nuclear magnetic resonance (NMR) spectroscopy was conducted at the Pacific Northwest National Laboratory in Richland, Washington. Unless otherwise described, seawater was sourced from Sequim Bay, which maintains an average salinity of 30.6 ± 0.8 psu ($n = 1009$ data points recorded over 45 months, $CV = 2.7\%$) with limited seasonal variation due to the lack of significant freshwater sources (i.e., rivers or streams) entering the bay and limited rainfall (<14 in. annually) (Gill et al. 2016). The laboratory’s seawater has an average pH of 7.83 ± 0.12 ($n = 988$; $CV = 1.5\%$), which fluctuates slightly on a seasonal basis due to algal growth in the bay (Table 1). Surface seawater in the Gulf of Mexico near the location of the Deepwater Platform is slightly higher at ~ 35.5 to 36 psu with a pH near 8.0; both salinity and pH drop slightly at greater depths; salinity values are around 34.9 psu and pH near 7.9 (Bianchi et al. 2014). Seawater is supplied to the laboratories as both unfiltered and filtered (Arkal Spin Klin filter system with a nominal pore size 40 μm) supplies. The filtered seawater can undergo further filtration in the laboratory if needed down to a nominal pore size of 0.22 μm for sterile conditions.

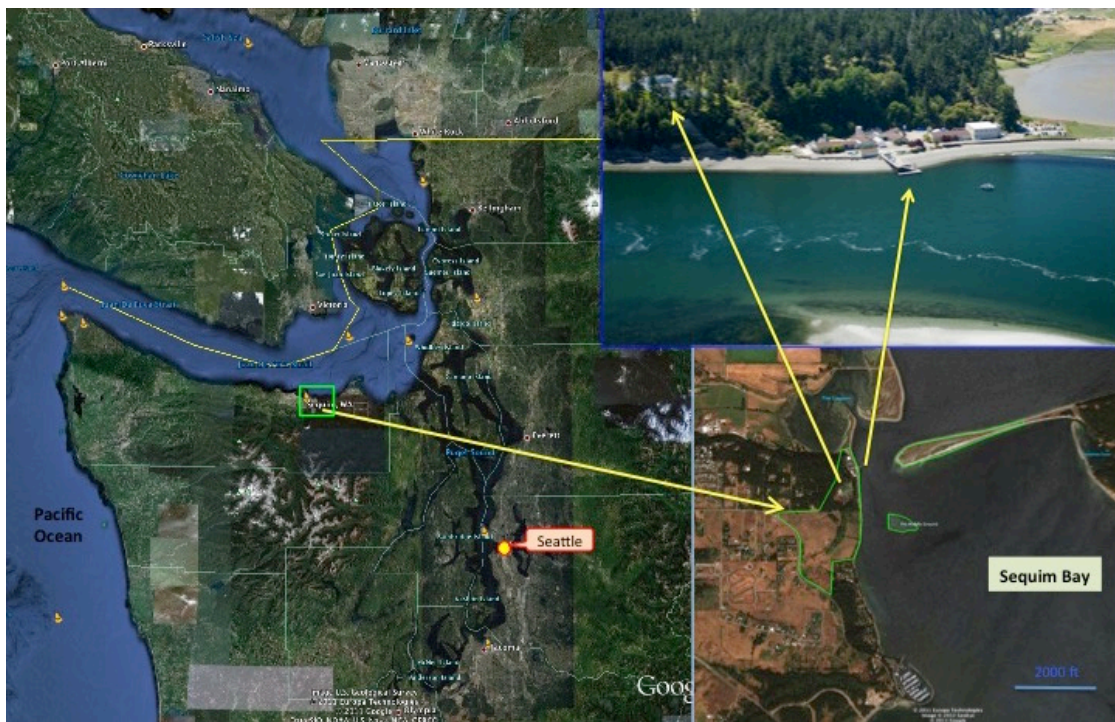


Figure 3.1. Location of the PNNL-Marine Science Laboratory on Sequim Bay in northwest Washington.

Table 3.1. Comparison of water properties: Sequim Bay, WA and Gulf of Mexico.

	Sequim Bay	Gulf of Mexico Surface Water	Gulf of Mexico Deep Water
pH	7.8	8.0	7.9
Salinity (psu)	30.6	35.5 to 36	34.9

3.2 Droplet Size Determination

Throughout the study, unless otherwise noted, droplet size was determined by digital photographic imaging using a Canon EOS 70D (20.2 MP) with attached 100 mm macro lens ($f/16$, ISO 6400) or GoPro Hero4 12 MP modified by replacing the original lens with an AXION 4.35 mm rectilinear lens (for use with the pressurized view cells). Size standards or a ruler were included in the field of view (FOV) for calibration, and the depth of field (DOF) was also measured to allow for volumetric calculations. High-speed photography proved to be the best approach for imaging droplets during vigorous mixing in flasks or in simulated blowouts, in situations with high oil or dispersant concentrations, and was the only means of collecting droplet size data in the blowout tanks.

The research team also visited Sequoia Instruments, located in nearby Bellevue, Washington, to run several tests with their technical staff using the LISST-100 and LISST-Holo to see if either could be used to image fluids in cuvettes and flow cells at the speeds and concentrations necessary for this study. These devices have been used in many other studies reporting droplet size distributions (see for example, Brandvik et al. 2013), but it was not possible to generate useful data with the off-the-shelf equipment. Significant adaptations and further testing would have been required to use the LISST devices in this study.

Images with sizable particles were processed using Fiji (ImageJ software with preloaded plugins for particle calling/recognition) (Schindelin et al. 2012). The images were first scale calibrated to rulers emplaced in the FOV and then processed by cropping to remove areas outside the calibrated FOV and DOF. Next, background subtraction and thresholding were used to remove noise and material surface effects. Then particles were identified by their degree of circularity to rule out images of overlapping droplets, clusters of small droplets that could be mistakenly identified as very large droplets, or other debris. Due to shear forces experienced during mixing or in simulated blowouts, the oil particles are circular. Large particles also have a greater likelihood of overlapping with smaller particles (located elsewhere in the DOF), which, despite representing only a very small portion of the overall volume of oil, were typically present in large numbers. A value of 30% circularity was selected for particle identification (Figure 3.2).

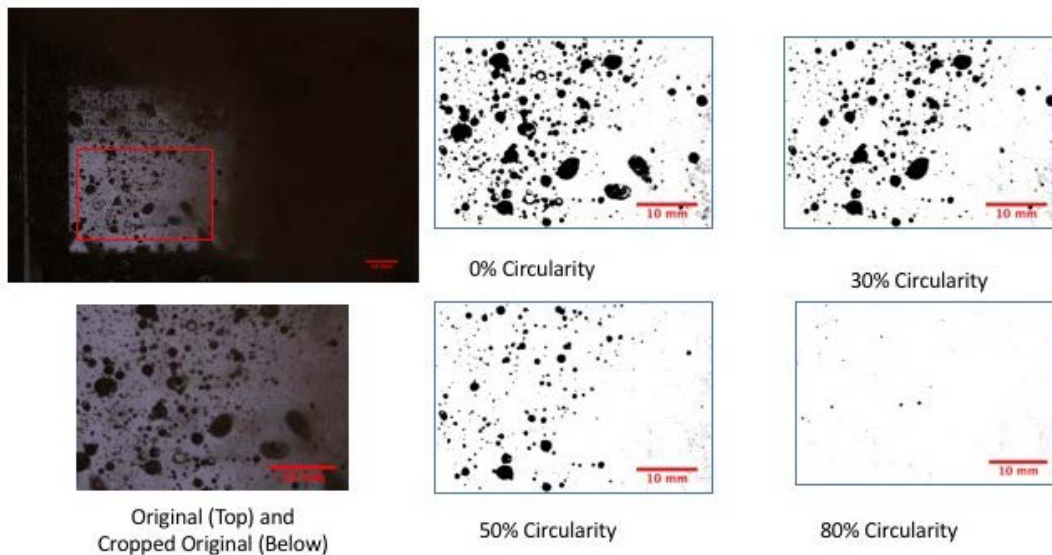


Figure 3.2. Example of particle (droplet) identification in a challenging blowout test image with larger droplets (left side of original) and a large cloud of atomized droplets (right side of original).

To prevent the addition of subjectivity to the particle identification the thresholding was automatically performed using the Otsu thresholding method for blowouts and the Triangle method for particle degradation testing. The Otsu method performs well in white background, clear solution situations and thus was well suited to the blowouts; however, it could not identify particles in biomass dense degradation solutions, so the Triangle method was used instead. After thresholding, the particles were then selected and size analyzed. Some particle sizing methods include a “fill holes” step prior to calling particles, but we chose to not include this step because the pressurized oil contained a portion of gas, which could be seen as bubbles in the water column. By not filling holes these bubbles were not identified as oil particles, because they had a solid edge and translucent center and thus maintained the fidelity of our particle size assessments.

Images were processed using the Batch-Macro Mode in Fiji using the following macro code:

```
run("Set Scale...", "distance=508.0157 known=10 pixel=1 unit=mm global");
makeRectangle(816, 1308, 2424, 1482);
run("Crop");
run("Subtract Background...", "rolling=200 light");
run("8-bit");
run("Auto Threshold", "method=Otsu");
setOption("BlackBackground", false);
run("Convert to Mask");
run("Analyze Particles...", " circularity=0.30-1.00 show=Masks display exclude");
run("Scale Bar...", "width=10 height=24 font=84 color=Red background=None
location=[Lower Right] bold overlay");
```

The scale numbers and rectangle coordinates noted in the code are specific to each batch of images and therefore variable, however the remaining code is unchanged between blowout image sets. Particle degradation image sets, as noted above, change the “Auto Threshold” method from “Otsu” to “Triangle.”

Image processing with Fiji produced a text file with the image label and estimated particle cross-sectional area, circumference, and other descriptors for each particle detected in a given image. The diameter was calculated as $d = 2 \sqrt{\text{area}/\pi}$ and the volume ($v = \frac{4}{3} \pi \left(\frac{d}{2}\right)^3$) of the associated sphere represented by each particle. The particle size distribution and volume fraction were calculated as in Mikkelsen et al. (2005). All 50 logarithmically spaced diameter bin sizes (microns) covered by the LISST-100 and the digital floc camera used in Mikkelsen et al. (2005) were used for easy comparison. Descriptive statistics were calculated for each image including the particle count, minimum, maximum, mean, and standard deviation of the particle area and diameter for each image.

A calibration experiment was conducted using 0.75 mm size standard polystyrene beads. The beads were placed in a seawater tank used to simulate oil blowouts and photographed with a ruler in the FOV (Figure 3.3). A subsection of the image was processed and 29 beads were selected at random and sized using the method described above, except that the beads had to be artificially darkened in the center to accurately calculate the cross-sectional area (the beads reflected light and each bead has a bright center that was misinterpreted as a hole, as seen in Figure 3.3B). Additionally, 29 beads were selected at random and the diameter of each was determined using a caliper. The results, provided in Table 3.2, show good agreement between the image processing and manual measurements: the image processing yielded a 3.8% difference in mean size relative to the manual measurement and a higher standard deviation.

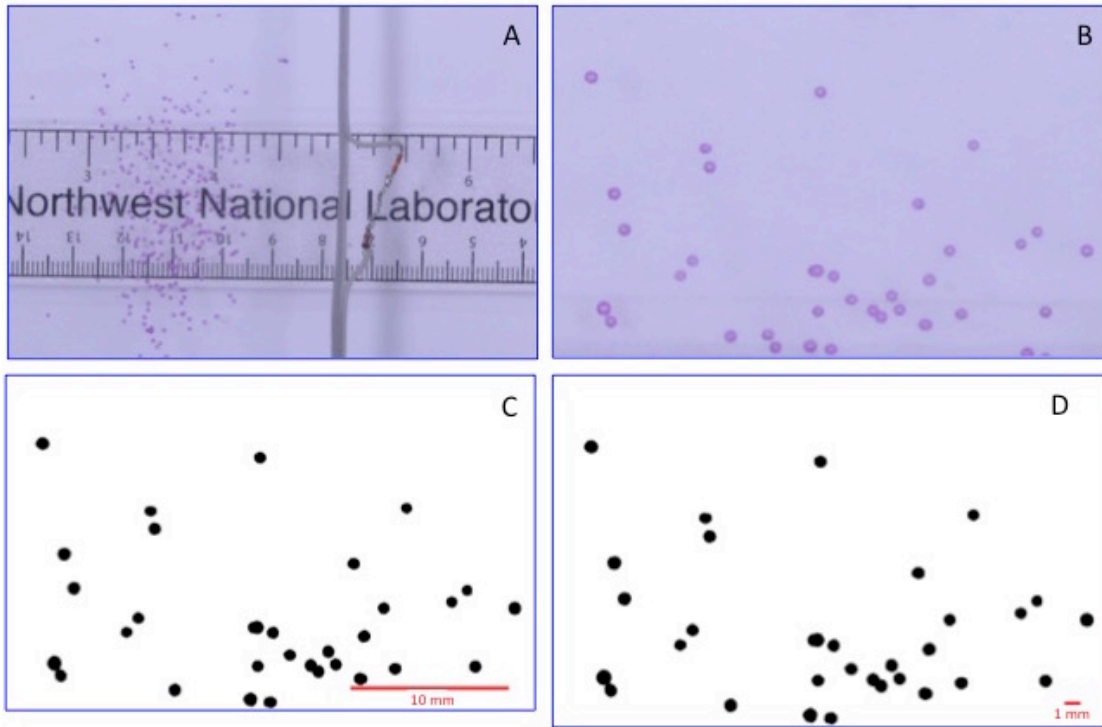


Figure 3.3. A) The original photo with ruler for scale; B) the cropped subsection of the photo used for particle size determination; C) a mask of the cropped image with a 10 mm scale bar; and D) a second mask with a 1 mm scale bar. The vertical object in image A is part of a thermal probe array that sits in the camera field of view.

Table 3.2. Particle size determination using a polystyrene bead standard.

Particle Size Analysis		Manual Particle Size Analysis (Caliper)	
Label	Diameter (mm)	Bead Number	Diameter (mm)
1	0.82	1	0.68
2	0.75	2	0.64
3	0.69	3	0.79
4	0.72	4	0.87
5	0.79	5	0.86
6	0.83	6	0.75
7	0.75	7	0.73
8	0.80	8	0.75
9	0.68	9	0.72
10	0.71	10	0.78
11	0.83	11	0.83
12	0.75	12	0.78
13	0.73	13	0.73
14	0.93	14	0.73
15	0.76	15	0.81
16	0.70	16	0.70
17	0.79	17	0.73
18	0.77	18	0.80
19	0.74	19	0.72
20	1.21	20	0.81

Particle Size Analysis		Manual Particle Size Analysis (Caliper)	
Label	Diameter (mm)	Bead Number	Diameter (mm)
21	0.75	21	0.85
22	1.08	22	0.81
23	0.75	23	0.91
24	0.78	24	0.88
25	0.77	25	0.80
26	0.81	26	0.74
27	0.79	27	0.73
28	0.86	28	0.81
29	0.79	29	0.84
Mean	0.81	Mean	0.78
SD	0.46	SD	0.06
Min	0.68	Min	0.64
Max	1.21	Max	0.91

Example raw data obtained from Fiji particle size analysis are shown below in Table 3.3. The raw data include the particle identification number, circular area, perimeter, and circularity. The raw particle data were imported into Microsoft Excel for further modification and analysis. Equations were used to convert the particle area to particle diameter and particle volume. The particle volumes of each identified particle in each image were summed to determine the total volume of particles imaged, by which each particle was then divided to calculate the volume fraction of each particle in the whole.

Table 3.3. Example of raw data obtained from Fiji particle size analysis.

	Label	Cross-Sectional Area	Circumference	Circularity
1	Blowout 6_01	4.21E-04	0.058	1
2	Blowout 6_01	0.001	0.116	1
3	Blowout 6_01	4.21E-04	0.058	1
4	Blowout 6_01	4.21E-04	0.058	1
5	Blowout 6_01	4.21E-04	0.058	1

To maintain consistency with other oil research the measured particles were binned according to their particle diameter and particle volume fraction percent. The bins used were those that have previously been used by the Sequoia LISST and digital floc camera devices (Table 3.4) (Mikkelsen et al. 2005).

Table 3.4. Sequoia LISST bins and digital floc camera bins used in particle size analysis research (Mikkelsen et al. 2005).

Lower limit, mid point and upper limit in microns for size bins 1–32 (bold , covered by the LISST) and size bins 25–50 (<i>italic</i> , covered by the DFC). The two instruments are seen to overlap in eight size bins, 25–32							
Size bin #	Lower limit (μm)	Mid point (μm)	Upper limit (μm)	Size bin #	Lower limit (μm)	Mid point (μm)	Upper limit (μm)
1	2.50	2.72	2.95	26	<i>156.90</i>	<i>170.44</i>	<i>185.15</i>
2	2.95	3.20	3.48	27	<i>185.15</i>	<i>201.13</i>	<i>218.49</i>
3	3.48	3.78	4.11	28	<i>218.49</i>	<i>237.35</i>	<i>257.83</i>
4	4.11	4.46	4.85	29	<i>257.83</i>	<i>280.09</i>	<i>304.26</i>
5	4.85	5.27	5.72	30	<i>304.26</i>	<i>330.52</i>	<i>359.05</i>
6	5.72	6.21	6.75	31	<i>359.05</i>	<i>390.04</i>	<i>423.70</i>
7	6.75	7.33	7.97	32	<i>423.70</i>	<i>460.27</i>	<i>500.00</i>
8	7.97	8.65	9.40	33	<i>500.00</i>	<i>543.15</i>	<i>590.03</i>
9	9.40	10.21	11.09	34	<i>590.03</i>	<i>640.96</i>	<i>696.28</i>
10	11.09	12.05	13.09	35	<i>696.28</i>	<i>756.38</i>	<i>821.66</i>
11	13.09	14.22	15.45	36	<i>821.66</i>	<i>892.58</i>	<i>969.61</i>
12	15.45	16.78	18.23	37	<i>969.61</i>	<i>1053.30</i>	<i>1144.20</i>
13	18.23	19.81	21.52	38	<i>1144.20</i>	<i>1243.00</i>	<i>1350.20</i>
14	21.52	23.37	25.39	39	<i>1350.20</i>	<i>1466.80</i>	<i>1593.40</i>
15	25.39	27.58	29.96	40	<i>1593.40</i>	<i>1730.90</i>	<i>1880.30</i>
16	29.96	32.55	35.36	41	<i>1880.30</i>	<i>2042.60</i>	<i>2218.90</i>
17	35.36	38.41	41.72	42	<i>2218.90</i>	<i>2410.40</i>	<i>2618.40</i>
18	41.72	45.32	49.23	43	<i>2618.40</i>	<i>2844.40</i>	<i>3089.90</i>
19	49.23	53.48	58.10	44	<i>3089.90</i>	<i>3356.60</i>	<i>3646.30</i>
20	58.10	63.12	68.56	45	<i>3646.30</i>	<i>3961.00</i>	<i>4302.90</i>
21	68.56	74.48	80.91	46	<i>4302.90</i>	<i>4674.30</i>	<i>5077.70</i>
22	80.91	87.89	95.48	47	<i>5077.70</i>	<i>5516.00</i>	<i>5992.10</i>
23	95.48	103.72	112.67	48	<i>5992.10</i>	<i>6509.30</i>	<i>7071.10</i>
24	112.67	122.39	132.96	49	<i>7071.10</i>	<i>7681.40</i>	<i>8344.30</i>
25	<i>132.96</i>	<i>144.43</i>	<i>156.90</i>	50	<i>8344.30</i>	<i>9064.50</i>	<i>9846.90</i>

4.0 Project Tasks, Experimental Design, and Findings

The eight study tasks are described in the following sections. They describe how the physical state of oil was characterized after treatment with a dispersant in a cold, deep, low turbulence setting; the influence of droplet size on biodegradation; the exploration of novel, noninvasive approaches to characterize emulsions and oil degradation in pressure chambers; the effect of deep water conditions on cell growth and the biodegradation of high concentrations of oil; the effects of pressure, time, DOR, and oil:water ratio on droplet size; oil blowout experiments conducted to determine the effect of pressure drop and temperature on oil droplet size; the effect of sediments on droplet size; and the BLOSOM.

4.1 Characterize the Physical State of Oil after Treatment with a Dispersant in a Cold, Deep, Low Turbulence Setting

Oil droplet size is considered an important factor controlling biodegradation and a primary objective of using dispersants is to render oil into small droplet sizes to enhance the rate of degradation. Furthermore, dispersants dilute a given volume of oil into a larger volume of seawater, presumably increasing the availability of oxygen and other nutrients to support microbial activity (Lessard and DeMarco 2000; Broje et al. 2014). Dispersants include surfactants, which are amphiphilic molecules having two distinct functional groups or sidechains: one attracted to oil (oleophilic) and one attracted to water (hydrophilic). In the absence of a surfactant, oil itself is hydrophobic (water “fearing”) and thus collects together into large droplets or slicks rather than mixing with the water. The surfactant creates an interface between the oil and water, effectively reducing the interfacial surface tension between the two and allowing the oil to be broken up into smaller droplets.

With surface slicks, a dispersant can be sprayed evenly over the slick and allowed to penetrate into the oil to mix with it. Wind, wave, and current action at the surface provides further mixing to break apart the slick and disperse the smaller droplets of oil into the water column. In a subsurface leak, the dispersant must be injected into the escaping plume of oil; the addition of a dispersant to oil as it leaks from a source requires thorough mixing energy from the blowout, the turbulent rising plume, or ocean currents to blend the dispersant with the oil and surrounding water.

Oil escaping from a deep ocean leak may initially experience extreme turbulence due to the pressure differential when exiting from the geological reserve (as much as 10,000 to 15,000 psi) into the ocean environment (approximately 2900 psi of hydrostatic pressure at 2 km depth) (USNC 2011). Degassing also contributes to the extreme turbulence as dissolved and free gas rapidly expands out of the oil upon release. As the plume of oil moves several meters from the leak orifice, some turbulence continues as gas and the buoyancy of larger oil droplets carry the plume upwards and additional oil and gas continue to be released and rise from the wellhead below. This turbulence may continue to diminish as the plume expands, if droplet sizes decrease and buoyancy decreases (i.e., oil density increases due to gas loss and diffusion of low molecular weight hydrocarbons), and if the gas content within the plume also decreases. Subsurface ocean currents are unlikely to provide turbulent mixing energy, but will affect the movement of the oil and gas plume, and may separate less buoyant droplets from rising, buoyant droplets.

The effect of dispersants on surface plumes is readily observed and reasonably well-studied (National Research Council 1989; Fingas 2014; Zeinstra-Helfrich et al. 2015). However, much less is known about the effects of dispersants on subsurface leaks, and such scenarios are difficult to recreate experimentally. This task was created to explore the physical properties of oil and oil:dispersant mixes under deep ocean conditions. The interfacial tension of the sample oil in seawater in the presence of different concentrations of dispersant was also examined. Experiments were designed to create a well-mixed plume of oil in

seawater with and without different concentrations of dispersant under pressure (up to 2900 psi, 197 atm). The initial vigorous mixing energy would then be reduced and the effect on droplet size observed. This section describes the experimental setup, observations, and key challenges that were addressed including 1) replicating and maintaining pressure during the experiments and observations; 2) reducing experimental artifacts, particularly from surfaces introduced by the pressure systems to which oil could stick; and 3) overcoming the effects of gravity and oil buoyancy to maintain droplet suspensions.

4.1.1 Oil and Dispersant Samples

For the study, Mississippi Canyon Block 252 well (“MC 252”) was provided by BP Exploration & Production Inc. (BP), herein referred to as Macondo crude. Some preliminary studies or experiments in which multiple samples of oil were desired for comparison also used a West Texas Intermediate (WTI) crude sample purchased from Texas Raw Crude and Alaskan North Slope (ANS) crude oil, supplied by the sponsor. Samples of Corexit 9500 were provided by BSEE/Ohmsett and samples of Finasol OSR 52 were purchased directly from Solvadis LLC.

4.1.2 Pressure Systems

Large volume pressure studies were carried out using 2 L pressure reactors (Parr Instruments) fabricated from 2205 duplex stainless steel and outfitted with Hasteloy C inner fittings to avoid corrosion when exposed to seawater or concentrated brines for extended periods. Four of the reactors included impeller mixing blades and two of the reactors had no internal mixers (Figure 4.1). All reactors were rated for 3000 psi at up to 300°C and included three separate sampling ports positioned to reach the bottom, middle, and upper portions of the cylinder (Figure 4.2). An additional port was used for a thermocouple to record temperature. When not operating at room temperature, the temperature of the reactors was maintained by immersing the reactor in an ethylene glycol-filled jacket that contained a recirculating copper tubing system also filled with ethylene glycol and connected to a temperature control unit (Figure 4.2). With added outer insulation, the jackets were connected to a chiller and used to bring the temperature of the reactor fluids down to ~4.5°C. Pressurized samples were withdrawn from each of the three sampling ports in the reactors using a 30 mL, 3000 psi rated sampling syringe. The samples were then depressurized and analyzed. The reactor systems were pressurized using a pneumatically driven Haskel AGD30 Double Acting Gas Booster pump connected to a standard gas cylinder filled with air (gas supply to pressurize the reactors) and the building’s pressurized air supply (~100 psi and ~40 SCFM) to drive the booster pump. The pump was also used to inject fresh seawater into the reactor (using the pressure sampling syringe) and to restore pressure after withdrawing a sample, and with this approach it was possible to collect multiple time point samples or to monitor and adjust pH.



Figure 4.1. Examples of a non-mixing (left) and mixing reactor (right) fitted with the ethylene glycol cooling systems (with insulation removed to show the cooling coils. The wall-mounted manifold to the left allows for independent control of cooling to each of the six reactors. The image on the right shows a mixing reactor without the cooling system.

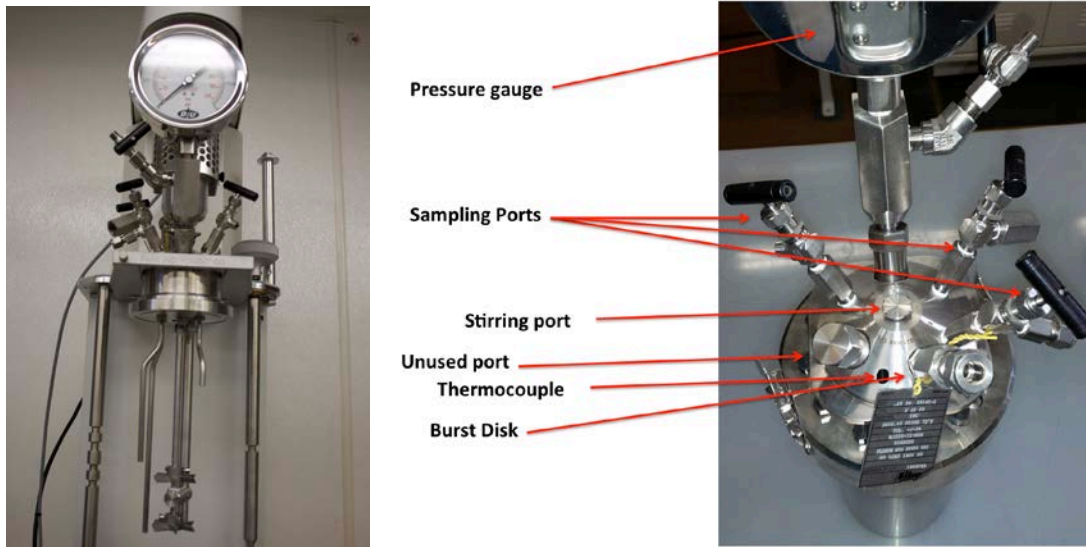


Figure 4.2. Photo of the sampling tubes and mixer assembly with the reactor vessel removed (left) and the reactor head (right- no mixing shaft installed) to show the arrangement of access ports.

4.1.3 Oleophobic Coatings

In studies with crude oil in an enclosed system (e.g., flask or tank), one difficulty is the tendency of the oil to stick to sidewalls, mixers, sampling tubes, and optical windows. This phenomenon can interfere with maintaining droplet suspensions, limit the ability to accurately measure droplet size and dispersion in water, and affect biodegradation studies because suspended oil droplets form a coating on available surfaces. In an attempt to minimize the effects of oil sticking to the sidewalls of the pressure systems, a

number of commercially available coatings were explored for their oleophobicity and potential toxicity (toxicity would interfere with biodegradation studies). A coating that would repel oil, while not affecting the marine microbial community by leaching biocidal compounds into the water, was sought. A clear coating was desired for the sapphire glass windows in the pressurized view cells (described below), but no such limitation was placed on coatings for the other surfaces. Prior work on anti-fouling coatings for marine energy devices and sensors had identified a set of coatings with promising attributes (Bonheyo et al. 2015). Coatings that were tested included the following:

- Intersleek 900 (International Paint-AkzoNobel), a fluoropolymer-based paint that is very hydrophobic and reported to be somewhat oleophobic
- Cerakote (NIC Industries, Inc. and MAD Custom Coating, Bremerton, WA), a very durable thin-film polymer-ceramic composite coating; several variations were tested for oleophobicity and three were tested for toxicity
- UltraSeal ABW from Nanofilm Ltd., a chlorofluoropolymer
- Aculon Glass Repellency (Aculon, Inc), a clear fluorinated alkane-based coating
- Aculon Anti-Fouling Treatment (AFT), an opaque fluorinated alkane-based coating
- 3M NeverWet Multisurface (2-step aerosol).

Coatings for oleophobicity testing were applied by following the manufacturers' instructions onto 1" × 3" coupons of steel, 316 stainless steel, and FR4 fiberglass. Optically clear coatings were applied to glass microscopy slides. Some surfaces were sanded to allow for good coating adhesion in accordance with the manufacturer's instructions. Control surfaces included Teflon, glass, stainless steel, steel, FR4 (glossy surface), and FR4 (sanded surface). Hydrophobicity was assessed using crude oil (ANS); some coatings were also tested with decane, an oleophobicity standard. Measurements were made using a ramé-hart 590-U1 Advanced Automated Goniometer/Tensiometer (Figure 4.3). Each droplet was 10 µl and measurements were made using images taken from the droplets. Six droplets, 3 drops could fit per long edge, were used and each droplet was imaged 8 times (0.1 second between each image acquired) for a total of 32 images per sample set. The number of drops measured was increased if the quality of the drop being imaged was suspect. A summary of the data is provided in Table 4.1 and Table 4.2.



Figure 4.3. A ramé-hart 590-U1 Advanced Automated Goniometer/Tensiometer used to measure contact angle of oil on surfaces to determine the oleophobicity of a surface and to measure the interfacial tension between fluids.

The UltraSeal ABW and Aculon coatings displayed comparable oleophobic properties that were better than those of Cerakote, NeverWet, or Intersleek. Ultimately, the Aculon Glass Repellency coating was chosen because it could be applied more easily on all exposed surfaces, including the mixing blades and exterior of the sampling ports in the Parr reactors.

Coatings used for biocidal effects testing were prepared on $\frac{1}{2}'' \times \frac{1}{2}''$, 316 stainless steel coupons, except for the Aculon Glass Repellency, which was painted onto $\frac{3}{4}'' \times \frac{3}{4}''$ glass microscopy coverslips. The biocidal effects testing was performed using a Microtox[®] assay, a standard method used by the U.S. Environmental Protection Agency (EPA) and other researchers to assess the toxicity of metals and organic compounds in liquid or solid phase (Fulladosa et al. 2005; Tsiridis et al. 2006; Backhaus et al. 2000; Lsi and Aoyama 2010; Park et al. 2016). The Microtox assay measures the luminescence of the bioluminescent marine bacterium *Aliivibrio fischeri* (ATCC 49387); the luminescent output is an indicator of cellular metabolism and the overall “health” of the organism. All tests were performed in triplicate to get an average and standard deviation values. Glass or 316 Stainless Steel coupons were used as non-toxic controls and to establish baseline luminescence values. Sea Hawk Islands 77 Plus (New Nautical Coatings, Inc), a copper- and tin-based biocidal coating was used as a positive (toxic) control. Cells were exposed to the coatings and leachate for 30 minutes in accordance with standard methods and luminescent output was measured using a Synergy HT microplate reader (BioTek Instruments, Inc) (Girotti et al. 2002).

Table 4.1. Contact angles using crude oil.

Coupon	Physical Prep	Surface Coating	Solution Tested	Average Angle	Std. Dev.
Steel	SandedCoupon	Sanded w ABW	ANS	89.15	2.11
FR4	SandedCoupon	Sanded w ABW	ANS	87.56	4.25
Stainless Steel	SandedCoupon	Sanded w Aculon AFT	ANS	87.39	1.42
FR4	SandedCoupon	Red Cerakote w ABW	ANS	82.90	1.86
FR4	SandedCoupon	Teal Cerakote w ABW	ANS	79.39	3.61
FR4	GlossyCoupon	Glossy w ABW	ANS	78.93	1.90
Steel	SandedCoupon	Teal Cerakote w ABW	ANS	78.28	1.53
Steel	SandedCoupon	Yellow Cerakote w ABW	ANS	76.98	3.15
Glass	Slide	HT Glossy Cerakote w ABW	ANS	76.63	1.85
Steel	SandedCoupon	Red Cerakote w ABW	ANS	75.11	7.66
FR4	SandedCoupon	Yellow Cerakote w ABW	ANS	69.45	4.56
Teflon	Slide	Blank	ANS	45.17	0.86
Steel	SandedCoupon	Red Cerakote	ANS	44.40	2.01
FR4	SandedCoupon	Teal Cerakote	ANS	44.27	2.55
Steel	SandedCoupon	Teal Cerakote	ANS	42.97	1.52
FR4	SandedCoupon	Red Cerakote	ANS	42.23	3.56
Steel	SandedCoupon	Yellow Cerakote	ANS	41.72	1.10
FR4	GlossyCoupon	NeverWet	ANS	41.58	3.03
FR4	SandedCoupon	Yellow Cerakote	ANS	39.26	2.11
Teflon	High Density Tape	Blank	ANS	36.18	1.47
Glass	Slide	HT Glossy Cerakote	ANS	35.52	1.43
Teflon	Coupon	Coupon w ABW	ANS	34.20	2.68
Glass	Slide	Blank	ANS	28.44	0.85
FR4	GlossyCoupon	Blank	ANS	27.38	22.31
Steel	Sanded Coupon	Blank	ANS	22.81	0.90
Teflon	Coupon	Blank	ANS	20.45	2.80
FR4	SandedCoupon	Blank	ANS	18.01	2.49
Stainless Steel	Sanded Coupon	Blank	WTI	16.96	2.36

ANS = Alaska North Slope crude oil; WTI = West Texas Intermediate crude oil

Table 4.2. Contact angles using decane.

Coupon	Physical Prep	Surface Coating	Solution Tested	Average Angle	Std. Dev.
Teflon	Matte Coupon	Coupon w ABW	Decane	26.82	2.19
Steel	SandedCoupon	Sanded Coupon w ABW	Decane	48.74	1.90
Polypropylene	SandedCoupon	Sanded Coupon w ABW	Decane	27.24	3.69
Glass	Slide	Slide 5 w ABW	Decane	55.28	3.02
Glass	Slide	Slide 1 CeraKote w ABW	Decane	39.80	2.95
Glass	Frosted Slide	Frosted Coupon w ABW	Decane	61.17	0.93
Glass	Coupon	Coupon w ABW	Decane	51.56	2.69
FR4	GlossyCoupon	Glossy Coupon w ABW	Decane	56.79	0.75

Coupon	Physical Prep	Surface Coating	Solution Tested	Average Angle	Std. Dev.
FR4	SandedCoupon	Sanded Coupon w ABW	Decane	56.16	1.77
FR4	SandedCoupon	Intersleek Gray w ABW	Decane	40.03	3.19
FR4	SandedCoupon	Intersleek Blue w ABW	Decane	41.78	2.37
FR4	SandedCoupon	Yellow Cerakote w ABW	Decane	41.32	2.04
FR4	SandedCoupon	Teal Cerakote w ABW	Decane	51.49	0.36
FR4	SandedCoupon	Red Cerakote w ABW	Decane	53.90	1.82
Steel	SandedCoupon	Yellow Cerakote w ABW	Decane	44.06	1.99
Steel	SandedCoupon	Teal Cerakote w ABW	Decane	47.97	2.41
Steel	SandedCoupon	Red Cerakote w ABW	Decane	45.77	1.85
FR4	SandedCoupon	Red Cerakote	Decane	14.66	4.80
FR4	SandedCoupon	Yellow Cerakote	Decane	16.95	0.05

*Intersleek coating exhibited swelling upon contact with decane.

The Islands 77 Plus coating exhibited a >99% decrease in luminescence compared to the negative control samples (Figure 4.4). None of the other coatings displayed significant toxicity in response to the coatings, indicating that all could be used in experiments examining microorganisms or in which microbial activity might affect the results (Figure 4.4 and Figure 4.5). Intersleek 900 had been previously tested and showed no antimicrobial activity (data not shown).

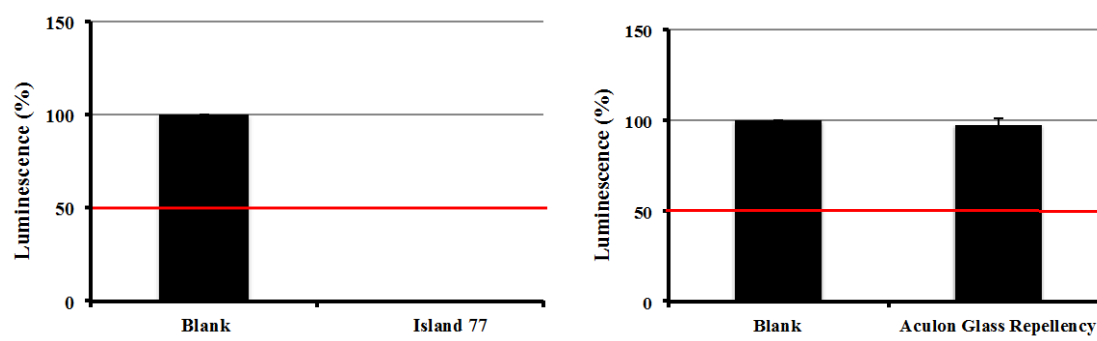


Figure 4.4. Left panel: Positive control test with Islands 77 showing >99% reduction in luminescence compared with the stainless steel negative control blank. Right panel: Aculon Glass Repellency coated glass coupon compared with uncoated glass negative control blank. Experiments were done in triplicate and average values are shown. Error bars represent the standard deviation values.

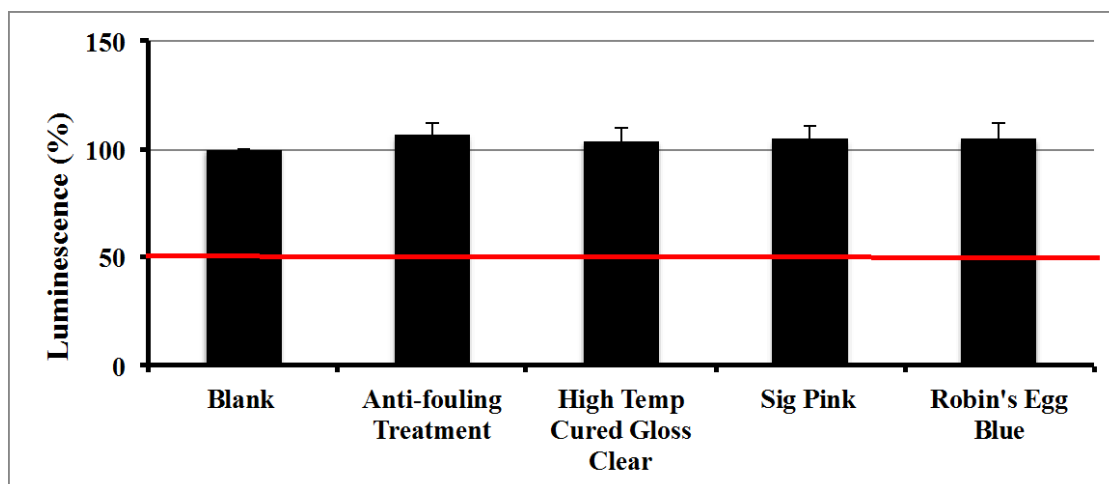


Figure 4.5. Coatings used on stainless steel coatings showed no toxic effects. Experiments were done in triplicate and average values are shown. Error bars represent the standard deviation values.

4.1.3.1 Challenges with the Parr Reactors

One challenge with the pressure chambers came from the process of pressurizing the systems. If the fluid level inside the chamber was high enough to submerge all of the sampling ports, the high-pressure air introduced into the oil and seawater during pressurization resulted in significant mixing and frothing of the oil. Reducing the water level created a significant headspace and less fluid for analysis. Under all fill levels, a gas:fluid interface existed at the top of the reactor, which allowed the oil to form a slick, even when droplet sizes were $<10\ \mu\text{m}$ in diameter and with mixing speeds fast enough to generate a vortex cone. Surface slicks could not be sampled through the sampling ports, and increasing the mixing energy to draw down the oil back into the water column affected the droplet size distribution, as was observed in unpressurized systems. Additionally, it appeared that with high mixing speeds, the impeller came into contact with the oil droplets, resulting in a mechanical reduction of the droplet sizes.

A second and fundamental challenge with working in pressurized systems is the ability to analyze samples under pressure. Withdrawing samples for size analysis using dynamic light scattering or photographic imaging proved to be impossible because the action of collecting a sample into a high-pressure sampling syringe resulted in atomization of the oil as it moved from the pressure vessel into the void space of the sampling syringe. Even partially pressurizing the syringe to reduce the effect of pressure drop could not be counted on to minimize effects. To overcome the effects of depressurization, efforts were made to identify noninvasive means of analyzing the pressurized fluids in the Parr reactors or in pressurized lines that could be used either to draw samples at pressure from the reactor or as standalone pressurized systems. Several methods that were investigated are described in Section 4.3 below.

4.1.4 View Cells

One method that did allow for examination of the pressurized fluids was to design a separate high-pressure reactor in which fluids could be pressurized, or into which pressurized fluids could be injected (while maintaining pressure) and observed. This high-pressure view cell included integrated sapphire glass view windows for direct observation of the pressurized fluids and oil droplets. Samples could also be withdrawn from the Parr reactors through high-pressure tubing into a high-pressure view cell. The view cells were milled from block 216 Stainless Steel with a $\frac{1}{2}$ in. (1.27 mm) diameter hole drilled in one direction intersecting a perpendicular hole $\frac{1}{8}$ in. (.3175 mm) in diameter (Figure 4.6). Two Teledyne

260D Syringe Pumps rated to 7500 psi and outfitted with cooling jackets for temperature control were used to control the withdrawal of samples from any of the three sampling ports into the view cell through the $\frac{1}{8}$ in. tubing and into the central chamber where droplets could be observed through a pipe affixed to a sapphire glass window and locked in the $\frac{1}{2}$ in. hole. A second pipe and window opposite the view window could be used with a fiber optic light source to illuminate the interior (Figure 4.6).

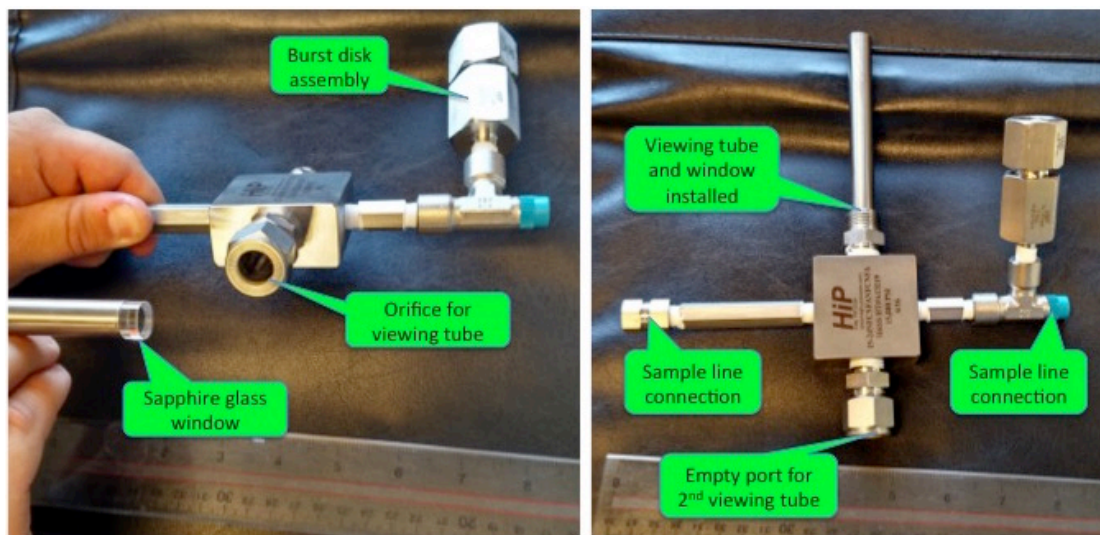


Figure 4.6. View cells disconnected from the Teledyne pump and Parr reactor. The viewing tubes are $\frac{1}{2}$ " OD and the sample line tubes are $\frac{1}{8}$ " OD. The inner chamber is $\frac{1}{2}$ " diameter \times $\frac{3}{4}$ " long.

Unavoidably, samples drawn through the sample port and connecting lines experienced some shear forces, which may have impacted droplet size. The small diameter sampling lines could not be treated effectively with any of the oleophobic coatings, and therefore, oil also coated the interior of the sampling lines. A third challenge was that oil within the Parr reactors that formed a surface slick could not be retrieved using the three sampling ports.

Alternatively, a Teledyne pump was used to pressurize a sample of oil and water injected directly in the view cell using the opposing sample port. After loading a sample, that port was sealed and the pump was used to pressurize the system through the port on the opposite side. Once pressurized, the second port was sealed off from the pump to maintain pressure in the view cell as a standalone system. Small magnetic stir bars were placed in the central view chamber and used to provide some mixing energy if the view cell was placed on a magnetic stir plate. However, because of poor coupling of the stir bar to the magnetic stir plate through the thick stainless steel view cell walls, only slow mixing speeds could be maintained: oil droplets were still affected by gravity and could stick to the walls of the view cell or to the sapphire glass windows, limiting observation times to a few seconds. A fiber optic variable intensity white light source provided illumination through the opposing viewing tube from the camera.

One difficulty with the flow cell was the ability to collect high-resolution images through the viewing tube. A custom attachment was made with a 3D printer to connect a Canon EOS 70D (20.2 MP) camera with an attached 100 mm macro lens ($f/16$, ISO 6400) to the viewing tube, but the large diameter of the lens relative to the diameter of the viewing tube resulted in poor-quality images. A boroscopic camera was also tested, but its resolution was too low. A second mount was created to connect a GoPro Hero4 12 MP camera to the viewing tube. The GoPro has a lens diameter that is similar in size to the viewing tube, and images (including video) could be taken; however, the effective FOV at the end of the tube was only <1 cm. Increasing the magnification of the image to resolve small droplets (<0.75 mm) was not very effective, particularly when the droplets were in motion due to stirring or gravity. The DOF relative to the

length of the view cell also diminished the quality of the images. Decreasing the length of the viewing tube was not possible because of the minimum focus distance of the camera. Because the challenge of collecting images down the view tube of the flow cell is similar to that of collecting images through the length of a microscope, an attempt was made to couple a microscope objective and camera mount to the viewing tube, but this proved challenging and could not be completed. Of the camera systems and methods tested, the GoPro Hero4 camera provided the best quality images and was used to conduct the experiments.

4.1.5 Interfacial Tension

When two immiscible liquids are present, the interfacial tension is a measure of force that holds the phases separate. Without external mixing forces, the two fluids separate to minimize the surface area between the two. The smallest possible surface area exists when the fluids are separated as two phases, i.e., all oil in one large drop or slick. As interfacial tension increases, so does the amount of energy needed to increase the amount of surface area between the fluids (i.e., creating smaller and smaller droplets of oil in the water). In contrast, an interfacial tension value of zero would indicate that the two materials may freely mix without an input of energy. Dispersants act as an interface between oil and water, reducing surface tension and allowing for greater surface area to be present with lower mixing energy.

The interfacial tension of Macondo oil in seawater, with and without different concentrations of dispersants, was measured using a ramé-hart 590-U1 Advanced Automated Goniometer/Tensiometer (Figure 4.3) and the DROPimage Advanced software package. The interfacial tension data may be used to help calculate the droplet size (e.g., Young-Laplace equation relating surface tension, droplet radius, and pressure differential across the fluid interface) and Weber number (relating fluid density, velocity, surface tension, and droplet size) to characterize the mixing media.¹⁷ The interfacial tension was measured using an inverted pendant drop phase methodology in which a droplet of oil is injected into a cuvette of seawater. This approach is used when the density of the drop phase (the oil in this case) is less than that of the external phase (the seawater). During the measurements, seawater temperature was held constant at 17.4°C or 17.8°C, which corresponded to room temperature on different days. The oil was also at room temperature or heated to 30°C. All measurements had to be made at 14.7 psi (1 atm). In these experiments, the dispersant was thoroughly premixed with the water, providing an idealized situation.

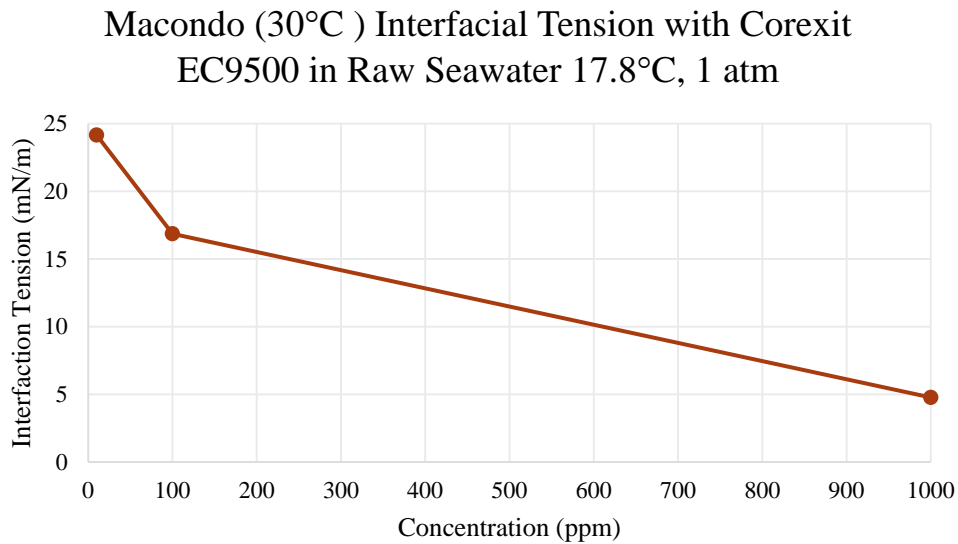
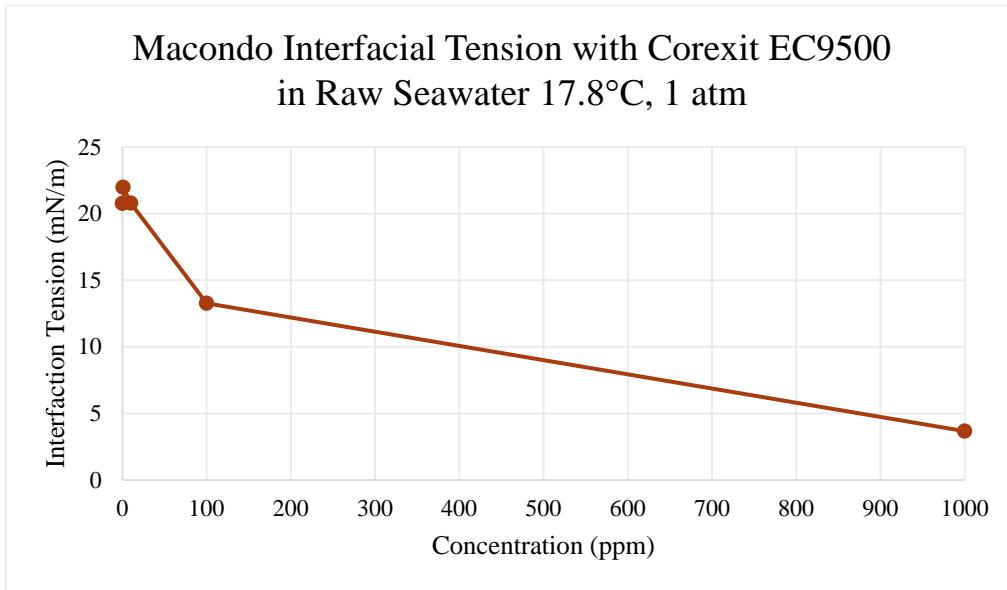
The interfacial tension of Macondo crude oil at 1 atm, 17.4°C, 0.8561 g/L density, in 17.4°C, 32 ppt salinity seawater was determined ($N = 3$) to be 21.79 mN/m (+/- Std. Dev. 0.68). The Macondo crude oil interfacial tension increased upon heating to 30°C and subsequently testing in 17.4°C, 32 ppt salinity seawater ($N = 3$) for a value of 23.39 mN/m (+/- Std. Dev. 0.13).

With 17.4°C seawater and oil, the addition of Corexit EC9500 at concentrations of 10 ppm or greater showed a reduction in the interfacial tension compared to the Macondo crude oil alone. Similarly, with 30°C oil in 17.4°C seawater, the addition of Corexit at concentrations of 100 ppm or greater reduced the interfacial tension compared to the 30°C Macondo alone, but the use of 10 ppm Corexit resulted in a slightly higher interfacial tension of 24.15 mN/m.

When the dispersant Finasol OSR 52 was used with 17.4°C seawater and oil, it reduced the surface tension at concentrations of 100 ppm or greater, but concentrations of 10 ppm and 1 ppm yielded surface tensions (21.88 mN/m and 21.72 mN/m, respectively) that were comparable to that of the Macondo oil alone. The same effect was seen when the oil was heated to 30°C: concentrations of Finasol at 100 ppm or greater reduced the surface tension of the oil compared to seawater with no dispersant, but the use of

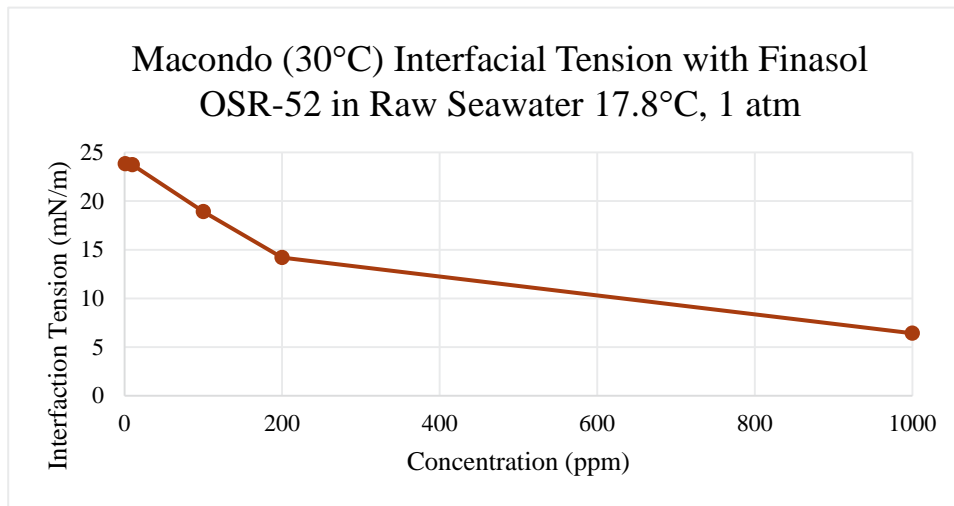
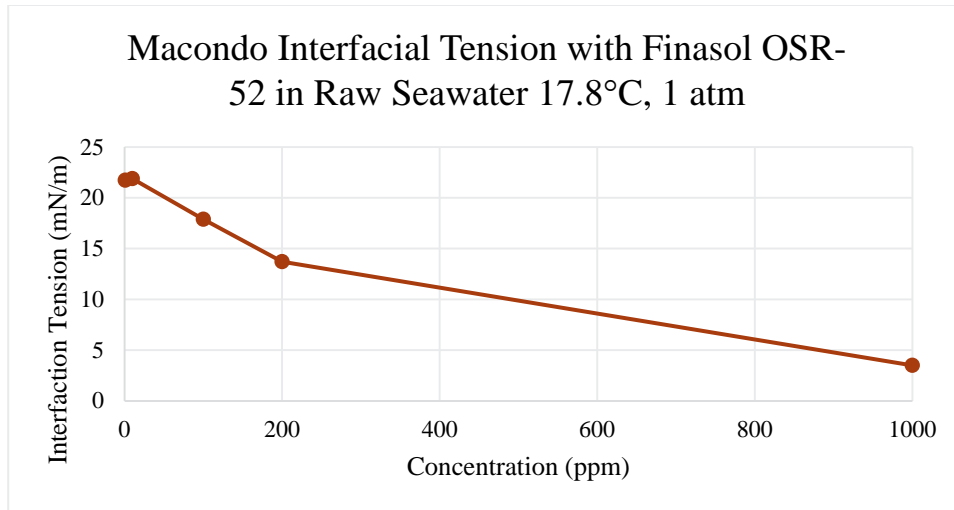
10 ppm and 1 ppm yielded surface tensions (23.72 mN/m and 23.83 mN/m, respectively) that were comparable to that of the Macondo oil alone.

In general, interfacial tension was found to increase slightly as the temperature difference between the oil and the water increased, and a somewhat greater effect was observed with the Corexit. The temperature-induced increase was not proportional to changes in DOR and might therefore be attributed to the oil. The effect of mismatched and matched dispersant and oil temperatures during mixing in a simulated blowout was explored more carefully under Tasks 5 and 6 below (Sections 4.5 and 4.6). Raw data for these measurements are provided in Appendix A and summaries for oil with Corexit 9500 and Finasol OSR 52 are provided below in Figure 4.7 and Figure 4.8, respectively.



Dispersant Dilution	Concentration (ppm)	Interfacial Tension 17.8°C			Interfacial Tension 30°C		
		Tension (mN/m)	N	Std Dev	Tension (mN/m)	N	Std Dev
1:10 dil	1000	3.67	30	0.45	4.77	3	0.42
1:100 dil	100	13.27	30	2.31	16.86	3	0.74
1:1000 dil	10	20.78	3	0.44	24.15	3	0.19

Figure 4.7. Effect of dispersant (Corexit 9500) concentration and temperature on the interfacial tension between oil and water.



Dispersant Dilution	Concentration (ppm)	Interfacial Tension 17.8°C)			Interfacial Tension (30°C)		
		Interfacial Tension	N	Std Dev	Interfacial Tension	N	Std Dev
1:10 dil	1000	3.5	3	*	6.42	3	0.84
1:50 dil	200	13.71	30	0.23	14.2	3	0.75
1:100 dil	100	17.88	30	0.38	18.91	3	0.69
1:1000 dil	10	21.88	30	0.97	23.72	3	0.46
1:10000 dil	1	21.72	30	0.49	23.83	3	0.63

Figure 4.8. Effect of dispersant (Finasol OSR 52) concentration and temperature on the interfacial tension between oil and water. *Approximation: the droplet would not remain formed long enough to test.

4.1.6 Visualization of the Effect of Pressure on Droplet Size

A series of tests was conducted to examine the effect of static pressure on droplet size once initial mixing energy was reduced or eliminated. Dispersants work by reducing the interfacial surface tension between oil and water, but mixing energy is also critical to the creation of small droplets. It was suspected that pressure might affect droplet size because crude oil can be more compressible than water, and the change in density might have a measureable impact on the surface tension of the oil droplet. The objective was to compare identical samples of oil, dispersant, and seawater at different pressures and with equivalent or no mixing energy to determine whether the observed droplet size distribution varied. To examine the effect of pressure on droplet size with different DORs, samples of oil and dispersant in seawater were injected into the high-pressure view cells using the Teledyne pumps and subjected to different pressures. The samples were premixed, loaded into the view cells, pressurized, and mixed with a stir bar. Stirring was stopped and the fluid was immediately imaged using a digital camera to assess the droplet sizes. The small view cells were used rather than the large Parr reactors because of the aforementioned difficulties in retrieving representative samples from the Parr reactors, particularly with larger drops. In these tests, pressure was maintained as a constant and the oil was not observed to degas. Experiments observing the effect of depressurization on droplet size and droplet size distributions are described later under Task 6 (Section 4.6).

For the effect of static pressure tests, Macondo crude was used with Corexit 9500 at DORs of 1:25, 1:50, and 1:100. Test solutions used 50 μ L of oil in 200 mL of seawater; however, some oil was expected to have coated the exposed inner surfaces of the flow cell and tubing despite the oleophobic treatment. Pressure was held at 14.7 psi (atmospheric), 1000 psi, 2000 psi, and 2900 psi (the equivalent of \sim 2 km water depth). One set of tests was conducted with the temperature held at room temperature (17.8°C) and a second set with the temperature held at 6°C to \sim 8°C. The small view cells have no means for temperature regulation, so fluids starting at 4°C warmed by 2°C to 4°C during the cold temperature experiments.

After several trials, droplets could not be accurately imaged within the view cell. While mixed with the stir bar, droplets may have moved too quickly to be imaged, but without mixing, droplets were still not visible; perhaps they rose out of view. A number of trials were conducted in which the concentration of oil was increased in the hope of capturing droplets in frame, but an appropriate concentration was not found: either no droplets were visible or the window became coated with oil and oil droplets could not be clearly resolved through the sheen (Figure 4.9). Neither the automated nor manual processing of the images was effective at identifying droplets.

Different coatings and wipes were tested in an attempt to keep the window clean when higher oil concentrations were used (Aculon Glass Repellency, Ultraseal ABW, and Tub O' Towels) without success. Interestingly, these treatments worked well on borosilicate glass beakers and flasks used in other tests, and it is not clear why the sapphire glass behaved differently. Oil with no dispersant, low DOR, and high DOR also did not work. An attempt was also made to mount the view cells onto a rotating axis (aligned parallel to the view tubes) in order to keep droplets suspended for a longer period of time, but this also failed. It is possible that some large droplets may not have been captured in the images if the droplet rapidly rose to the surface.

Ongoing work at PNNL is attempting to identify better coatings to prevent the buildup of oil on the windows. Another possible solution may be to use the Parr reactors with vigorous mixing to create an oil in water suspension and to draw pressurized samples through the view cell using the Teledyne pumps. This would require further improvements to the camera mount (using custom-designed optics based upon those used for microscopy). Another possibility is to use a modified Parr reactor with a large window and interior white backdrop positioned within 1–2 cm of the window to enable the use of standard high-speed

photography. This latter approach worked well with the blowout tests described in later under Task 6 (Section 4.6).

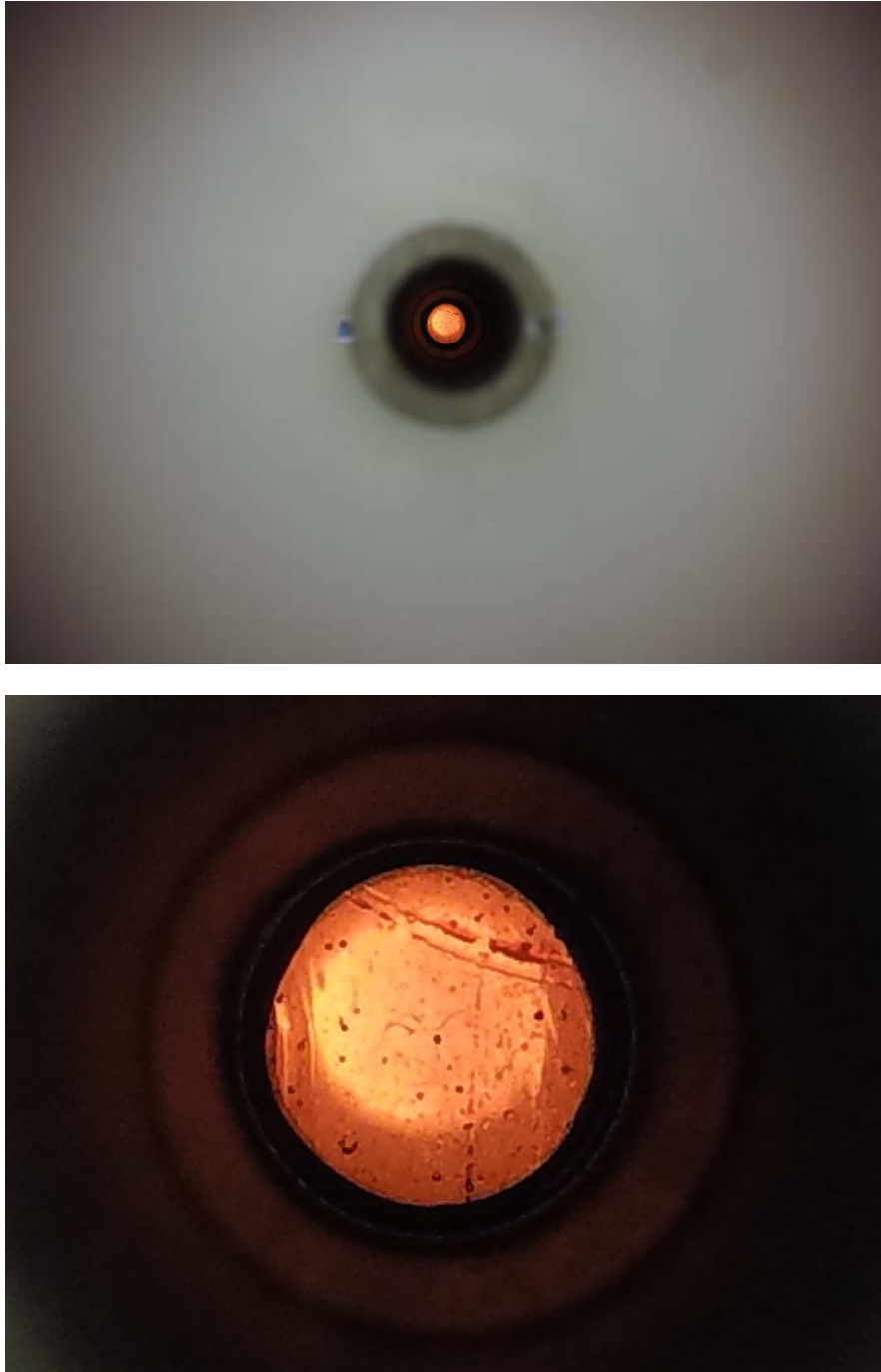


Figure 4.9. Original (top) and cropped (bottom) images taken of 400 μL oil with 16 μL Corexit in 200 mL seawater at 17.8°C. In this image, the view cell window has become coated with oil. In the original image, the wide outer white area is the plastic coupler used to join the camera to the view tube, the silver ring is the top edge of the view tube, the black ring is the inside of the view tube, and the orange circle is the field of view through the sapphire glass window.

4.2 Examine the Influence of Droplet Size on Biodegradation

A long-held assumption is that oil droplet size is an important factor controlling the rate of biodegradation, and a primary objective of using dispersants is to render oil into small droplet sizes to enhance the rate of degradation (National Research Council 2005; Prince et al. 2016). The potential benefits of reducing droplet size include, for example: 1) smaller droplets have a larger surface to area ratio, allowing microbes to colonize the surface of the oil while still accessing water and oxygen to promote the metabolism of hydrocarbons; and 2) dispersion distributes a given quantity of oil through a larger volume of water, potentially slowing or reducing the rates at which key nutrients are depleted and toxic waste products accumulate. However, an accurate measure of the difference in metabolic rate as a function of droplet size does not appear to have been empirically tested. Consequently, it is difficult to ascertain the relative improvement in biodegradation rates when trying to establish, for example, 1 mm or 0.1 mm mean droplet sizes. An understanding of how biodegradation rates scale with droplet size would help inform whether a significant benefit can be achieved by using larger amounts of dispersant.

To explore this dynamic, methods were tested to establish different droplet size distributions and to maintain a consistent droplet size distribution for many hours or days, or to at least create a stable decay in size over time. Ideally, a series of experiments would use cultures in which different oil droplet size distributions could be maintained in suspension for a period of days in order to conduct microbial biodegradation studies. Alternatively, cultures could be created with different starting size distributions. In order to isolate droplet size as the critical variable, tests were conducted to identify means of establishing different distributions and to assess how the method of creating the distribution affected cellular growth.

The first section below identifies the different means of creating and maintaining suspensions of droplets that were explored. These methods were assessed to examine their ability to stabilize and maintain droplet size and for their effect on microbial growth and metabolism. The second section identifies the microorganisms used in the assays. Combinations of stabilizers, emulsifiers, and mixing energy could not be highly toxic to the cells. However, some promotion or repression of growth and metabolism was deemed acceptable, provided the effect could be accounted for and test results could be normalized to subtract the effect. The final section outlines the biodegradation study.

4.2.1 Means of Creating and Maintaining Droplet Suspensions

Molten soft agar suspensions using Noble Agar, Bacto Agar, and Gelrite were tested as a means of capturing droplets into a semi-solid matrix, but this also failed to create an even droplet distribution: some oil separated from the agar before it set and additional oil “bled out” of the agar after it cooled. An ultrasonic water bath with variable frequency and intensity control was also tested as a means of providing mechanical energy to maintain an emulsion; however, the initial emulsions decayed and formed surface slicks of oil. Carbon black, which is used to stabilize some emulsions after mechanical mixing, was found to be toxic to cell growth and interfered with the ability to take photographs or optical density readings. The surfactant sodium dodecyl sulfate, even at low concentrations, resulted in foaming during mixing, and also contributed to cell death. Other surfactants, Dawn dish detergent, Corexit, and Finasol, were tested more extensively as described below.

4.2.2 Microorganisms Used in the Experiments

A pair of oil metabolizing bacteria, *Alcanivorax borkumensis* ATCC 700651 and *Pseudomonas putida* ATCC 700007, and a single oil metabolizing fungus, *Hormoconis resinae* ATCC 22711 (Figure 4.10), were used in the tests as identified below. The bacteria grow as single cells and are believed to only

colonize or interact with the surface of oil droplets, and would therefore be most likely to be affected by droplet size. *H. resiniae*, on the other hand, is an example of a filamentous fungus whose mycelia can penetrate into an oil droplet, and may thus be less limited by droplet size. The use of defined cultures of organisms eliminates the potential variability and uncertainty found in natural or complex mixed cultures caused by different species growing at different and unpredictable rates. However, for tests requiring a greater diversity of metabolism, an undefined mixture of microorganisms was prepared from freshly collected seawater. The seawater mix was concentrated 50-fold via filtration to capture the cells followed by resuspension in seawater supplemented with glycerol. Individual aliquots were frozen at -80°C until needed.



Figure 4.10. Left to right: *Hormoconis resiniae*, *Alkanivorax borkumensis*, and *Pseudomonas putida* grown on agar media. Petri dishes are 100 mm across.

4.2.2.1 Characterization of Dispersant Impact on Substrate Biodegradation by Microorganisms

For tests using dispersants to control droplet size, it was important to understand the impact the dispersants might have on microbial growth (cell division) and metabolism in order to normalize or subtract these impacts from the results to assess the impact of other factors such as temperature, pH, or droplet size. A number of studies have examined the impact of dispersants, including Corexit 9500, on microbial metabolism and the results have been highly variable. Some have shown increased metabolism, others no effect, and still other studies have shown inhibition (Prince et al. 2016; Kleindienst et al. 2015; Macias-Zamora et al. 2014; Prince and Butler 2014). A series of control tests were therefore performed to examine the potential effects of the dispersant on cell growth. Assays included direct analysis of toxicity using Microtox assays, assessing the impact on growth curves, and assessing any impact on the metabolism of various substrates.

To assess the impact on metabolism by the selected organisms and with the same samples of dispersant to be used in the droplet size study, an analysis was performed to look for any potential impacts on the metabolism of either carbohydrate (sugar) or protein. Glucose was used as a model sugar and bovine serum albumin (BSA) as the model protein. Preliminary tests with two different commercial assay kits, D-glucose assay kit (Megazyme Inc., IL, USA) and Quick Start Bradford Protein Assay (Bio-Rad, CA, USA), were performed to confirm that the kits could detect different concentrations of substrates (D-glucose and BSA). Each substrate was prepared in sterile ultrapure (18 MΩ resistance) water at the following concentrations: 0.125, 0.2, 0.5, 1, 2, 5, 10, and 20 mg/mL. The assays were done using 96-well plates and absorbance was measured using a Synergy HT microplate reader (Biotek, VT, USA). Figure 4.11 (glucose assay) and Figure 4.12 (protein assay) show the results from preliminary tests and both worked well. All assays were done in triplicate. Average values are shown and error bars represent standard deviation values.

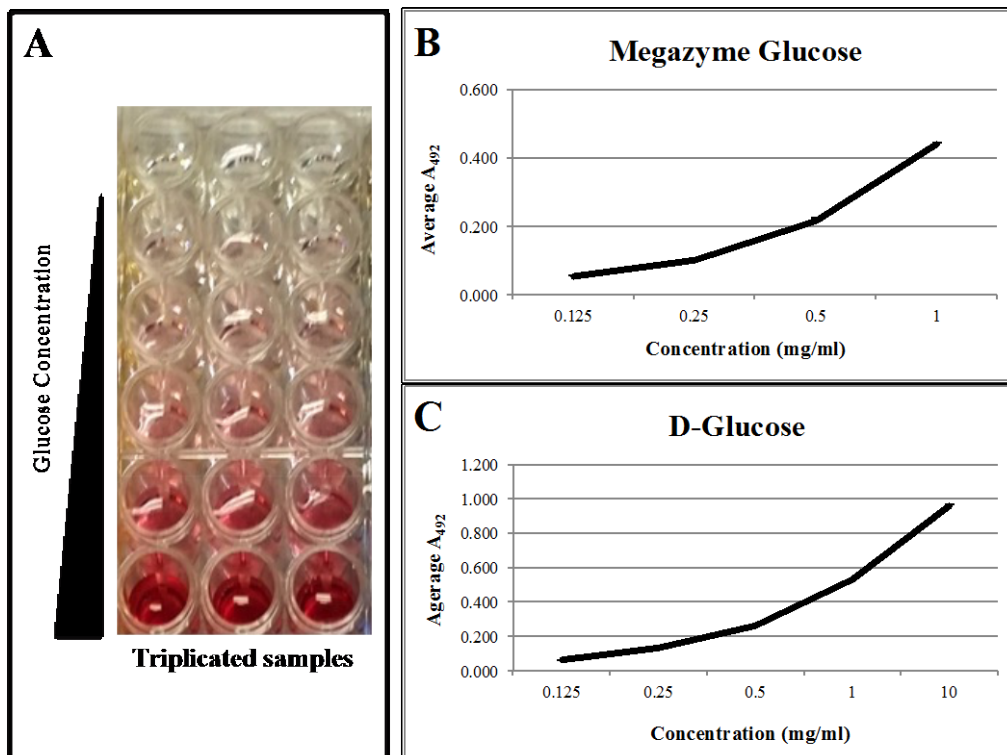


Figure 4.11. Preliminary glucose assays. (A) After 20-minute incubation at 45°C, the D-glucose standard and Glucose Determination Reagent (GOPOD reagent) mixture changed color and the higher the glucose concentration, the darker the color was. All samples were tested in triplicate. (B) Glucose assay result with the manufacturer's glucose standard: absorbance of light at wavelength 492 (A_{492}) values were proportional to glucose concentrations. (C) Glucose assay result with “homemade” D-glucose standard: A_{492} values were proportional to glucose concentrations.

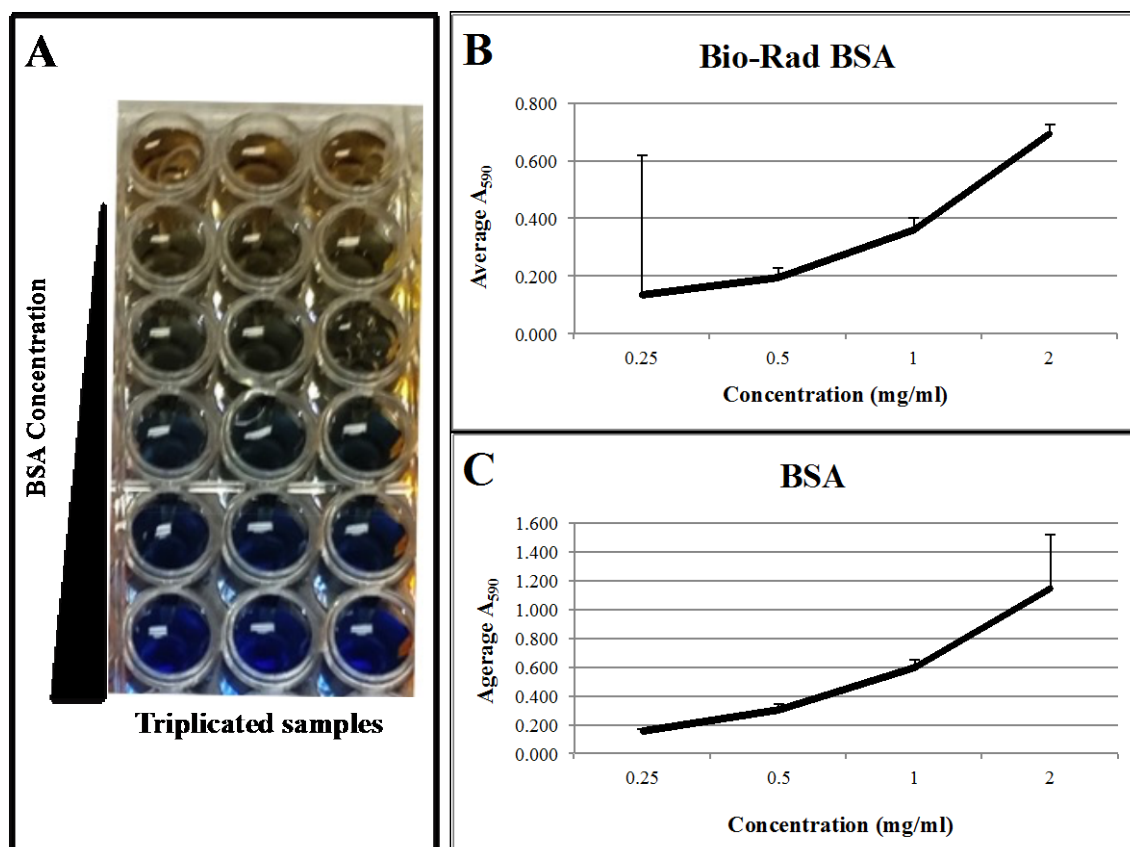


Figure 4.12. Preliminary protein assays. (A) After 5-minute incubation at room temperature, the Bovine Albumin Serum (BSA) standard and Dye Reagent mixture changed color and the higher the glucose concentration, the darker the color was. All samples were tested in triplicate. (B) Protein assay result with the manufacturer's BSA standard: absorbance of light at wavelength 590 (A_{590}) values were proportional to protein concentrations. (C) Protein assay result with “homemade” BSA standard: A_{590} values were proportional to protein concentrations.

Following the successful test with substrates prepared in ultrapure water, the assays were repeated using sterile filtered seawater as a solvent because it would be used later to cultivate the microorganisms during the biodegradation tests. Samples prepared for glucose quantification included D-glucose in sterile 18 M Ω water as a solvent, D-glucose in sterile seawater, D-glucose + BSA in sterile 18 M Ω water, and D-glucose + BSA in sterile seawater. Samples prepared for protein quantification included BSA in sterile 18 M Ω water as a solvent, BSA in sterile seawater, BSA + D-glucose in sterile 18 M Ω water, and BSA + D-glucose in sterile seawater. The two standards were combined in some samples to verify that each substrate could be detected in the presence of the other, which would allow for a reduction in the number of samples to be prepared for the biodegradation assays. Figure 4.13 and Figure 4.14 show new control assay results. The conclusion was that neither the use of seawater nor mixing the two substrates had any effect on D-glucose and BSA detection.

After validating the test methods in seawater, samples were created to examine the impact of Corexit, Finasol, and Dawn dish detergent on metabolism by *H. resiniae*, *A. borkumensis*, and an undefined, mixed inoculum of seawater microorganisms prepared using filtration to concentrate the microbial content of

raw seawater 50-fold. *A. borkumensis* has not been shown to metabolize glucose or protein in laboratory culture and served as a negative control. *H. resiniae* (syn. *Cladosporium resiniae* and *Amorphotheca resiniae*) can metabolize glucose, but is unlikely to metabolize protein. The mixed microbial community was expected to harbor organisms that metabolize both substrates.

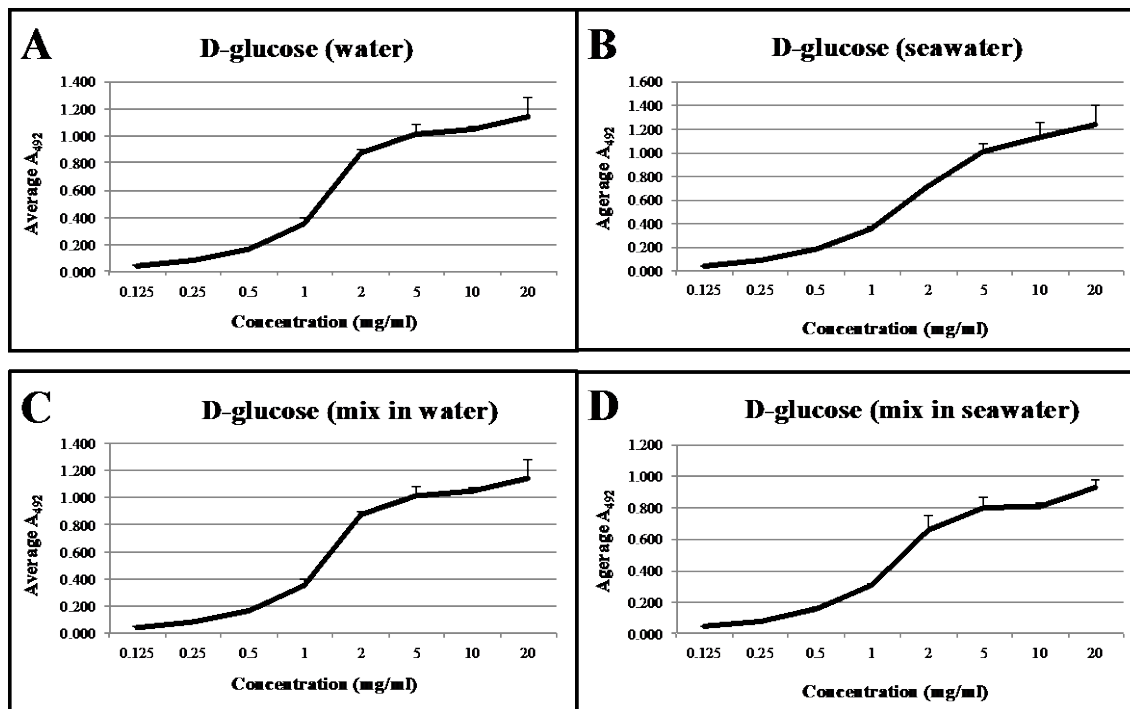


Figure 4.13. Glucose assays. Two different solvents, water and seawater, were used to make various concentrations of D-glucose. (A) D-glucose standards dissolved in sterile water and (B) D-glucose standards dissolved in sterile seawater. (C&D) D-glucose and BSA (dissolved in either water or seawater) were mixed at a 1:1 ratio and then used to measure D-glucose concentrations. All assays were done in triplicate and error bars represent standard deviation values.

Corexit, Finasol, and Dawn dish detergent were tested at final concentrations of 0.625%, 1.25%, 2.5% and 5%. BSA and D-Glucose were combined at concentrations of 1 mg/mL each, and 0.1 mg/mL each. Control sets that included either no inoculum, no dispersant, or no BSA or D-Glucose were also created. All samples were prepared using filter-sterilized seawater and a barcode system was used to label and track the samples. Tube caps were left loose to prevent the generation of anaerobic conditions. 0.1 mL samples were collected at Time 0, 1 day, 5 days, 6 days, and 7 days. Collected samples were stored at -20 °C until analysis.

No substrate degradation was observed, even in the samples to which no dispersant or emulsifier was added. Samples were also collected at Time 0 and after 5 days to inoculate petri dish media (potato dextrose agar for samples inoculated with *H. resiniae*, and marine agar for samples inoculated with *A. borkumensis*) to check cell viability. The Time 0 plates showed visible growth (both *A. borkumensis* and *H. resiniae*) on agar plates. After 5 days, based on spread plate results, however, *A. borkumensis* was no longer viable, while *H. resiniae* still had viability. Results for *A. borkumensis* and *H. resiniae* are shown in Figure 4.15 and Figure 4.16, respectively. All experiments were done in triplicate.

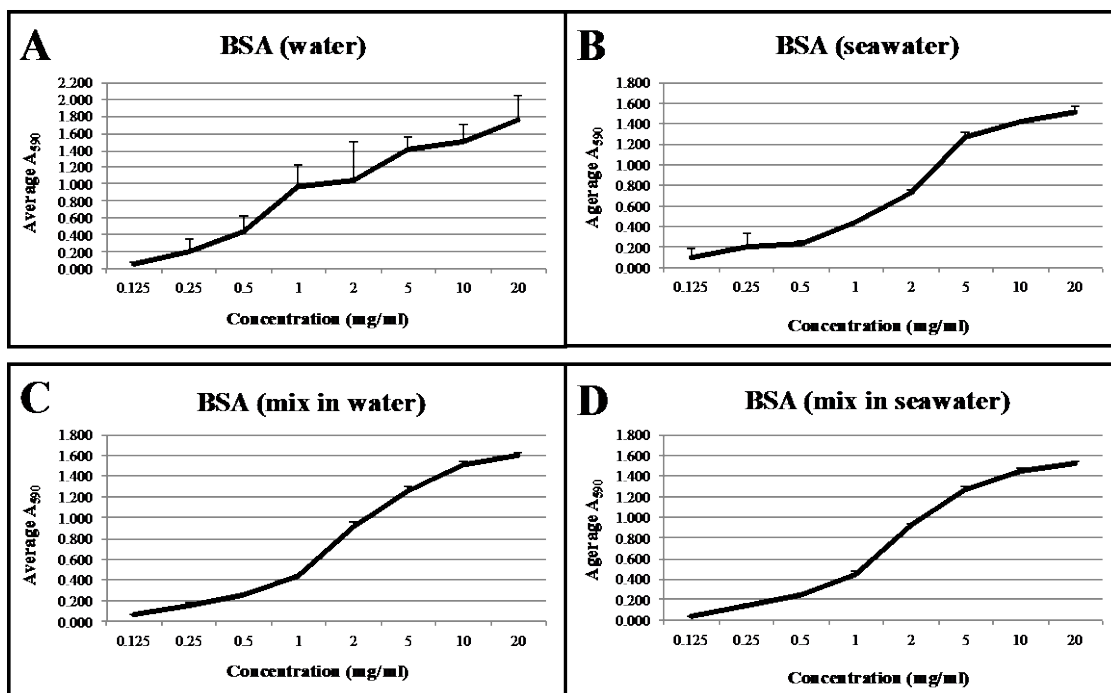


Figure 4.14. Protein assays. Two different solvents, water and seawater, were used to make various concentrations of Bovine Serum Albumin (BSA). (A) BSA standards dissolved in sterile water and (B) BSA standards dissolved in sterile seawater. (C&D) D-glucose and BSA (dissolved in either water or seawater) were mixed at a 1:1 ratio and then used to measure BSA concentrations. All assays were done in triplicate and error bars represent standard deviation values.

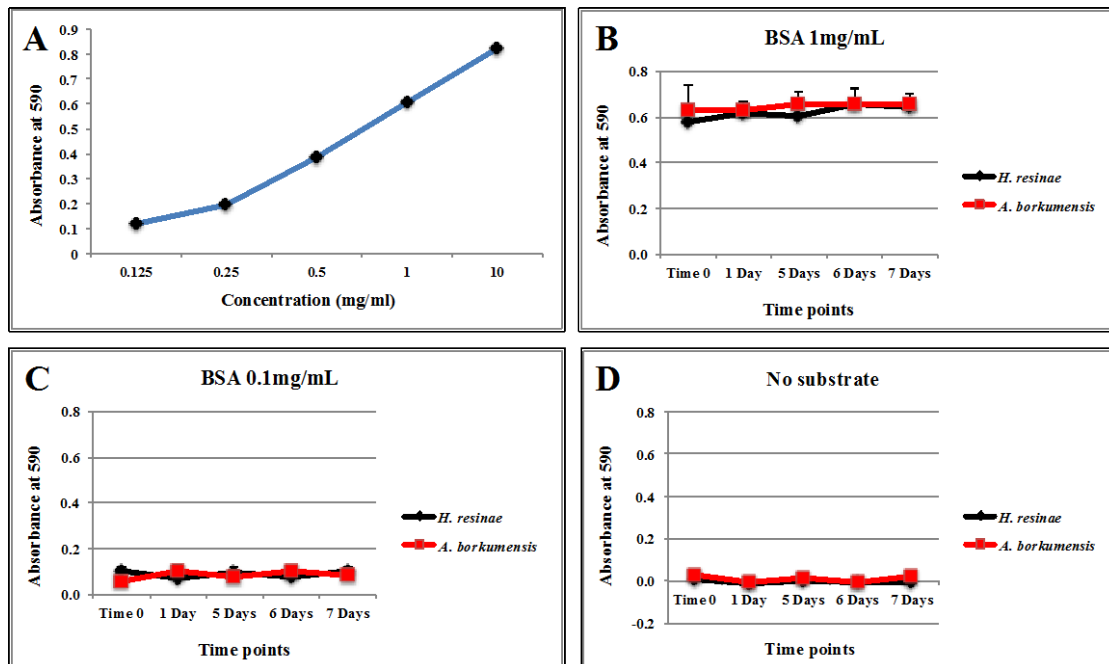


Figure 4.15. Protein assays. (A) Protein assay results from the BSA & D-glucose mix: A590 values were proportional to protein concentration. (B) Protein assay results from samples containing 1 mg/mL of BSA. (C) Protein assay results from samples containing 0.1 mg/mL of BSA. (D) Protein assay results from samples containing no substrate. All experiments were done in triplicate and average values are shown. Standard deviation values are shown as error bars.

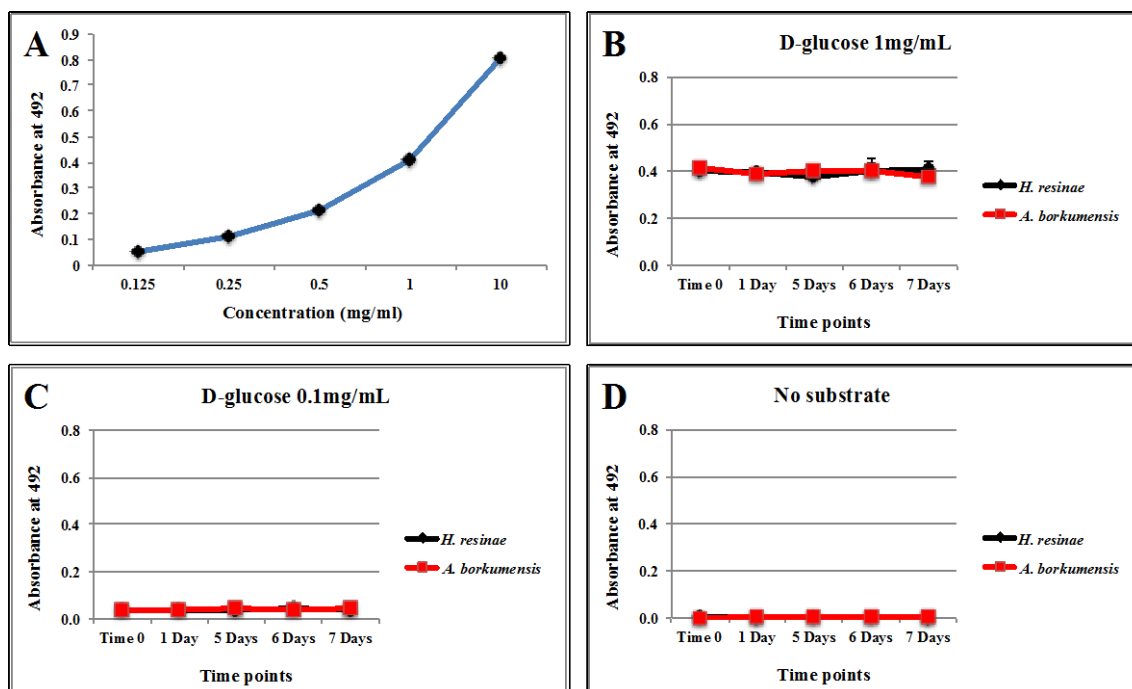


Figure 4.16. Glucose assays. (A) Glucose assay results from the BSA & D-glucose mix: A492 values were proportional to glucose concentration. (B) Glucose assay results from samples containing 1 mg/mL of D-glucose. (C) Glucose assay results from samples containing 0.1 mg/mL of D-glucose. (D) Glucose assay results from samples containing no substrate. All experiments were done in triplicate and average values are shown. Standard deviation values are shown as error bars.

The results for *A. borkumensis* were expected: it is not known to metabolize glucose or protein in laboratory culture. The results for *H. resiniae* and the seawater inoculum were more puzzling, because *H. resiniae* was expected to metabolize glucose but not protein and the seawater mix was expected to metabolize both substrates.

A second approach to examining the impact of dispersant/emulsifier on substrate biodegradation by microorganisms was to test how dispersant/emulsifier affected cell growth. Cultures were prepared in 96-well microtiter plates using marine broth growth medium supplemented with Corexit, Finasol, or Dawn dish detergent at concentrations of 0%, 0.5%, 0.625%, 1%, 2%, 2.5%, and 5% (v/v). One plate was created inoculated with *A. borkumensis* and a second plate with the concentrated seawater mixture of organisms. *H. resiniae* was not used for this experiment because it has a filamentous growth habit that results in uneven turbidity in liquid culture. Figure 4.17 shows the experimental setup. Each concentration of dispersant or detergent was tested in triplicate (Cultures 1–3); columns 10–12 were sterile controls (no inoculum) used as reference samples for determining the change in optical density (O.D.). The O.D.₅₉₀ was measured every 10 minutes for 3 days using a Synergy HT microplate reader (Biotek, VT, USA). Results are shown in Figure 4.18 and Figure 4.19.

	Corexit 9500A			Finasol OSR 52			Dawn dishsoap			None		
	1	2	3	4	5	6	7	8	9	10	11	12
A	0%	0%	0%	0%	0%	0%	0%	0%	0%	0%	0%	0%
B	0.5%	0.5%	0.5%	0.5%	0.5%	0.5%	0.5%	0.5%	0.5%	0%	0%	0%
C	0.625%	0.625%	0.625%	0.625%	0.625%	0.625%	0.625%	0.625%	0.625%	0%	0%	0%
D	1%	1%	1%	1%	1%	1%	1%	1%	1%	0%	0%	0%
E	1.25%	1.25%	1.25%	1.25%	1.25%	1.25%	1.25%	1.25%	1.25%	0%	0%	0%
F	2%	2%	2%	2%	2%	2%	2%	2%	2%	0%	0%	0%
G	2.5%	2.5%	2.5%	2.5%	2.5%	2.5%	2.5%	2.5%	2.5%	0%	0%	0%
H	5%	5%	5%	5%	5%	5%	5%	5%	5%	0%	0%	0%
	Culture 1	Culture 2	Culture 3	Culture 1	Culture 2	Culture 3	Culture 1	Culture 2	Culture 3	Culture 1	Culture 2	Culture 3

Figure 4.17. Experimental setup for testing the effect of dispersant/emulsifier on cell growth. The growth curve study was done with various concentrations of dispersants and emulsifiers. 96-well plates and a microplate reader were used. Test organisms were *A. borkumensis* and seawater organism mix and experiments were done in triplicate.

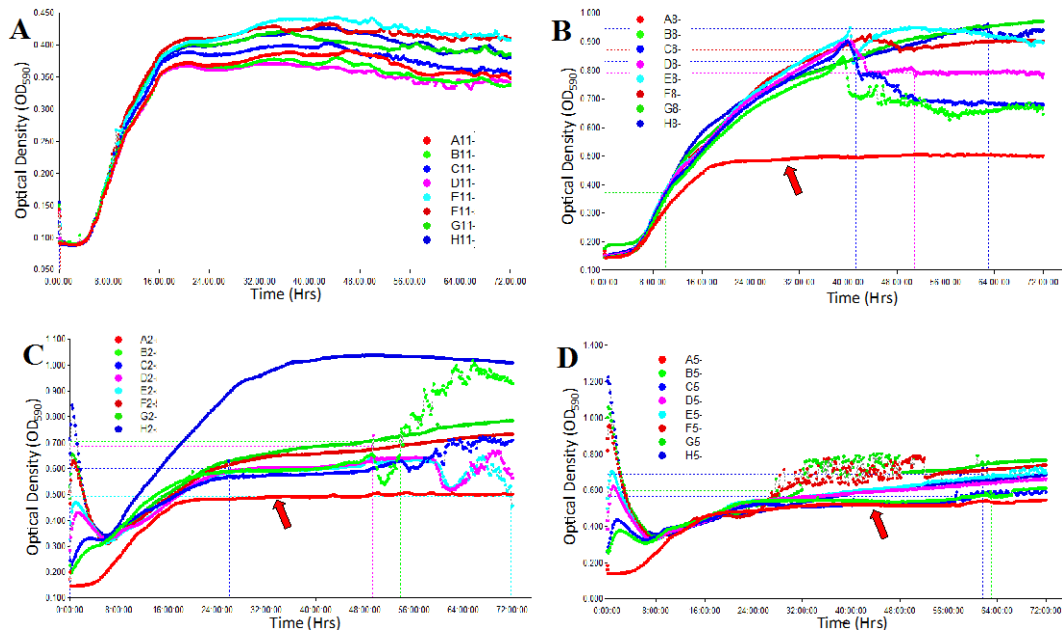


Figure 4.18. Impact of dispersant/emulsifier on *A. borkumensis*. (A) No dispersant or emulsifier, (B) Dawn dish soap, (C) Corexit 9500A, and (D) Finasol OSR 52. (B–D): The red arrow indicates the control well (red line): growth curve in the absence of dispersant or emulsifier. Each graph presents data for a single column of wells on a microtiter plate; each line represents one representative well (culture) on the microtiter plate.

Each line in panels B–D of Figure 4.18 represents the average of three identical wells (i.e., Cultures 1–3) for a given treatment and concentration. Similarly in panel A, each line represents an average of three identical wells, although all wells and lines come from identical control cultures. In summary, *A. borkumensis* growth was not inhibited but instead enhanced by both dispersants and the Dawn dish soap. Panel A of Figure 4.18 shows consistent growth rates and peak optical densities in the dispersant- and detergent-free control cultures. Panels B and C show similar rates of growth and that higher optical cell

densities were achieved using Dawn dish detergent (B) and Corexit (C). This implies that the cells were able to use either addition as a carbon or nutrient source. Panel D shows a moderate elevation in the final optical density with the addition of Finasol. The “no additive” control culture for each panel is shown in red and is indicated by a black arrow (Figure 4.18 B–D).

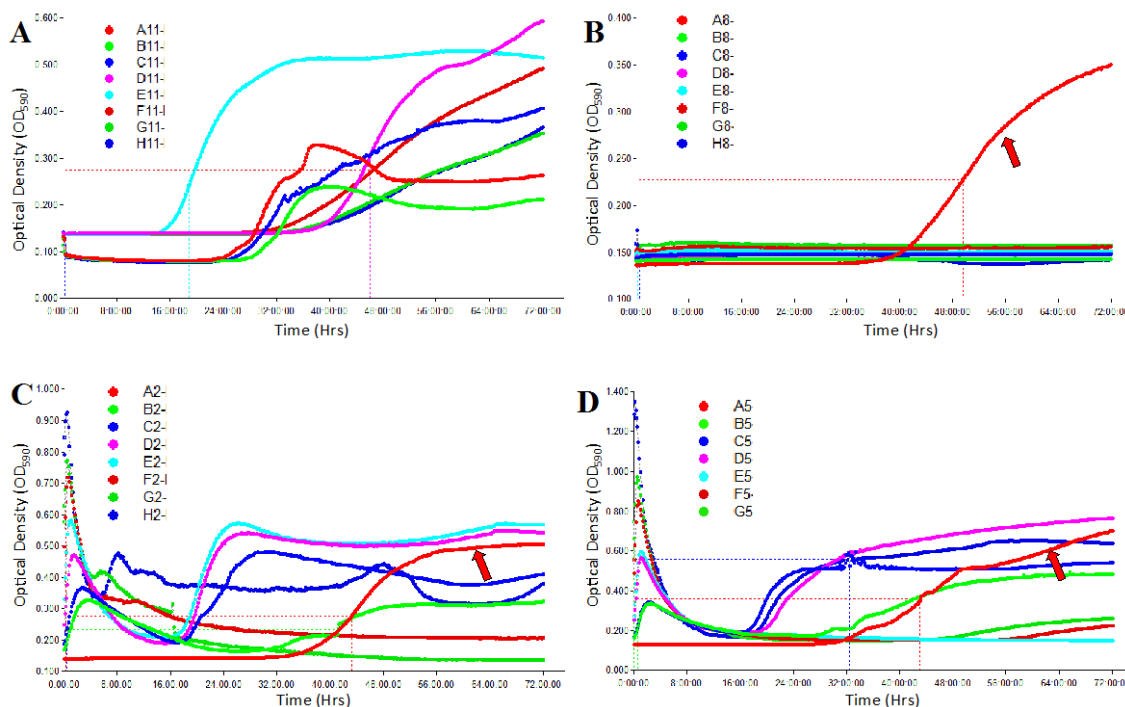


Figure 4.19. Impact of dispersant/emulsifier on seawater microorganism mix. (A) No dispersant or emulsifier, (B) Dawn dish soap, (C) Corexit 9500A, and (D) Finasol OSR 52. (B–D): The red arrow indicates growth curve (red line) in the absence of dispersant or emulsifier. Each graph presents data for a single column of wells on a microtiter plate; each line represents one representative well (culture) on the microtiter plate.

The results from the growth experiments using the seawater organism mix are less definitive. The mixed inoculum contains many unknown organisms and the distribution of growth curves resulting from the control (no additive) cultures in panel A perhaps indicate that there is no dominant, fast-growing species in the mixture. In contrast to the results obtained using *A. borkumensis*, Dawn dish soap had a clearly negative impact on the growth of the mixed seawater organisms (Figure 4.19 B). It is possible that with additional time, one or more resistant species might have begun to grow, but the effect ruled out the use of Dawn dish soap as a means of manipulating oil droplet size during biodegradation tests. For some cultures, Corexit and Finasol appeared to support the rapid onset of growth, but not of higher density growth (Figure 4.19 A, C, and D), and some growth curves for each dispersant also indicated inhibition of growth by the dispersant.

As a further test of the toxicity of the additives, Microtox[®] assays were performed to see whether dispersant or emulsifier would have toxic effects. The Microtox assay measures the light output of a bioluminescent bacterium, *Alivibrio fischeri* following a 30-minute exposure to a test sample or solution. When a test material is toxic, it diminishes metabolism by *A. fischeri*, resulting in reduced bioluminescence (Girotti et al. 2002; Park et al. 2016). Toxic levels of a substance are identified by the EC₅₀ value, the effective concentration that reduces bioluminescence to ≤50% of the control (no additive) value. A culture of *A. fischeri* was aliquoted into a microtiter plate and individual wells were then spiked

with a dispersant or Dawn detergent to create concentrations of 0.5 $\mu\text{L}/\text{mL}$, 0.625 $\mu\text{L}/\text{mL}$, 1 $\mu\text{L}/\text{mL}$, 1.25 $\mu\text{L}/\text{mL}$, 2 $\mu\text{L}/\text{mL}$, 2.5 $\mu\text{L}/\text{mL}$, and 5 $\mu\text{L}/\text{mL}$. Zinc sulfate was used as a positive (lethal) control for comparison and validation. Triplicate samples were created and readings were taken using a Synergy HT microplate reader (Biotek, VT, USA).

The Microtox results are shown in Figure 4.20. Both dispersants, Corexit 9500A and Finasol OSR 52 did not show toxicity (Figure 4.20 C & D), while Dawn resulted in EC_{50} at lower concentrations, 0.5 $\mu\text{L}/\text{mL}$ through 1 $\mu\text{L}/\text{mL}$. Surprisingly, at concentrations of 1.25 to 5 $\mu\text{L}/\text{mL}$, Dawn was less toxic to *A. fischeri*; it is unclear why this occurred. The results also demonstrated increased light output with increasing concentration for Corexit and an uneven increase in luminescence with increasing concentration for Finasol. The rapid (≤ 30 min) stimulation of luminescence indicates that the response is due to an increase in metabolism rather than cell growth. All of the results are pretty consistent with the growth curves, indicating that Corexit and Finasol are not toxic.

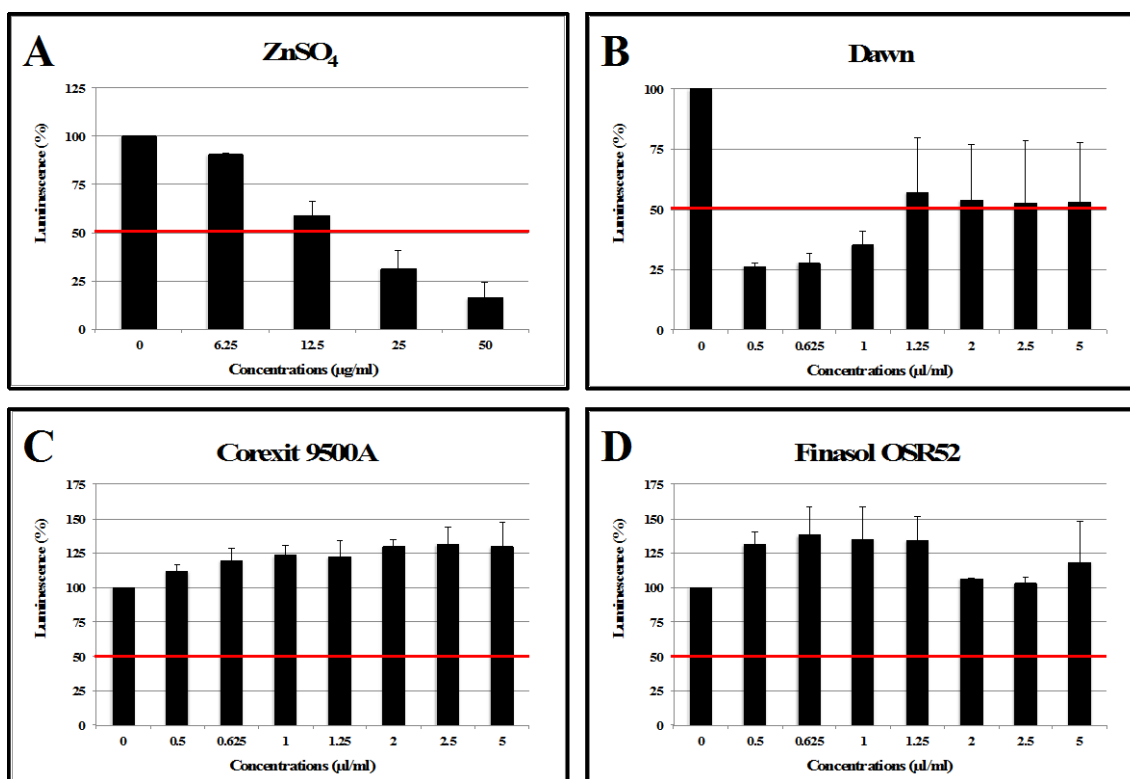


Figure 4.20. Microtox[®] assay results.

4.2.3 Experimental Setup to Examine the Effect of Droplet Size on Biodegradation

Ultimately, Corexit 9500 was used with constant stirring (by magnetic stir bars) to set the initial droplet size distribution. All samples were subjected to the same vigorous mixing speed (identical magnetic stir bars at 400 rpm) to create the droplet size distribution and to sustain the suspension of oil in seawater, while also providing consistent aeration for the cells. The temperature for all samples was kept at 18°C and the incubation lasted for 7 days. The flasks and stir bars were all treated with Aculon Glass Repellency to minimize oil adhesion to the borosilicate flask wall or Teflon coated stir bar. The Aculon coating was previously shown to have no effect on cell growth (Figure 4.4). Samples were kept in a

darkened room to prevent photo-degradation of hydrocarbons, except during periods when the samples were examined, photographed, or ultimately processed to quantify hydrocarbons.

A preliminary test found seawater to be an inappropriate medium for the test because cell growth was stunted within 24–48 hr, presumably due to the limited availability of key nutrients. A modified seawater medium enriched with nitrogen and phosphate (0.45 μm filtered seawater supplemented with 5 mM NH_4Cl and 2.2 mM K_2HPO_4) was thus employed to sustain growth over several days. Tests with this medium and oil resulted in dense cell cultures after ~72 hr.

In one set of tests, each sample was inoculated with the oil metabolizing bacteria, *A. borkumensis* (ATCC 700651) and *P. putida* (ATCC 700007). In a second set of tests, the samples were inoculated with the fungus, *H. resinae* (ATCC 22711). The bacteria and fungi were used separately to test for evidence that growth habit (with or without penetrating mycelia) might influence the dependence on droplet size. A set of preliminary tests was used to determine growth rates, inoculum volume, and oil in water concentrations. Table 4.3 shows the composition of the individual samples that were ultimately created and analyzed in the study. Fourteen samples were created on Day 1 and used for the biodegradation study. Included were control samples without oil to monitor the growth of the organisms. On the final day of the incubations and prior to sample processing to quantify hydrocarbons, a fifteenth sample, Sample O, was created with the bacterial inoculum and oil as a “no biodegradation control.” A DOR of 1:20 was arbitrarily selected for that sample. The inoculum and Corexit were included in case the presence of cells or dispersant might bias the polycyclic aromatic hydrocarbon (PAH) analysis.

Each day after inoculation, the stir plate was stopped briefly to allow for photography that was used to calculate droplet size. The volume of fluids was also noted and any missing volume (presumably due to evaporation), which was minimal on all days, was replaced with dH_2O to maintain salinity.

Quantification of hydrocarbons was performed according to a modified EPA method for dispersed oil in water (40 CFR Ch. I, Pt 300, App. C) (EPA 2003) and a previously developed gas chromatography-mass spectrometry (GC-MS) method developed at PNNL-MSL (Huesemann et al. 2003, 2004). The collected water samples (50–100 mL) were spiked with surrogate recovery standards (5 α -androstande, naphthalene-d8, acenaphthene-d10, phenanthrene-d10, chrysene-d12, and perylene-d12) followed by liquid-liquid extraction with dichloromethane three times. The extracts were then dewatered by sodium sulfate and carefully concentrated under N_2 to ~5 mL. Silica column chromatography was used for the further cleanup and fractionation into alkanes and PAHs. The extracts were then concentrated and solvent-exchanged into hexane.

GC-internal standards (d10-fluorene and d12-benzo[*a*]pyrene) were added to the final concentrated extracts prior to GC-MS analysis. The GC-MS system was an Agilent 6890N GC interfaced to an Agilent 5973 inert MS using electron impact in selective ion monitoring mode. A DB5-MS capillary column (J&W Inc., 30 m length, 0.25 mm diameter, 0.25 μm thickness) was used to achieve chromatographic separation of the alkanes and PAHs. Identification of target analytes was based on their retention times and confirmed by the abundance of a secondary ion relative to the molecular ion. Alkanes included normal and branched aliphatics ranging in carbon number from 10 to 35 as well as pristane and phytane. PAHs include 16 parent PAHs (naphthalene, phenanthrene, anthracene, fluorene, dibenzothiophene, fluoranthene, pyrene, chrysene, benzo[*b*]fluoranthene, benzo[*k*]fluoranthene, benzo[*e*]pyrene, benzo[*a*]pyrene, perylene, indeno[1,2,3-*cd*]pyrene, dibenzo[*a,h*]anthracene, benzo[*g,h,i*]perylene), as well as 22 alkylated homologues of naphthalene, fluorene, dibenzothiophene, phenanthrene, anthracene, fluoranthene, pyrene, and chrysene. The measured hydrocarbon concentrations were then normalized to the concentration of a conserved biomarker within the oil 17 α (H),21 β (H)-hopane for the quantification of biodegradation (Prince et al. 1994).

Table 4.3. Composition of samples used to study the effect of droplet size on biodegradation.^(a)

Addition	Sample A	Sample B	Sample C	Sample D	Sample E
mL Seawater + NP medium	200	200	200	200	200
mL <i>Alcanivorax borkumensis</i>	3	3	3	3	3
mL <i>Pseudomonas putida</i>	3	3	3	3	3
mL <i>Hormoconis resinae</i>	0	0	0	0	0
mL Corexit	0	0	1	2	5
mL oil	0	200	200	200	200
DOR	NA	0	1:200	1:100	1:40
DWR	NA	0	1:200000	1:100000	1:40000

Addition	Sample F	Sample G	Sample H	Sample I	Sample J
mL Seawater + NP medium	200	200	200	200	200
mL <i>Alcanivorax borkumensis</i>	3	3	0	0	0
mL <i>Pseudomonas putida</i>	3	3	0	0	0
mL <i>Hormoconis resinae</i>	0	0	6	6	6
mL Corexit	10	20	0	0	1
mL oil	200	200	0	200	200
DOR	1:20	1:10	NA	0	1:200
DWR	1:20000	1:10000	NA	0	1:200000

Addition	Sample K	Sample L	Sample M	Sample N	Sample O
mL Seawater + NP medium	200	200	200	200	200
mL <i>Alcanivorax borkumensis</i>	0	0	0	0	3
mL <i>Pseudomonas putida</i>	0	0	0	0	3
mL <i>Hormoconis resinae</i>	6	6	6	6	0
mL Corexit	2	5	10	20	10
mL oil	200	200	200	200	200
DOR	1:100	1:40	1:20	1:10	1:20
DWR	1:100000	1:40000	1:20000	1:10000	1:20000

(a) Samples with bacteria are highlighted in green and samples with fungi in orange.
NA = not applicable.

4.2.4 Results of the Droplet Study

The samples prepared as described in the section above and in Table 4.3 were analyzed daily to calculate droplet size and at the conclusion of the experiment to measure changes in PAH concentration. The complete results of the hydrocarbon analysis are provided in a series of tables in Appendix B and the droplet size data are provided in Appendix C. In summary, droplet sizes changed throughout the course of the experiment. This may have been caused by a combination of factors: evaporation of aromatic hydrocarbons, biodegradation of hydrocarbons, biodegradation of the Corexit, and flocculation of cells or cell-oil aggregates. Although changes in droplet size were expected because of these factors, the observed changes were inconsistent and do not appear to scale with the DOR and initial sizes. Nonetheless, the data do provide a perspective on the influence of different initial DORs and size ranges on biodegradation, and a detailed analysis of the biodegradation of specific hydrocarbons as a function of initial DOR. The

results are specific to the organisms used in the tests and the test conditions; discrepancies in the findings reported by different researchers have been attributed to the experimental setup, organisms, and methods of analysis. The control tests described at the beginning of this chapter also demonstrate that the organisms tested did not appear to be negatively affected by the presence of Corexit.

The histograms in Appendix C show the distribution of droplet sizes found in the flasks throughout the course of the experiment. The graphs follow the method of droplet size distribution representation presented by Brandvik et al. 2013 and Johansen et al. 2013, in which the theoretical droplet size range was represented as a series of bins of equal logarithmic intervals (Johansen et al. 2013; Brandvik et al. 2013). After sizing, each particle was placed into its corresponding bin, which was labeled on the x-axis by its median diameter. The y-axis (volume fraction) is the percent of the total volume of oil represented by all of the droplets in each bin. Table 4.4 and Table 4.5 summarize the droplet size data, showing minimum and maximum droplet sizes, mean droplet diameter, and the mode median bin diameter (bin representing the greatest fraction of the total volume of oil) from the distributions shown in Appendix C.

Droplet size measurements were also taken for the two samples with no oil or dispersant (Samples A and H). Small aggregates of cells were captured in those photographs and were likely also captured in the photos of samples with oil and dispersants. The larger *H. resiniae* cells and mycelia likely account for the bimodal distributions seen in Samples I through N. The coloration of the microorganisms was too similar to that of similarly sized oil droplets to filter them out. Thus, the cells likely influenced the recorded distributions toward smaller size ranges.

The data provided in Table 4.6 and Table 4.7 and in Appendix B indicate that the inoculated samples have lower concentrations of several PAHs than the values from the Time 0 sample (Sample O). Some of the observed loss could be explained by effects other than biodegradation. For example, 2-ring PAHs (especially the naphthalene) can be lost by evaporation more easily than other PAHs. Therefore, the significant concentration decrease of those PAHs could be a combined effect of evaporation and biodegradation. The concentration of other PAHs, such as phenanthrene, did decrease compared to Sample O. The results of the hydrocarbon analysis were noisy and showed no significant trends relative to DOR or droplet size, or even to the presence or absence of dispersant.

If there were any inhibitory effects of the dispersant, they appeared to have been fairly small and perhaps constrained to specific hydrocarbons. A more suitable comparison might have been to compare these tests with a sample in which the oil was maintained as a surface slick; the actual droplet size distribution may not be as important as simply creating a suspension of the oil droplets in the water column. If a future study validates that hypothesis, then only the minimum amount of dispersant necessary to prevent slick formation (in a deep ocean release) would be needed. Studies described in Section 4.6 of this report examine droplet size distributions generated from simulated blowouts with and without added dispersant. They note that the turbulent nature of a discharge and subsequent degassing results in some atomization and emulsification of oil without added dispersants.

Table 4.4. Summary of the droplet size data for the *Alcanivorax borkumensis* and *Pseudomonas putida* samples.

	Sample A	Sample B	Sample C	Sample D	Sample E	Sample F	Sample G
oil	0	200 uL					
DOR	NA	0	1:200	1:100	1:40	1:20	1:10
DWR	NA	0	1:200000	1:100000	1:40000	1:20000	1:10000
Time (hrs)	Minimum Droplet Diameter (mm)						
24	0.008806	0.008892	0.008283	0.007737	0.006605	0.009496	0.009495
48	0.011683	0.011260	0.011161	0.010655	0.010625	0.010220	0.010079
72	0.010477	0.010622	0.010685	0.010565	0.010655	0.010625	0.010625
96	0.011063	0.011312	0.010869	0.011079	0.010966	0.010931	0.010802
120	0.010390	0.010595	0.010536	0.010477	0.010593	0.010419	0.010332
148	0.010595	0.010474	0.010477	0.010535	0.010777	0.010896	0.010777
	Maximum Droplet Diameter (mm)						
24	0.032948	0.050463	0.035682	0.181946	0.159577	0.192156	0.155536
48	0.050463	0.327035	0.334731	0.425206	0.050463	0.151388	0.231249
72	0.050463	0.276395	0.247215	0.222837	0.107047	0.087404	0.188814
96	0.035682	0.188814	0.259772	0.249777	0.142730	0.142730	0.437019
120	0.035682	0.185412	0.192156	0.228479	0.050463	0.087404	0.178412
148	0.035682	0.198672	0.242010	0.271750	0.100925	0.118345	0.147123
	Volume Fraction, Mode Median Bin Diameter (mm)						
24	0.008685	0.008685	0.008685	0.00736	0.074735	0.171025	0.14493
48	0.01209	0.331655	0.20182	0.391375	0.010245	0.010245	0.171025
72	0.010245	0.122815	0.14493	0.122815	0.010245	0.010245	0.010245
96	0.010245	0.01209	0.122815	0.122815	0.010245	0.010245	0.46185
120	0.010245	0.171025	0.122815	0.122815	0.010245	0.010245	0.171025
148	0.010245	0.074735	0.074735	0.14493	0.010245	0.122815	0.074735
	Mean Droplet Diameter (mm)						
24	0.010059	0.010312	0.009319	0.009367	0.009606	0.011245	0.012511
48	0.013742	0.013546	0.016052	0.013968	0.012598	0.012081	0.012213
72	0.012002	0.016551	0.015111	0.016497	0.012900	0.012684	0.013262
96	0.012977	0.014421	0.016773	0.015021	0.012837	0.012692	0.014553
120	0.011680	0.013614	0.014177	0.015690	0.012751	0.012276	0.012863
148	0.011790	0.022674	0.022807	0.020043	0.012087	0.012523	0.018737

Table 4.5. Summary of the droplet size data for the *Hormiconis resinae* samples.

	Sample H	Sample I	Sample J	Sample K	Sample L	Sample M	Sample N
oil	0	200 uL					
DOR	NA	0	1:200	1:100	1:40	1:20	1:10
DWR	NA	0	1:200000	1:100000	1:40000	1:20000	1:10000
Time (hr)	Minimum Droplet Diameter (mm)						
24	0.010080	0.010221	0.010386	0.010418	0.011634	0.011861	0.010074
48	0.011227	0.010165	0.010715	0.010418	0.010068	0.010194	0.010476
72	0.010505	0.010505	0.010604	0.010565	0.010445	0.010522	0.010742
96	0.010979	0.010803	0.010924	0.010715	0.010837	0.010652	0.010361
120	0.010655	0.010472	0.010638	0.010443	0.010586	0.010554	0.010432
148	0.010902	0.010770	0.010837	0.010832	0.010559	0.010633	0.011888
	Maximum Droplet Diameter (mm)						
24	0.112838	0.222837	0.050463	0.123608	0.050463	0.118345	0.174808
48	0.050463	0.262212	0.079788	0.247215	0.147123	0.147123	0.155536
72	0.050463	0.133512	0.071365	0.257310	0.163518	0.133512	0.138198
96	0.050463	0.298541	0.050463	0.208063	0.100925	0.151388	0.112838
120	0.061804	0.321142	0.071365	0.178412	0.151388	0.112838	0.228479
148	0.050463	0.405275	0.050463	0.112838	0.112838	0.123608	0.071365
	Volume Fraction, Mode Median Diameter (mm)						
24	0.010245	0.14493	0.010245	0.010245	0.012049	0.012049	0.012049
48	0.01209	0.23816	0.010245	0.23816	0.010245	0.010245	0.14493
72	0.010245	0.010245	0.010245	0.23816	0.010245	0.010245	0.14493
96	0.010245	0.281045	0.010245	0.010245	0.010245	0.010245	0.010245
120	0.010245	0.281045	0.010245	0.010245	0.010245	0.010245	0.010245
148	0.010245	0.281045	0.010245	0.010245	0.010245	0.010245	0.010245
	Mean Droplet Diameter (mm)						
24	0.011598	0.013157	0.011844	0.012391	0.013269	0.013948	0.013411
48	0.012972	0.012420	0.012720	0.012120	0.012316	0.011873	0.012765
72	0.012367	0.012038	0.012130	0.012872	0.012876	0.012260	0.013380
96	0.012680	0.013146	0.013119	0.013002	0.012665	0.012434	0.012251
120	0.012412	0.012993	0.012486	0.012718	0.012667	0.012628	0.012279
148	0.011919	0.020472	0.012001	0.013023	0.011992	0.011812	0.013586

Table 4.6. Percent loss of hydrocarbon after 148 hrs compared to Sample O; bacterial exposures. ^(a)

Compound	MDL (ug/L)	Sample B	Sample C	Sample D	Sample E	Sample F	Sample G
DOR		0	1:200	1:100	1:40	1:20	1:10
		% loss					
Naphthalene	0.0026	100.00%	100.00%	100.00%	100.00%	100.00%	99.97%
2,6-Dimethylnaphthalene	0.0011	99.59%	99.69%	99.56%	99.46%	99.90%	99.52%
C1-Naphthalenes	0.0023	100.00%	100.00%	100.00%	100.00%	100.00%	100.00%
C2-Naphthalenes	0.0096	97.85%	98.19%	97.47%	97.18%	99.04%	97.53%
C3-Naphthalenes	0.0112	78.07%	79.57%	76.44%	82.23%	87.26%	77.47%
C4-Naphthalenes	0.0113	52.57%	53.68%	49.47%	57.07%	64.92%	51.23%
Biphenyl	0.0005	100.00%	100.00%	100.00%	100.00%	100.00%	100.00%
Fluorene	0.0011	83.60%	84.73%	82.30%	85.67%	88.58%	81.10%
1-Methyl fluorene	0.0010	53.20%	54.79%	50.11%	58.16%	65.72%	53.16%
C1-Fluorenes	0.0035	56.57%	54.88%	53.58%	63.32%	66.14%	52.94%
C2-Fluorenes	0.0026	26.87%	25.57%	19.77%	30.68%	39.25%	24.35%
C3-Fluorenes	0.0131	12.27%	9.22%	6.70%	12.00%	24.42%	13.50%
Dibenzothiophene	0.0012	52.58%	53.67%	51.75%	58.01%	65.50%	49.90%
C1-Dibenzothiophenes	0.0030	31.60%	29.26%	30.34%	35.35%	46.74%	27.58%
C2-Dibenzothiophenes	0.0023	19.66%	15.17%	12.90%	18.93%	33.96%	15.23%
C3-Dibenzothiophenes	0.0031	16.48%	11.68%	12.01%	12.66%	28.77%	13.37%
C4-Dibenzothiophenes	0.0022	19.25%	18.45%	12.37%	17.62%	31.44%	18.30%
Phenanthrene	0.0025	43.82%	45.13%	43.74%	49.58%	59.35%	39.68%
Anthracene	0.0002	26.42%	18.11%	24.67%	36.51%	39.64%	27.24%
1-methyl Phenanthrene	0.0008	20.39%	17.51%	17.99%	21.95%	37.99%	17.08%
3,6-DMP	0.0009	12.53%	12.76%	7.45%	15.35%	31.26%	12.85%
2,6-DMP	0.0003	11.55%	6.84%	3.21%	13.29%	30.90%	5.90%
1,7-DMP	0.0006	11.85%	10.39%	-1.04%	13.67%	27.02%	2.60%
C1-Phen/An	0.0034	22.22%	19.80%	18.89%	25.53%	38.75%	21.13%
C2-Phen/An	0.0038	14.49%	11.38%	11.08%	16.66%	31.12%	11.44%
C3-Phen/An	0.0028	11.03%	6.21%	4.88%	11.34%	28.85%	10.05%
C4-Phen/An	0.0041	8.54%	5.86%	4.28%	10.90%	27.41%	7.49%
Fluoranthene	0.0004	20.13%	20.09%	28.50%	25.52%	48.21%	23.67%
Pyrene	0.0015	7.68%	3.71%	3.55%	5.63%	24.73%	7.60%
C1-Fluor/Py	0.0008	9.46%	5.36%	1.81%	5.44%	27.64%	8.98%
C2-Fluor/Py	0.0013	10.64%	4.09%	4.40%	9.28%	28.84%	8.75%
C3-Fluor/Py	0.0022	9.27%	5.73%	5.44%	12.35%	31.66%	10.33%
Benzo [a] anthracene	0.0003	6.70%	17.57%	14.76%	14.49%	52.66%	14.81%
Chrysene	0.0006	10.44%	3.99%	2.51%	8.60%	42.33%	16.45%
C1-Chrysenes	0.0008	13.93%	7.84%	9.69%	10.90%	49.83%	19.18%
C2-Chrysenes	0.0030	13.96%	9.29%	11.13%	7.13%	46.99%	18.24%
C3-Chrysenes	0.0066	10.97%	10.74%	5.50%	7.14%	45.40%	12.14%
C4-Chrysenes	0.0141	17.97%	12.96%	12.87%	10.02%	47.07%	18.74%

Compound	MDL (ug/L)	Sample B	Sample C	Sample D	Sample E	Sample F	Sample G
DOR		0	1:200	1:100	1:40	1:20	1:10
		% loss					
Benzo [b] fluoranthene	0.0008	-4.78%	-0.70%	-1.49%	9.93%	56.32%	1.67%
Benzo [k] fluoranthene	0.0010	100.00%	100.00%	100.00%	100.00%	100.00%	100.00%
Benzo [e] pyrene	0.0011	18.58%	10.29%	21.50%	14.70%	58.71%	25.60%
Benzo [a] pyrene	0.0010	41.48%	39.52%	47.21%	64.77%	81.12%	76.79%
Perylene	0.0010	8.25%	-0.99%	1.69%	7.38%	51.48%	8.05%
Indeno [1,2,3-c,d] pyrene	0.0002	100.00%	100.00%	100.00%	100.00%	100.00%	100.00%
Dibenzo [a,h] anthracene	0.0003	79.74%	87.29%	92.29%	90.67%	100.00%	90.31%
Benzo [g,h,i] perylene	0.0002	73.93%	73.97%	84.06%	81.18%	92.50%	81.88%
Recovery							
d8-Naphthalene		77%	68%	63%	70%	45%	76%
d10-Acenaphthene		91%	84%	80%	90%	51%	84%
d10-Phenanthrene		105%	98%	95%	105%	64%	96%
d12-Chrysene		78%	67%	74%	69%	70%	79%
d12-Perylene		85%	67%	77%	80%	77%	84%

(a) Green, orange, and blue highlighting provided solely to color-code samples

Table 4.7. Percent loss of hydrocarbon after 148 hrs compared to Sample O; fungal exposures. ^(a)

Compound	MDL (ug/L)	Sample I	Sample J	Sample K	Sample L	Sample M	Sample N
DOR		0	1:200	1:100	1:40	1:20	1:10
		% loss					
Naphthalene	0.0026	100.00%	100.00%	100.00%	100.00%	100.00%	100.00%
2,6-Dimethylnaphthalene	0.0011	99.43%	97.57%	95.37%	93.11%	92.00%	96.74%
C1-Naphthalenes	0.0023	100.00%	100.00%	100.00%	100.00%	100.00%	100.00%
C2-Naphthalenes	0.0096	98.75%	96.09%	94.05%	91.12%	89.96%	95.11%
C3-Naphthalenes	0.0112	83.85%	75.87%	68.55%	64.38%	64.74%	72.58%
C4-Naphthalenes	0.0113	49.83%	46.05%	38.54%	33.93%	38.59%	42.79%
Biphenyl	0.0005	100.00%	100.00%	100.00%	99.28%	100.00%	100.00%
Fluorene	0.0011	85.55%	79.87%	78.30%	71.02%	72.25%	77.06%
1-Methyl fluorene	0.0010	54.97%	52.33%	46.18%	39.03%	44.17%	47.63%
C1-Fluorenes	0.0035	52.47%	48.89%	42.39%	36.46%	40.03%	45.93%
C2-Fluorenes	0.0026	21.82%	23.99%	18.74%	13.91%	20.10%	21.69%
C3-Fluorenes	0.0131	-1.05%	13.66%	11.55%	8.27%	8.28%	5.71%
Dibenzothiophene	0.0012	56.89%	49.45%	46.23%	38.96%	42.98%	45.67%
C1-Dibenzothiophenes	0.0030	27.94%	24.07%	22.24%	14.46%	18.82%	19.51%
C2-Dibenzothiophenes	0.0023	9.82%	14.78%	10.80%	7.22%	11.90%	10.27%
C3-Dibenzothiophenes	0.0031	4.56%	13.06%	7.77%	2.86%	5.12%	7.46%
C4-Dibenzothiophenes	0.0022	-0.44%	7.88%	4.63%	0.44%	3.77%	2.70%
Phenanthrene	0.0025	48.28%	41.91%	39.09%	30.54%	38.10%	39.84%

Compound	MDL (ug/L)	Sample I	Sample J	Sample K	Sample L	Sample M	Sample N
DOR		0	1:200	1:100	1:40	1:20	1:10
		% loss					
Anthracene	0.0002	44.79%	21.18%	24.50%	5.20%	25.57%	23.41%
1-methyl Phenanthrene	0.0008	17.26%	20.70%	17.44%	11.77%	17.37%	18.12%
3,6-DMP	0.0009	8.45%	10.77%	8.59%	7.16%	11.62%	10.44%
2,6-DMP	0.0003	7.01%	8.52%	11.82%	0.24%	10.71%	2.20%
1,7-DMP	0.0006	8.35%	7.68%	5.81%	5.70%	10.29%	2.78%
C1-Phen/An	0.0034	19.70%	20.46%	17.09%	13.02%	17.62%	19.20%
C2-Phen/An	0.0038	7.91%	12.18%	10.82%	7.52%	9.74%	12.28%
C3-Phen/An	0.0028	3.73%	9.41%	6.87%	3.48%	4.88%	6.50%
C4-Phen/An	0.0041	2.94%	8.11%	3.95%	0.31%	2.38%	1.89%
Fluoranthene	0.0004	17.58%	31.74%	23.34%	27.24%	33.67%	21.64%
Pyrene	0.0015	7.30%	14.81%	12.53%	10.96%	14.23%	14.06%
C1-Fluor/Py	0.0008	-0.04%	3.93%	3.10%	-2.70%	3.69%	-0.08%
C2-Fluor/Py	0.0013	0.81%	9.39%	5.86%	4.64%	3.89%	6.07%
C3-Fluor/Py	0.0022	1.01%	5.13%	6.56%	4.66%	6.69%	3.16%
Benzo [a] anthracene	0.0003	3.12%	18.92%	2.01%	4.48%	20.99%	14.95%
Chrysene	0.0006	6.73%	12.32%	12.43%	6.85%	10.99%	11.10%
C1-Chrysenes	0.0008	6.96%	12.84%	12.38%	10.79%	11.17%	11.17%
C2-Chrysenes	0.0030	6.64%	12.84%	13.67%	9.10%	14.43%	12.23%
C3-Chrysenes	0.0066	5.66%	13.92%	16.30%	10.45%	14.24%	12.37%
C4-Chrysenes	0.0141	9.74%	14.45%	20.43%	18.10%	19.27%	13.37%
Benzo [b] fluoranthene	0.0008	12.96%	18.12%	14.25%	25.78%	21.98%	27.78%
Benzo [k] fluoranthene	0.0010	100.00%	100.00%	100.00%	100.00%	100.00%	100.00%
Benzo [e] pyrene	0.0011	11.60%	24.20%	11.30%	17.94%	11.64%	19.32%
Benzo [a] pyrene	0.0010	43.75%	64.91%	33.72%	56.22%	52.66%	66.55%
Perylene	0.0010	11.82%	16.90%	7.79%	3.15%	12.59%	15.39%
Indeno [1,2,3-c,d] pyrene	0.0002	100.00%	100.00%	100.00%	100.00%	100.00%	100.00%
Dibenzo [a,h] anthracene	0.0003	88.95%	90.22%	5.78%	100.00%	100.00%	89.74%
Benzo [g,h,i] perylene	0.0002	78.02%	77.72%	5.63%	78.49%	85.76%	85.42%
Recovery							
d8-Naphthalene		68%	64%	71%	67%	72%	80%
d10-Acenaphthene		89%	88%	94%	88%	95%	99%
d10-Phenanthrene		110%	101%	112%	102%	109%	114%
d12-Chrysene		74%	76%	86%	80%	81%	81%
d12-Perylene		86%	85%	88%	81%	86%	93%

(a) Green, orange, and blue highlighting provided solely to color-code samples

4.3 Explore Novel, Noninvasive Approaches to Characterizing Emulsions and Oil Degradation in Pressure Chambers

One challenging aspect of hyperbaric research is that withdrawing samples from a pressure system may result in alteration of the sample. This held particularly true for the high-pressure studies using oil because of the degassing of the oil following a drop in pressure and changes in oil droplet size due to the change in pressure and mixing energies introduced by sample extraction and pressure release. Although changes in pressure during sample extraction were not expected to significantly affect the chemical state of the oil (other than the rapid loss of dissolved and free gas), the aforementioned physical changes would have interfered with the analysis of dispersant effectiveness (oil droplet size), and the process of sample extraction and fluid exchange is particularly slow.

A few methods used for other high-pressure studies were explored to determine whether they could be used to characterize the physical and chemical properties of the pressurized fluids and gases. The methods and tests undertaken are described in the sections that follow.

4.3.1 Nuclear Magnetic Resonance Spectroscopy

NMR spectroscopy is a powerful tool that allows the determination of average molecular and chemical contributions of complex mixtures. Recently, ^1H and $^{13}\text{C}\{^1\text{H}\}$ NMR spectroscopy were used to thoroughly characterize the molecular sub-structures contained within a number of diesel fuels and coal liquids (Canella et al. 2013a, b; Bays 2014). Fuels and coal liquids are complex mixtures in which contributions from individual species cannot readily be resolved because the mixture comprises thousands of unique molecular species. Similarly for an oil spill, an understanding of the interactions of dispersants, such as Corexit and Finasol, with the crude or processed oil will mean observing the influence of the oil on the dispersant. These interactions will have a time and chemical condition (temperature, pressure, dispersant concentration, etc.) dependency that should be measured while the process is occurring, *operando*, and at the conditions most representative of those being studied, *in situ*, as opposed to *ex situ* measurements where the results must be extended to conditions observed in the environment.

Proton nuclear magnetic resonance (^1H -NMR) techniques were applied as a means of measuring droplet/micelle size and formation of oil/dispersant in water at high pressures. High-pressure reaction vessels are fully enclosed so there are not many means for performing *in situ* analyses. Samples were tested using both ^1H -NMR and ^1H -DOSY (diffusion ordered spectroscopy). Before the tests were performed, several aspects were investigated, including 1) the feasibility of using NMR with the high salt concentration found in seawater of the Gulf of Mexico, which could have caused electrical grounding of the NMR cell, resulting in arcing and precluding its use; and 2) whether salt concentrations were within range for testing and whether accurate particle sizes could be measured. A 300 MHz ^1H frequency Agilent Varian NMR System (VNMR) equipped with a direct detect dual band probe was used for diffusion experiments. Diffusion coefficients were measured using the ^1H -DOSY (Wu et al. 1995) in the VnmrJ 4.2 software suite. Experimental parameters included 128 scans, 2–3 ms gradient pulse lengths, and diffusion delays of 0.05–0.2 s. The gradient strengths were varied from 0–20 G cm^{-1} .

Initial ^1H -DOSY testing of Corexit EC9500A and Finasol OSR 52 was conducted in pure deuterated water (D_2O) and the results for Finasol OSR 52 are shown in Figure 4.21.

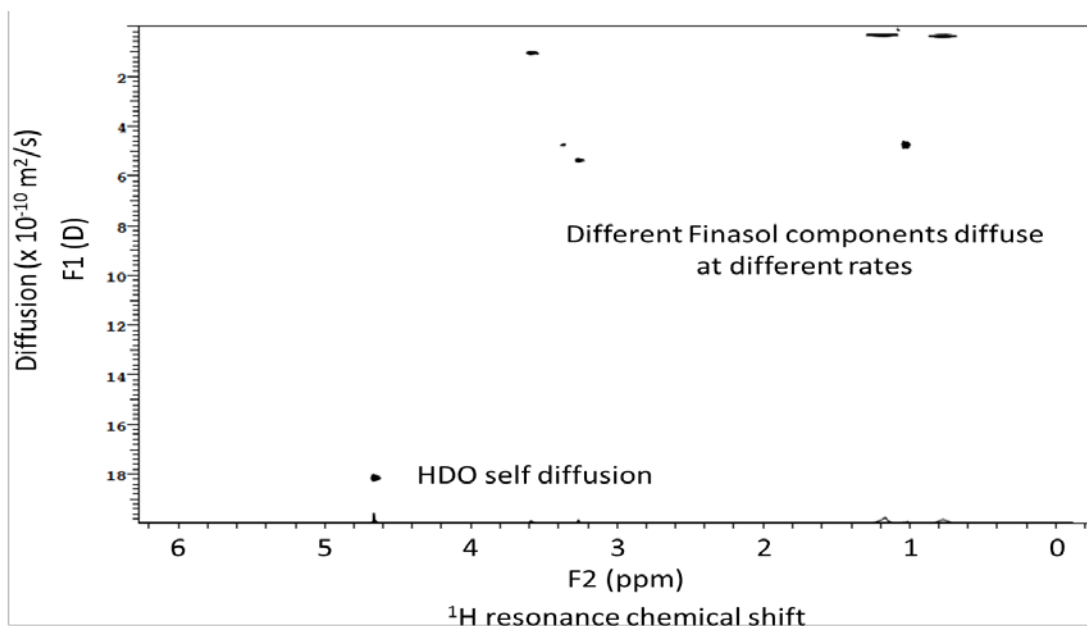


Figure 4.21. Diffusion ordered spectrum of Finasol OSR 52 in deuterium oxide (D_2O). The x-axis represents 1H -NMR resonances indicative of the structural characteristics of each Finasol OSR 52 component. The y-axis represents the rate at which each of the Finasol OSR 52 components diffuses through the deuterated water. The same rate of diffusion for different resonances suggests that they are part of the same molecule or same cluster of molecules, as would be the case for a micelle. Clearly, two major chemical components make up Finasol OSR 52: one with a diffusion constant (D) slightly less than $1 \times 10^{-10} \text{ m}^2/\text{s}$ and one with a diffusion constant of $4.4 \times 10^{-10} \text{ m}^2/\text{s}$. HDO is D_2O that has exchanged a proton for a deuteron with residual water. The diffusion rate of HDO in D_2O serves as an internal standard in all samples.

Sampling in the pure D_2O indicated that the compositional components of the Finasol OSR 52 could be detected. Using the Stokes-Einstein equation, which assumes that each of the particles behaves as a spherical agglomeration or micelle, the radius of the agglomerations or micelles was calculated to be 3–5 nm for the Finasol OSR 52 in D_2O , which is reasonable for a cluster of molecules below the critical micelle concentration. The dispersant samples were subsequently tested in salt-modified D_2O . Two salt concentrations made by adding Instant Ocean[®] sea salt to D_2O were tested for proof of concept: 36 ppt (mimicking that of Gulf of Mexico seawater) and 360 ppt (an extreme brine environment; ocean brine pools are around 150 ppt). The high salt concentrations did not cause grounding or arcing in the NMR cell and a good signal was obtained. After mixing Instant Ocean[®] sea salt into the Finasol- D_2O mixture to create a solution with a salinity of 36 ppt, the spectral components became broader, the diffusion coefficient became smaller (corresponding to a higher diffusion rate), and the radius of the micelles or agglomerations decreased from 0.3–5.5 nm to 0.61 nm. The radius is much smaller with the salt than without it. These results indicate that the two dispersants tested may behave in a different manner when applied in variable salt conditions (e.g., in a high salt environment like a brine pool).

To confirm that signal information could be obtained in the increased salt solution, 1 μm diameter polystyrene beads from Magsphere (Pasadena, CA) were tested (Figure 4.22). While good peak signals could be obtained for the polystyrene beads in 1H -NMR testing, the beads were not amenable to particle sizing in 1H -DOSY, because the material was (and behaved like) a solid particle and 1H -DOSY testing requires diffusion of materials to be able to measure particles in the test chamber.

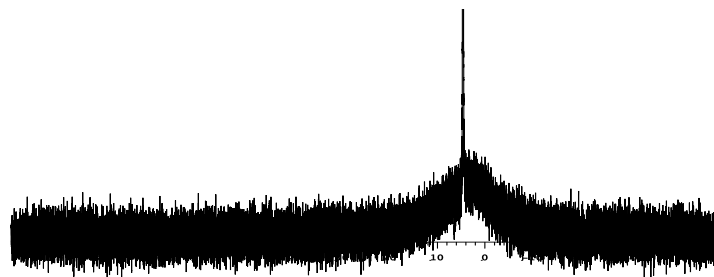


Figure 4.22. ^1H -NMR spectrum of 1 micron diameter polystyrene beads.

^1H -NMR spectroscopy was used to measure stock samples of dispersant to determine whether they comprised any materials that would show up as distinct signals that could be tracked in a mixed component sample. Dioctyl sodium sulfosuccinate (DOSS), a primary component of many dispersants that is often used to track dispersant in the environment, was also tested. ^1H -NMR comparison results for DOSS and the dispersants are shown in Figure 4.23. The results show that the DOSS spectra are visible in the spectra obtained for Finasol and Corexit. Particle sizes of the dispersants in pure D_2O and in salt-modified D_2O could be measured, so varying concentrations of dispersant in D_2O were tested as well as the addition of oil (WTI crude) to the samples. Table 4.8 provides a list of samples and results.

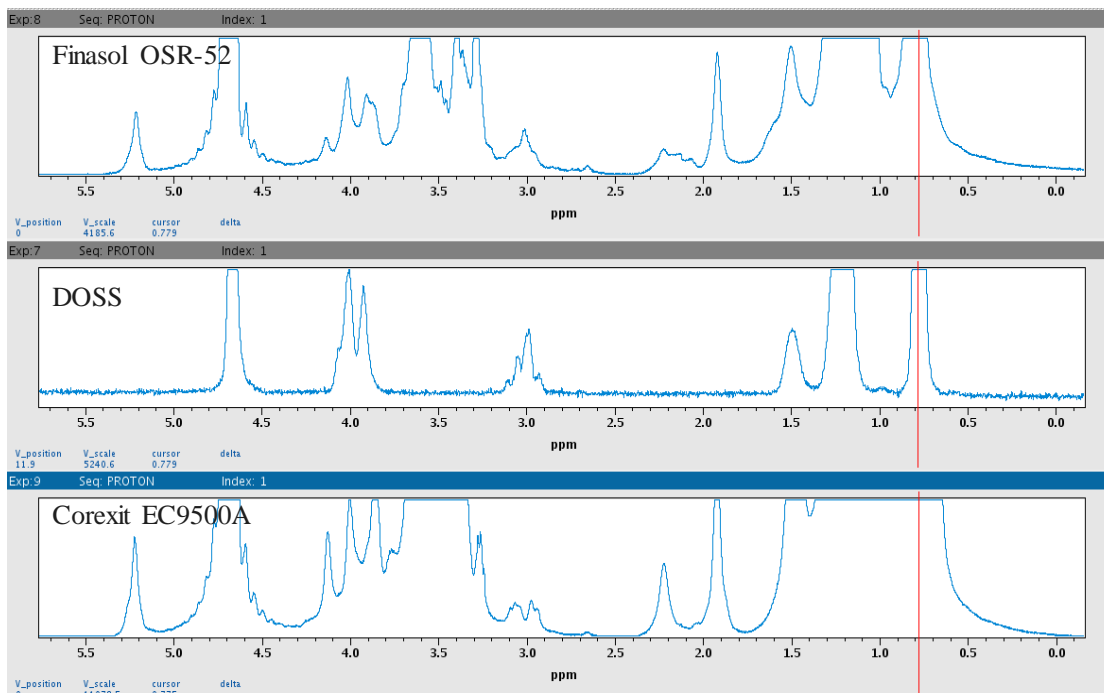


Figure 4.23. Three spectra aligned vertically obtained by ^1H -NMR spectroscopy for Finasol OSR 52, DOSS, and Corexit EC9500A (from top to bottom, respectively). Each DOSS ^1H -NMR component showed overlapping signal with other dispersant components.

At high dispersant concentrations ($\geq 1:25$ dispersant to D_2O) the phases separated in the NMR cell. The addition of crude oil resulted in an oil layer on top of the D_2O with a rapid phase separation. This separation and top layer formation prevented particle size determination using the ^1H -DOSY method. In an attempt to maintain dispersion and micelle formation after mixing,

higher DOR ratios were used. Diffusion behaviors of species observable by $^1\text{H-NMR}$ were not sensitive to the DOR ratios up to 3:1

Table 4.8. Tests performed on the $^1\text{H-NMR}$ spectrometer for *in situ* particle size determination and micelle diffusion analysis. The testing time given is the time for a single test. Each experiment required 4–5 tests for proper analysis.

Sample	Dispersant: D ₂ O ratio (v/v)	Oil:D ₂ O ratio (v/v)	Salinity (ppt)	Relaxation Time (s)	Diffusion Coefficient x10 ⁻¹⁰ (m ² /s)	Particle Size (nm)	Testing Time (hr)
Finasol OSR 52	1:50	Not Tested	0	Not Measured	0.3-5.5	0.3-5.5	2
Finasol OSR 52	1:25	Not Tested	36	0.6-8	2.5-5.6	0.3-0.7	1-2
Corexit EC9500A	1:25	Not Tested	36	0.6-2	2-5.5	0.3-0.8	1-2
Finasol OSR 52	1:5000	Not Tested	0	Not Measured	0.2-5.5	0.3-8	>12
Corexit EC9500A	1:5000	Not Tested	0	Not Measured	0.8-3	0.2-3	>12
Finasol OSR 52	1:1000	Not Tested	0	Not Measured	0.5-6.0	0.3-3.5	8
Corexit EC9500A	1:1000	Not Tested	0	Not Measured	0.3-5.2	0.3-5.8	8
Finasol OSR 52	1:1000	1:100	36	Not Measured	0.5-5.1	0.3-3.5	8
Diocetyl Sodium Sulfosuccinate	1:25	Not Tested	0	Not Measured	2	0.9	1-2

(Table 4.9). It is possible that some micelle formation did occur, but the majority of the species in solution seemed to be those formed with Finasol OSR 52 alone and due to resonance overlap in the $^1\text{H-NMR}$ spectrum, any difference in speciation was not observable by this technique. Figure 4.24 shows the $^1\text{H-DOSY}$ spectra of A) 1:50 Finasol OSR 52: D₂O ratio and B) 1:1 ODR in a 1:50 analyte mixture:D₂O (analyte mixture = 1:1 oil-dispersant mixture), which are essentially identical. The addition of oil in a 3:1 DOR and 1:50 oil:D₂O ratios resulted in rapid phase separation and the particle size could not be determined by DOSY methods.

Ultimately, the use of NMR was abandoned because of the number of difficulties and the conclusion that oil droplets and other fluids would need to be maintained in a motionless state for several minutes or longer to achieve the resolution needed to make accurate characterization of either physical or chemical properties.

Table 4.9. Samples and ratios used to try and force micelle formation for particle size determination and diffusion analysis.

Sample	Dispersant:		Analyte Mixture:	Diffusion	Particle Size (nm)
	D ₂ O ratio (v/v)	DOR (v/v)	D ₂ O ratio (v/v)	Coefficient x10 ⁻¹⁰ (m ² /s)	
Finasol OSR 52	1:50	1:50	1:50	0.3-5.5	0.3-5.5
Finasol OSR 52	1:50	1:50	1:50	0.4-5	0.3-4.5
Finasol OSR 52	1:100	1:1	1:50	0.4-5	0.3-4.5
Finasol OSR 52	1:100	3:1	1:50	0.4-5	0.3-4.5

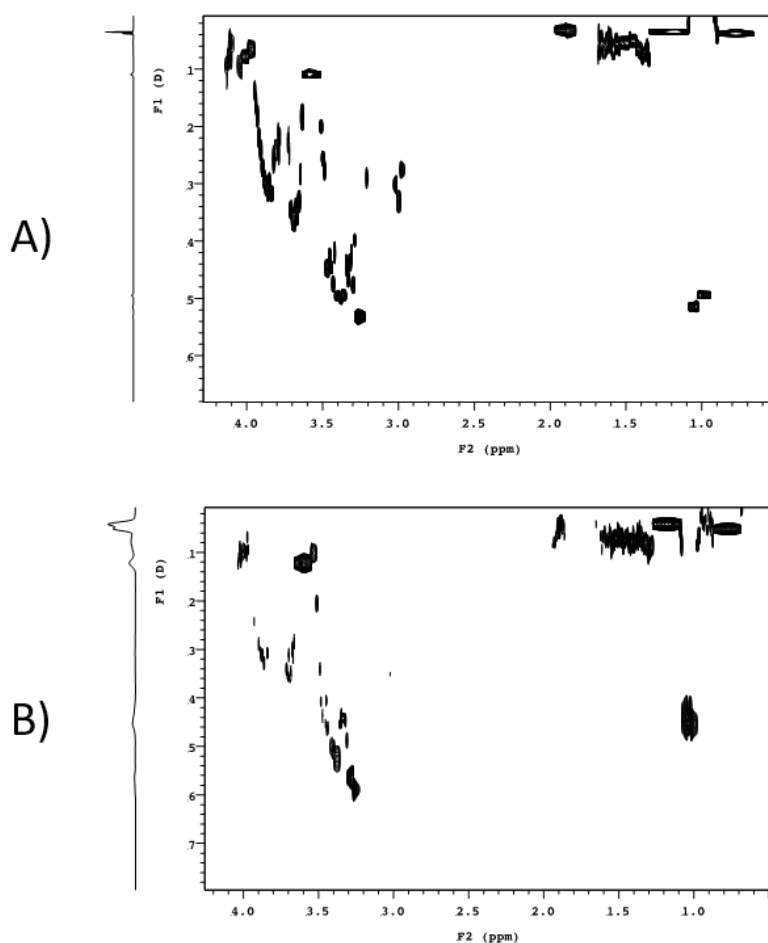


Figure 4.24. ¹H-DOSY spectra of A) 1:50 Finasol OSR 52: D₂O ratio and B) 1:1 DOR in a 1:50 analyte mixture:D₂O (analyte mixture = 1:1 oil-dispersant mixture). No significant changes were observed upon addition of oil. The expansion of dot size and the few additional dots that arise were data noise peaks and not significant.

4.3.2 Investigation of Other Spectroscopic Approaches

A rapid and low-cost method of quickly determining oil:dispersant:seawater ratios was desired because typical methods (e.g., liquid chromatography [LC]-MS, GC-MS) are time-/labor-intensive and produce significant chemical waste in the form of harsh solvents. Spectroscopic approaches (i.e., light-based) were investigated as a solution for on-the-fly quantitation of oil:dispersant:seawater and to detect changes in the chemical composition of samples subject to degradation. Briefly, spectroscopy approaches exploit the optical characteristics that are unique to each compound (e.g., absorption spectra of water, Figure 4.25). With the introduction of the sapphire glass view cell into the pressure system (Figure 4.6), light spectroscopic methods were also explored in an attempt to identify a means of characterizing pressurized samples of seawater, oil, and dispersant without having to withdraw or perform solvent extractions on the samples.

Fluorescence spectroscopy, for example, provides a very high level of sensitivity capable of parts per billion and lower limits of detection. Fluorescence spectroscopy has been used for the high-pressure study of the solubility of organometallic compounds, chemical extraction processes, catalytic reactions, new materials synthesis and purification, and the characterization of fundamental chemical processes. All conjugated organic compounds fluoresce to some degree and the emission spectrum, emission lifetime, and emission efficiency are largely a function of the molecular structure. Consequently the fluorescence spectrum and lifetime collected from the high-pressure system could provide a means of determining the gross molecular composition of the seawater-oil-dispersant emulsion. Shorter wavelength fluorescence spectra with shorter lifetimes would indicate smaller organic compounds with simple conjugation. Longer wavelength spectra (in the red for very large polyaromatic hydrocarbons) with longer lifetimes would indicate a higher degree of conjugation, a higher content of polyaromatic hydrocarbons, and in general higher molecular weight (lower volatility) components of oil.

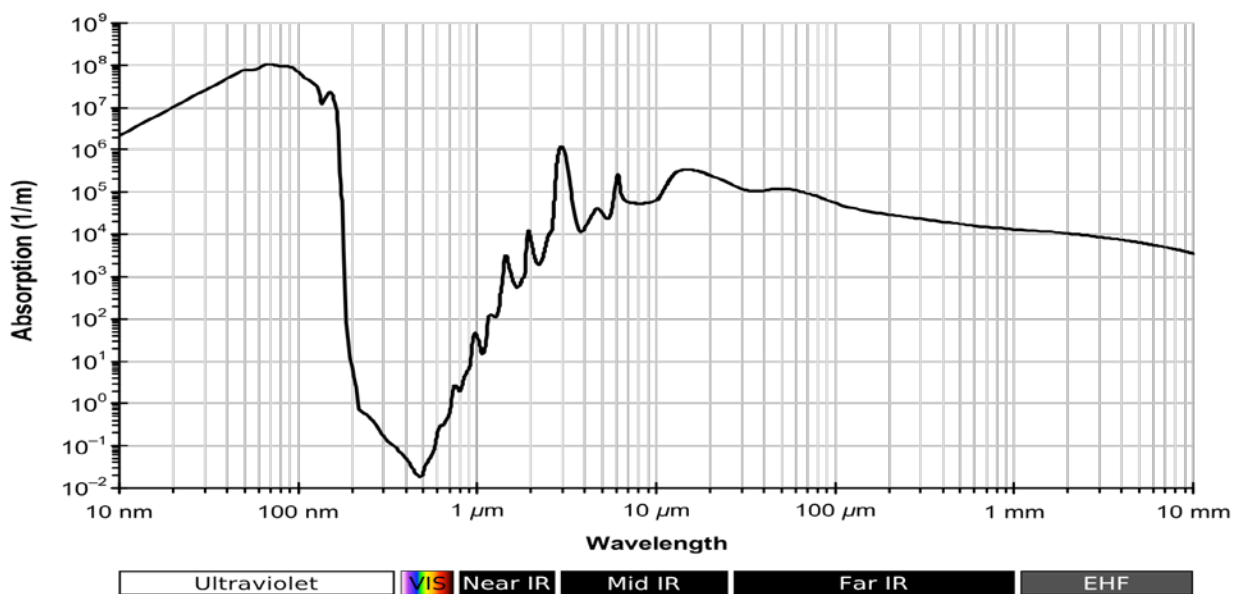


Figure 4.25. Absorption spectra of water.

For each of the methods described below, the first round of evaluation was carried out in unpressurized systems to facilitate movement and rapid exchange of samples between systems. Studies using pressurized systems were then performed with any methods that were successful.

When a compound absorbs light of a particular wavelength, it may emit light at a different wavelength—a phenomenon known as fluorescence. Oil, dispersant, and seawater all fluoresce; seawater, for example, fluoresces because of the presence of organic contaminants (e.g., proteins and DNA). The particular excitation and emission spectra, as well as the timing of the fluorescence, all have the potential to help identify compounds, and the intensity of the fluorescence may also be used to quantify the compounds. To determine the fluorescent spectra of a compound, two components are needed: a monochromatic illumination source to produce light of a single wavelength and a spectrophotometer to detect light of a particular wavelength.

A BioTek Synergy4 multi-detection microplate reader was explored as a high-throughput tool for measuring fluorescence. It provided both the illumination source and the spectrophotometer with a plate reader and attached automated microplate stacker for rapid, automated analysis of hundreds of samples. It provided three measurement modes: absorption, transmission, and fluorescence illumination from 250 nm to 650 nm; detection from 300 nm to 700 nm, and the ability to perform automated excitation/ emission scans of compounds.

An experiment was carried out to determine whether the instrument could detect unique fluorescent signatures from oil or dispersant in seawater. The rationale was that if each compound has a unique fluorescent signature, then ratios of fluorescence measurements should be directly related to ratios of the compounds. Test materials included dispersants (Corexit and Finasol), crude oil (ANS and WTI), unfiltered and 0.22 μm filtered seawater, and specific dispersant components (1,2-propanediol, kerosene, dipropylene glycol methyl ether, 2-butoxyethanol, and dioctyl sulfosuccinate).

The spectra are provided in Appendix D and results are summarized here. Seawater, Corexit, Finasol, ANS, and WTI all fluoresced in ultraviolet light. Peak excitation differed between compounds, but there was some overlap and the peaks were not particularly sharp. This might be resolved by using a different instrument. The dispersant components did not display any significant fluorescence. The conclusion was that fluorescence spectroscopy might be a viable approach if background fluorescence does not wash out unique signatures.

A second experiment was aimed at determining whether pre-determined ratios of oil, dispersant, and seawater mixtures could be related to fluorescence ratios. The rationale was based on each compound fluorescing at unique wavelengths. For this set of experiments, test materials included dispersants (Corexit and Finasol), crude oil (ANS and WTI), and unfiltered seawater. Samples consisted of 180 μL raw seawater + 10 μL oil + 10 μL dispersant. Spectra are provided in Appendix E and results are summarized here. Mixtures of oil, dispersant, and seawater fluoresced across a range of wavelengths. Inconsistent results were acquired across dilutions of dispersant, most likely due to an inability to stabilize emulsions of oil/dispersant/seawater because the oil tended to accumulate on edges of the wells and/or stick to bottom of the plates. The conclusion was that at dilutions at which dispersant would be used in the ocean it would be unlikely to be able to distinguish the dispersant's fluorescence from background seawater/oil fluorescence.

Hyperspectral analysis was also performed to determine whether more complex spectral profiles might be useful. Using a contrast dye in the water allowed visualization of the dye in a more discriminatory manner than the oil. However, dispersant and oil emulsions quickly blocked the imaging system. The available system only went to ~ 1100 nm and most infrared testing of oil occurs at ~ 3300 nm. With an extended spectrum system, it may be possible to measure oil directly. It may also be possible to use a “void in water” signal to measure the size of oil droplets at low concentrations, or even to measure droplets in higher concentration emulsions using a very short path length.

4.4 Examine the Effect of Deep Water Conditions on Cell Growth and the Biodegradation of High Concentrations of Oil

Compared with studies at atmospheric pressure, only a very small number of studies have examined the effect of high pressure on cellular metabolism (Kumar and Libchaber 2013; Marietou and Bartlett 2014; Follonier et al. 2012). Fewer still have examined the biodegradation of oil under high pressure (Schedler et al. 2014; Juarez et al. 2015; Scoma et al. 2016). In the deep ocean⁵, high pressure is accompanied by cold temperatures (3–4°C), a lack of sunlight, and other confounding factors that may include elevated salinity, reduced oxygen, and less mixing energy than in wave- and wind-driven surface waters. Each of these factors has the potential to slow down microbial growth and metabolism, particularly on complex carbon sources.

Microorganisms in the deep pelagic ocean are typically slow-growing heterotrophic and chemoautotrophic organisms that live off of detritus and other nutrients sourced from the upper water column or gradients created by thermal or chemical seeps on the ocean floor. Many of the organisms found in the deep ocean are also believed to be transient; i.e., transported to the deep ocean from the upper water column attached to sinking particulates. Studies have also shown that many organisms from surface environments are capable of growth at elevated pressures (Kumar and Libchaber 2013; Marietou and Bartlett 2014; Scoma et al. 2016) and upwelling events bring microbial communities from the deep ocean up to the surface (Kerkhof et al. 1999), thereby adding to the diversity of these environments.

A set of experiments was designed to explore the relative importance of temperature, pressure, dispersant concentration, and droplet size as independent variables on microbial growth and metabolism. The effects of dispersants and droplet size were described previously in Chapter 2.0. Studies concerning the metabolism of hydrocarbons have typically used very low concentrations of oil (e.g., Schedler et al. [2014] used <2 mM; McFarlin et al. [2014] used 2.5 and 15 ppm) to facilitate the monitoring of the hydrocarbons and to control the suspension of hydrocarbons in the test chamber. A key objective of this study that was established by the sponsor was to examine oil degradation with >1% (v:v) crude oil in seawater with little mixing energy. Such conditions would likely occur in close proximity to a natural seep or leak plume.

4.4.1 Microbiology: Strain Selection

The objective was to use a natural consortium of microorganisms from seawater rather than to rely on a single organism or specified mix that would necessarily fail to represent the genetic and metabolic diversity of the natural environment. However, natural microbial communities collected at a single location constantly vary in composition due to many factors, including seasonal, tidal, and diurnal cycles. This variation could introduce inconsistencies between experiments started on different dates using inocula freshly collected from the field each time. Therefore, to maintain consistency across all experiments, microbes were collected from 252 L of seawater at PNNL-MSL through serial filtration onto 0.45 µm and 0.22 µm filters. The microorganisms were then resuspended from the filters into 2520 mL of seawater + 2520 mL 50% glycerol. The suspension was then divided into both 0.8 mL and 40 mL sample tubes that were frozen at -80°C to create a supply of virtually identical inocula. The preparation also provided a 50x concentration factor to help when inoculating a large volume of sterile medium. A frozen sample was used to inoculate sterile growth media to demonstrate the viability of the frozen organisms. Another was used to inoculate an oil-containing sample of seawater to show that at least some of the microorganisms were in fact capable of consuming oil.

⁵ Microbiologists generally define the deep ocean as greater than 1000 m (Jannasch and Taylor 1984; Prieur 2011)

A DNA fingerprint of the frozen stock was also generated to create a profile of the prokaryote and eukaryote content. The fingerprint method used polymerase chain reaction (PCR) amplification of a hyper-variable region of the small subunit rRNA encoding domain to generate DNA fragments of different lengths for the different organisms in the sample. The presence of a fragment identifies the presence of a corresponding organism and thus the collection of fragments represents the community. This allowed for tracking and comparison of changes in microbial content during the biodegradation tests.

In some instances where tighter control of variables was desired, cultures of single, pairs, or triplets of isolated species were used. Two bacteria, *A. borkumensis* (ATCC 700651) and *P. putida* (ATCC 700007), and one fungus, *H. resinae* (ATCC 22711), were used. All are known to metabolize petroleum products. *A. borkumensis* is globally distributed in the ocean and has been isolated in the Gulf of Mexico (Kosita et al. 2011). Strains of *P. putida* and *H. resinae* have also been isolated from marine environments, but may not have been specifically identified in Gulf of Mexico isolations to date. Both a bacterium and a fungus were used to consider the effects on prokaryotes and eukaryotes and differences between unicellular species (*A. borkumensis*) that might be expected to only colonize the surface of an oil droplet and a filamentous fungus potentially capable of extending mycelia to penetrate into droplets of oil or tar.

The initial plan was to conduct a series of studies of emulsified oil in seawater using different concentrations of dispersant and under different pressures. Numerous studies have examined the effect of these and other factors on very low concentrations of oil in seawater, with typical values of parts per million and below (Prince et al. 2013; McFarlin et al. 2014; Kleindienst et al. 2015; Schedler et al. 2014). In this study, the objective was to examine degradation using much higher concentrations of oil—parts per thousand or parts per hundred—and to use low-mixing conditions. The study described in Chapter 2.0, and the work of others have generated inconsistent results concerning the effect of dispersants on cellular growth and metabolism, particularly on oil (Kleindienst et al. 2015; Prince et al. 2016; Kleindienst et al. 2015; Macias-Zamora et al. 2014; Prince and Butler 2014). Consequently, a decision was made to not proceed with further studies concerning dispersant effects.

Oil sticking to the inner walls of the Parr reactors and forming a surface slick remained problematic. A similar effect was observed during another study for BSEE that examined the use of an absorbant-like particulate material as a means to deliver microorganisms and promote the biodegradation of oil. One observation from that study was that because microorganisms did not degrade the small quantities of oil that formed a slick on the sides of glassware and on the water surface slick as quickly as oil droplets in suspension, the non-degraded slick oil confounded the ability to conduct high sensitivity measurements of hydrocarbon degradation in the water column (Bonheyo et al. 2017). Due to time and funding constraints and in consultation with BSEE, a decision was made to perform a literature review regarding hyperbaric microbiology and the impact of pressure on metabolism and to conduct an experiment comparing the relative impact of pressure and temperature on the growth of microorganisms from surface environments (i.e., that may be introduced into a deep water setting).

Each liter of growth medium consisted of 1 L of sterile filtered seawater supplemented with 1 g pyruvate, 50 mg yeast extract, 5 mg tryptone, and 50 mg NH₄Cl. The 2 liter Parr reactors were filled with 1.6 L of growth medium and inoculated with 40 mL of the frozen seawater microbial community and 10 mL of an overnight *A. borkumensis* culture. The reactors were then sealed and incubated at either room temperature (~17.8°C) or 4°C. For each pair of temperatures, one reactor was kept at atmospheric pressure and another at 2500 psi (equivalent to ~1700m depth). The mixing impellers were used to provide gentle mixing. Samples were collected every 24 hr to measure turbidity (O.D.₆₀₀), at which time pressure was first slowly released from the pressurized reactors, a sample was withdrawn, and then the system was repressurized. This allowed for fresh gas exchange on a daily basis.

With the exception of the atmospheric pressure culture at 4°C, all other cultures showed signs of growth within 24 hr. Not surprisingly, the culture maintained at atmospheric pressure and room temperature exhibited the fastest growth and achieved the highest optical density reading, which peaked at 48 hr at 0.179. Surprisingly, the unpressurized sample at 4°C showed no increase in O.D. throughout the test. The growth profile of the samples pressurized at 2500 psi were all similar, regardless of temperature: the 4°C culture reached an O.D. of 0.020 after 24 hr then fell slightly to 0.019, whereas the room temperature sample reached an O.D. of 0.018 at 24 hr and 0.019 after 48 hr. Samples spread onto agar plates and incubated at 18°C showed unidentifiable, but mixed colony morphotypes.

4.5 Characterize the Effects of Pressure, Time, DOR, and Oil:Water Ratio on Droplet Size

Dispersants reduce the interfacial tension between the oil and water, permitting small droplets of oil to exist without coalescence. A number of factors influence droplet size and the potential for coalescence; among these are the viscosity and density of the fluids, surfactant concentration, dilution of the oil in water, and interfacial shear (Auflem et al. 2001).

As described in Section 4.1, an investigation was conducted to determine whether pressure affected oil droplet size over a range of DORs. A range of oil in water concentrations was tested using the small view cells for imaging, but the oil was either not visible, or quickly obscured the windows. Greater success was found using a series of simulated blowouts to characterize droplet sizes (described in Section 4.6) and we were instead tasked with characterizing the viscosity and interfacial tension of the oil and dispersants.

4.5.1 Oil and Dispersant Physical Characteristics: Rheometrics

To understand how the dispersants (Finasol OSR 52 and Corexit EC9500) and crude oils (ANS and Macondo) may behave in a blowout scenario we obtained rheology data on each material. One factor that was examined was whether matching the temperature and density of the dispersant with the ejected oil had any effect on the extent of oil and dispersant mixing and thus the emulsification of the oil. Although data for each of the materials could be found online, experiments were conducted to obtain high-quality density and viscosity data as a function of temperature, recognizing that age (weathering, degassing), and batch (dispersant) or date of extraction (oil) can influence the properties of the materials. The initial rheological data were obtained through automated sample analysis at the Southwest Research Institute (SwRI, San Antonio, TX). SwRI was able to deliver density values for each of the four materials at 20°C and at 70°C (except for Macondo, which had too much off-gassing to obtain an accurate density measurement) as well as dynamic (absolute) viscosity from 4°C to 100°C at a shear rate of 100/s, consistent with previous literature. It is necessary to maintain consistency between tests because these materials are non-Newtonian and thus instead of exhibiting a consistent dynamic viscosity no matter what the applied shear force, these materials exhibited shear-thinning behavior (Figure 4.26).

Corexit EC9500 Dynamic Viscosity vs Shear Rate

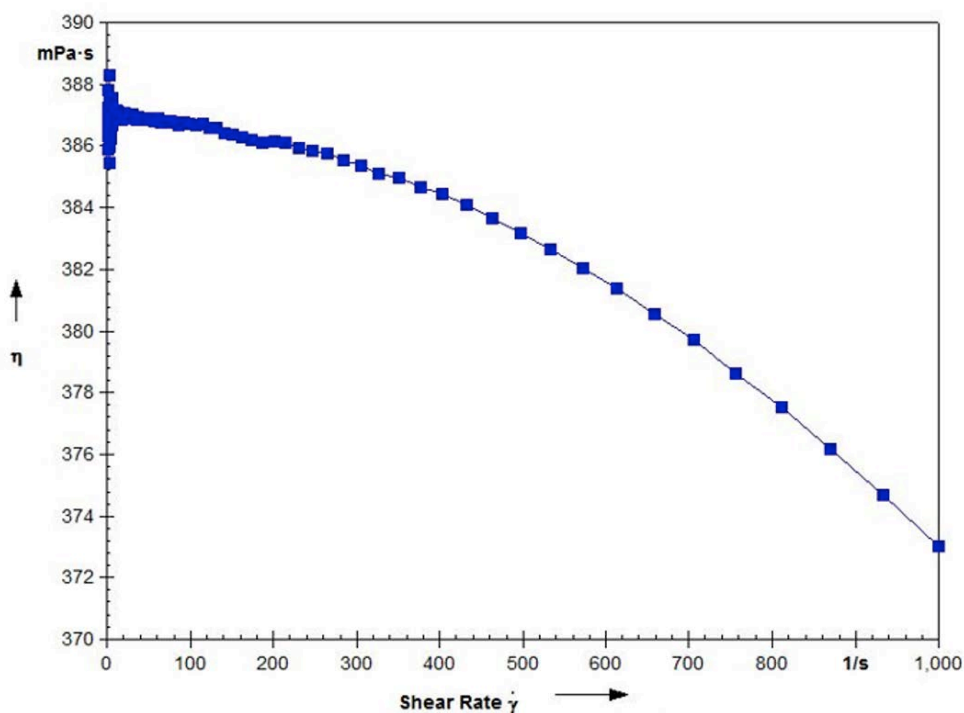


Figure 4.26. Non-Newtonian shear-thinning behavior exhibited by Corexit EC9500 during a viscosity vs. shear rate sweep. Viscosity is shown in mPascal-seconds; 1 mPa-s equals 1 cP.

Both stock samples as well as weathered samples were evaluated using a single shear rate for all samples as opposed to different rates for fresh vs. weathered samples. As can be seen in Figure 4.26 however, this choice will not necessarily result in a large change in the measured viscosity, because at low shear rates the samples are close to Newtonian. During a blowout scenario, shear-thinning behavior may drastically change the oil-dispersant-water interactions as the viscosity of each sample reaches that of water (1.61 cP), a Newtonian fluid, during high stress. This behavior may increase phase separation, thereby decreasing dispersant effectiveness, or it could minimize interfacial tension between the oil and dispersant to ultimately increase dispersant effectiveness.

Of the four materials tested, the viscosity of Corexit EC9500 was approximately 10–20 times higher than the other materials (Figures 4.27, 4.28, 4.29, and 4.30). Finasol OSR 52 had an average dynamic viscosity of 223.67 cP at 4°C. Corexit EC9500 had an average dynamic viscosity of 2057 cP at 4°C. ANS crude oil had an average dynamic viscosity of 110.33 cP at 4°C. Macondo crude oil had an average dynamic viscosity of 70.1 cP at 4°C. While this is the lowest viscosity of the samples tested, it is still ~35x that of raw seawater, which is 1.61 cP at 5°C and 33 ppt.

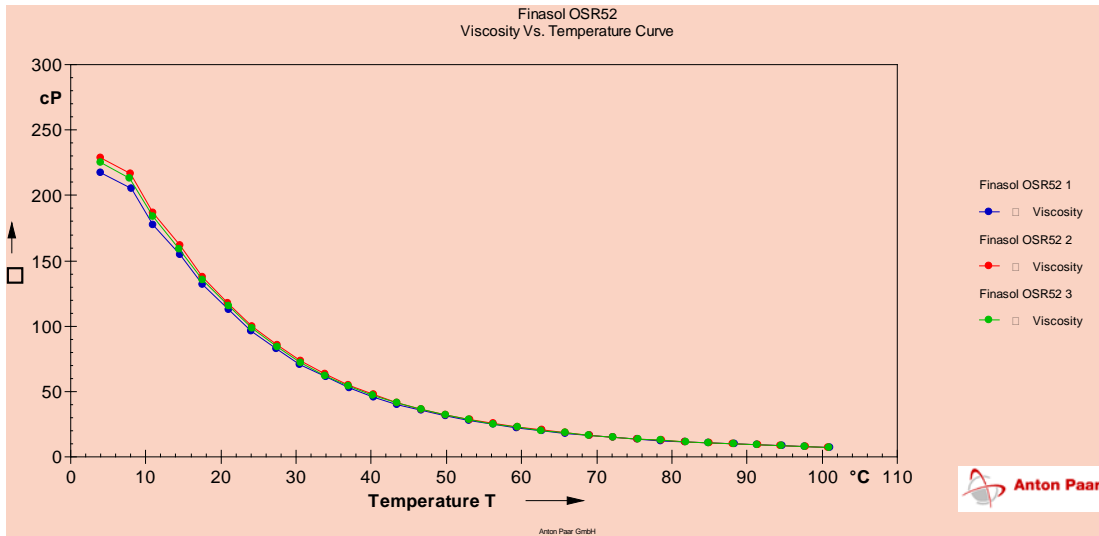


Figure 4.27. Finasol OSR 52 viscosity vs. temperature curve. Testing performed by SwRI.

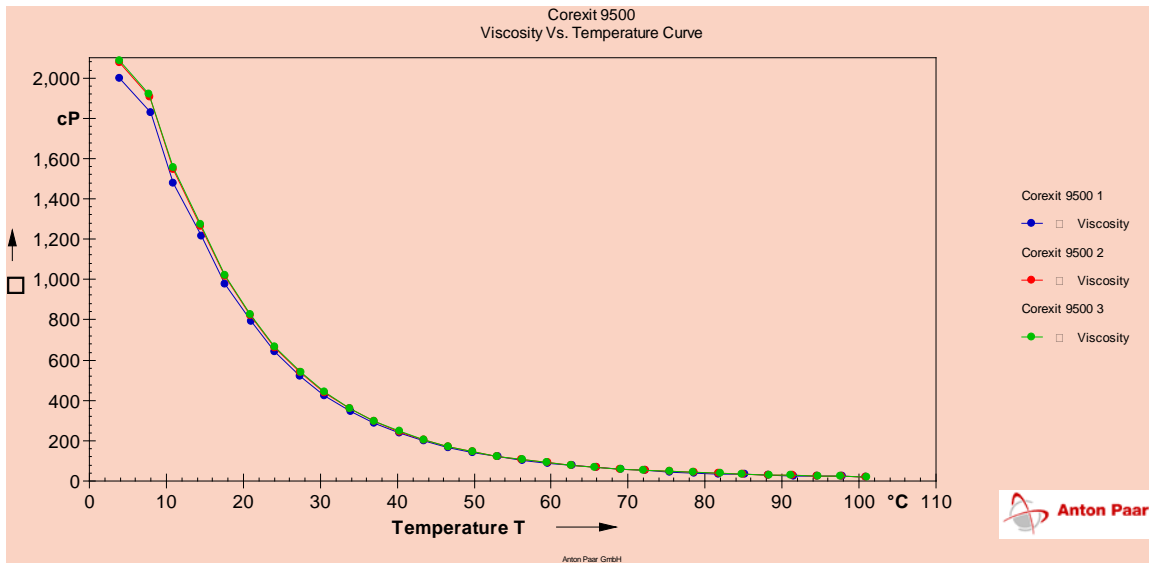


Figure 4.28. Corexit EC9500 viscosity vs. temperature curve. Testing performed by SwRI.

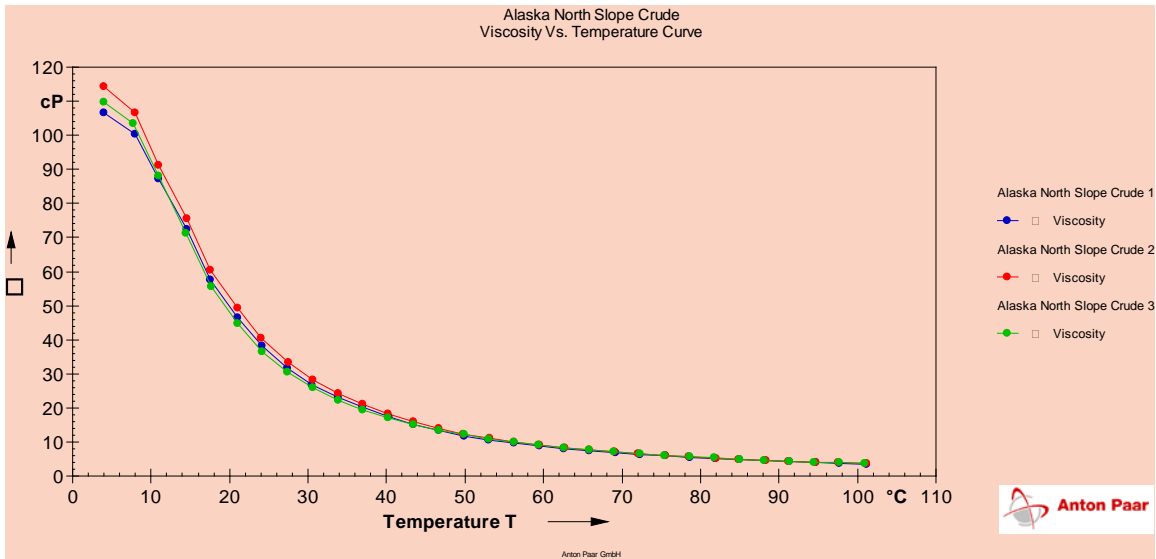


Figure 4.29. Alaska North Slope crude oil viscosity vs. temperature curve. Testing performed by SwRI.

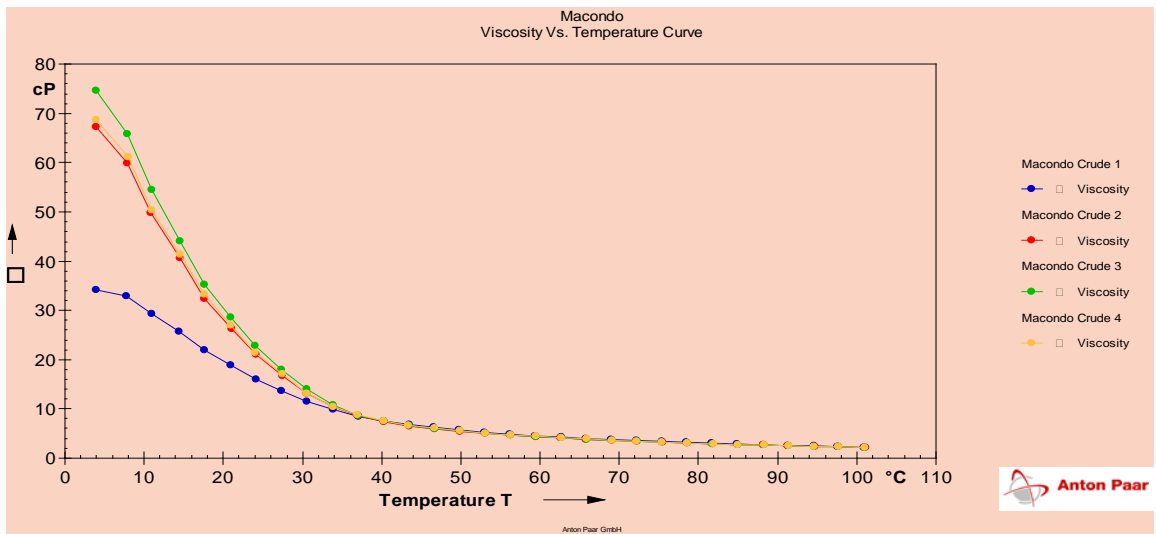


Figure 4.30. Macondo crude oil viscosity vs temperature curve. The Macondo sample was tested four times because the first test yielded an anomalous result (blue line). Testing performed by SwRI.

The measured density of each material is given in Table 4.10. Raw seawater at 20°C and 33 ppt salinity has a density of 1.023 g/cm³ at the surface and a density of 1.036 g/cm³ at 4°C and 35 ppt salinity at a depth of 2000 m. Of the four materials tested, only Corexit EC9500 had a density greater than that of seawater. Density of a material is proportional to the temperature of the material and, while density measurements were not made at 70°C by SwRI, the Radwag USA (Miami, FL) density determination kit was used to track the Macondo oil density as it cooled from 52.5°C to 19.5°C (Figure 4.31). The value obtained at 20°C (0.8575) has a percent difference equal to 0.17% derived from the SwRI data confirming the accuracy of the results.

Table 4.10. Density measurements of Finasol OSR 52, Corexit EC9500, Alaska North Slope crude oil, and Macondo crude oil obtained at 20°C and at 70°C.

Sample	Density (g/cm ³) Measurements			
	20°C	Std. Dev.	70°C	Std. Dev.
Finasol OSR 52	1.0045	0.0001	0.9650	0.0003
Corexit EC9500	1.0635	0.0000	1.0249	0.0000
Alaska North Slope Crude Oil	0.8909	0.0002	0.8562	0.0002
Macondo Crude Oil	0.8561	0.0001	Not Measured	Not Measured

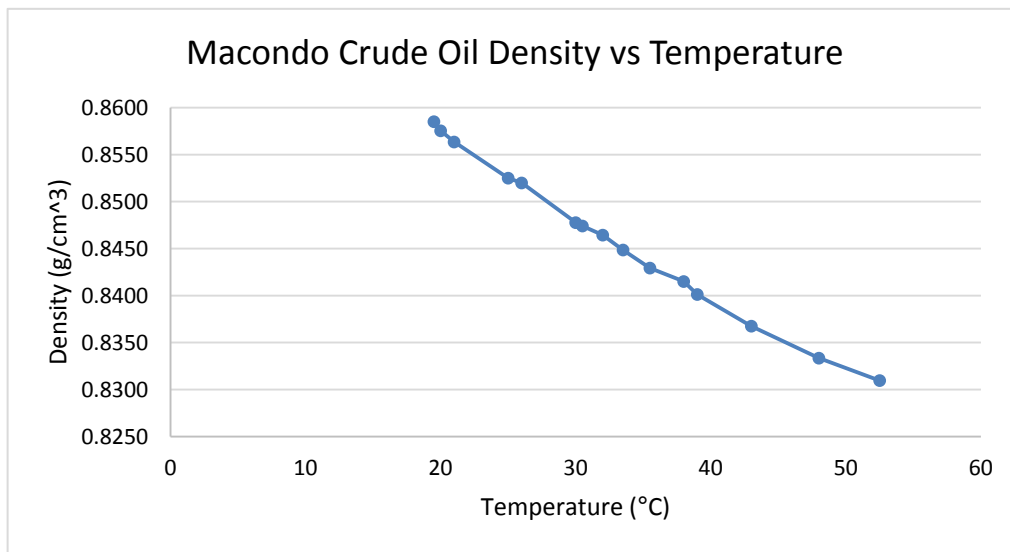


Figure 4.31. Graph illustrating the increase in density of Macondo crude oil while cooling from 52.5°C to 19.5°C.

4.6 Characterize the Effect of Pressure Drop and Temperature on Oil Droplet Size

To better understand various characteristics of oil blowouts at depth, a small-scale system was developed to simulate the ejection of oil at a higher initial pressure than the hydrostatic pressure of the marine environment. Specifically, tests were designed to examine droplet size distributions immediately following ejection and to explore whether different methods of dispersant injection would affect the size distribution. The experimental system developed used a pressurized 2 L Parr reactor to eject oil (starting pressure of 2900 psi) into an aquarium filled with unfiltered seawater. Initial tests attempted to use the Teledyne syringe pumps, which are rated to 7500 psi and can be used to generate accurate pressures in closed systems, but pressure could not be sustained during the injection.

In several of the planned tests, heated oil and or dispersant was to be ejected into cold seawater. One possible method for tracking the movement of the fluids would be to monitor temperature throughout the system. Thermal imaging cameras were unsuitable for the task due to the absorption and poor transmission of infrared radiation in water and shielding by the aquarium glass. Instead, a thermal probe sensor array was developed to track the temperature of fluids in the aquarium (Figure 4.32), which is described in more detail below. Visible spectrum videography was performed using the GoPro cameras,

still images for assessing droplet sizes were taken using the Canon EOS camera, and lighting was provided by two LimoStudio 500 watt equivalent, 5500 K temperature light-emitting diode (LED) light banks (Figure 4.33). The aquarium setup was placed inside a chemical safety cabinet for ventilation and containment.



Figure 4.32. Test tank showing a 4×3 thermal probe array. Each wire had three thermistors along its length to interrogate the top, middle, and bottom depths of the tank.

Natural, unfiltered seawater (33 ppt) was stored in 5 gallon pails in a walk-in refrigerator until needed to provide chilled seawater of 7.8°C to 8.2°C during the experiments. When heating was needed for the oil, a Parr reactor containing the oil or oil and dispersant premixture was stored overnight in a 65°C incubator. The measured temperature of the oil or oil:dispersant mix during the injection was typically ~55.4°C because of rapid cooling during setup or ineffective heating in the incubator. This still provided a significant temperature differential with the cold water.

Oil was ejected through ¼ in. OD (6.35 mm) 0.172 in. ID (4.37 mm) high-pressure stainless steel tubing. Dispersant was ejected through ⅛ in. OD (3.18 mm) 0.069 in. ID (1.27 mm) stainless steel tubing. The duration of the blowout was 2–3 seconds during which 121 g to 165 g of oil and gas were released. Oil in the Parr reactor was pressurized either by injecting the gas through the oil, which resulted in considerable solvation of the gas, or by injecting the gas into the head space above the oil, which resulted in less gas dissolving into the oil (measured by weight gain during pressurization).



Figure 4.33. Laboratory setup for the blowout tank.

4.6.1 Sensor Array Development

An inexpensive sensor array system for tracking temperature was developed using thermistors (MF58H 10K) for the sensing element. Thermistors were chosen over thermocouples because they are easily multiplexed, allowing a single analog-to-digital converter (ADC) to read as many thermistors as there are digital output pins. An ATmega2560 microcontroller was chosen to drive the system because it has a 10-bit ADC and up to 56 digital output pins. The system was developed to have 36 thermistors, thereby allowing for future expandability (up to 56 thermistors can be driven). The thermistors were arrayed in a $4 \times 3 \times 3$ (depth, width, height) arrangement. Clamps to attach lead weights to the data cables were designed and 3D printed. Software was developed in C to run on the microcontroller, which returned temperature data a universal serial bus. A host script was written in Python to run on a PC, which collected temperature data from the microcontroller. The host script also operated a camera (see Section 4.6.3 on particle size analysis), which took photos at regular intervals. Multiple photos were taken in quick succession during the initial 10 s of the blowout, and then the rate of photography decreased over the remaining 10 min of the experiment. Photos and temperature data were synchronized to the PC's clock. Lighting was provided by a pair of LimoStudio 500-watt equivalent, 5500 K temperature LED lights.

4.6.2 Results from the Thermal Array

Results indicated a change in temperature in the water after the blowout, but the spatial resolution was not high enough to provide a good picture of the mixing. Both heating and cooling were observed in the array from the injection of warm or hot oil and the release of rapidly expanding gas (Figure 4.34).

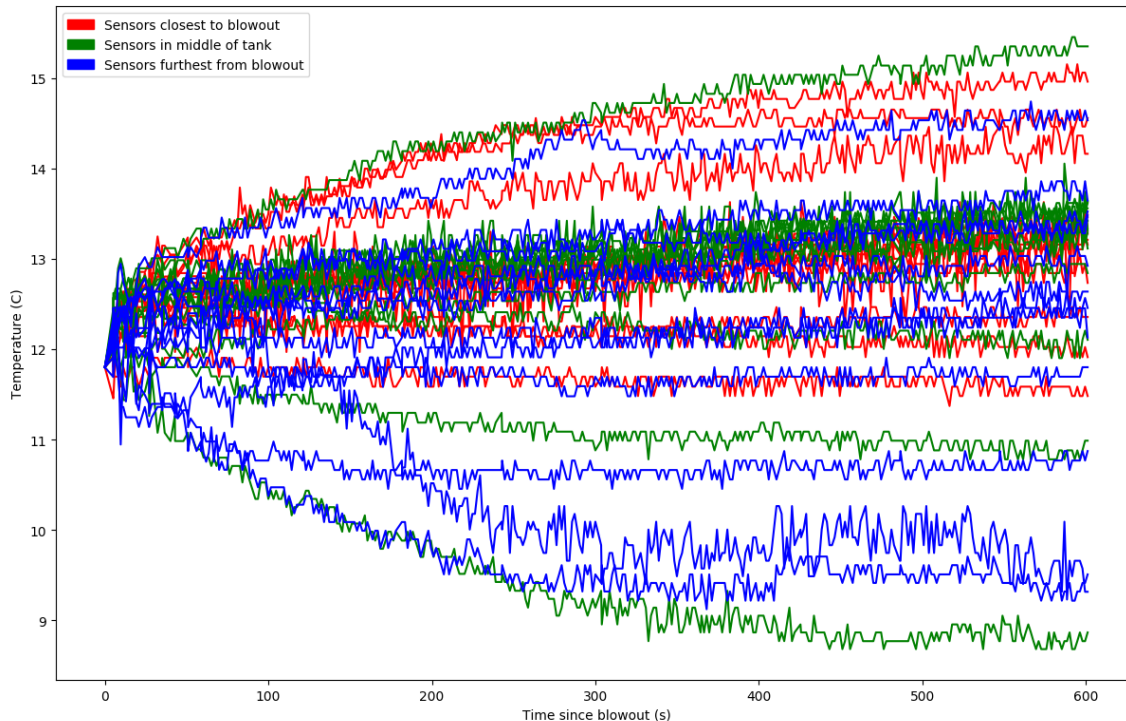


Figure 4.34. Sample data from the thermal array indicating the temperature of the surrounding water. Sensors closest to the point of oil injection recorded a rise in temperature, but a few sensors farther from the point of injection recorded a drop in temperature.

4.6.3 Blowout Testing: Particle Size Analysis

Blowout particle size analysis was performed using images taken with a Canon EOS 70D digital camera with the attached 100 mm macro lens ($f/16$, ISO 6400). The camera was located 38 cm from the tank. Images were obtained as a time series that started at a time coinciding with the initiation of a simulated oil blowout and ended 10 minutes after initiation. Particle size analysis was performed using images collected at 5 s after blowout to assess blowout dynamics and again at 10 min after blowout (well after the initial turbulent release) to assess the evolution of the size distribution and to maintain consistency and correlation of data with research using swirling and baffled flask tests, in which data are collected after 10 minutes of mixing.

Images were scaled to a submerged ruler affixed to a polytetrafluoroethylene (PTFE) board. The PTFE board was placed 7 cm from the tank wall to reduce the overall path length through which a portion of the oil plume was imaged. Even with this reduced path length, blowouts with increased concentrations of oil or highly dispersed (small particle cloud) could easily obscure the FOV such that direct imaging was ineffective (Figure 4.35).



Figure 4.35. Image acquired at 10 min after blowout (136 g of 60°C Macondo oil at 2400 psi [390 psi drop from blowout] into 63226.5 g of raw seawater [33 ppt; 11.8°C]). The particles are too fine (sub 0.01 μm) and too dense to effectively image and quantitate oil distribution in the water column. One of the temperature sensors emplaced in the water tank is barely visible in the center-right of the image.

As described in detail in Section 3.0, images with sizable particles were converted to 8-bit grayscale in Adobe Photoshop and then the particle size distribution was calculated using Fiji (Image J with particle size analysis plugin). The submerged ruler was used to scale the resultant images. Identified particles were required to have a circularity of at least 0.30 to prevent overlapping particles from being measured as a single large particle.

Figure 4.36 shows sample images collected from a test blowout analysis of approximately 50 g of 60°C Macodo crude oil released at 2200 psi into 60,000 g of raw seawater at 12°C.

Qualitatively tracking the blowout plume in the tank, large particles of oil can be seen within a cloud of smaller particles. When the large particles reach the surface of the water, some spread out along the surface forming a thick layer, but the blowout turbulence induces some mixing in the tank as well. This mixing of the large and small particles resulted in a distribution of fine oil particles in the water column 10 min after blowout (see Table 4.11 and data described later in Figure 4.7 through Figure 4.15 in Section 4.6.6). At both 5 s and 10 min after blowout droplets were measured at the smallest size discernable with this imaging system; however, the maximum particle size observed at 5-seconds had a cross-sectional area almost 2 orders of magnitude higher than the largest particle observed at 10-minutes.

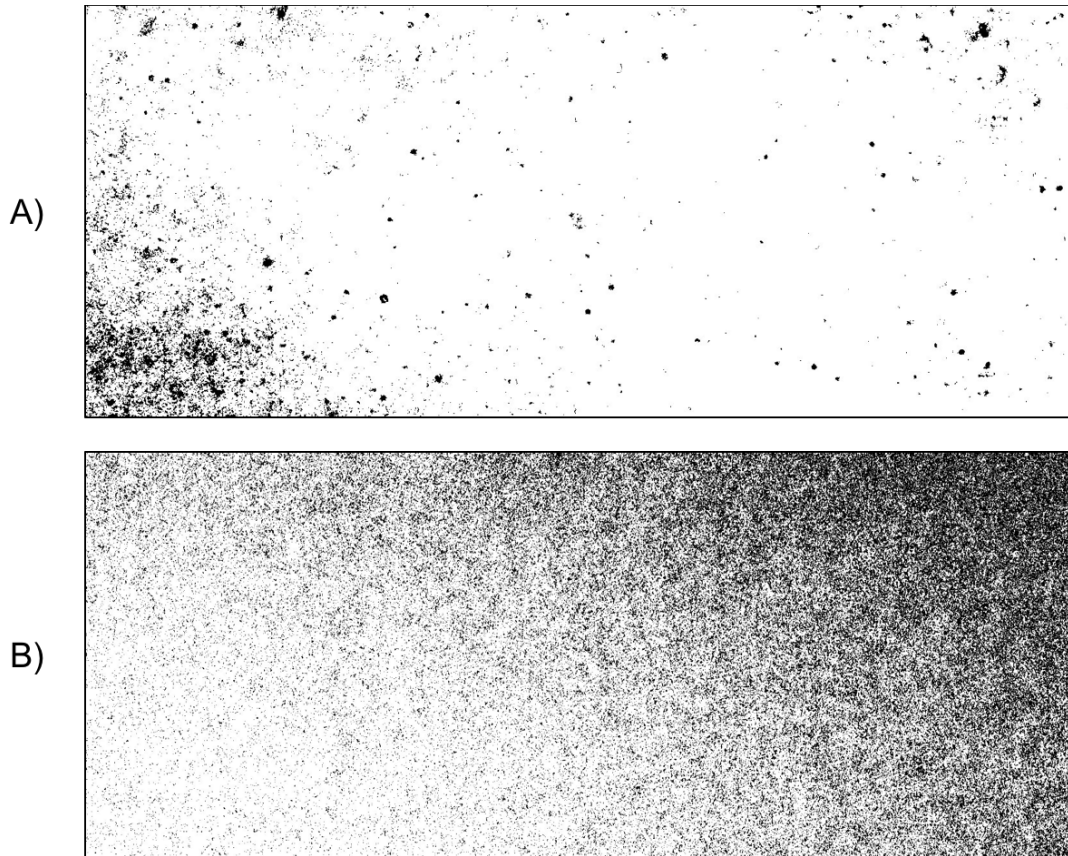


Figure 4.36. A) A subsection of the camera field of view imaged at 5 s post-blowout and B) a subsection of the camera field of view imaged at 10 min post-blowout.

Table 4.11. Cross-sectional area of oil particles at 5 s and 10 min after a test blowout with no dispersant.

Values in mm ²	5-Second Image	10-Minute Image
Mean Area	0.003	0.001
SD	0.021	0.001
Min	4.53E-04	4.53E-04
Max	1.113	0.033

4.6.4 Dispersant Injection

The timing, and placement of dispersant injection was critical to facilitate mixing with the oil and seawater and ultimately dispersion of the oil throughout the water column. Figure 4.37 shows a scenario whereby little to no mixing may occur even though the dispersant and oil are co-injected at approximately the same time and the same XYZ coordinates in a water column. In this instance, the rapid degassing of the oil prevented the dispersant from mixing with the oil.



Figure 4.37. Time series of images during a Macondo crude oil blowout (43 grams released at 60°C and 2400 psi) with coinjection of 1.0 g of Corexit EC9500 (17.4°C and 1 atm) into raw seawater (11.8°C and 1 atm). The still image A) represents Time 0 at which point the blowout had initiated and the Corexit was injected; B) is at a time approximately 0.5 s after blowout initiation; and C) is an image captured approximately 1 s after blowout initiation. The Corexit dispersant is encircled in red and tracked through the three images.

As can be seen in this small-scale blowout, injecting dispersant at the same XYZ coordinate as the blowout was initiated did not result in efficient mixing. The dispersant did not mix with the oil or disperse into the water column. It was instead carried up through the water column as a single large droplet with the gas. Upon reaching the surface of the water the droplet of dispersant was noted to break up into smaller droplets that later dispersed surface oil. If the oil and dispersant were evenly mixed throughout the water column the concentration of oil would have been 43 g in 51,419 total grams of solution or 836.27 ppm and the DOR would have been 1:43.

4.6.5 The Tests

A number of preliminary tests were conducted to optimize the photography, process, location, and orientation for releasing the oil and injecting dispersant. The simulated blowouts described in section 4.6.6 were performed to assess the impact of temperature, DOR, and method of introducing dispersant into the blowout. In instances where the oil and dispersant were “premixed,” this was done by adding dispersant to a 40 mL subvolume of the oil in a 50 mL centrifuge tube, mixing with a vortex, then adding that mix to the remaining oil and stirring to mix in the dispersant. This created an idealized mixing situation.

4.6.6 Test Results

Table 4.12 shows the test parameters that were used for the simulated blowouts and Figure 4.38 – Figure 4.46 provide the droplet size distributions (following the methods used by Brandvik et al. 2013 and Johansen et al. 2013) at approximately 5 s after the start of the blowout and again after 10 min after blowout start. In each case, the seawater was chilled to an initial temperature of 4°C. Dispersant was either premixed with the oil or injected into the oil plume to allow mixing. Tests analyzed whether it was

important to match the temperature of the dispersant to the oil to enable better mixing. The Parr reactor with the oil and gas was weighed before and after the injection to calculate the amount of material injected into the tank.

In all blowout tests, a cloud of atomized oil droplets $<10\ \mu\text{m}$ (with many droplets $<1\ \mu\text{m}$) was created and lingered for >10 minutes in the tank. In the absence of dispersant, the cloud eventually formed a gravity-based gradient with some clearing at the bottom of the tank and increased density of particles (opaque appearance) at the top of the tank. Although the cloud was visually dense, the oil entrained in the cloud amounted to a very small volume, typically less than 0.1 percent of the volume of water. Also during the tests, rising oil droplets created a slick on the water surface. In the presence of dispersant (co-injected or premixed), this slick was discontinuous. With the introduction of dispersant, particularly with premixed dispersant, a chemocline envelope formed around the plume that kept the oil:dispersant:entrained seawater separate from the surrounding seawater. Despite the initial highly energetic turbulence and continued degassing and rising of buoyant droplets, this chemocline remained stable for 30 to 90 minutes in the tank, but eventually “collapsed” and oil freely dispersed throughout the tank before density differences eventually caused droplets to rise. The initial sinking and spread of the oil droplets was presumed to be driven by interfacial tension. However, there was no significant difference in droplet size distributions when the dispersant was premixed or co-injected with the oil.

A bimodal distribution frequently resulted when no dispersant was added. This was observed as the cloud of small, $<800\ \mu\text{m}$ droplets that were very numerous, but represented only a small fraction of the total volume of oil. Only a small number of large ($>2\ \text{mm}$) droplets are needed to represent a significant fraction of the oil released. With or without dispersant, the force of the blowout generated small-sized droplets. Additionally, the mode of introducing the dispersant, the ultimate DOR, and any temperature differential between the dispersant and the oil did not appear to have any effect. This latter finding is encouraging for modelers in that it simplifies the number of parameters that need to be considered when building a particle size distribution and spill migration model.

It is important to note that some or all of the larger droplets released in the absence of dispersant might break up into smaller droplets while rising through the water column because of the turbulence from continued degassing and the continued upwelling of gas and oil from below. This study did not examine the fate of the smaller droplets over an extended period of time. The dispersants may act to prevent coalescence of the droplets during the first minutes to hours following oil release and before physical separation alone might prevent droplets from contacting each other.

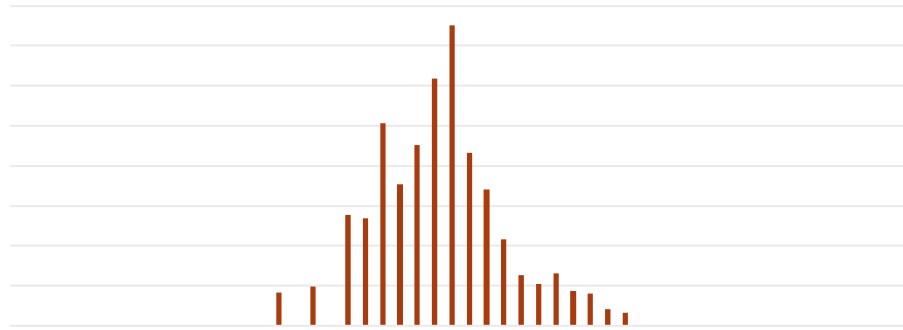
Table 4.12. Test parameters used for the simulated blowouts.^(a)

Test #	2	2.2	3	3.2	3.3
Seawater Temp	4°C	4°C	4°C	4°C	4°C
Oil Temp	60°C	16.8°C	16.8°C	16.8°C	16.8°C
Dispersant Temp	60°C	16.8°C	none	none	none
Injection Style	premixed	premixed	NA	NA	NA
Pressurization	Headspace	Headspace	in oil	Headspace	Headspace
Starting Pressure	2370	2300	2390	2290	2330
Ending Pressure	1705	1950	1920	1890	1940
Drop	665	450	470	400	390
Dispersant	1.575	1.32	0	0	0
Oil + Gas released	165	132	161	149.5	139 g
Oil Released	157.5	132	161	149.5	139 g
DOR	1:100	1:100	NA	NA	NA
Seawater	62013.5	63215.5	64519	64948.5	64433.5
Test #	4	4.2	5	6	
Seawater Temp	4°C	4°C	4°C	4°C	
Oil Temp	60°C	60°C	60°C	60°C	
Dispersant Temp	none	none	4°C	60°C	
Injection Style	NA	NA	Coinjection	Coinjection	
Pressurization	Headspace	Headspace	Headspace	Headspace	
Starting Pressure	2345	2410	2300	2370 psi	
Ending Pressure	1775	1930	1850	1705 psi	
Drop	570	480	410	665 psi	
Dispersant	0	0	2.13 g	1.43 g	
Oil + Gas released	151 g	121 g	131.5 g	157.5 g	
Oil Released	151 g	118.5 g	128 g	165 g*	
DOR	NA	NA	1:60	1:110	
Seawater	64020.5	63994	63106	62014.5	

(a) Blue (4°C) and red (60°C) font is used for ease of identifying temperature combinations

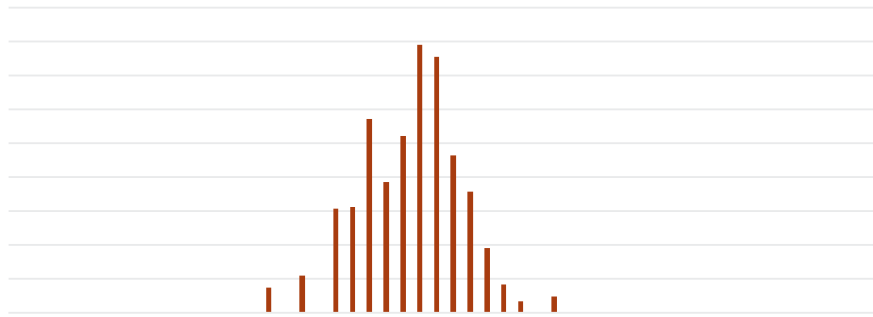
*Likely due to continued off-gassing from reactor.

NA = not applicable.



released 165

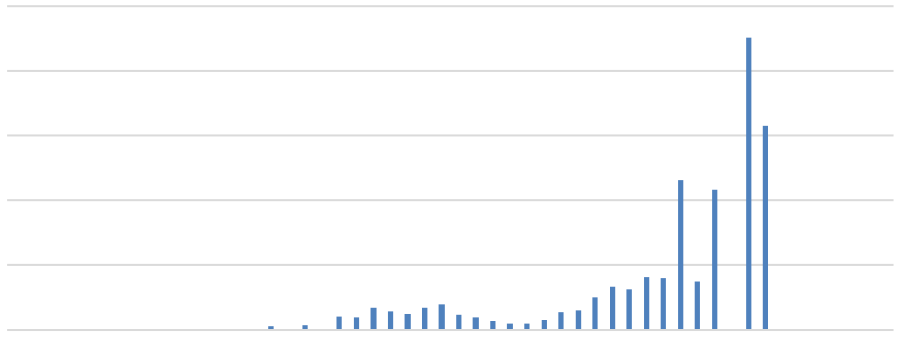
Figure 4.38. Droplet size distributions for blowout #2 at approximately 5 s after the start of the blowout and again after 10 min after blowout start.



ter

63215.5

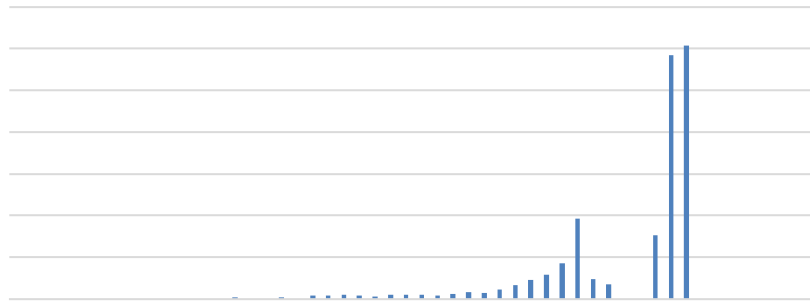
Figure 4.39. Droplet size distributions for blowout #2-2 at approximately 5 s after the start of the blowout and again after 10 min after blowout start.



released 161

Figure 4.40. Droplet size distributions for blowout #3 at approximately 5 s after the start of the blowout and again after 10 min after blowout start.

4.60



ter 64948.5

Figure 4.41. Droplet size distributions for blowout #3-2 at approximately 5 s after the start of the blowout and again after 10 min after blowout start.

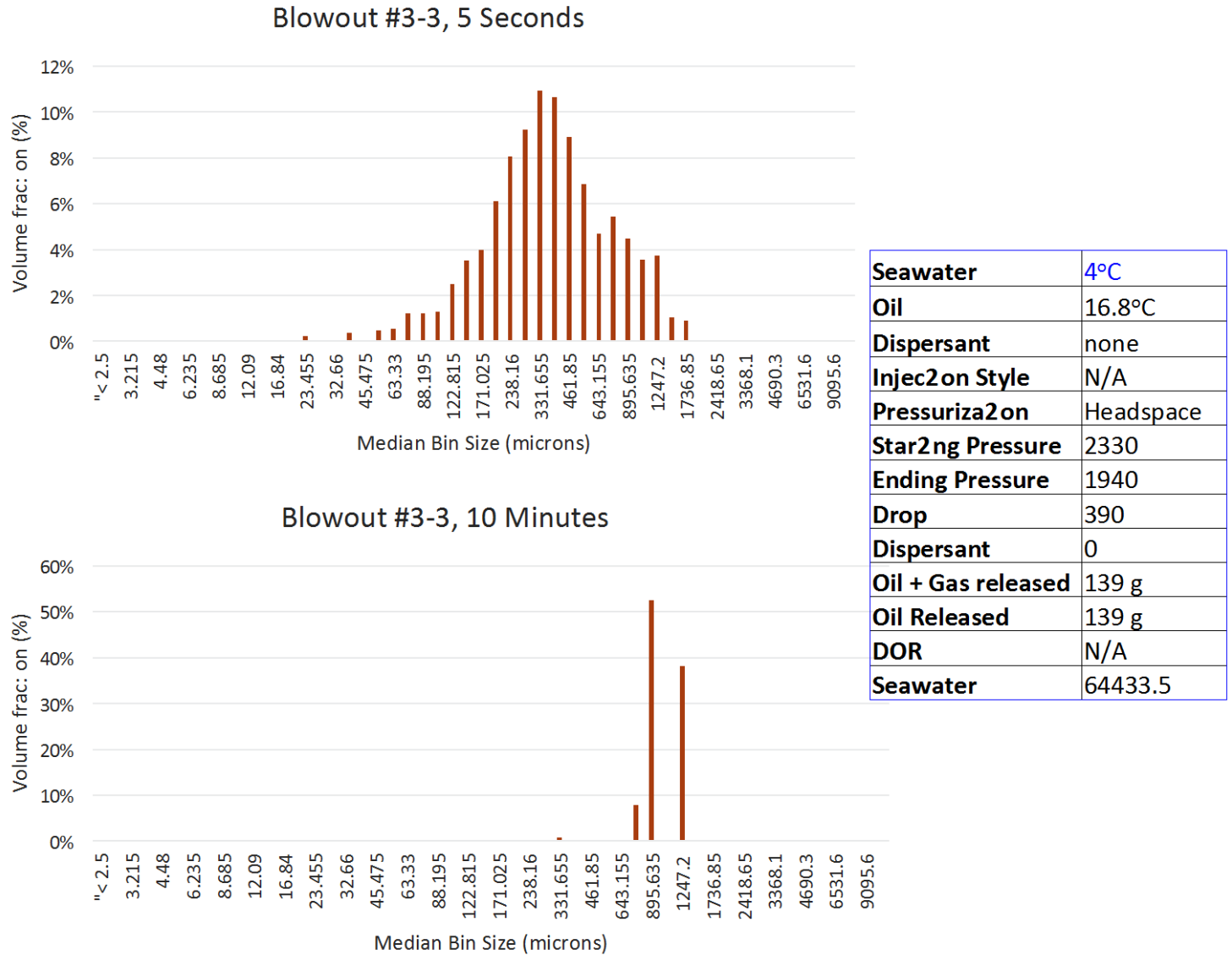


Figure 4.42. Droplet size distributions for blowout #3-3 at approximately 5 s after the start of the blowout and again after 10 min after blowout start.

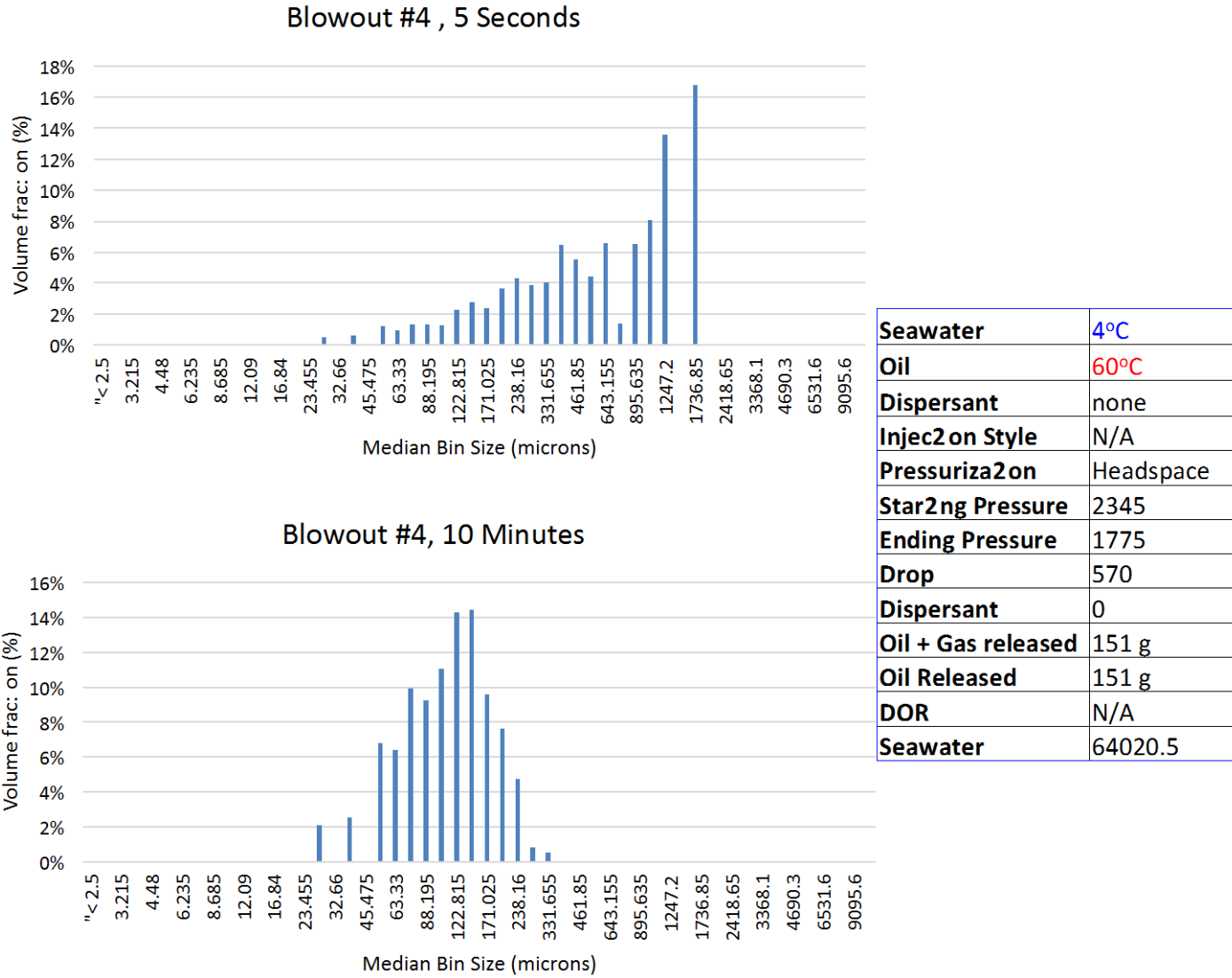


Figure 4.43. Droplet size distributions for blowout #4 at approximately 5 s after the start of the blowout and again after 10 min after blowout start.

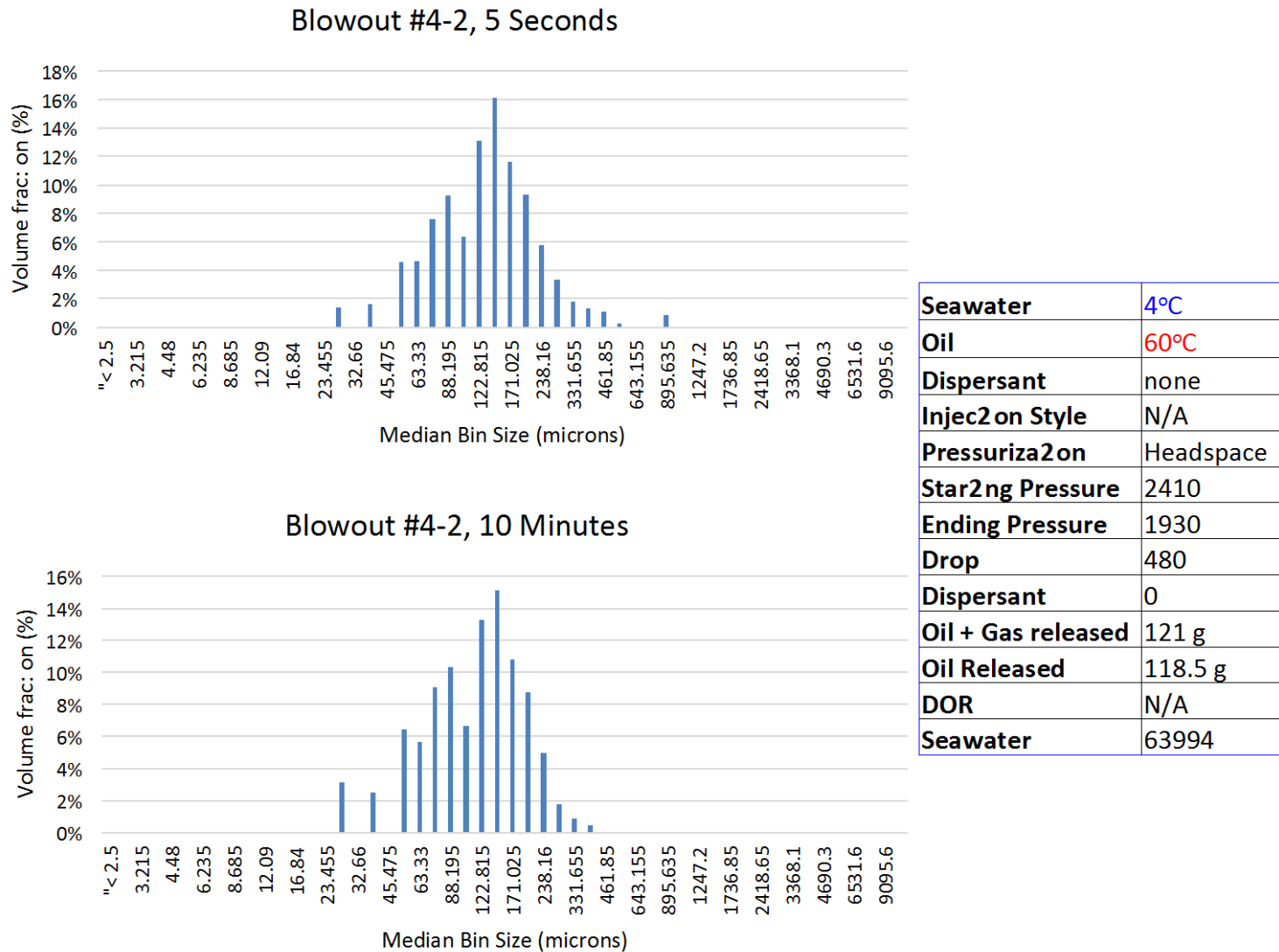
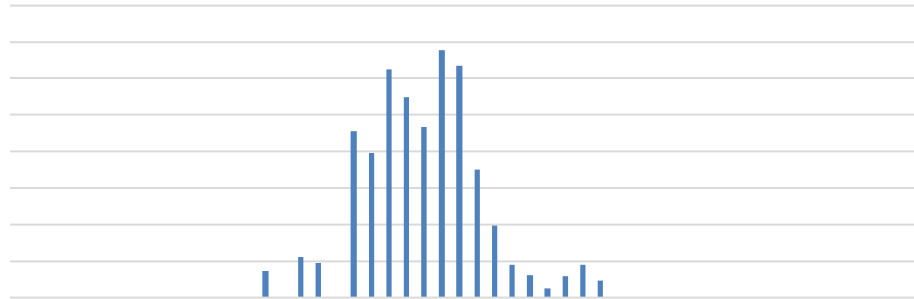


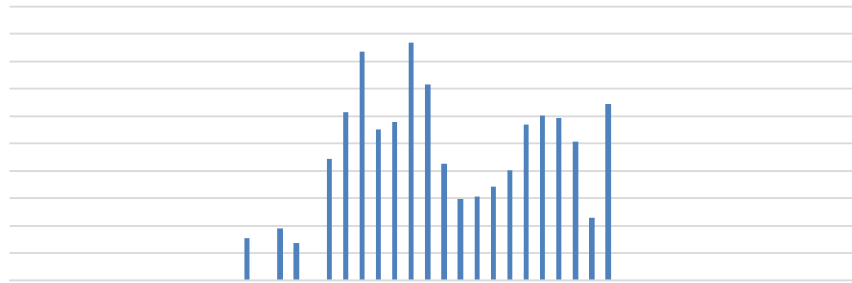
Figure 4.44. Droplet size distributions for blowout #4-2 at approximately 5 s after the start of the blowout and again after 10 min after blowout start.



Seawater

63106

Figure 4.45. Droplet size distributions for blowout #5 at approximately 5 s after the start of the blowout and again after 10 min after blowout start.



DOR

165 g*

Figure 4.46. Droplet size distributions for blowout #6 at approximately 5 s after the start of the blowout and again after 10 min after blowout start.

4.7 Explore the Effect of Sediments on Droplet Size

Organic and inorganic particles found in crude oil and the water column may have an impact on droplet size during a blowout. The formation of stable oil-particle-aggregates (OPAs) in coastal environments following a spill is well-documented (Fitzpatrick et al. 2015; Lee et al. 2003; Khelifa et al. 2002; Stoffyn-Egli 2002; Le Floch et al. 2002). This phenomenon is, however, typically noted with weathered oil, and in particular with oil that has sunk to the benthos. One important factor in the formation of these aggregates along the shoreline is turbulence, and the turbulent discharge of oil from a leaking well might promote the formation of aggregates.

The potential formation of OPAs during a deep ocean release would have important ramifications for the fate and transport of the oil. OPAs have a lower interfacial tension with water than does oil alone, and are thus less likely to coalesce (Lee 2002). OPAs also tend to have a higher specific gravity and to sink in water (Fitzpatrick et al. 2015). OPAs may form with a wide range of sediment and mineral types, or with phytoplankton, and will form when the concentration of sediment is as low as 100 mg sediment per liter of seawater (Fitzpatrick et al. 2015).

To examine the impact that particulates might have on freshly ejected (unweathered) oil, the initial plan was to mix sediments with crude oil samples to be ejected at high pressure into the seawater test tank. However, safety concerns arose about the potential for creating a blockage in the pressure lines. Instead, 200 μL of oil with and without 50 mg of fine sediment (diatomaceous earth) was added to 200 mL of seawater (1:1000 oil to water ratio) in 500 mL glass beakers, and mixing energy was provided by a magnetic stir bar at 240 rpm. The oil-sediment-seawater mix was agitated for 5 min, and then the mixing energy was stopped to allow for photography (within a few seconds of stopping) and particle size determination. Photos of the water surface and potential oil slick formation were taken after 2–3 min without mixing. Mixing was restored and then 4 μL of Corexit 9500 was added to each beaker to achieve a DOR of 1:50. Mixing continued for 5 min at which point a second set of photographs were taken. Mixing was again restored and an additional 4 μL of Corexit was added to achieve a DOR of 1:25. A control flask with the sediment remained turbid when mixing ceased; a large portion of the diatom frustules are of low enough density to remain suspended for at least a few minutes without active mixing and would have a rapid impact on causing an adhered portion of the oil to rise or sink in the water column.

The results (Table 4.13 and Figures 4.47 through 4.49) show that prior to the addition of the dispersant, samples with and without sediment had a fairly similar droplet size distribution in the smaller bin sizes, but the sample with no sediment had larger droplets representing a significant fraction of the total volume. With the addition of Corexit at a DOR of 1:50, however, the samples with sediment had a distinctly lower size distribution with a maximum diameter of 62 μm , while the sample without sediment had droplets with a maximum diameter of 359 μm . Similarly, the mode median diameter (representing a large fraction of the total volume of oil) of the sediment containing sample was 12 μm , while that of the sample without sediment was 202 μm . With a DOR of 1:25, the sediment sample had a bimodal distribution with larger droplets, up to 160 μm , while the sediment-free sample still had larger droplets of up to 257 μm and a more even distribution (not including the largest bin size). Droplet sizes in the 10 to 20 μm range may be associated with the diatomaceous earth, whose particles fell in that size range. The smaller sizes may be due to oil associating with the diatom frustules to form OPAs, or perhaps due to some physical action in the mixing in which the diatom frustules “bombard” and break apart the droplets. Photographs of the beakers (Figure 4.50 and Figure 4.51) show that the stir bar in the beaker with the sediment was much cleaner than the stir bar in the beaker without sediment, which had a very apparent coating of oil. However, images of the water surface taken a few minutes after the mixing was stopped showed that in

the absence of sediment, much of the oil with dispersant remained in suspension and did not readily form a slick. In the presence of sediment, the water column remained an orange-tinted turbid color, but oil droplets began to aggregate at the surface to form a slick. This would appear to fit the bimodal distribution with the larger droplets rising to the surface, but it was surprising that the largest droplets in the sediment mix were ~40% smaller than the largest droplets in the flask without sediment.

Table 4.13. Summary of droplet size data (mm).

Minimum Diameter			Maximum Diameter		
Treatment	Without Sediment	With Sediment	Treatment	Without Sediment	With Sediment
No Corexit	0.01045	0.01022	No Corexit	0.25231	0.12866
1:50 DOR	0.01045	0.01022	1:50 DOR	0.35860	0.06180
1:25 DOR	0.01057	0.01033	1:25 DOR	0.25731	0.15958

Mean Diameter			Mode Median Bin Diameter		
Treatment	Without Sediment	With Sediment	Treatment	Without Sediment	With Sediment
No Corexit	0.01264	0.01285	No Corexit	0.23816	0.01245
1:50 DOR	0.01869	0.01233	1:50 DOR	0.20182	0.01245
1:25 DOR	0.01426	0.01193	1:25 DOR	0.23816	0.14493

Geometric Mean		
Treatment	Without Sediment	With Sediment
No Corexit	0.01210	0.01222
1:50 DOR	0.01438	0.01186
1:25 DOR	0.01313	0.01156

While this study demonstrated that sediments entrained in oil during a blowout can alter droplet size distributions when compared to oil without sediment, the results are based upon a single sediment type. The experiments used diatomaceous earth, a silicate, with particles ranging from 10 to 20 μm in diameter. Further studies might examine particles of varying sizes and compositions, including carbonates, other silicates, organic particles, and mixtures. Crude oil adheres to virtually any surface, but may preferentially adhere to other sediment types. Intact diatom frustules are hollow and have a low density compared with solid silicates or other mineral types. The frustules also have very intricate nano-scale surface features that could potentially increase or decrease oil adsorption and retention. Both the chemistry and surface structure of sediment particles would likely affect the formation of OPAs during blowouts. The density of the sediment would also likely affect the migration of the oil.

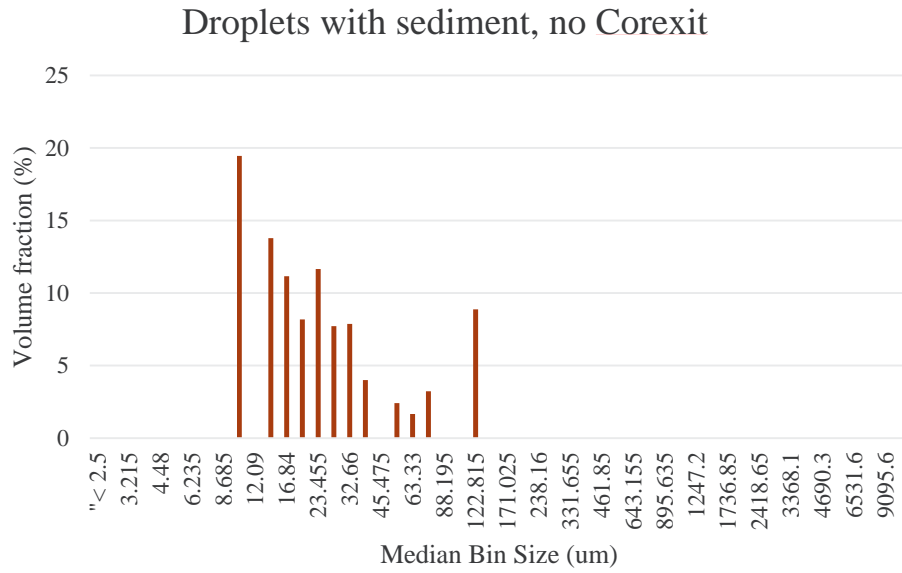
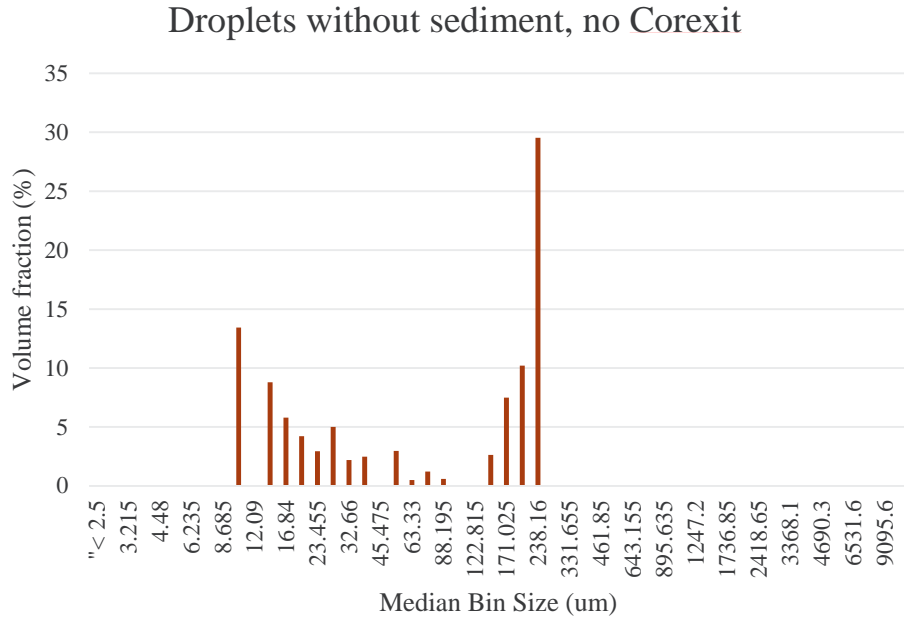


Figure 4.47. Size distributions for samples with and without sediment and no dispersant.

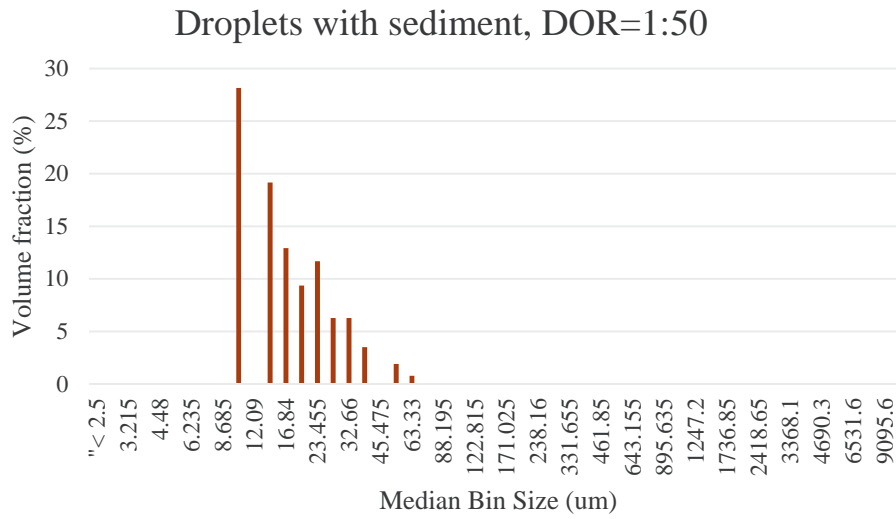
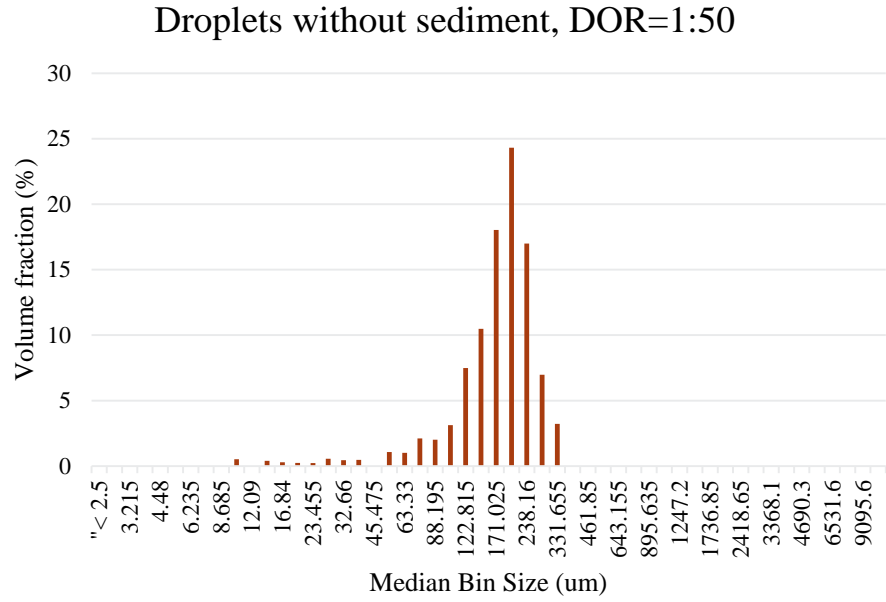


Figure 4.48. Size distributions for samples with and without sediment and a DOR of 1:50.

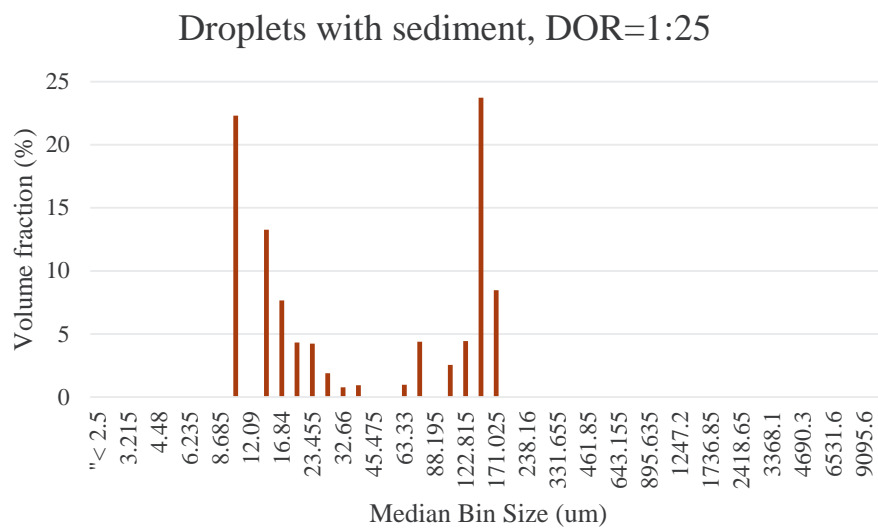
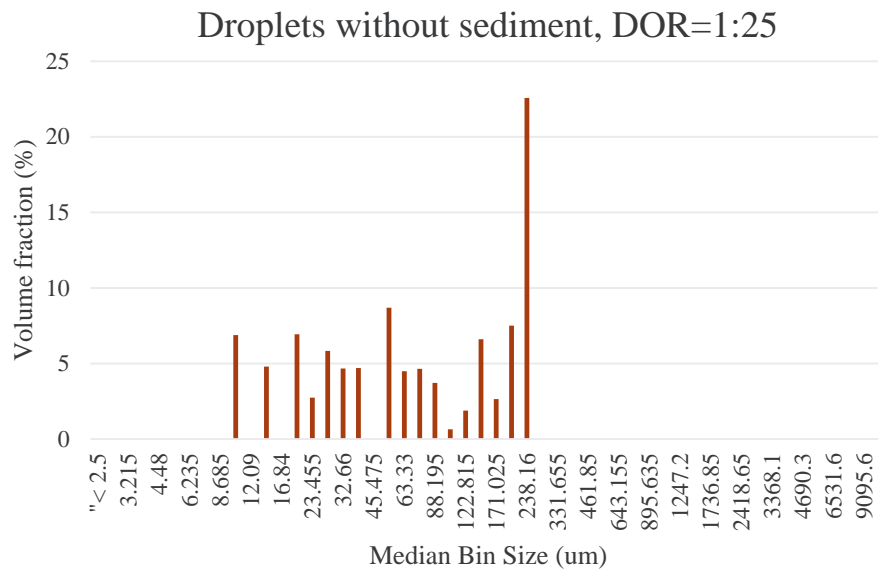


Figure 4.49. Size distributions for samples with and without sediment and a DOR of 1:25.

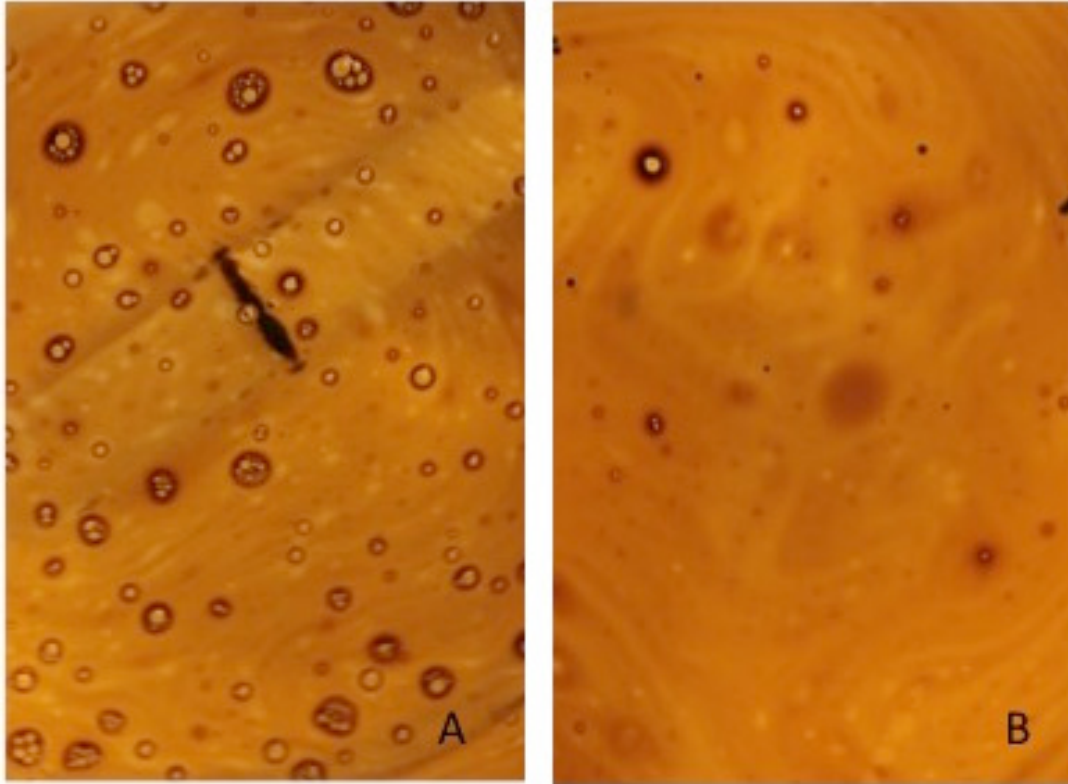


Figure 4.50. Oil suspensions without sediment (A) and with sediment (B) after mixing but prior to the addition of Corexit. The stir bar in the flask without sediment became coated with oil and remained coated even after the addition of Corexit.

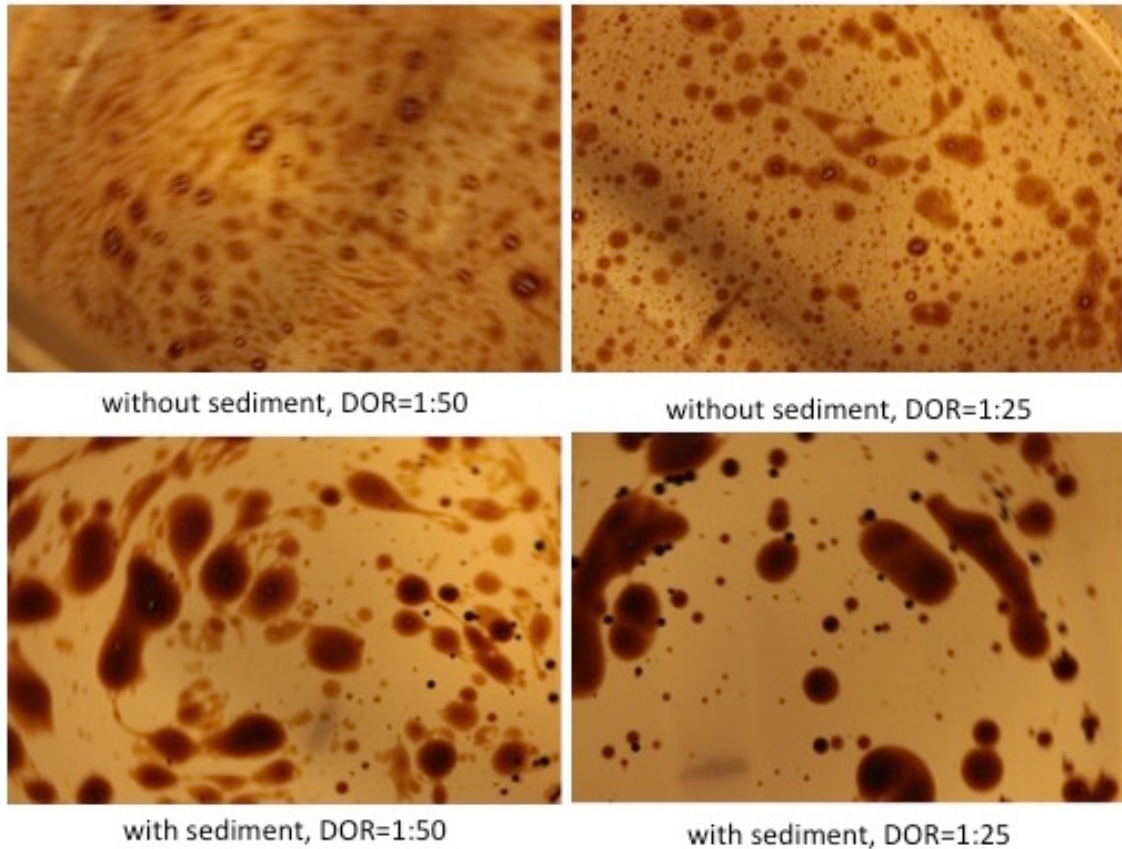


Figure 4.51. Surface expression of oil without sediment (top) and with sediment (bottom) after the addition of dispersant.

4.8 Update BLOSOM (Blowout and Spill Occurrence Model) to Incorporate Dispersant Effects on Droplet Size Distributions

Numerical simulations are a critical part of scientific progress when complicated natural systems are studied, along with observations at field and measurements in controlled laboratory conditions. Simulations allow for the testing of hypotheses that cannot be tested in laboratories. Likewise, the comprehensive information in space and time obtained as a numerical solution is simply not possible in real-life conditions. These realities have long motivated the development and testing of numerical models and will continue to do so into the foreseeable future.

Numerical models are complicated enough that they present several challenges of their own. While verification, validation, and confirmation of numerical models of natural systems is impossible (Oreskes et al. 1994), their evaluation is fundamentally important (Oreskes et al. 1998). Testing a model is critical to making sure that it model is behaving as expected. It also is important to test a model’s validity, in particular to avoid a misleading sense of truth that may arise from not paying due attention to the limitations that are inherent to all models (Sterman 2994).

As part of this study, the numerical BLOSOM was upgraded to simulate the addition of dispersants at depth during a blowout—a scenario that was first experienced during the Deepwater Horizon accident. During the time of the accident, different models were used to track oil at the sea surface to support policy decisions and emergency response planning and implementation. However, no model was readily

accessible at that time to help evaluate the consequences *a priori*, or to help guide the process during the administration of dispersants. Experiments, observational campaigns, and the development of models have resulted in enough progress in our understanding of complicated deep sea blowouts that we can now begin to simulate the application of dispersants during a blowout event. This effort—one of the first of its kind—implements a dispersant module in BLOSOM and presents some simulations highlighting its capabilities and limitations. As mentioned above, understanding the capabilities and limitations of any model is an important part of the progress made toward using them efficiently in policy and scientific applications.

At the beginning of this effort, BLOSOM already computed a droplet size distribution (DSD) as described by Johansen (2003). The construction of BLOSOM’s dispersant module began with the addition of the DSD proposed by Johansen et al. (2013; Figure 4.52). Two versions of the Johansen et al. (2013) distribution were added to BLOSOM: the original formulation as proposed in the 2013 paper and a variant of the droplet distribution with corrected coefficient values as outlined by Brandvik et al. (2014). These updated coefficients were described as preliminary in the Scope of Work. With the addition of the updated coefficients, BLOSOM provides the capability for comparing the original and updated versions, and other DSDs.

Some proprietary oil-spill models are able to simulate the addition of dispersants at depth (e.g., OSCAR, MIKE and OILMAP), while freely distributed models are only able to include the use of dispersants at the sea surface. Thus, to the best of our knowledge, BLOSOM is the only open-source blowout and oil-spill model capable of simulating the addition of dispersants at depth. The depth should only be limited by the bathymetry and ocean model data that is provided.

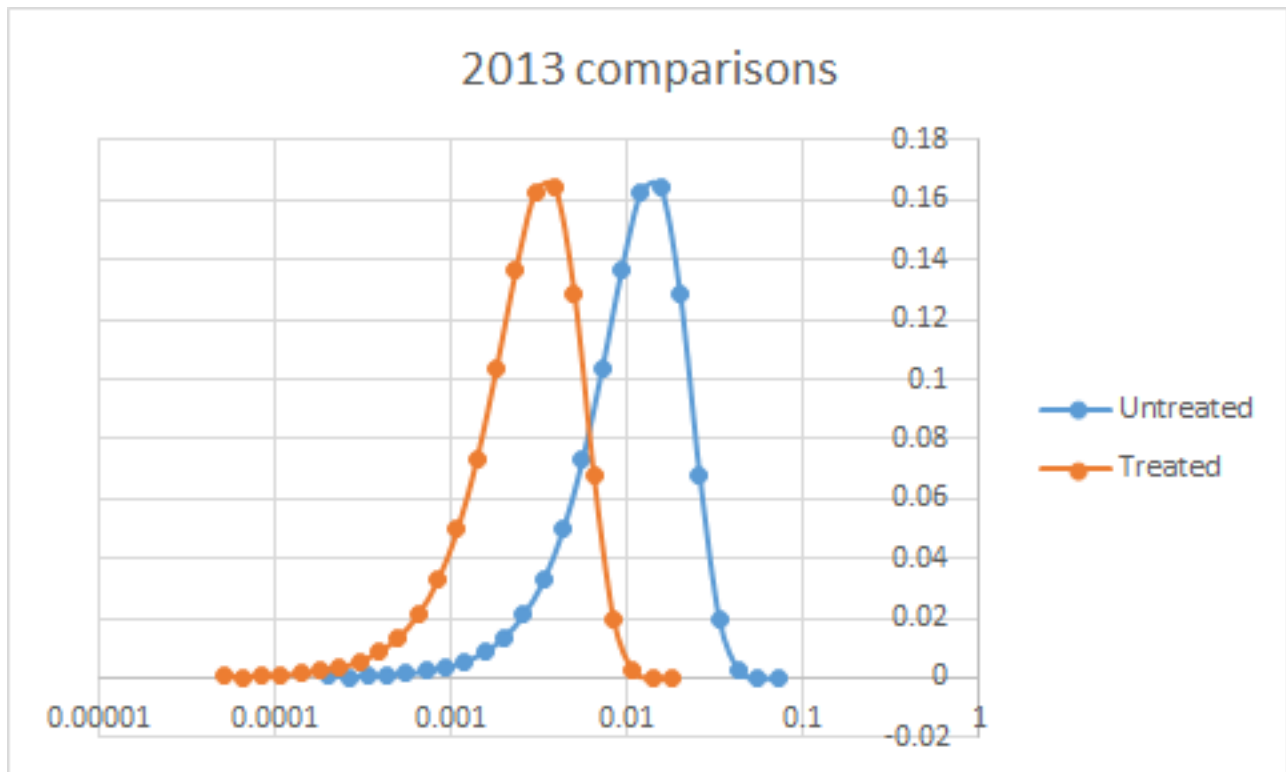


Figure 4.52. Johansen et al (2013) distributions for oil droplet size (ordinate, fraction mass) as a function of droplet size (abscissa, microns) as computed by BLOSOM internally.

BLOSOM requires a minimum droplet size value to be supplied and this functionality was already present in the original model; however, an optional upper boundary on droplet size was also added as a user argument. Two preset droplet size ranges, one preset representing droplet sizes in the presence of dispersants and another representing sizes in the absence of dispersants, were also added. The values used for the presets were taken from Johansen et al. (2013).¹⁷ A separate option was added to BLOSOM's settings to allow users to select which droplet model to use to initiate the simulation.

In addition to adding the option to select the Johansen 2013 DSD, steps were taken to further enhance BLOSOM's dispersant module. To simulate the effectiveness of dispersant application, an efficiency coefficient needs to be present, as well as two DSDs: one to apply to untreated oil and one to apply to treated oil. For the efficiency coefficient, users can supply their own value, or it can be derived from relationships extracted from the literature (see findings below in Section 4.8.1.4). The capability to specify a second DSD for treated oil and an efficiency value were both added to BLOSOM. Explicit spatiality was introduced by allowing the user to specify regions of dispersant influence—as a circle on the surface (simulating surface application) or as a sphere below the surface (simulating subsurface application). Any spill parcel or jet/plume control volume that intersects a dispersant application region may be marked as having been treated, modifying the DSD according to the selected treated DSD and efficiency value.

Several simulations were carried out to compare the PNNL experimental DSDs to those derived from literature that have been implemented as part of BLOSOM. A series of BLOSOM simulations were carried out: two for each DSD built into BLOSOM and each experimental DSD provided by the PNNL experiments. Each DSD was tested under static ambient conditions (i.e., with no ocean currents or wind), as well as with hydrodynamic ocean model data derived from the NCOM-AmSeas model for the simulated period from May 20, 2010 through July 19, 2010 on 6 hr intervals. For each simulation in the constant and hydrodynamic categories, only the selected DSD and droplet size boundaries varied according to the input information.

The PNNL experiments fall into two main categories: oil at 16.8°C and 60°C. Within each category, DSD from blowouts with dispersant and DSD from blowouts without dispersant were calculated (Figure 4.53 and Figure 4.54). Table 4.14 includes the main experimental characteristics of each blowout.

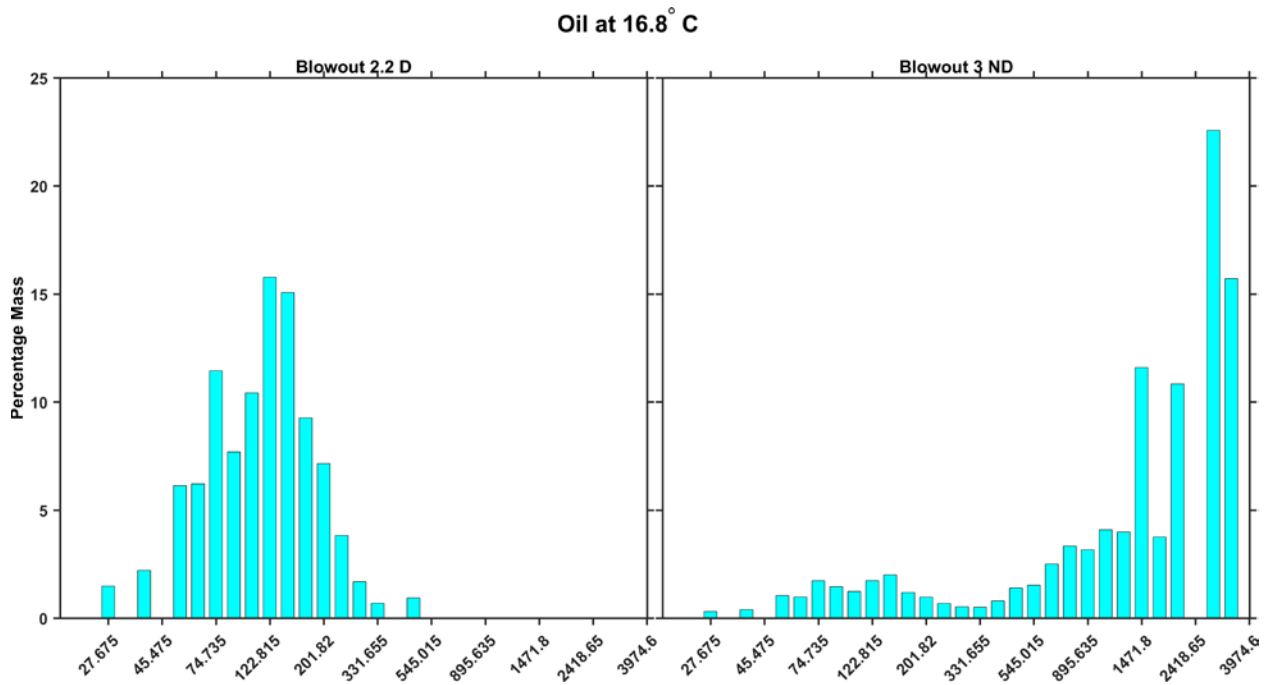


Figure 4.53. Droplet size distributions (fraction mas, ordinate) as a function of droplet size (abcissa, microns) for experiments using oil at 16.8°C with application of dispersant (D, left panel) and without dispersant (ND, right panel). The details for each experiment can be seen in Table 4.14.

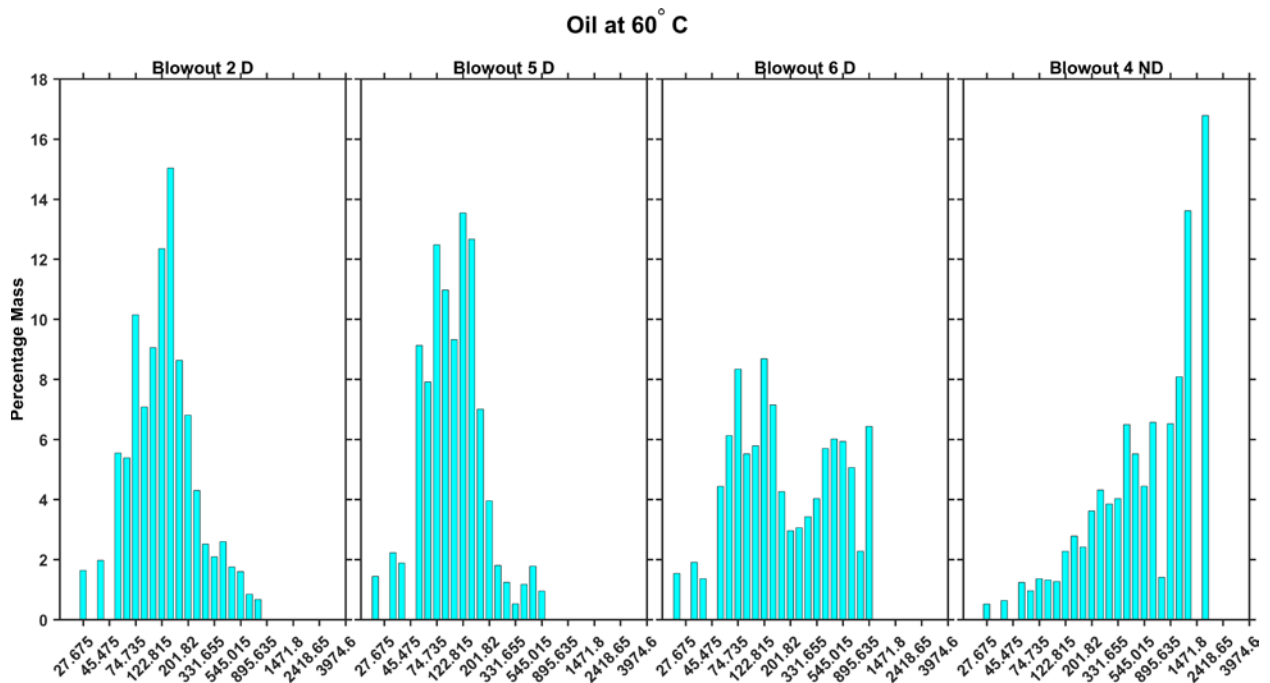


Figure 4.54. Droplet size distributions (fraction mas, ordinate) for blowouts with oil at 60°C as a function of droplet size (abcissa, microns). The three panels on the left are for distributions using the application of dispersant, and the distribution on the right is under comparable conditions but with no application of dispersants. The details for each experiment can be seen in Table 4.14.

Table 4.14. Experimental setup for each blowout.^(a)

Blowout number	2	2.2	3	4	4.2	5	6
Seawater Temp	4°C	4°C	4°C	4°C	4°C	4°C	4°C
Oil Temp	60°C	16.8°C	16.8°C	60°C	60°C	60°C	60°C
Dispersant Temp	60°C	16.8°C	none	none	none	4°C	60°C
Injection Style	premixed	premixed	NA	NA	NA	Coinjection	Coinjection
Pressurization	Headspace	Headspace	in oil	Headspace	Headspace	Headspace	Headspace
Starting Pressure	2370	2300	2390	2345	2410	2300	2370 psi
Ending Pressure	1705	1950	1920	1775	1930	1850	1705 psi
Drop	665	450	470	570	480	410	665 psi
Dispersant	1.575	1.32	0	0	0	2.13 g	1.43 g
Oil + Gas released	165	132	161	151 g	121 g	131.5 g	157.5 g
Oil Released	157.5	132	161	151 g	118.5 g	128 g	165 g
DOR	1:100	1:100	NA	NA	NA	1:60	1:110
Seawater	62013.5	63215.5	64519	64020.5	63994	63106	62014.5

(a) Blue (4°C) and red (60°C) font is used for ease of identifying temperature combinations

NA = not applicable.

The oil temperature did not seem to have a strong effect on the droplet distribution; the DSDs for blowouts without dispersant (Figure 4.55) and with dispersant (Figure 4.56) were similar. Therefore, two distributions were enough to represent the DSDs for when no dispersant is applied (blowout 3 was used for this case) and for when dispersant is applied (blowout 2.2 was used for this case). By plotting these two representative distributions together, the effect of the dispersant can be evaluated (Figure 4.57).

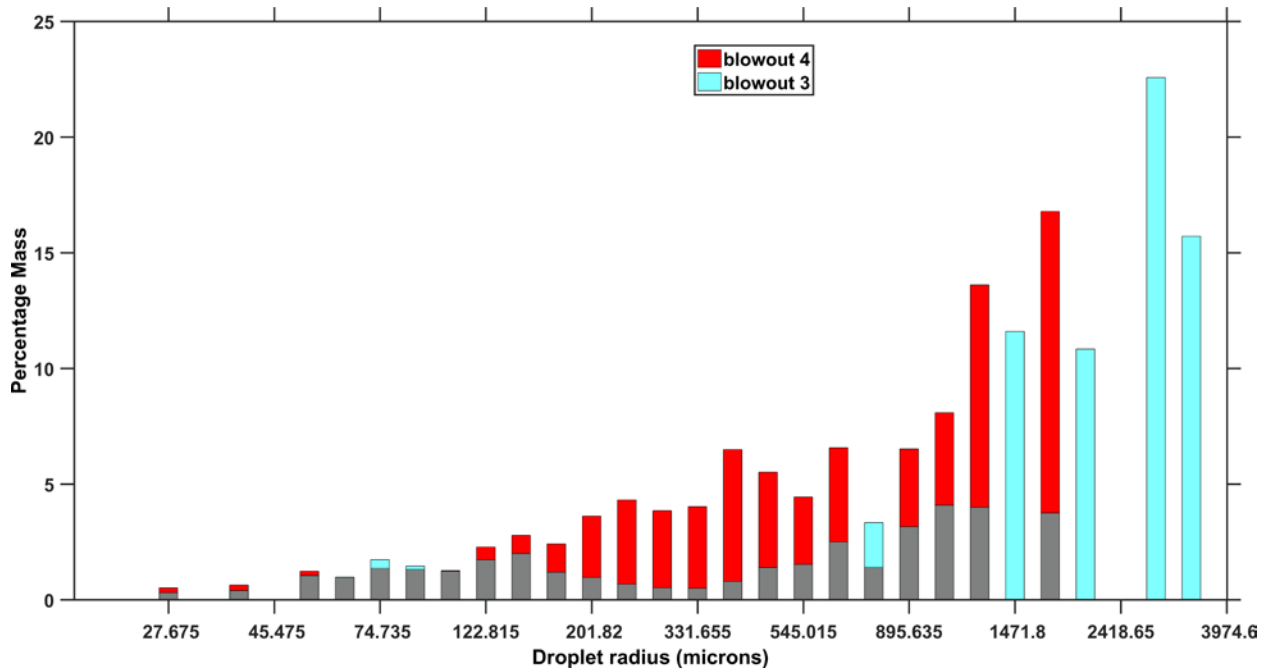


Figure 4.55. Normalized droplet size distribution (fraction mas, ordinate) as a function of droplet size (abscissa, microns) for two experiments (blowouts 3 and 4) without any dispersant applied. Gray indicates the intersection of the two distributions.

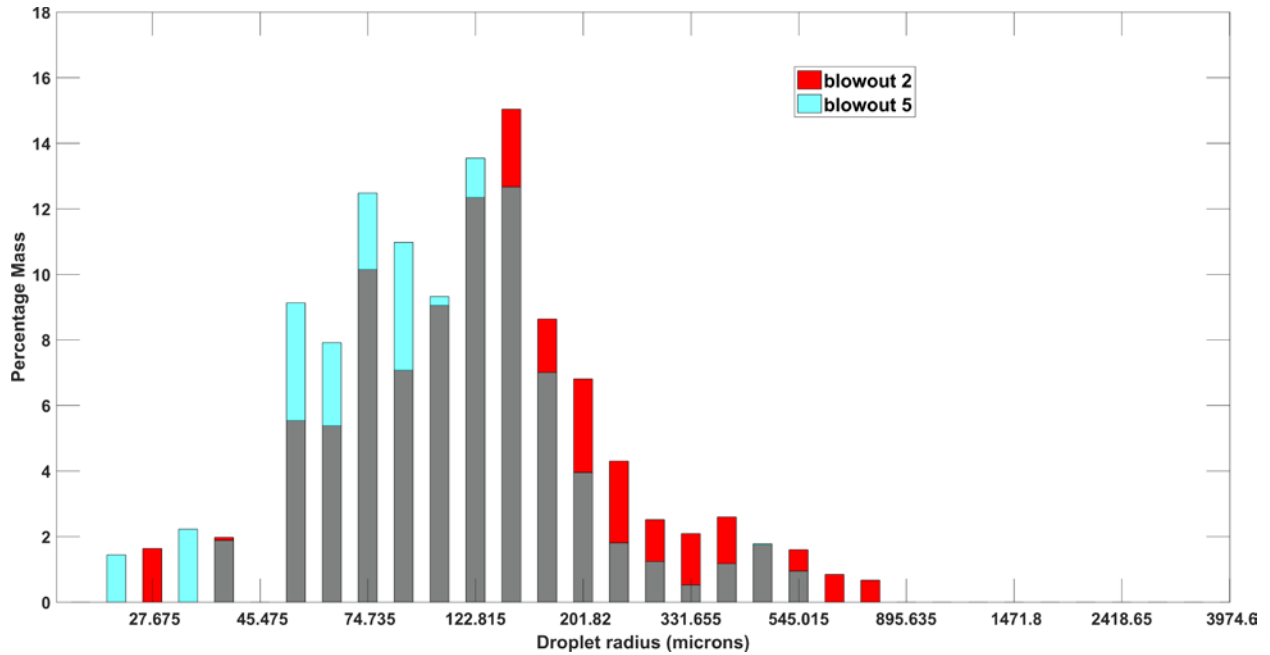


Figure 4.56. Normalized droplet size distribution (fraction mas, ordinate) as a function of droplet size (abscissa, microns) for two experiments (blowouts 2 and 5) with dispersant applied. Gray indicates the intersection of the two distributions.

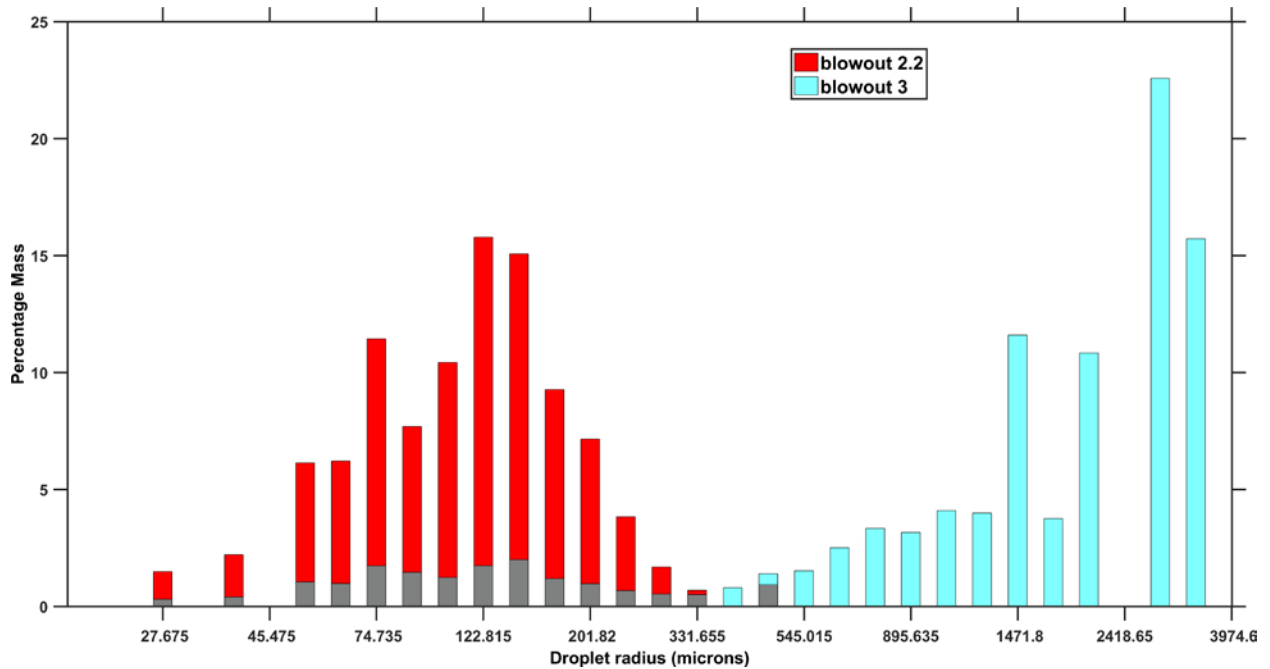


Figure 4.57. Droplet size distribution (fraction mas, ordinate) as a function of droplet size (abscissa, microns) for the blowout without dispersant (cyan) and the blowout with dispersant (red) used for BLOSOM simulations. Gray indicates the intersection of the two distributions.

The viscosity of oil has a strong effect on the effectiveness of applied dispersant; specifically, the more viscous the oil, the less effective dispersant application will be (ITOPF 2011). Viscosity can be seen as a measure of mechanical resistance to mechanical breakup, and how readily a body of oil breaks into

smaller droplets under mechanical stress (ITOPF 2011). Because BLOSOM tracks the viscosity of simulated crude oil, it can be used as a proxy of the efficiency of applied dispersant. This relationship is explored through literature research.

4.8.1 Results: Numerical Simulations

Numerical simulations were conducted for static and hydrodynamic conditions.

4.8.1.1 Static Conditions

The output from BLOSOM simulations using constant ambient conditions was used to confirm that the distributions of droplet sizes when using the J2013 (Figure 4.58) and PNNL2017 (Figure 4.59) distributions agreed with the distributions obtained in the corresponding studies (Figure 4.52 and Figure 4.57, respectively). When oil is treated with dispersant, the PNNL2017 droplet radii range between about 20 and 250 μm , while the treated J2013 distribution ranges between 50 and 1800 μm (red bars in Figures 4.58 and Figure 4.59). When oil was not treated with dispersant, PNNL2017 ranged between 13 and 1700 μm , while J2013 ranged between 200 and 72,000 μm (cyan bars in Figure 4.58 and Figure 4.59).

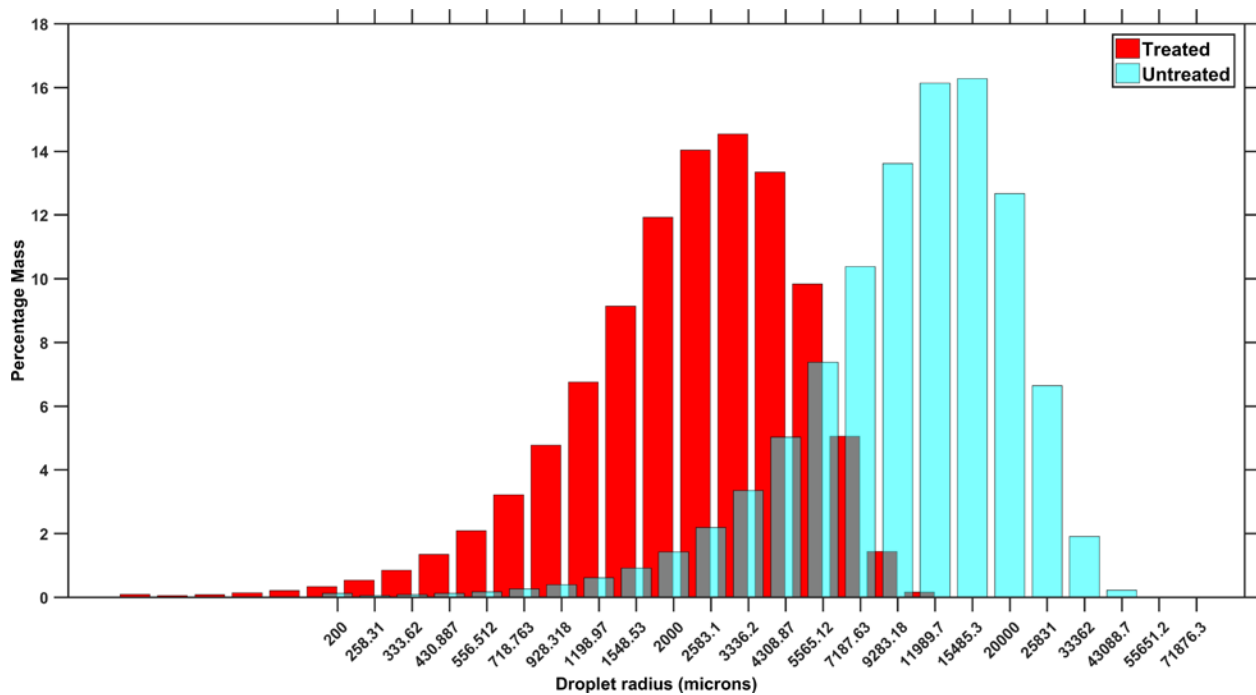


Figure 4.58. Droplet size distributions from Johansen et al. (2013) as implemented in BLOSOM for both dispersant-treated and untreated oil.

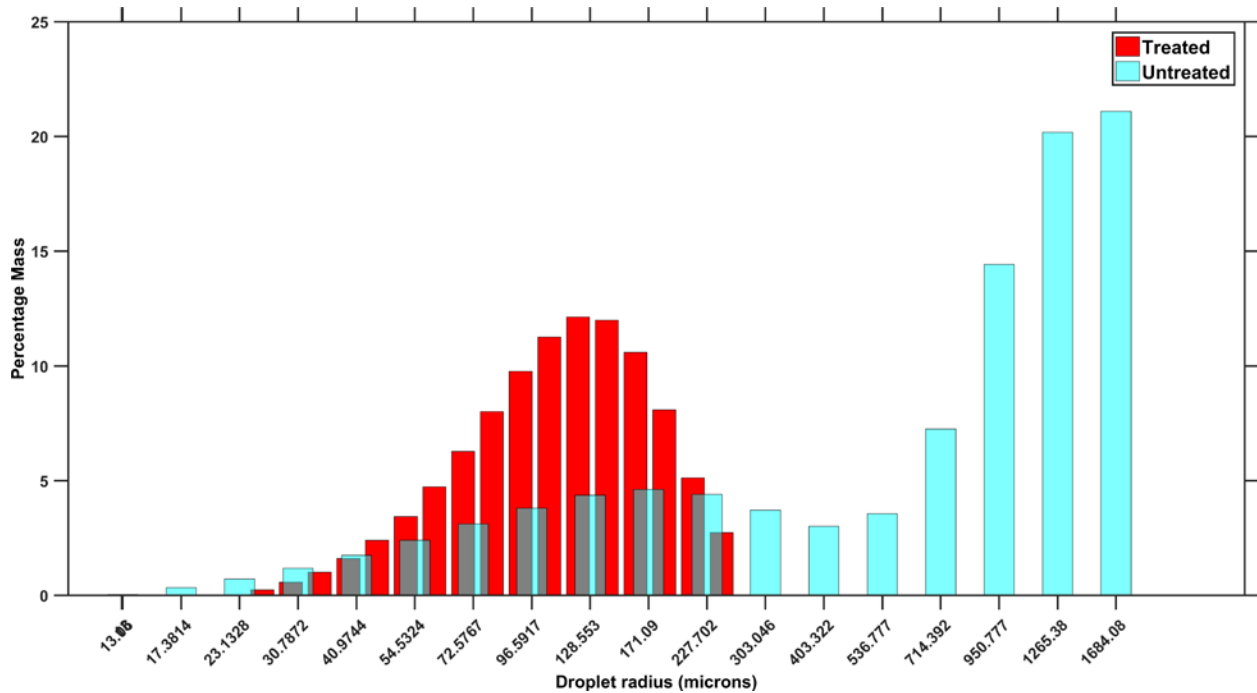


Figure 4.59. The droplet size distributions from the experimentally derived observations, as implemented in BLOSOM. Both dispersant-treated and untreated oil droplets are represented.

4.8.1.2 Hydrodynamic Conditions

When the output from a numerical ocean model is included, a realistic simulation of a deep blowout becomes possible. For this purpose, output from the Navy Coastal Ocean Model (NCOM) simulating ocean currents during the Deepwater Horizon event (May 20–July 18, 2010) was used.

Figure 4.60, Figure 4.61, Figure 4.62, and Figure 4.63 show the final outcomes for simulations using the J2013 distribution with untreated droplet sizes, the J2013 distribution using treated droplet sizes, the PNNL2017 untreated distribution and droplet sizes, and the PNNL2017 treated distribution and droplet sizes, respectively. As can be seen in the figures, a much greater amount of oil reached the surface in the J2013 simulations (Figure 4.60 and Figure 4.61), while the PNNL2017 simulations (Figure 4.62 and Figure 4.63) produced a much sparser surface slick. This discrepancy can be attributed to the fact that the PNNL2017 distributions produce droplet sizes that are roughly an order of magnitude smaller than those from the J2013 simulations. Both the dispersant-treated simulations (Figure 4.61 and Figure 4.63) show a larger concentration of oil below the water surface than their untreated counterparts (Figure 4.60 and Figure 4.62). This is expected, because dispersants reduce the size of droplets in an oil plume to a point at which they will stay suspended in the water column, thereby increasing the likelihood of colliding with the ocean floor (Johansen et al. 2013; McNutt et al. 2012).

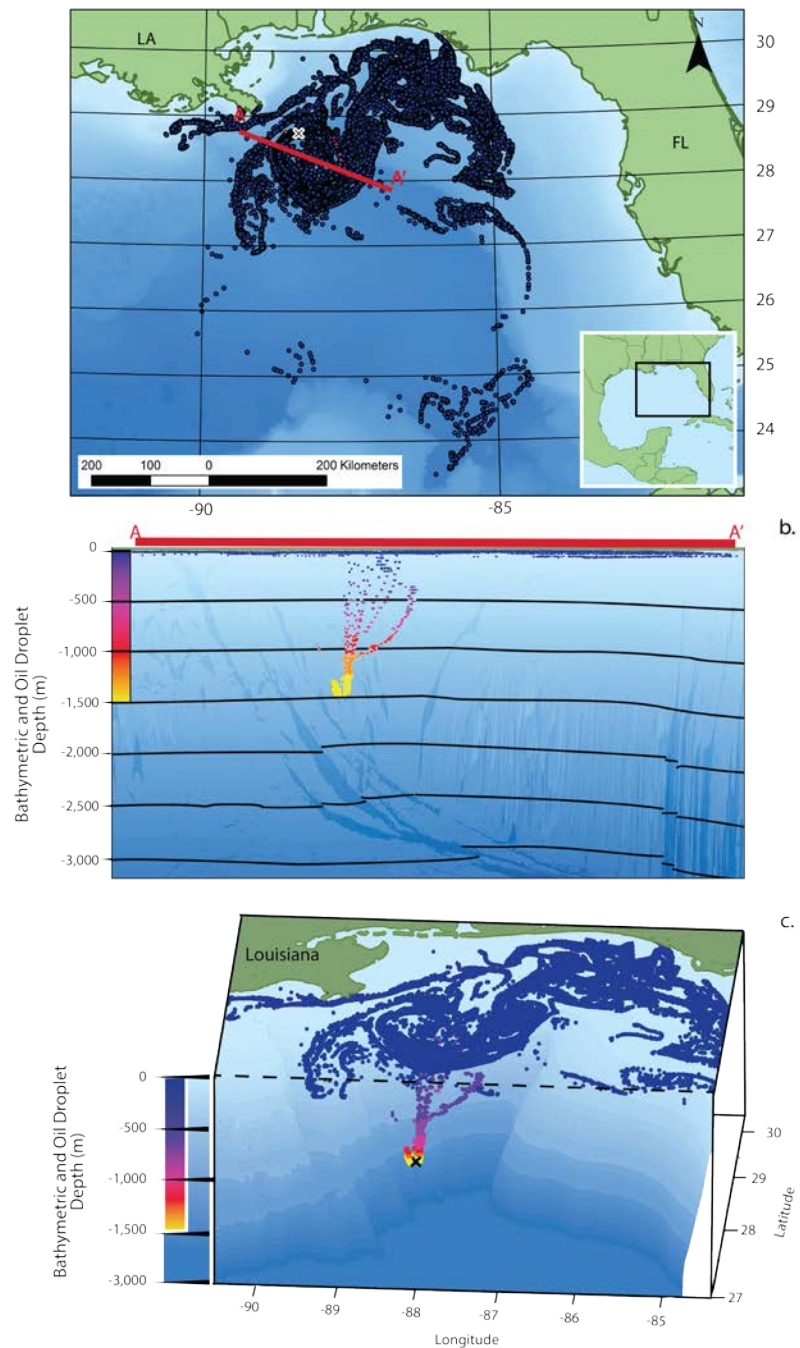


Figure 4.60. Oil blowout as simulated with BLOSOM after a 30-day simulation using the distribution from Johansen et al. (2013) for untreated droplet sizes.¹⁷ a) Plan view of the blowout at the sea-surface after a 30-day simulation originating at the Macondo Well initialized on May 2010 using realistic hydrodynamic conditions as simulated by NCOM, and using the J2013 distribution for oil not treated with dispersant. The red line indicates the location of a vertical cross-section. b) Vertical cross-section along the red line in panel a) showing the distribution as a function of depth (ordinate). The color scale indicates the depth of each droplet. c) Three-dimensional view of the blowout shown in panels a) and b), the color again indicates the depth of the droplet.

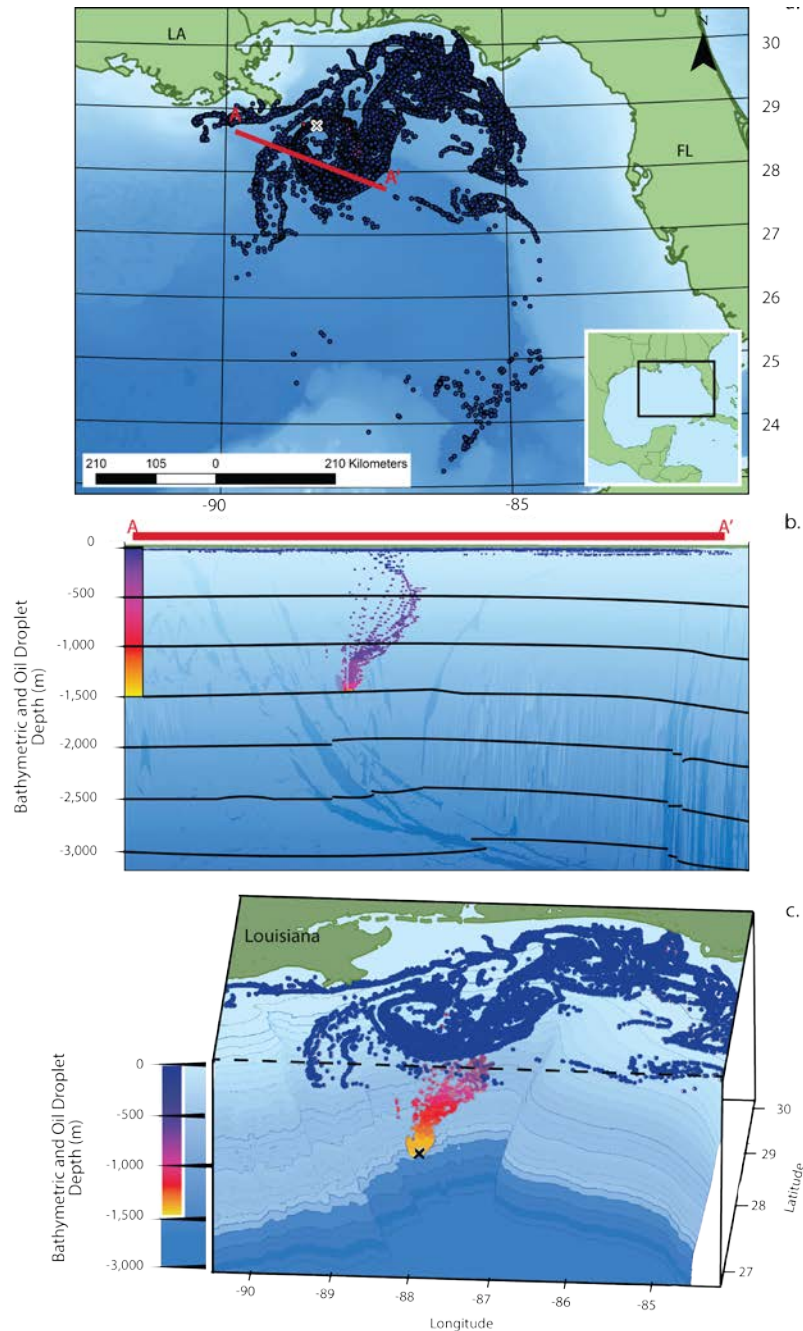


Figure 4.61. Oil blowout as a function of longitude, latitude, and depth, after a 30-day simulation with BLOSOM, using the distribution from Johansen et al. (2013) for treated droplet sizes.¹⁷ a) Plan view of the blowout at the sea-surface after a 30-day simulation originating at the Macondo Well initialized on May 2010 using realistic hydrodynamic conditions as simulated by NCOM, and using the J2013 distribution for oil treated with dispersant. The red line indicates the location of a vertical cross-section. b) Vertical cross-section along the red line in panel a) showing the distribution as a function of depth (ordinate). The color scale indicates the depth of each droplet. c) Three-dimensional view of the blowout shown in panels a) and b), the color again indicates the depth of the droplet.

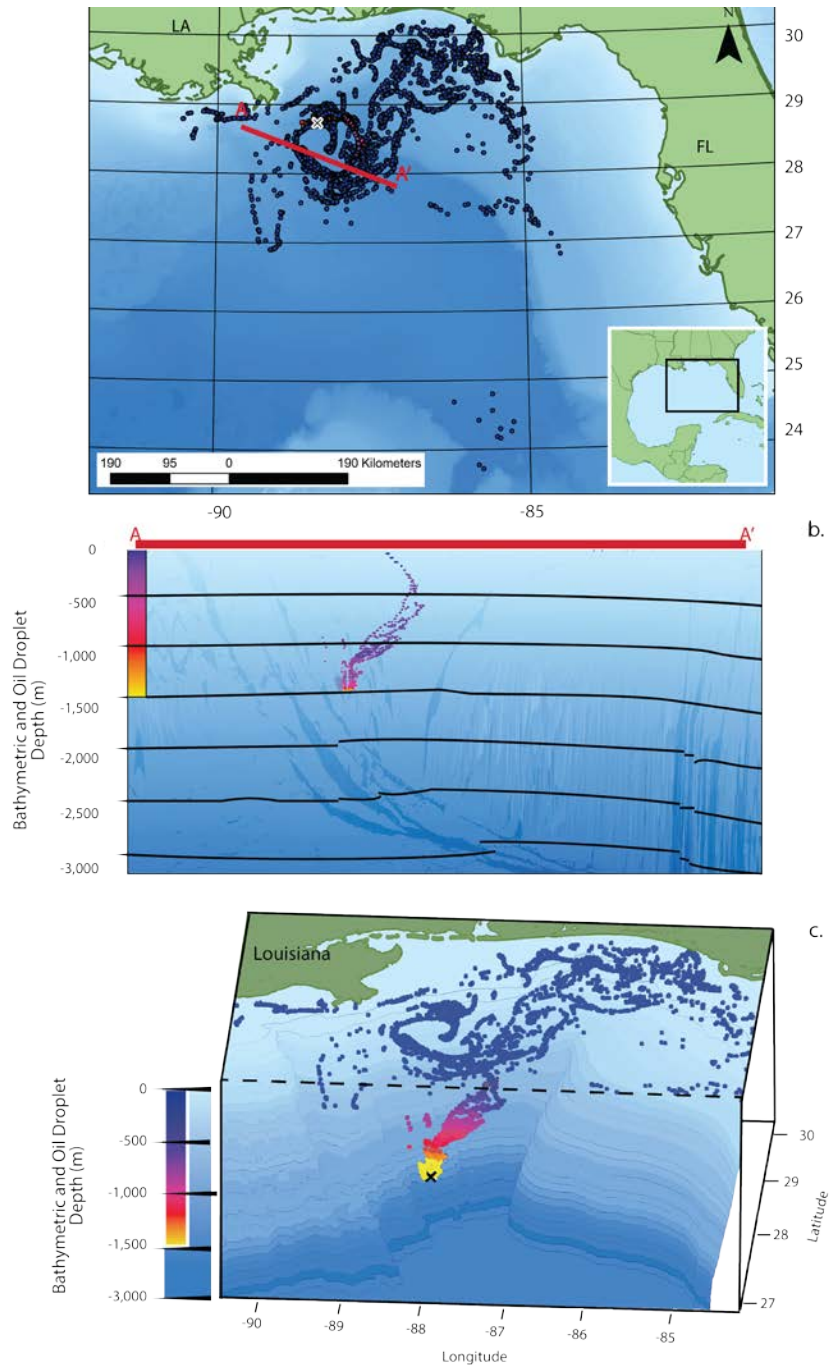


Figure 4.62. Oil blowout as simulated with BLOSOM after a 30-day simulation using the distribution from PNNL for untreated droplet sizes. a) Plan view of the blowout at the sea-surface after a 30-day simulation originating at the Macondo Well initialized on May 2010 using realistic hydrodynamic conditions as simulated by NCOM, and using the PNNL distribution for oil not treated with dispersant. The red line indicates the location of a vertical cross-section. b) Vertical cross-section along the red line in panel a) showing the distribution as a function of depth (ordinate). The color scale indicates the depth of each droplet. c) Three-dimensional view of the blowout shown in panels a) and b), the color again indicates the depth of the droplet.

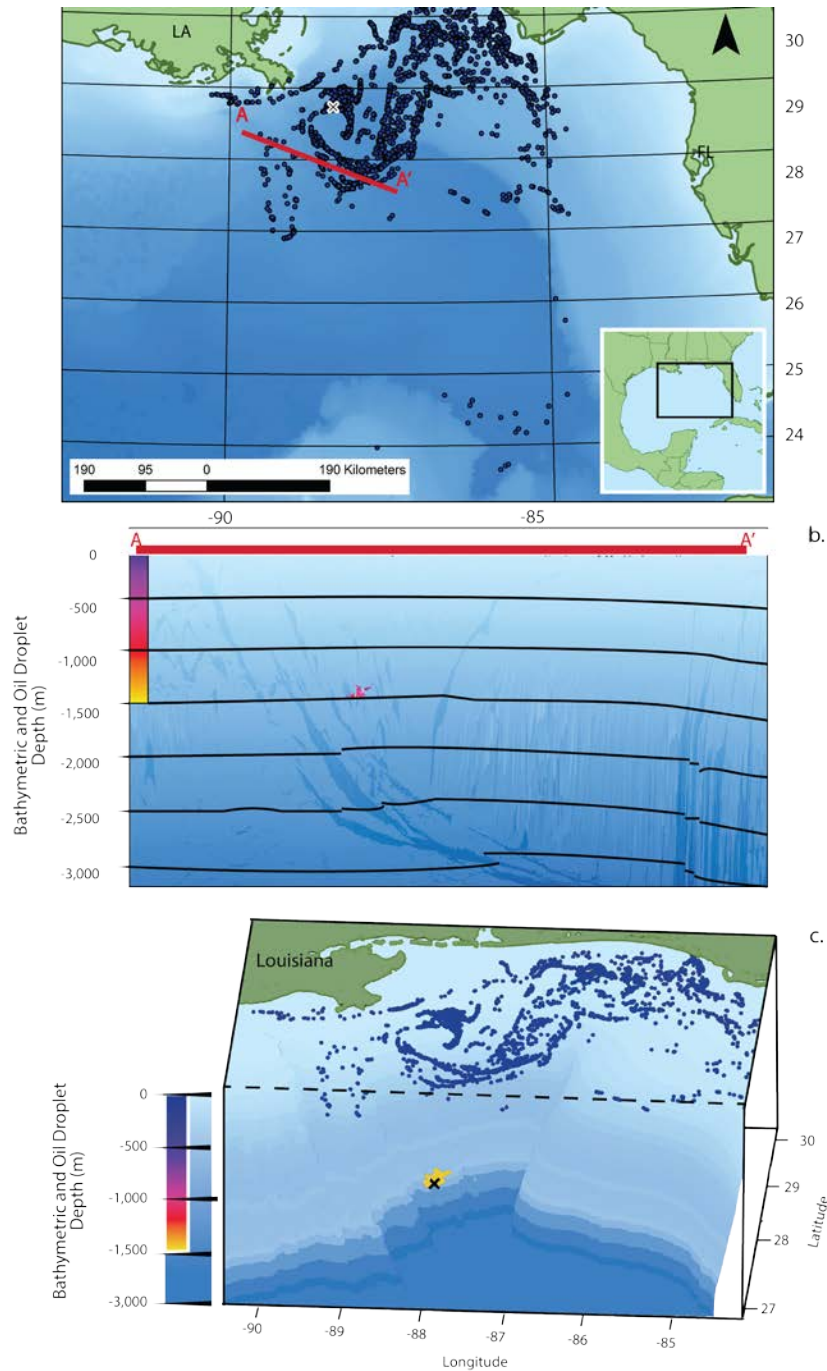


Figure 4.63. Oil blowout as simulated with BLOSOM after a 30-day simulation using the distribution from PNNL for treated droplet sizes. a) Plan view of the blowout at the sea-surface after a 30-day simulation originating at the Macondo Well initialized on May 2010 using realistic hydrodynamic conditions as simulated by NCOM, and using the PNNL distribution for oil treated with dispersant. The red line indicates the location of a vertical cross-section. b) Vertical cross-section along the red line in panel a) showing the distribution as a function of depth (ordinate). The color scale indicates the depth of each droplet. c) Three-dimensional view of the blowout shown in panels a) and b), the color again indicates the depth of the droplet.

Table 4.15. Percent of oil mass by depth for each of the four BLOSOM simulations

	0–250 m	250–500 m	500–750 m	750–1000 m	1000–1250 m	<-1250 m
J2013 T	42.1	0.6	0.9	1.3	2.2	52.9
J2013 NT	87.1	0.6	0.7	0.8	1	9.9
PNNL T	2.7	0	0	0	0	97.3
PNNL NT	3.8	0.3	0.3	0.6	1.8	93

Johansen et al. 2013 distribution treated (J2013 T) and untreated (J2013 NT), and PNNL experimental distributions treated (PNNL T) and untreated (PNNL NT).

4.8.1.3 Discussion

As noted, the PNNL2017 distributions produced droplet sizes that were roughly an order of magnitude smaller than those from the J2013 simulations. This was likely due to the experimental conditions under which the DSDs were derived. In this study we compared them “as derived.”

Because the J2013 DSDs were comparable to Deepwater Horizon conditions, BLOSOM successfully simulated oil remaining at depth when using the J2013 DSD for treated oil. The amount of oil remaining at depth is about 53%, which is roughly consistent with the amount of oil believed to never have surfaced (McNutt et al. 2012). It should be noted that most of the oil in this simulation becomes sunk as the ocean currents and turbulent diffusion moved oil onto the bottom, but only when oil droplets remained at depth long enough. Oil remaining at depth was more limited (roughly 10% of oil) when the untreated J2013 DSD was used. Because both PNNL distributions are small compared to the J2013 distribution for treated oil, the PNNL2017 simulations resulted in a large amount of oil remaining at depth.

4.8.1.4 Literature Findings

There has recently been a large body of literature published discussing the behavior of dispersants as they interact with plumes of crude oil. A literature review was undertaken to tease out any common variables that appear to have an influence on dispersant-crude oil interactions.⁶ Several articles describing physical experimentation with dispersants were evaluated, with a number of experimental variables recorded which could potentially effect dispersant effectiveness (DE). DE is measured by the reduction in droplet sizes (Mukherjee 2011) and therefore, the inverse relationship between DE and droplet size occurs by definition. This relationship is useful if you know the reduction in DSDs (before vs after dispersant application) and you want to calculate DE. Relevant variables captured during the literature review include dispersant brand, dispersant concentration, crude oil type, pressure, temperature, mixing method and rate, mixing time, salinity, SARA concentrations, and degree of crude weathering. While there was some signal associated with temperature and salinity, the strongest signals came from mixing efficiency and oil viscosity. While mixing efficiency had the strongest signal, the viscosity correlation was chosen to include in BLOSOM since viscosity is already explicitly included as part of the BLOSOM simulation.

A three-parameter model incorporating the hyperbolic tangent was found to give a good fit to the experimental viscosity data in Figure 4.64. The generalized relationship is given in terms of the hyperbolic tangent function as well as the adjustable parameters A, B, and C.

⁶ Abdelrahim et al. 2014; Belore et al. 2009; Brandvik et al. 2013; Brandvik et al. 2016; Chandraskar et al. 2003; Fu et al. 2014; Moles et al. 2002; Mukherjee et al. 2011; Nagamine 2014; Nyankson et al 2015a; Nyankson et al 2015b; Pan et al. 2016; Wang et al. 2013.

$$\% \text{ Effectiveness} = A \left(1 + \tanh \left(\frac{B - \mu}{C} \right) \right) \quad (4.1)$$

Here, μ is the oil viscosity in units of centipoise (cP).

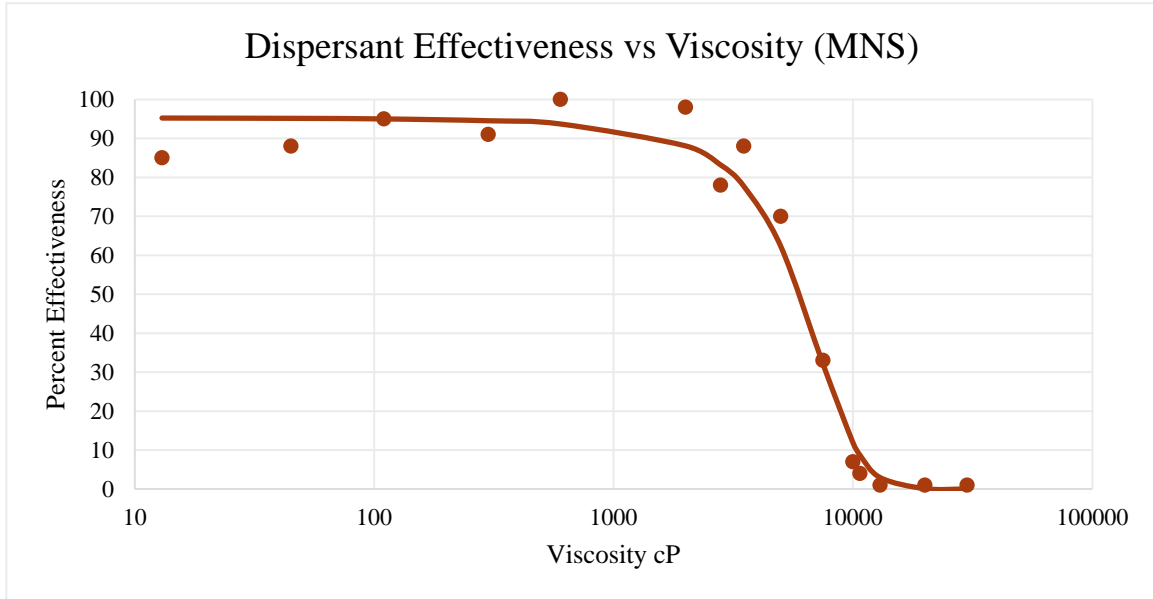


Figure 4.64. Curve fit for dispersant effectiveness (percentage, ordinate) as a function of oil viscosity (cP, abscissa).

The parameters A, B, and C in Equation (4.1) are dependent on the type of test protocol used to determine the viscosity. Both the Institut Français du Pétrole and Mackay, Nadeau, and Steelman test protocols are commonly used. Values for A, B, and C for use in the prediction of dispersant percent effectiveness associated with viscosity values obtained using either of these protocols are given in Table 4.16.

Table 4.16. Values for parameters A, B, and C used to determine dispersant effectiveness as a function of viscosity values obtained using either the IFP or MNS test protocol.

Parameter	Test Protocol	
	IFP	MNS
A	49.3	50
B	1890	6000
C	3330	4000

4.8.2 Future Enhancements: BLOSOM

Many enhancements can be made to increase BLOSOM’s utility when simulating the application of dispersants on oil spills. One such enhancement would be to treat the dispersant application sites as actual clouds, rather than just spheres of influence. This would mean that they could be affected by ambient

factors, and perhaps dissipate over time. Such a modification would greatly increase the complexity of the present implementation, but would yield more physically defensible results.

Another enhancement would be to add a means to heuristically calculate the minimum droplet size used to anchor the active DSD. Currently, this is a user-supplied value, or a specific, fixed value taken from literature. Ideally, this value could be derived from relationships as they exist within a simulation. Such an automated setup would enable less-knowledgeable users to simulate the application of dispersants that to achieve desirable results. To achieve this degree of emergent behavior, additional correlations would need to be derived from the present (or future) literature.

Still another enhancement would be to further refine the heuristics used to derive dispersant effectiveness to include the input from a wider range of environmental variables. During the literature review, several promising leads were noted for additional correlative relationships that could be boiled down into equations, but there was insufficient evidence to sufficiently justify their use. An expanded literature review could further elucidate such relationships to the point where they are defensible, and they could be incorporated into BLOSOM's dispersant module.

Finally, the PNNL2017 DSDs could be further integrated into BLOSOM's framework to better take advantage of user adjustments. For the purposes of this project the droplet sizes were fixed to a specific range, because these values were derived from direct observational results. Modifying the droplet size boundaries for the PNNL2017 DSDs to be adjustable by the modeler (as they are for the current J2013 DSD) opens up the possibility of fitting the derived distributions to match observations from any other experimental setup.

5.0 Conclusions and Next Steps

Ongoing exploration in the deep ocean environment of the U.S. Outer Continental Shelf requires continued high pressure research to characterize the phenomena affecting blowouts and response strategies. New and improved methods and capabilities will be needed to accurately simulate conditions and to collect meaningful data that may be used to inform oil spill models and response. Particular needs include equipment for simulating blowouts and oil suspensions in closed cells and methods for measuring and monitoring the evolution of DSDs within pressure cells. Non-invasive methods for monitoring oil and dispersant chemistry would also be beneficial. Field tests in the open ocean would also help reduce some uncertainties regarding the correlation and scaling of laboratory tests with real world scenarios, as noted below.

The DSDs derived from the PNNL experimental results produced droplets that were an order of magnitude smaller than the droplets sizes observed during *Deepwater Horizon* (Johansen et al. 2013; compare Figs. 4.8.7 and 4.8.8). This is due to the experimental design, including the methods and equipment that were used (e.g., nozzle size, GOR, discharge rate). The physical constraints and limitations of tank experiments will invariably produce DSDs of a different scale than are produced by a full-scale blowout in the open ocean. Challenges therefore exist in understanding how to properly establish equivalencies of scale between the experimental parameters and full scale 'real world' parameters, and for how to transform data and

observations from an experiment to the equivalent real-world scale. Finding the proper extrapolation method for the lab results from PNNL is therefore encouraged as a direction for future research. Another important direction for future research is simulating the evolution of the initial DSD (known as a dynamic DSD) to capture variations in size as the blowout evolves within the ocean, and at its surface.

The results of the experiment examining the effect of droplet size on the rate of biodegradation indicate that the scale of the droplets may not have a significant effect on the rate of biodegradation, but this may only be true within the scale examined (<10 μm through $\sim 500 \mu\text{m}$). There may be a critical threshold of larger droplet size that may significantly impact the rate of biodegradation. Additional work is necessary, however, to identify an approach for generating and maintaining larger droplet size distributions in laboratory scale environments. The formation of OPAs when mixing diatomaceous earth with oil or oil and dispersant may have identified an alternative approach and it may be possible to use the size of the particulate to control scale. Hollow (as with the diatom frustules) or porous particulate matter would be preferable and it would be necessary to quantify what fraction of the volume of the OPAs consists of oil.

The blowout experiments demonstrated that the vigorous and turbulent action of the blowout results in the atomization of a fraction of the oil. Differences in DSD between the PNNL and Johansen et al. 2013 study also demonstrate that the specific physical aspects of the blowout (e.g., orifice diameter, discharge rate, GOR) will impact the resulting initial droplet size distribution. It would likely be very important to monitor the DSD some distance from the blowout with and without the introduction of dispersant. Results from the BLOSOM model indicate that generating very small DSDs would result in driving a greater portion of the oil to the seafloor. Deep ocean seafloor sequestration of a significant portion of the oil may be beneficial, but this would need to be evaluated for the specific location. Biodegradation of the oil at the seafloor (due to cold temperatures and low oxygen) would be considerably slower than biodegradation of oil in the water column. Results of the BLOSOM model and the droplet size biodegradation study indicate that the motivation for controlling droplet size with DOR should be to direct what fraction of the oil is in the water column, water surface, or benthos: reducing droplet size below $500 \mu\text{m}$ is unlikely to increase the rate of biodegradation.

The blowout experiments also demonstrated that the extent of mixing of dispersant into the oil plume at or near the location of the blowout orifice may have little consequence. Premixing the dispersant with the oil (as was also done by Johansen et al. 2013), perhaps simulating an injection of dispersant into the well or riser pipe below a blowout orifice did not have a significant effect on the DSD when compared with injecting the dispersant into the ejection plume. An important caveat is to monitor the dispersant injection to assure that degassing of the oil does not separate the dispersant from the plume.

Another possible phenomenon that might impact oil-dispersant-seawater mixing and emulsification is the formation of methane hydrates during a deep ocean blowout. Methane hydrates can form when liquid or gaseous methane comes in contact with cold water and elevated pressures. The hydrates will form on the surface of gas bubbles, but can also nucleate on other surfaces, including sediments carried with the oil. Hydrate formation during a deep ocean oil release would reduce the amount of gas ordinarily contributing to the upward driving force on

the oil; if a significant quantity of gas was affected, the upward mobility of the plume would become increasingly dependent upon droplet size and buoyancy. The effect of dispersant concentration on hydrate formation is also poorly characterized. Further, the formation of hydrates within the ejection plume may pull water out of the mixture and thus impede the emulsification of the oil by the dispersant at the very location where turbulent mixing energy is available.

6.0 References

- Abdelrahim, M. A., and Rao, D. N. Measurement of Interfacial Tension in Hydrocarbon/Water/Dispersant Systems at Deepwater Conditions. From Oil Spill Remediation: Colloid Chemistry-based Principles and Solutions. 2014. 1st Ed. John Wiley & Sons, Inc. pp 295-315.
- Auflem, I. H.; Kallevik, H.; Westvik, A.; Sjöblom, J., Influence of pressure and solvency on the separation of water-in-crude-oil emulsions from the North Sea. *Journal of Petroleum Science and Engineering* **2001**, *31* (1), 1-12.
- Backhaus, T.; Scholze, M.; Grimme, L. H., The single substance and mixture toxicity of quinolones to the bioluminescent bacterium *Vibrio fischeri*. *Aquatic Toxicology* **2000**, *49* (1–2), 49-61.
- Bays, J. *13C NMR Analysis of Blind Canyon and Illinois #6 Coal Liquids*; Pacific Northwest National Laboratory: Richland, WA, 2014.
- Becker, K. W.; Lindblom, G. P., PERFORMANCE EVALUATION OF A NEW VERSATILE OIL SPILL DISPERSANT. *International Oil Spill Conference Proceedings* **1983**, *1983* (1), 61-64.
- Belore, R. C.; Trudel, K., Guarino, A., Large-scale cold water dispersant effectiveness experiments with Alaskan crude oils and Corexit 9500 and 9527 dispersants. *Marine Pollution Bulletin*: **2009**, *58* (1), 118-128.
- Bianchi, T. S.; Osburn, C.; Shields, M. R.; Yvon-Lewis, S.; Young, J.; Guo, L.; Zhou, Z., Deepwater Horizon Oil in Gulf of Mexico Waters after 2 Years: Transformation into the Dissolved Organic Matter Pool. *Environmental Science & Technology* **2014**, *48* (16), 9288-9297.
- Bonheyo, G.; Winder, E.; Park, J.; Avila, A.; Jeters, R.; Larimer, C. *Advanced Materials and Manufacturing Reliability: Performance Analysis of Antifouling Coatings*; Pacific Northwest National Laboratory: Richland, WA, 2015; p 30.
- Bonheyo, G.; Jeters, R.; Shin, Y.; Park, J.; Kuo, L.; Avila, A.; Symes, M. *E15PG00037: Multifunctional Herding-Sorbent Agents for Use in Icy Water*; PNNL-26504; Pacific Northwest National Laboratory: Richland, WA, May, 2017, 2017; pp 1-84.
- Brandvik, P. J.; Johansen, Ø.; Leirvik, F.; Farooq, U.; Daling, P. S., Droplet breakup in subsurface oil releases – Part 1: Experimental study of droplet breakup and effectiveness of dispersant injection. *Marine Pollution Bulletin* **2013**, *73* (1), 319-326.
- Brandvik, P. J.; Johansen, Ø.; Farooq, U.; Angell, G.; Leirvik, F. *Sub-surface oil releases – Experimental study of droplet distributions and different dispersant injection techniques- version 2. A scaled experimental approach using the SINTEF Tower basin*; SINTEF report no: A26122; SINTEF Trondheim, Norway 2014; pp 1-134.

Brandvik, P. J., Davies, E., Bradly, C., Storey, C. Leirvik, F., Subsurface oil releases – Verification of dispersant effectiveness under high pressure. 2016. Final Report. SINTEF Materials and Chemistry, pp 1-62.

Broje, V.; Gala, W.; Nedwed, T.; Twomey, J., A Consensus on the State of the Knowledge and Research Recommendations on the Fate and Effects of Deep Water Releases of Oil, Dispersants and Dispersed Oil. *International Oil Spill Conference Proceedings* **2014**, 2014 (1), 225-237.

Campo, P.; Venosa, A. D.; Suidan, M. T., Biodegradability of Corexit 9500 and Dispersed South Louisiana Crude Oil at 5 and 25 °C. *Environmental Science & Technology* **2013**, 47 (4), 1960-1967.

Cannella, W. F., C.; Arboleda, P.; Bays, T.; Dettman, H.; Foster, M.; Gieleciak, R.; Gunter, G.; Hager, D.; Lay, C.; Lewis, S.; Luecke, J.; Sluder, S.; Zigler, B. *Detailed Characterization of the Physical and Chemical Properties of the Reformulated FACE Diesel Fuels: FD2B, FD4B, and FD7B*; AVFL-19-1 Coordinating Research Council, Inc: Alpharetta, GA, Jan 2013, 2013; p 150.

Cannella, W. F., C.; Gieleciak, R.; Arboleda, P.; Bays, T.; Dettman, H.; Foster, M.; Gunter, G.; Hager, D.; King, D.; Lay, C.; Lewis, S.; Luecke, J.; Sluder, S.; Zigler, B.; Natarajan, M. *Advanced Alternative and Renewable Diesel Fuels: Detailed Characterization of Physical and Chemical Properties*; CRC Report No. AVFL-19-2; Coordinating Research Council: Alpharetta, GA, 2013.

Chandraskar, S., Sorial, G., and Weaver, J. W. 2003. Determining Dispersant Effectiveness Data for a Suite of Environmental Conditions. Presented at International Oil Spill Conference, Vancouver, Canada, April 7-10, 2003.

EPA method 40 CFR Ch. 1, part 300, Appendix C. Swirling flask dispersant effectiveness test, revised standard dispersant toxicity test, and bioremediation agent effectiveness test. . 7-1-03 ed.; US-EPA, Ed.

Fingas, M. *A Review of Literature Related to Oil Spill Dispersants 2011-2014*; Anchorage, Alaska, 2014; p 52.

Fitzpatrick, F. A.; Boufadel, M. C.; Johnson, R.; Lee, K. W.; Graan, T. P.; Bejarano, A. C.; Zhu, Z.; Waterman, D.; Capone, D. M.; Hayter, E.; Hamilton, S. K.; Dekker, T.; Garcia, M. H.; Hassan, J. S. *Oil-particle interactions and submergence from crude oil spills in marine and freshwater environments: review of the science and future research needs*; 2015-1076; Reston, VA, 2015; p 44.

Follonier, S.; Panke, S.; Zinn, M., Pressure to kill or pressure to boost: a review on the various effects and applications of hydrostatic pressure in bacterial biotechnology. *Appl Microbiol Biotechnol.* **2012**, 93 (5), 1805-1815.

Fu, J., Gong, Y., Zhao, X., O'Reilly, S.E., Zhao, D., Effects of Oil and Dispersant on Formation of Marine Oil Snow and Transport of Oil Hydrocarbons. *Environmental Science and Technology* **2014**, 48 (24), 14392-14399.

Fulladosa, E.; Murat, J.-C.; Villaescusa, I., Study on the toxicity of binary equitoxic mixtures of metals using the luminescent bacteria *Vibrio fischeri* as a biological target. *Chemosphere* **2005**, 58 (5), 551-557.

Gill, G. A.; Kuo, L.-J.; Janke, C. J.; Park, J.; Jeters, R. T.; Bonheyo, G. T.; Pan, H.-B.; Wai, C.; Khangaonkar, T.; Bianucci, L.; Wood, J. R.; Warner, M. G.; Peterson, S.; Abrecht, D. G.; Mayes, R. T.; Tsouris, C.; Oyola, Y.; Strivens, J. E.; Schlafer, N. J.; Addleman, R. S.; Chouyyok, W.; Das, S.; Kim, J.; Buessler, K.; Breier, C.; D'Alessandro, E., The Uranium from Seawater Program at the Pacific Northwest National Laboratory: Overview of Marine Testing, Adsorbent Characterization, Adsorbent Durability, Adsorbent Toxicity, and Deployment Studies. *Industrial & Engineering Chemistry Research* **2016**, 55 (15), 4264-4277.

Girotti, S.; Bolelli, L.; Roda, A.; Gentilomi, G.; Musiani, M., Improved detection of toxic chemicals using bioluminescent bacteria. *Analytica Chimica Acta* **2002**, 471 (1), 113-120.

Government_Accountability_Office. *Oil Dispersants: Additional Research Needed, Particularly on Subsurface and Arctic Applications*; Government Accountability Office: May 30, 2012, 2012; p 73.

Huesemann, M. H.; Hausmann, T. S.; Fortman, T. J., Assessment of bioavailability limitations during slurry biodegradation of petroleum hydrocarbons in aged soils. *Environmental Toxicology and Chemistry* **2003**, 22 (12), 2853-2860.

Huesemann, M. H.; Hausmann, T. S.; Fortman, T. J., Does Bioavailability Limit Biodegradation? A Comparison of Hydrocarbon Biodegradation and Desorption Rates in Aged Soils. *Biodegradation* **2004**, 15 (4), 261-274.

Use of Dispersants to Treat Oil Spills. Technical Information paper ed.; International Tanker Owners Pollution Federation Limited (ITOPF) 2011; pp 4-5.

Jannasch, H.W. and Taylor, C.D. Deep-Sea Microbiology. *Ann. Rev. Microbiol.* **1984**, 38, 487-514.

Johansen, Ø., Development and verification of deep-water blowout models. *Marine Pollution Bulletin* **2003**, 47 (9), 360-368.

Johansen, Ø.; Brandvik, P. J.; Farooq, U., Droplet breakup in subsea oil releases – Part 2: Predictions of droplet size distributions with and without injection of chemical dispersants. *Marine Pollution Bulletin* **2013**, 73 (1), 327-335.

Juarez, A. G. V.; Kadimesetty, H. S.; Achatz, D. E.; Schedler, M.; Muller, R., Online Monitoring of Crude Oil Biodegradation at Elevated Pressures. *IEEE Journal Of Selected Topics In Applied Earth Observations And Remote Sensing* **2015**, 8 (2), 872-878.

Kerkhof, L. J.; Voytek, M. A.; Sherrell, R. M.; Millie, D.; Schofield, O., Variability in bacterial community structure during upwelling in the coastal ocean. In *Molecular Ecology of Aquatic Communities*, Zehr, J. P.; Voytek, M. A., Eds. Springer Netherlands: Dordrecht, 1999; pp 139-148.

Khelifa, A.; Stoffyn-Egli, P.; Hill, P. S.; Lee, K., Characteristics of Oil Droplets Stabilized by Mineral Particles: Effects of Oil Type and Temperature. *Spill Science & Technology Bulletin* **2002**, 8 (1), 19-30.

Kleindienst, S.; Seidel, M.; Ziervogel, K.; Grim, S.; Loftis, K.; Harrison, S.; Malkin, S. Y.; Perkins, M. J.; Field, J.; Sogin, M. L.; Dittmar, T.; Passow, U.; Medeiros, P. M.; Joye, S. B., Chemical dispersants can suppress the activity of natural oil-degrading microorganisms. *Proceedings of the National Academy of Sciences of the United States of America* **2015**, 112 (48), 14900-14905.

Kleindienst, S.; Paul, J. H.; Joye, S. B., Using dispersants after oil spills: impacts on the composition and activity of microbial communities. *Nat Rev Micro* **2015**, 13 (6), 388-396.

Klump, E., Oil Drillers Rush Back to the Gulf of Mexico: BP's oil spill is a distant memory as companies invest billions. *Businessweek* November 14, 2013, 2013.

Kostka, J.E., Prakash, O., Overholt, W.A., Green, S.J., Gina Freyer, G., Canion, A., Delgardio, J., Norton, N., Hazen, T.C., Huettel, M. Hydrocarbon-Degrading Bacteria and the Bacterial Community Response in Gulf of Mexico Beach Sands Impacted by the Deepwater Horizon Oil Spill. *Appl Environ Microbiol.* **2011** 77(22), 7962–7974.

Kumar, P.; Libchaber, A., Pressure and Temperature Dependence of Growth and Morphology of *Escherichia coli*: Experiments and Stochastic Model. *Biophysical Journal* **2013**, 105 (3), 783-793.

Le Floch, S.; Guyomarch, J.; Merlin, F.-X.; Stoffyn-Egli, P.; Dixon, J.; Lee, K., The Influence of Salinity on Oil–Mineral Aggregate Formation. *Spill Science & Technology Bulletin* **2002**, 8 (1), 65-71.

Lee, K., Oil–Particle Interactions in Aquatic Environments: Influence on the Transport, Fate, Effect and Remediation of Oil Spills. *Spill Science & Technology Bulletin* **2002**, 8 (1), 3-8.

Lee, K.; Stoffyn-Egli, P.; Tremblay, G. H.; Owens, E. H.; Sergy, G. A.; Guénette, C. C.; Prince, R. C., Oil–Mineral Aggregate Formation on Oiled Beaches: Natural Attenuation and Sediment Relocation. *Spill Science & Technology Bulletin* **2003**, 8 (3), 285-296.

- Lei, L.; Aoyama, I., Effect-directed investigation and interactive effect of organic toxicants in landfill leachates combining Microtox test with RP-HPLC fractionation and GC/MS analysis. *Ecotoxicology* **2010**, *19* (7), 1268-1276.
- Lessard, R. R.; DeMarco, G., The Significance of Oil Spill Dispersants. *Spill Science & Technology Bulletin* **2000**, *6* (1), 59-68.
- Jon E. Lindstrom, D. M. W., Joan F. Braddock *Biodegradation of dispersed Oil Using COREXIT 9500*; The Alaska Department of Environmental Conservation Division of Spill Prevention and Response: 1999.
- Lindstrom, J. E.; Braddock, J. F., Biodegradation of petroleum hydrocarbons at low temperature in the presence of the dispersant Corexit 9500. *Marine Pollution Bulletin* **2002**, *44* (8), 739-747.
- Macías-Zamora, J. V.; Meléndez-Sánchez, A. L.; Ramírez-Álvarez, N.; Gutiérrez-Galindo, E. A.; Orozco-Borbón, M. V., On the effects of the dispersant Corexit 9500© during the degradation process of n-alkanes and PAHs in marine sediments. *Environmental Monitoring and Assessment* **2014**, *186* (2), 1051-1061.
- Marietou, A.; Bartlett, D. H., Effects of High Hydrostatic Pressure on Coastal Bacterial Community Abundance and Diversity. *Applied and Environmental Microbiology* **2014**, *80* (19), 5992-6003.
- McFarlin, K. M.; Prince, R. C.; Perkins, R.; Leigh, M. B., Biodegradation of Dispersed Oil in Arctic Seawater at -1°C. *PLoS ONE* **2014**, *9* (1), e84297.
- McNutt, M. K.; Camilli, R.; Crone, T. J.; Guthrie, G. D.; Hsieh, P. A.; Ryerson, T. B.; Savas, O.; Shaffer, F., Review of flow rate estimates of the Deepwater Horizon oil spill. *Proceedings of the National Academy of Sciences* **2012**, *109* (50), 20260-20267.
- Mikkelsen, O. A.; Hill, P. S.; Milligan, T. G.; Chant, R. J., In situ particle size distributions and volume concentrations from a LISST-100 laser particle sizer and a digital floc camera. *Continental Shelf Research* **2005**, *25* (16), 1959-1978.
- Moles, A., Holland, L., and Short, J., Effectiveness in the Laboratory of Corexit 9527 and 9500 in Dispersing Fresh, Weathered, and Emulsion of Alaska North Slope Crude Oil under Subarctic Conditions. *Spill Science & Technology Bulletin* **2002**, *7*(5-6), 241-247.
- Mukherjee, B., Turner, J., Wrenn, B. A., Effect of Oil Composition on Chemical Dispersion of Crude Oil. *Environmental Engineering Science* **2011**, *28*(7), 496-507.
- Mulkins-Phillips, G. J.; Stewart, J. E., Effect of Four Dispersants on Biodegradation and Growth of Bacteria on Crude Oil. *Applied Microbiology* **1974**, *28* (4), 547-552.
- Nagamine, S. I. 2014. 'The Effects of Chemical Dispersants on Buoyant Oil Droplets'. MS thesis. University of Hawai'i, Mānoa.

Using Oil Dispersants on the Sea; National Research Council; National Academy Press: Washington, DC, 1989, 1989; pp 24-69.

Oil Spill Dispersants: Efficacy and Effects; National Research Council; National Academy Press: Washington, D.C., 2005; p 400.

Nyankson, E., DeCuir, M. J., and Gupta, R.B., Soybean Lecithin as a Dispersant for Crude Oil Spills. *ACS Sustainable Chemical Engineering* **2015**, 3(5), 920-931.

Nyankson, E., Olasehinde, O., John, T. V., and Gupta, R. B., Surfactant-Loaded Halloysite Clay Nanotube Dispersants for Crude Oil Spill Remediation. *Industrial and Engineering Chemistry Research* **2015**, 54(38), 9328-9341

Oreskes, N.; Shrader-Frechette, K.; Belitz, K., Verification, Validation, and Confirmation of Numerical Models in the Earth Sciences. *Science* **1994**, 263 (5147), 641.

Oreskes, N., Evaluation (not validation) of quantitative models. *Environmental Health Perspectives* **1998**, 106 (Suppl 6), 1453-1460.

Pan, Z., Zhao, L., Boufadel, M.C., King, T., Conmy, R., Lee, K., Impact of mixing time and energy on the dispersion effectiveness and droplets size of oil. *Chemosphere* **2017**, 166, 246-254.

Park, J.; Jeters, R. T.; Kuo, L.-J.; Strivens, J. E.; Gill, G. A.; Schlafer, N. J.; Bonheyo, G. T., Potential Impact of Seawater Uranium Extraction on Marine Life. *Industrial & Engineering Chemistry Research* **2016**, 55 (15), 4278-4284.

Prieur, D., 2011, Deep-Sea Microbiology. *Encyclopedia of Astrobiology*. M. Gargaud, R. Amils, J. C. Quintanilla et al. Berlin, Heidelberg, Springer Berlin Heidelberg: 414-415.

Prince, R. C.; Elmendorf, D. L.; Lute, J. R.; Hsu, C. S.; Haith, C. E.; Senius, J. D.; Dechert, G. J.; Douglas, G. S.; Butler, E. L., 17.alpha.(H)-21.beta.(H)-hopane as a conserved internal marker for estimating the biodegradation of crude oil. *Environmental Science & Technology* **1994**, 28 (1), 142-145.

Prince, R. C.; McFarlin, K. M.; Butler, J. D.; Febbo, E. J.; Wang, F. C. Y.; Nedwed, T. J., The primary biodegradation of dispersed crude oil in the sea. *Chemosphere* **2013**, 90 (2), 521-526.

Prince, R. C.; Butler, J. D., A protocol for assessing the effectiveness of oil spill dispersants in stimulating the biodegradation of oil. *Environmental Science and Pollution Research* **2014**, 21 (16), 9506-9510.

Prince RC, K. B. a. B. J., Three Widely-Available Dispersants Substantially Increase the Biodegradation of otherwise Undispersed Oil. *Journal of Marine Science: Research & Development* **2016**, 6 (1), 4.

- Schedler, M.; Hiessl, R.; Valladares Juárez, A. G.; Gust, G.; Müller, R., Effect of high pressure on hydrocarbon-degrading bacteria. *AMB Express* **2014**, *4*, 77-77.
- Schindelin, J.; Arganda-Carreras, I.; Frise, E.; Kaynig, V.; Longair, M.; Pietzsch, T.; Preibisch, S.; Rueden, C.; Saalfeld, S.; Schmid, B.; Tinevez, J.-Y.; White, D. J.; Hartenstein, V.; Eliceiri, K.; Tomancak, P.; Cardona, A., Fiji: an open-source platform for biological-image analysis. *Nat Meth* **2012**, *9* (7), 676-682.
- Scoma, A.; Barbato, M.; Hernandez-Sanabria, E.; Mapelli, F.; Daffonchio, D.; Borin, S.; Boon, N., Microbial oil-degradation under mild hydrostatic pressure (10 MPa): which pathways are impacted in piezosensitive hydrocarbonoclastic bacteria? *Scientific Reports* **2016**, *6*, 23526.
- Sterman, J. D., The Meaning of Models. *Science* **1994**, *264* (5157), 329.
- Stoffyn-Egli, P.; Lee, K., Formation and Characterization of Oil–Mineral Aggregates. *Spill Science & Technology Bulletin* **2002**, *8* (1), 31-44.
- Tamburini, C.; Goutx, M.; Guigue, C.; Garel, M.; Lefevre, D.; Charriere, B.; Sempere, R.; Pepa, S.; L.Peterson, M.; Wakeham, S.; Lee, C., Effects of hydrostatic pressure on microbial alteration of sinking fecal pellets. *Deep-Sea Research II* **2009**, *56*, 1533–1546.
- Tsiridis, V.; Petala, M.; Samaras, P.; Hadjispyrou, S.; Sakellaropoulos, G.; Kungolos, A., Interactive toxic effects of heavy metals and humic acids on *Vibrio fischeri*. *Ecotoxicology and Environmental Safety* **2006**, *63* (1), 158-167.
- U.S._Coast_Guard. *On scene coordinator report: Deepwater Horizon oil spill*; U.S. Department of Homeland Security, U.S. Coast Guard: Washington, DC, 2011.
- U.S. Crude Oil and Natural Gas Proved Reserves*; US Energy Information Administration (US-EIA) 2011; p 10.
- Gulf of Mexico Fact Sheet*; US Energy Information Administration (US-EIA) 2013 Accessed March 31, 2014 at http://www.eia.gov/special/gulf_of_mexico/data.cfm (updated July 1, 2013).
- US Energy Information Administration (US-EIA). 2017. 'Gulf of Mexico crude oil production, already at annual high, expected to keep increasing.' *Today in Energy*. Accessed 9/24/2017 at <https://www.eia.gov/todayinenergy/detail.php?id=30752> (last updated April 12, 2017)
- USNC. *Macondo: the Gulf oil disaster: Chief Counsel's report*; United States National Commission On The BP Deepwater Horizon Oil Spill And Offshore Drilling: Washington, D.C., 2011; p 371.
- Venosa, A. D.; Holder, E. L., Biodegradability of dispersed crude oil at two different temperatures. *Marine Pollution Bulletin* **2007**, *54* (5), 545-553.

Wang, W., Zheng, Y., and Lee, K. 2013. Chemical dispersion of oil with mineral fines in a low temperature environment. *Marine Pollution Bulletin* **2013**, 72(1), 205-212.

Wu, D. H.; Chen, A. D.; Johnson, C. S., An Improved Diffusion-Ordered Spectroscopy Experiment Incorporating Bipolar-Gradient Pulses. *Journal of Magnetic Resonance, Series A* **1995**, 115 (2), 260-264.

Zeinstra-Helfrich, M.; Koops, W.; Murk, A. J., The NET effect of dispersants — a critical review of testing and modelling of surface oil dispersion. *Marine Pollution Bulletin* **2015**, 100 (1), 102-111.

Appendix A
Interfacial Tension Data

Appendix A

Interfacial Tension Data

Sample: Macondo Crude in unfiltered seawater at 17.8°C with Corexit 9500 1:10 dilution at 1 atm pressure.

Number	Gamma	Beta	R0	Area	Volume	Theta	Height	Width	Opt
1	4.44	0.252	0.826	9.89	3.14	127.14	1.925	1.732	2
2	4.36	0.256	0.825	9.93	3.15	126.56	1.935	1.732	2
3	4.29	0.259	0.824	9.96	3.16	126.00	1.943	1.732	2
4	4.28	0.260	0.824	9.99	3.17	125.79	1.952	1.732	2
5	4.21	0.264	0.823	10.02	3.18	125.19	1.959	1.731	2
6	4.19	0.266	0.823	10.04	3.19	124.92	1.966	1.732	2
7	4.13	0.268	0.822	10.06	3.20	124.43	1.972	1.731	2
8	4.11	0.270	0.822	10.08	3.20	124.12	1.979	1.731	2
9	4.11	0.270	0.822	10.11	3.21	124.00	1.985	1.732	2
10	4.05	0.273	0.821	10.12	3.22	123.47	1.991	1.731	2
11	3.18	0.305	0.770	9.31	2.81	117.36	1.958	1.633	2
12	3.19	0.305	0.770	9.30	2.80	117.36	1.960	1.633	2
13	3.16	0.306	0.769	9.30	2.80	117.03	1.962	1.632	2
14	3.18	0.306	0.769	9.31	2.81	117.12	1.963	1.636	2
15	3.17	0.306	0.769	9.30	2.80	116.96	1.965	1.636	2
16	3.16	0.307	0.769	9.32	2.81	116.71	1.968	1.637	2
17	3.13	0.309	0.768	9.31	2.81	116.36	1.971	1.638	2
18	3.12	0.310	0.768	9.35	2.81	116.12	1.974	1.639	2
19	3.09	0.313	0.767	9.33	2.81	115.54	1.980	1.640	2
20	3.15	0.308	0.768	9.34	2.81	116.32	1.975	1.641	2
21	3.76	0.291	0.816	10.31	3.27	119.36	2.057	1.728	2
22	3.72	0.293	0.815	10.32	3.27	118.94	2.061	1.727	2
23	3.72	0.293	0.815	10.33	3.28	118.74	2.064	1.727	2
24	3.69	0.295	0.814	10.34	3.28	118.32	2.069	1.724	2
25	3.71	0.294	0.815	10.36	3.28	118.4	2.072	1.728	2
26	3.67	0.296	0.814	10.36	3.28	118.01	2.075	1.725	2
27	3.63	0.298	0.813	10.35	3.28	117.42	2.080	1.723	2
28	3.61	0.300	0.812	10.37	3.28	117.01	2.086	1.722	2
29	3.67	0.296	0.814	10.39	3.29	117.41	2.088	1.726	2
30	3.61	0.300	0.812	10.39	3.29	116.79	2.092	1.724	2
Mean:	3.67	0.290	0.800	9.89	3.09	119.84	2.000	1.700	2
Std. Dev:	0.45	0.02	0.02	0.45	0.21	3.89	0.06	0.04	0

Sample: Macondo Crude in unfiltered seawater at 17.8°C with Corexit 9500 1:100 dilution at 1 atm pressure.

Number	Gamma	Beta	R0	Area	Volume	Theta	Height	Width	Opt
1	14.26	0.212	1.357	27.09	13.48	126.44	3.333	2.823	2
2	14.03	0.215	1.356	27.11	13.48	125.65	3.343	2.822	2
3	14.06	0.215	1.356	27.14	13.50	125.29	3.350	2.823	2
4	14.05	0.215	1.356	27.17	13.51	124.96	3.357	2.823	2
5	13.83	0.217	1.354	27.18	13.51	124.19	3.367	2.821	2
6	13.66	0.220	1.353	27.19	13.50	123.50	3.375	2.818	2
7	1.620	0.220	1.352	27.21	13.51	123.07	3.382	2.818	2
8	13.59	0.221	1.352	27.23	13.51	122.57	3.389	2.818	2
9	13.43	0.223	1.350	27.23	13.51	121.88	3.398	2.815	2
10	13.32	0.224	1.349	27.25	13.51	121.27	3.406	2.814	2
11	13.17	0.218	1.323	25.88	12.58	125.11	3.272	2.754	2
12	13.12	0.219	1.322	25.89	12.58	124.68	3.278	2.754	2
13	13.00	0.220	1.321	25.90	12.58	124.19	3.285	2.753	2
14	12.92	0.221	1.320	25.91	12.58	123.81	3.290	2.752	2
15	12.86	0.222	1.320	25.92	12.58	123.39	3.296	2.751	2
16	12.78	0.223	1.319	25.95	12.59	122.95	3.303	2.750	2
17	12.75	0.224	1.319	25.96	12.59	122.58	3.308	2.750	2
18	12.63	0.225	1.318	25.96	12.59	122.05	3.315	2.748	2
19	12.70	0.224	1.318	25.98	12.60	121.87	3.319	2.750	2
20	12.56	0.227	1.317	26.00	12.60	121.28	3.327	2.748	2
21	14.95	0.212	1.389	28.44	14.45	125.21	3.433	2.889	2
22	14.75	0.214	1.387	28.46	14.45	124.33	3.444	2.887	2
23	14.57	0.216	1.386	28.47	14.45	123.65	3.453	2.885	2
24	14.56	0.216	1.386	28.49	14.46	123.13	3.461	2.886	2
25	14.47	0.217	1.385	28.52	14.47	122.62	3.470	2.885	2
26	14.29	0.220	1.384	28.53	14.47	121.78	3.480	2.882	2
27	14.17	0.221	1.382	28.55	14.47	121.06	3.489	2.881	2
28	14.15	0.221	1.382	28.58	14.48	120.52	3.498	2.882	2
29	14.08	0.222	1.382	28.6	14.48	119.83	3.508	2.881	2
30	13.87	0.225	1.380	28.62	14.49	118.89	3.519	2.878	2
Mean:	13.27	0.220	1.350	27.21	13.52	123.06	3.380	2.820	2
Std. Dev:	2.31	0.00	0.03	1.08	0.78	1.80	0.08	0.06	0.00

Sample: Macondo Crude in unfiltered seawater at 17.8°C with Corexit 9500 1:1000 dilution at 1 atm pressure.

Number	Gamma	Beta	R0	Area	Volume	Theta	Height	Width	Opt
1	20.48	0.211	1.622	39.37	23.09	110.99	4.203	3.373	2
2	20.58	0.212	1.631	40.03	23.57	104.81	4.296	3.394	2
3	21.28	0.209	1.647	40.58	24.15	109.79	4.276	3.425	2
Mean:	20.78	0.210	1.630	39.99	23.60	108.53	4.260	3.400	2
Std. Dev:	0.44	0.00	0.01	0.61	0.53	3.28	0.05	0.03	0.00

Sample: Macondo Crude in unfiltered seawater at 17.8°C with Corexit 9500 1:10,000 dilution at 1 atm pressure.

Number	Gamma	Beta	R0	Area	Volume	Theta	Height	Width	Opt
1	21.49	0.202	1.628	39.21	23.06	116.92	4.128	3.381	2
2	22.65	0.204	1.680	41.99	25.43	110.84	4.332	3.490	2
3	21.77	0.206	1.655	40.79	24.35	110.87	4.273	3.438	2
Mean:	21.97	0.200	1.650	40.66	24.28	112.88	4.240	3.440	2
Std. Dev:	0.61	0.00	0.03	1.39	1.19	3.50	0.10	0.05	0.00

Sample: Macondo Crude in unfiltered seawater at 17.8°C with Corexit 9500 1:100,000 dilution at 1 atm pressure.

Number	Gamma	Beta	R0	Area	Volume	Theta	Height	Width	Opt
1	20.83	0.207	1.622	39.05	22.94	117.12	4.122	3.370	2
2	21.15	0.204	1.621	38.75	22.75	120.37	4.069	3.365	2
3	20.29	0.203	1.586	36.99	21.29	122.76	3.948	3.293	2
Mean:	20.76	0.200	1.610	38.26	22.33	120.08	4.050	3.340	2
Std. Dev:	0.43	0.00	0.02	1.11	0.90	2.83	0.09	0.04	0.00

Sample: Macondo Crude in unfiltered seawater at 17.8°C with Finasol OSR 52 1:50 dilution at 1 atm pressure.

Number	Gamma	Beta	R0	Area	Volume	Theta	Height	Width	Opt
1	14.82	0.221	1.412	29.92	15.43	117.48	3.612	2.942	2
2	14.63	0.223	1.410	29.95	15.43	115.98	3.631	2.941	2
3	14.54	0.224	1.410	30.03	15.47	114.64	3.650	2.942	2
4	14.36	0.227	1.409	30.09	15.49	112.86	3.673	2.94	2
5	14.20	0.229	1.407	30.14	15.50	110.85	3.697	2.938	2
6	14.09	0.230	1.406	30.21	15.52	108.69	3.723	2.937	2
7	13.98	0.232	1.405	30.29	15.54	106.05	3.754	2.936	2
8	13.87	0.233	1.404	30.38	15.55	102.17	3.795	2.935	2
9	13.93	0.232	1.405	30.50	15.55	95.31	3.859	2.934	2
10	19.78	0.175	1.452	30.94	15.62	48.07	4.077	2.976	2
11	13.93	0.222	1.372	28.17	14.15	119.78	3.481	2.858	2
12	13.86	0.222	1.371	28.20	14.16	118.96	3.492	2.859	2
13	13.67	0.225	1.369	28.25	14.17	117.71	3.509	2.857	2
14	13.60	0.226	1.369	28.28	14.18	116.67	3.522	2.856	2
15	13.40	0.229	1.367	28.32	14.19	115.28	3.541	2.853	2
16	13.34	0.23	1.366	28.36	14.20	114.11	3.555	2.852	2
17	13.19	0.232	1.365	28.39	14.20	112.73	3.573	2.851	2
18	13.11	0.233	1.364	28.44	14.21	111.17	3.591	2.85	2
19	12.99	0.235	1.363	28.49	14.23	109.43	3.613	2.848	2
20	12.92	0.236	1.362	28.53	14.23	107.66	3.632	2.848	2
21	14.01	0.220	1.372	28.13	14.14	120.70	3.468	2.859	2
22	14.01	0.220	1.372	28.17	14.15	120.03	3.478	2.860	2
23	13.79	0.223	1.371	28.22	14.17	118.71	3.496	2.859	2
24	13.68	0.225	1.37	28.25	14.18	117.6	3.511	2.859	2
25	13.56	0.227	1.369	28.31	14.20	116.6	3.526	2.858	2
26	13.48	0.228	1.368	28.34	14.21	115.52	3.539	2.856	2
27	13.31	0.230	1.367	28.38	14.22	114.09	3.557	2.853	2
28	13.22	0.231	1.366	28.42	14.23	112.66	3.575	2.853	2
29	13.13	0.233	1.366	28.47	14.24	111.29	3.593	2.852	2
30	13.01	0.234	1.364	28.51	14.20	109.51	3.613	2.850	2
Mean:	13.71	0.230	1.380	28.90	14.60	113.25	3.600	2.880	2
Std. Dev:	0.51	0.00	0.02	0.88	0.62	5.66	0.10	0.04	0

Sample: Macondo Crude in unfiltered seawater at 17.8°C with Finasol OSR 52 1:100 dilution at 1 atm pressure.

Number	Gamma	Beta	R0	Area	Volume	Theta	Height	Width	Opt
1	18.39	0.203	1.509	33.53	18.35	122.07	3.766	3.113	2
2	18.32	0.204	1.509	33.56	18.36	121.39	3.776	3.135	2
3	18.09	0.206	1.508	33.62	18.40	120.50	3.790	3.133	2
4	18	0.207	1.508	33.66	18.42	119.98	3.798	3.133	2
5	17.84	0.209	1.507	33.71	18.45	118.95	3.813	3.133	2
6	17.8	0.209	1.507	33.73	18.45	118.52	3.818	3.134	2
7	17.64	0.211	1.506	33.78	18.48	117.41	3.834	3.133	2
8	17.58	0.212	1.506	33.81	18.49	116.88	3.841	3.133	2
9	17.46	0.213	1.505	33.85	18.51	115.83	3.855	3.132	2
10	17.3	0.215	1.504	33.87	18.51	115.10	3.865	3.131	2
11	18.27	0.204	1.507	33.45	18.28	121.79	3.765	3.128	2
12	18.2	0.204	1.506	33.47	18.29	121.19	3.773	3.129	2
13	18.08	0.206	1.506	33.50	18.30	120.53	3.786	3.128	2
14	17.98	0.207	1.505	33.52	18.31	119.86	3.792	3.127	2
15	17.7	0.210	1.504	33.54	18.31	119.04	3.804	3.124	2
16	17.58	0.211	1.503	33.56	18.32	118.32	3.811	3.124	2
17	17.54	0.211	1.502	33.59	18.33	117.67	3.820	3.124	2
18	17.47	0.212	1.502	33.62	18.34	116.95	3.830	3.124	2
19	17.31	0.213	1.501	33.65	18.35	116.12	3.841	3.122	2
20	17.19	0.215	1.500	33.66	18.35	115.40	3.850	3.120	2
21	18.6	0.210	1.540	35.39	19.79	116.26	3.935	3.206	2
22	18.47	0.211	1.541	35.42	19.80	115.52	3.945	3.206	2
23	18.34	0.212	1.541	35.47	19.82	114.32	3.96	3.206	2
24	18.24	0.213	1.540	35.51	19.84	113.33	3.973	3.205	2
25	18.09	0.215	1.539	35.55	19.85	111.98	3.991	3.204	2
26	17.96	0.216	1.538	35.59	19.86	110.65	4.006	3.203	2
27	17.87	0.217	1.538	35.64	19.88	109.19	4.023	3.202	2
28	17.78	0.218	1.537	35.68	19.88	107.64	4.041	3.202	2
29	17.66	0.219	1.536	35.73	19.89	105.68	4.063	3.200	2
30	17.58	0.220	1.535	35.78	19.90	103.22	4.089	3.199	2
Mean:	17.88	0.210	1.520	34.28	18.87	116.04	3.880	3.150	2
Std. Dev:	0.38	0.00	0.02	0.94	0.71	4.83	0.10	0.04	0.00

Sample: Macondo Crude in unfiltered seawater at 17.8°C with Finasol OSR 52 1:1000 dilution at 1 atm pressure.

Number	Gamma	Beta	R0	Area	Volume	Theta	Height	Width	Opt
1	22.97	0.199	1.670	41.00	24.72	119.84	4.118	3.464	2
2	22.86	0.200	1.670	41.06	24.76	118.74	4.203	3.465	2
3	22.92	0.200	1.671	41.10	24.79	118.75	4.205	3.467	2
4	22.76	0.201	1.670	41.16	24.83	118.02	4.217	3.466	2
5	22.80	0.201	1.671	41.20	24.86	117.80	4.221	3.468	2
6	22.80	0.201	1.672	41.24	24.89	117.43	4.227	3.470	2
7	22.64	0.202	1.671	41.25	24.89	116.85	4.235	3.469	2
8	22.63	0.202	1.671	41.30	24.93	116.45	4.241	3.470	2
9	22.64	0.202	1.672	41.33	24.95	116.19	4.245	3.470	2
10	22.61	0.203	1.671	41.35	24.95	115.85	4.250	3.471	2
11	22.51	0.199	1.653	40.13	23.96	120.6	4.135	3.429	2
12	22.38	0.200	1.652	40.16	23.98	120.21	4.142	3.429	2
13	22.52	0.199	1.653	40.20	24.01	120.01	4.145	3.431	2
14	22.46	0.200	1.654	40.24	24.04	119.79	4.150	3.431	2
15	22.38	0.200	1.653	40.26	24.05	119.46	4.155	3.431	2
16	22.24	0.202	1.653	40.27	24.06	119.1	4.161	3.430	2
17	22.30	0.201	1.653	40.30	24.08	118.9	4.163	3.432	2
18	22.26	0.201	1.654	40.32	24.09	118.67	4.168	3.432	2
19	22.10	0.203	1.653	40.33	24.10	118.29	4.174	3.431	2
20	22.12	0.203	1.653	40.34	24.10	118.06	4.176	3.432	2
21	20.62	0.206	1.609	38.36	22.35	117.69	4.078	3.343	2
22	20.56	0.206	1.609	38.36	22.35	117.57	4.080	3.342	2
23	20.63	0.206	1.609	38.37	22.35	117.62	4.080	3.343	2
24	20.57	0.206	1.609	38.37	22.35	117.48	4.082	3.343	2
25	20.58	0.206	1.609	38.37	22.35	117.32	4.083	3.343	2
26	20.57	0.206	1.609	38.38	22.36	117.27	4.084	3.343	2
27	20.56	0.206	1.609	38.38	22.36	117.23	4.085	3.343	2
28	20.48	0.207	1.608	38.38	22.35	117.05	4.087	3.342	2
29	20.47	0.207	1.608	38.37	22.35	116.91	4.088	3.341	2
30	20.58	0.206	1.609	38.39	22.36	116.97	4.088	3.343	2
Mean:	21.88	0.200	1.640	39.94	23.75	118.07	4.150	3.410	2
Std. Dev:	0.97	0.00	0.03	1.20	1.06	1.25	0.06	0.05	0.00

Sample: Macondo Crude in unfiltered seawater at 17.8°C with Finasol OSR 52 1:10,000 dilution at 1 atm pressure.

Number	Gamma	Beta	R0	Area	Volume	Theta	Height	Width	Opt
1	22.49	0.199	1.654	40.31	24.04	117.16	4.180	3.431	2
2	22.51	0.199	1.654	40.32	24.04	117.06	4.181	3.432	2
3	22.43	0.200	1.653	40.32	24.05	116.88	4.184	3.431	2
4	22.52	0.199	1.654	40.35	24.07	116.74	4.186	3.433	2
5	22.39	0.200	1.654	40.36	24.07	116.56	4.189	3.431	2
6	22.40	0.200	1.653	40.36	24.07	116.42	4.190	3.432	2
7	22.33	0.201	1.653	40.37	24.08	116.27	4.193	3.431	2
8	22.40	0.200	1.654	40.38	24.08	116.18	4.194	3.432	2
9	22.19	0.202	1.653	40.38	24.08	115.93	4.199	3.430	2
10	22.25	0.201	1.653	40.38	24.08	115.91	4.198	3.431	2
11	21.42	0.208	1.649	40.69	24.20	107.42	4.301	3.428	2
12	21.45	0.208	1.649	40.70	24.21	107.30	4.302	3.429	2
13	21.43	0.208	1.649	40.71	24.21	107.17	4.304	3.429	2
14	21.38	0.209	1.649	40.68	24.19	107.10	4.305	3.427	2
15	21.47	0.208	1.649	40.71	24.21	106.85	4.306	3.429	2
16	21.45	0.208	1.649	40.73	24.22	106.66	4.309	3.429	2
17	21.44	0.208	1.649	40.72	24.21	106.53	4.310	3.429	2
18	21.37	0.209	1.649	40.72	24.21	106.36	4.313	3.428	2
19	21.37	0.209	1.649	40.72	24.21	106.15	4.315	3.428	2
20	21.34	0.209	1.649	40.73	24.21	106.06	4.317	3.427	2
21	21.32	0.209	1.647	40.61	24.13	107.53	4.297	3.423	2
22	21.36	0.208	1.647	40.62	24.13	107.36	4.298	3.425	2
23	21.39	0.208	1.648	40.63	24.14	107.17	4.300	3.425	2
24	21.37	0.208	1.647	40.62	24.14	107.02	4.301	3.425	2
25	21.36	0.208	1.648	40.63	24.14	106.90	4.303	3.424	2
26	21.36	0.208	1.648	40.64	24.15	106.68	4.305	3.425	2
27	21.32	0.209	1.647	40.64	24.14	106.48	4.307	3.424	2
28	21.28	0.209	1.647	40.63	24.13	106.39	4.308	3.424	2
29	21.32	0.209	1.647	40.64	24.14	106.23	4.310	3.424	2
30	21.34	0.209	1.647	40.63	24.14	105.99	4.313	3.425	2
Mean:	21.72	0.210	1.650	40.56	24.14	110.02	4.270	3.430	2
Std. Dev:	0.49	0.00	0.00	0.16	0.06	4.69	0.06	0.00	0.00

Sample: 30°C Macondo Crude in unfiltered seawater at 17.8°C with Finasol OSR 52 1:10 dilution at 1 atm pressure.

Number	Gamma	Beta	R0	Area	Volume	Theta	Height	Width	Opt
1	5.53	0.266	0.927	13.24	4.66	120.02	2.361	1.949	2
2	6.51	0.274	1.021	16.59	6.36	109.32	2.768	2.154	2
3	7.21	0.267	1.060	17.77	7.05	109.49	2.864	2.232	2
Mean:	6.42	0.270	1.000	15.87	6.02	112.94	2.660	2.110	2
Std. Dev:	0.84	0.00	0.07	2.35	1.23	6.13	0.27	0.15	0.00

Sample: 30°C Macondo Crude in unfiltered seawater at 17.8°C with Finasol OSR 52 1:50 dilution at 1 atm pressure.

Number	Gamma	Beta	R0	Area	Volume	Theta	Height	Width	Opt
1	15.06	0.225	1.408	30.00	15.39	111.31	3.681	2.934	2
2	13.72	0.227	1.347	27.47	13.54	114.66	3.493	2.811	2
3	13.81	0.227	1.352	27.68	13.68	114.21	3.510	2.821	2
Mean:	14.20	0.230	1.370	28.38	14.20	113.39	3.560	2.860	2
Std. Dev:	0.75	0.00	0.03	1.40	1.03	1.82	0.10	0.07	0.00

Sample: 30°C Macondo Crude in unfiltered seawater at 17.8°C with Finasol OSR 52 1:100 dilution at 1 atm pressure.

Number	Gamma	Beta	R0	Area	Volume	Theta	Height	Width	Opt
1	18.76	0.211	1.52	34.55	19.01	112.07	3.928	3.161	2
2	19.66	0.207	1.54	35.30	19.66	114.16	3.947	3.201	2
3	18.31	0.216	1.52	34.87	19.19	106.28	4.004	3.164	2
Mean:	18.91	0.210	1.53	34.91	19.29	110.84	3.960	3.180	2
Std. Dev:	0.69	0.00	0.01	0.38	0.34	4.08	0.04	0.02	0.00

Sample: 30°C Macondo Crude in unfiltered seawater at 17.8°C with Finasol OSR 52 1:1000 dilution at 1 atm pressure.

Number	Gamma	Beta	R0	Area	Volume	Theta	Height	Width	Opt
1	23.58	0.206	1.683	41.97	25.57	117.09	4.273	3.496	2
2	23.34	0.205	1.672	41.45	25.08	116.95	4.247	3.474	2
3	24.23	0.205	1.700	42.88	26.34	115.31	4.335	3.532	2
Mean:	23.72	0.210	1.690	42.10	25.66	116.45	4.290	3.500	2
Std. Dev:	0.46	0.00	0.01	0.72	0.64	0.99	0.05	0.03	0.00

Sample: 30°C Macondo Crude in unfiltered seawater at 17.8°C with Finasol OSR 52 1:10,000 dilution at 1 atm pressure.

.Number	Gamma	Beta	R0	Area	Volume	Theta	Height	Width	Opt
1	23.32	0.206	1.675	41.75	25.26	113.01	4.303	3.480	2
2	24.54	0.205	1.712	43.66	26.95	110.20	4.424	3.556	2
3	23.63	0.204	1.677	41.65	25.22	115.88	4.270	3.482	2
Mean:	23.83	0.210	1.690	42.35	25.81	113.03	4.330	3.510	2
Std. Dev:	0.63	0.00	0.02	1.13	0.99	2.84	0.08	0.04	0.00

Sample: 30°C Macondo Crude in unfiltered seawater at 17.8°C with Corexit 9500 1:10 dilution at 1 atm pressure.

Number	Gamma	Beta	R0	Area	Volume	Theta	Height	Width	Opt
1	4.29	0.297	0.863	11.86	3.95	114.32	2.275	1.829	2
2	4.93	0.249	0.846	10.40	3.37	127.47	1.978	1.774	2
3	5.08	0.279	0.909	12.83	4.47	118.87	2.326	1.920	2
Mean:	4.77	0.280	0.870	11.70	3.93	120.22	2.190	1.840	2
Std. Dev:	0.42	0.02	0.03	1.22	0.55	6.68	0.19	0.07	0.00

Sample: 30°C Macondo Crude in unfiltered seawater at 17.8°C with Corexit 9500 1:100 dilution at 1 atm pressure

Number	Gamma	Beta	R0	Area	Volume	Theta	Height	Width	Opt
1	17.10	0.205	1.429	30.00	15.60	124.44	3.537	2.969	2
2	17.45	0.213	1.472	32.27	17.27	118.01	3.742	3.061	2
3	16.03	0.213	1.413	29.67	15.28	120.46	3.563	2.940	2
Mean:	16.86	0.210	1.440	30.65	16.05	120.97	3.610	2.990	2
Std. Dev:	0.74	0.00	0.03	1.42	1.07	3.25	0.11	0.06	0.00

Sample: 30°C Macondo Crude in unfiltered seawater at 17.8°C with Corexit 9500 1:1000 dilution at 1 atm pressure.

Number	Gamma	Beta	R0	Area	Volume	Theta	Height	Width	Opt
1	24.37	0.205	1.707	43.54	26.72	103.83	4.474	3.546	2
2	24.09	0.204	1.695	42.8	26.13	108.50	4.395	3.520	2
3	24.00	0.206	1.697	43.19	26.32	98.91	4.498	3.526	2
Mean:	24.15	0.210	1.700	43.18	26.39	103.75	4.460	3.530	2
Std. Dev:	0.19	0.00	0.01	0.37	0.30	4.80	0.05	0.01	0.00

Sample: 30°C Macondo Crude in unfiltered seawater at 17.4°C at 1 atm pressure.

Number	Gamma	Beta	R0	Area	Volume	Theta	Height	Width	Opt
1	23.38	0.204	1.67	41.49	24.98	110.83	4.307	3.468	2
2	23.52	0.207	1.684	42.38	25.72	106.89	4.392	3.499	2
3	23.26	0.208	1.682	42.57	25.73	97.03	4.488	3.496	2
Mean:	23.39	0.210	1.68	42.15	25.48	104.92	4.400	3.490	2
Std. Dev:	0.13	0.00	0.01	0.58	0.43	7.11	0.09	0.02	0.00

Sample: 17.4°C Macondo Crude in unfiltered seawater at 17.4°C at 1 atm pressure.

Number	Gamma	Beta	R0	Area	Volume	Theta	Height	Width	Opt
1	22.54	0.202	1.666	41.12	24.69	112.89	4.265	3.457	2
2	21.22	0.195	1.547	38.22	23.17	90.11	4.031	3.199	2
3	21.61	0.203	1.634	39.54	23.30	114.05	4.173	3.391	2
Mean:	21.79	0.200	1.620	39.63	23.72	105.68	4.160	3.350	2
Std. Dev:	0.68	0.00	0.06	1.45	0.84	13.50	0.12	0.13	0.00

Appendix B

PAH Analysis Following Biodegradation

The data provided in Table 4.6 and Table 4.7 and here in Appendix B indicate that the inoculated samples have lower concentrations of several PAHs than the values from the Time 0 sample (Sample O). Some of the observed loss could be explained by effects other than biodegradation. For example, 2-ring PAHs (especially the naphthalene) can be lost by evaporation more easily than other PAHs. Therefore, the significant concentration decrease of those PAHs could be a combined effect of evaporation and biodegradation. The concentration of other PAHs, such as phenanthrene, did decrease compared to Sample O. The results of the hydrocarbon analysis were noisy and showed no significant trends relative to DOR or droplet size, or even to the presence or absence of dispersant.

Appendix B

PAH Analysis Following Biodegradation

#	Compound	MDL (ug/L)	PAHs (ug/L)				
			Sample A	Sample B	Sample C	Sample D	Sample E
1	Naphthalene	0.0026	U	U	U	U	U
2	2,6-Dimethylnaphthalene	0.0011	U	2.95	2.27	3.17	3.96
3	C1-Naphthalenes	0.0023	U	U	U	U	U
4	C2-Naphthalenes	0.0096	U	57.98	48.90	68.15	76.10
5	C3-Naphthalenes	0.0112	U	444.57	414.24	477.71	360.26
6	C4-Naphthalenes	0.0113	U	376.09	367.33	400.64	340.37
7	Biphenyl	0.0005	U	U	U	U	U
8	Acenaphthylene	0.0004	U	U	U	U	U
9	Acenaphthene	0.0004	U	U	U	U	U
10	Fluorene	0.0011	U	16.09	14.97	17.36	14.05
11	1-Methyl fluorene	0.0010	U	109.58	105.85	116.82	97.96
12	C1-Fluorenes	0.0035	U	149.49	155.31	159.78	126.25
13	C2-Fluorenes	0.0026	U	344.82	350.95	378.28	326.82
14	C3-Fluorenes	0.0131	U	332.46	344.02	353.57	333.46
15	Dibenzothiophene	0.0012	U	10.78	10.53	10.97	9.54
16	C1-Dibenzothiophenes	0.0030	U	58.69	60.70	59.77	55.47
17	C2-Dibenzothiophenes	0.0023	U	106.04	111.98	114.98	107.01
18	C3-Dibenzothiophenes	0.0031	U	90.04	95.21	94.87	94.16
19	C4-Dibenzothiophenes	0.0022	U	37.75	38.13	40.97	38.51
20	Phenanthrene	0.0025	U	92.04	89.90	92.18	82.61
21	Anthracene	0.0002	U	4.01	4.46	4.10	3.46
22	1-methyl Phenanthrene	0.0008	U	117.38	121.62	120.91	115.07
23	3,6-DMP	0.0009	U	57.27	57.11	60.59	55.42
24	2,6-DMP	0.0003	U	59.94	63.13	65.59	58.76
25	1,7-DMP	0.0006	U	68.76	69.90	78.82	67.34
26	C1-Phen/An	0.0034	U	557.88	575.23	581.75	534.15
27	C2-Phen/An	0.0038	U	798.99	828.03	830.88	778.72
28	C3-Phen/An	0.0028	U	508.88	536.43	544.05	507.08
29	C4-Phen/An	0.0041	U	141.18	145.32	147.75	137.53
30	Fluoranthene	0.0004	U	3.70	3.70	3.31	3.45

#	Compound	PAHs (ug/L)				
		Sample F	Sample G	Sample H	Sample I	Sample J
1	Naphthalene	U	0.07	U	0.00	U
2	2,6-Dimethylnaphthalene	0.71	3.52	U	4.11	17.63
3	C1-Naphthalenes	U	U	U	U	U
4	C2-Naphthalenes	25.91	66.73	U	33.62	105.55
5	C3-Naphthalenes	258.30	456.86	U	327.39	489.13
6	C4-Naphthalenes	278.18	386.71	U	397.84	427.82
7	Biphenyl	U	U	U	U	U
8	Acenaphthylene	U	U	U	U	U
9	Acenaphthene	U	U	U	U	U
10	Fluorene	11.20	18.54	U	14.17	19.74
11	1-Methyl fluorene	80.27	109.66	U	105.43	111.62
12	C1-Fluorenes	116.55	161.95	U	163.57	175.92
13	C2-Fluorenes	286.42	356.68	U	368.60	358.38
14	C3-Fluorenes	286.40	327.78	U	382.92	327.18
15	Dibenzothiophene	7.84	11.39	U	9.80	11.49
16	C1-Dibenzothiophenes	45.70	62.14	U	61.83	65.16
17	C2-Dibenzothiophenes	87.17	111.89	U	119.04	112.49
18	C3-Dibenzothiophenes	76.79	93.40	U	102.90	93.73
19	C4-Dibenzothiophenes	32.05	38.20	U	46.96	43.07
20	Phenanthrene	66.60	98.83	U	84.74	95.17
21	Anthracene	3.29	3.96	U	3.01	4.29
22	1-methyl Phenanthrene	91.43	122.25	U	121.99	116.91
23	3,6-DMP	45.00	57.06	U	59.94	58.42
24	2,6-DMP	46.82	63.76	U	63.01	61.98
25	1,7-DMP	56.93	75.98	U	71.49	72.02
26	C1-Phen/An	439.28	565.65	U	575.94	570.47
27	C2-Phen/An	643.63	827.50	U	860.50	820.57
28	C3-Phen/An	406.97	514.46	U	550.62	518.12
29	C4-Phen/An	112.05	142.80	U	149.83	141.83
30	Fluoranthene	2.40	3.54	U	3.82	3.16

#	Compound	PAHs (ug/L)				
		Sample K	Sample L	Sample M	Sample N	Sample O
1	Naphthalene	U	U	U	U	227.85
2	2,6-Dimethylnaphthalene	33.60	50.05	58.10	23.67	726.26
3	C1-Naphthalenes	U	U	U	U	1011.24
4	C2-Naphthalenes	160.50	239.48	270.90	131.75	2696.94
5	C3-Naphthalenes	637.65	722.20	714.97	555.89	2027.47
6	C4-Naphthalenes	487.33	523.92	486.94	453.68	792.95
7	Biphenyl	U	1.03	U	U	142.76
8	Acenaphthylene	U	U	U	U	U
9	Acenaphthene	U	U	U	U	U
10	Fluorene	21.29	28.42	27.22	22.50	98.07
11	1-Methyl fluorene	126.01	142.76	130.71	122.61	234.14
12	C1-Fluorenes	198.28	218.68	206.40	186.10	344.17
13	C2-Fluorenes	383.14	405.91	376.73	369.21	471.48
14	C3-Fluorenes	335.19	347.61	347.57	357.29	378.95
15	Dibenzothiophene	12.22	13.87	12.96	12.35	22.73
16	C1-Dibenzothiophenes	66.72	73.40	69.65	69.07	85.81
17	C2-Dibenzothiophenes	117.74	122.47	116.28	118.45	132.00
18	C3-Dibenzothiophenes	99.44	104.73	102.29	99.77	107.81
19	C4-Dibenzothiophenes	44.59	46.54	44.99	45.49	46.75
20	Phenanthrene	99.81	113.80	101.43	98.57	163.85
21	Anthracene	4.11	5.16	4.05	4.17	5.45
22	1-methyl Phenanthrene	121.72	130.08	121.82	120.72	147.43
23	3,6-DMP	59.84	60.78	57.87	58.64	65.47
24	2,6-DMP	59.75	67.60	60.50	66.27	67.76
25	1,7-DMP	73.47	73.56	69.98	75.84	78.01
26	C1-Phen/An	594.62	623.83	590.85	579.48	717.22
27	C2-Phen/An	833.24	864.14	843.40	819.60	934.37
28	C3-Phen/An	532.64	552.04	544.04	534.77	571.95
29	C4-Phen/An	148.27	153.87	150.68	151.44	154.36
30	Fluoranthene	3.55	3.37	3.07	3.63	4.63

#	Compound	MDL (ug/L)	PAHs (ug/L)				
			Sample A	Sample B	Sample C	Sample D	Sample E
31	Pyrene	0.0015	U	9.48	9.89	9.91	9.69
32	C1-Fluor/Py	0.0008	U	60.89	63.65	66.04	63.60
33	C2-Fluor/Py	0.0013	U	93.10	99.93	99.60	94.52
34	C3-Fluor/Py	0.0022	U	102.95	106.96	107.29	99.46
35	Benzo [a] anthracene	0.0003	U	7.96	7.03	7.27	7.29
36	Chrysene	0.0006	U	33.13	35.52	36.07	33.82
37	C1-Chrysenes	0.0008	U	74.40	79.67	78.07	77.03
38	C2-Chrysenes	0.0030	U	94.94	100.10	98.07	102.48
39	C3-Chrysenes	0.0066	U	64.72	64.89	68.70	67.50
40	C4-Chrysenes	0.0141	U	38.67	41.03	41.07	42.41
41	Benzo [b] fluoranthene	0.0008	U	5.95	5.72	5.77	5.12
42	Benzo [k] fluoranthene	0.0010	U	U	U	U	U
43	Benzo [e] pyrene	0.0011	U	6.69	7.37	6.45	7.00
44	Benzo [a] pyrene	0.0010	U	1.29	1.33	1.16	0.78
45	Perylene	0.0010	U	9.27	10.21	9.94	9.36
46	Indeno [1,2,3-c,d] pyrene	0.0002	U	U	U	U	U
47	Dibenzo [a,h] anthracene	0.0003	U	2.93	1.84	1.12	1.35
48	Benzo [g,h,i] perylene	0.0002	U	1.87	1.87	1.15	1.35

U: below method detection limit

Recovery	MDL (ug/L)	Sample A	Sample B	Sample C	Sample D	Sample E
d8-Naphthalene		84%	77%	68%	63%	70%
d10-Acenaphthene		111%	91%	84%	80%	90%
d10-Phenanthrene		51%	105%	98%	95%	105%
d12-Chrysene		84%	78%	67%	74%	69%
d12-Perylene		219%	85%	67%	77%	80%

#	Compound	PAHs (ug/L)				
		Sample F	Sample G	Sample H	Sample I	Sample J
31	Pyrene	7.73	9.49	U	9.52	8.75
32	C1-Fluor/Py	48.67	61.22	U	67.28	64.61
33	C2-Fluor/Py	74.14	95.07	U	103.34	94.41
34	C3-Fluor/Py	77.54	101.74	U	112.32	107.64
35	Benzo [a] anthracene	4.04	7.26	U	8.26	6.91
36	Chrysene	21.34	30.91	U	34.50	32.44
37	C1-Chrysenes	43.37	69.87	U	80.43	75.35
38	C2-Chrysenes	58.50	90.22	U	103.01	96.18
39	C3-Chrysenes	39.69	63.87	U	68.58	62.58
40	C4-Chrysenes	24.95	38.31	U	42.55	40.33
41	Benzo [b] fluoranthene	2.48	5.59	U	4.94	4.65
42	Benzo [k] fluoranthene	U	U	U	3.43	2.06
43	Benzo [e] pyrene	3.39	6.11	U	7.26	6.22
44	Benzo [a] pyrene	0.42	0.51	U	1.24	0.77
45	Perylene	4.91	9.30	U	8.91	8.40
46	Indeno [1,2,3-c,d] pyrene	U	U	U	U	U
47	Dibenzo [a,h] anthracene	U	1.40	U	1.60	1.42
48	Benzo [g,h,i] perylene	0.54	1.30	U	1.58	1.60

U: below method detection limit

Recovery	Sample F	Sample G	Sample H	Sample I	Sample J
d8-Naphthalene	45%	76%	94%	68%	64%
d10-Acenaphthene	51%	84%	120%	89%	88%
d10-Phenanthrene	64%	96%	73%	110%	101%
d12-Chrysene	70%	79%	131%	74%	76%
d12-Perylene	77%	84%	240%	86%	85%

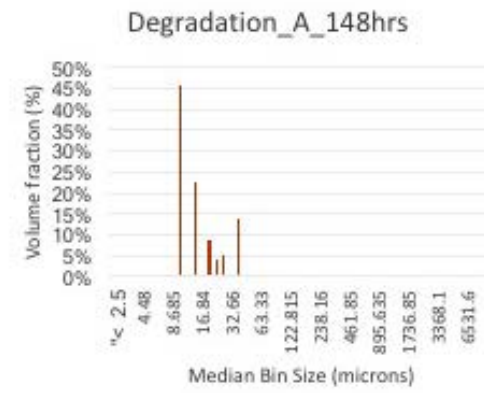
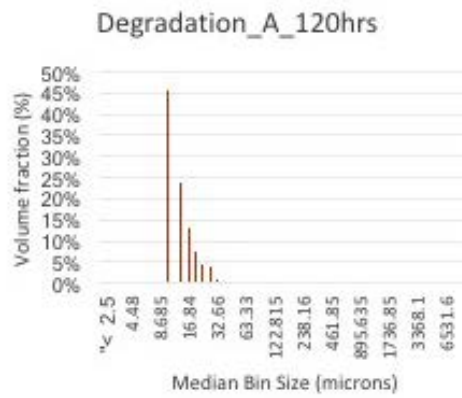
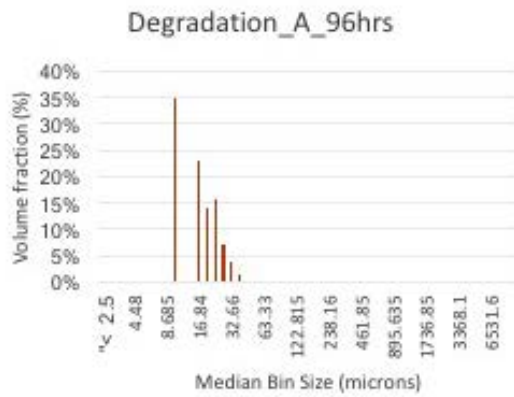
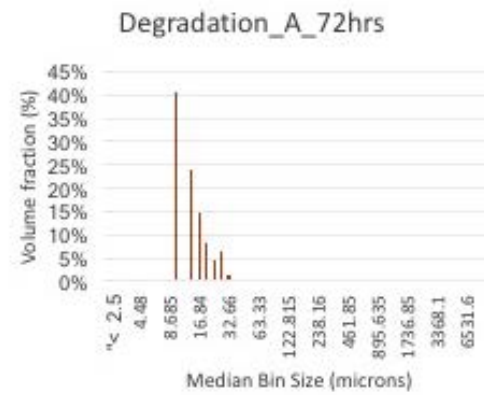
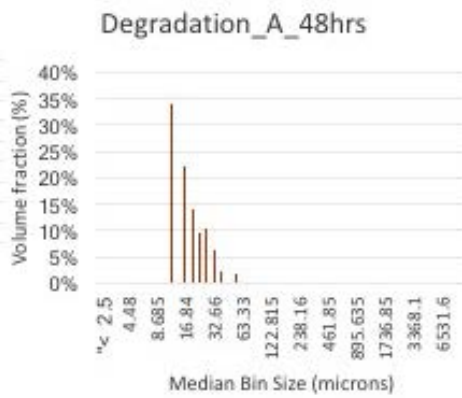
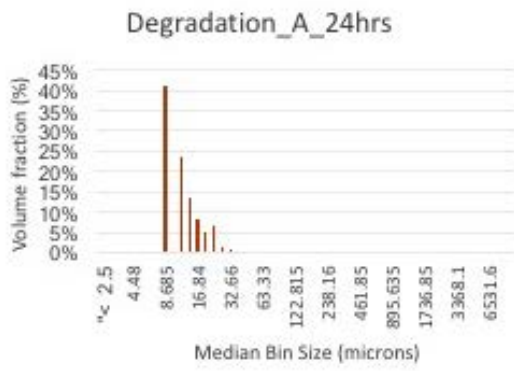
#	Compound	PAHs (ug/L)				
		Sample K	Sample L	Sample M	Sample N	Sample O
31	Pyrene	8.98	9.14	8.81	8.83	10.27
32	C1-Fluor/Py	65.17	69.07	64.77	67.31	67.25
33	C2-Fluor/Py	98.08	99.35	100.13	97.87	104.19
34	C3-Fluor/Py	106.02	108.18	105.87	109.88	113.46
35	Benzo [a] anthracene	8.36	8.14	6.74	7.25	8.53
36	Chrysene	32.40	34.46	32.93	32.89	37.00
37	C1-Chrysenes	75.75	77.12	76.79	76.79	86.45
38	C2-Chrysenes	95.26	100.30	94.42	96.85	110.35
39	C3-Chrysenes	60.85	65.10	62.35	63.70	72.69
40	C4-Chrysenes	37.51	38.61	38.06	40.83	47.14
41	Benzo [b] fluoranthene	4.87	4.22	4.43	4.10	5.68
42	Benzo [k] fluoranthene	3.68	3.52	3.27	3.54	4.49
43	Benzo [e] pyrene	7.28	6.74	7.26	6.62	8.21
44	Benzo [a] pyrene	1.46	0.96	1.04	0.74	2.20
45	Perylene	9.32	9.79	8.84	8.55	10.11
46	Indeno [1,2,3-c,d] pyrene	5.89	U	U	U	6.13
47	Dibenzo [a,h] anthracene	13.65	U	U	1.49	14.48
48	Benzo [g,h,i] perylene	6.78	1.55	1.02	1.05	7.19

U: below method detection limit

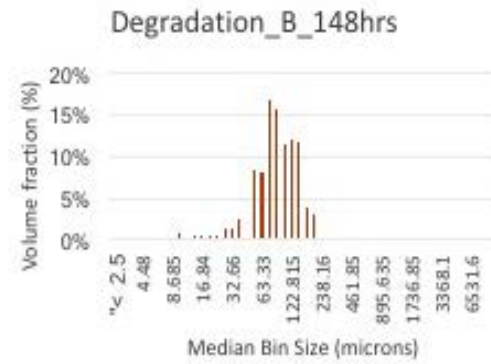
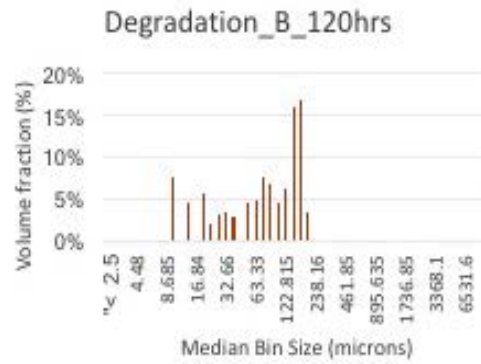
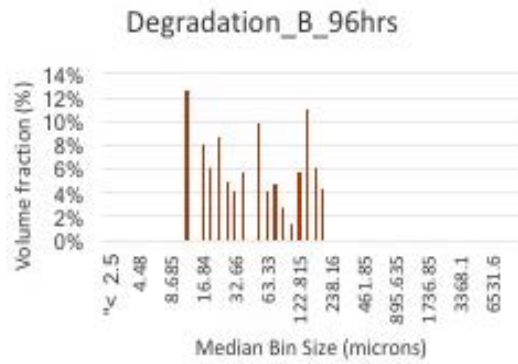
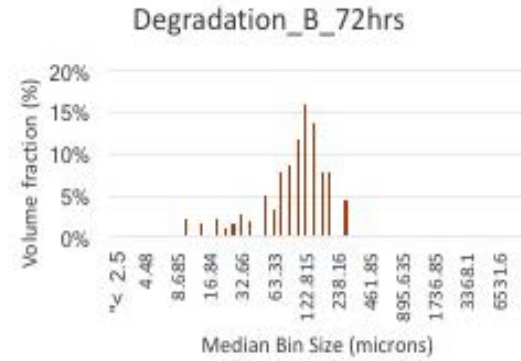
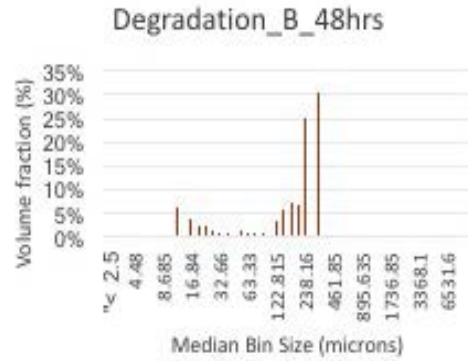
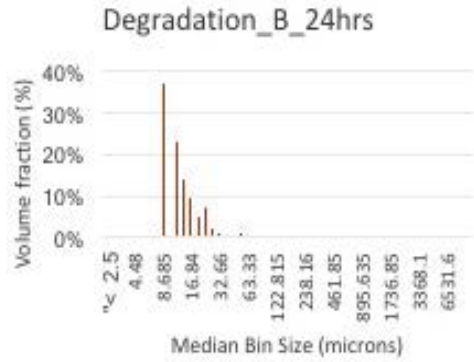
Recovery	Sample K	Sample L	Sample M	Sample N	Sample O
d8-Naphthalene	71%	67%	72%	80%	91%
d10-Acenaphthene	94%	88%	95%	99%	95%
d10-Phenanthrene	112%	102%	109%	114%	107%
d12-Chrysene	86%	80%	81%	81%	77%
d12-Perylene	88%	81%	86%	93%	91%

Appendix C

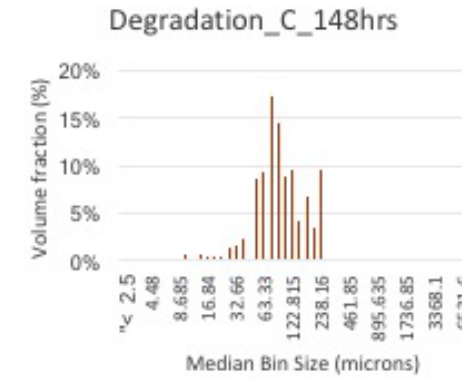
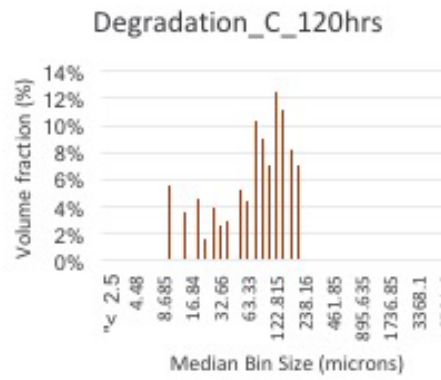
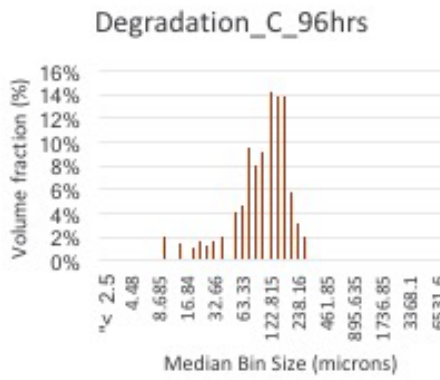
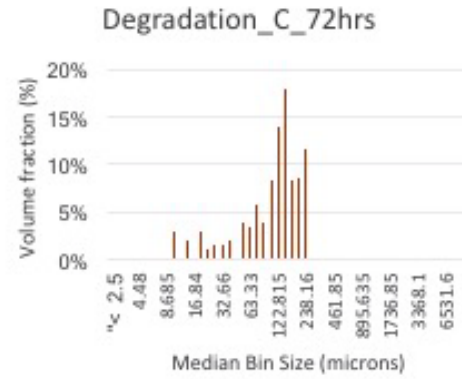
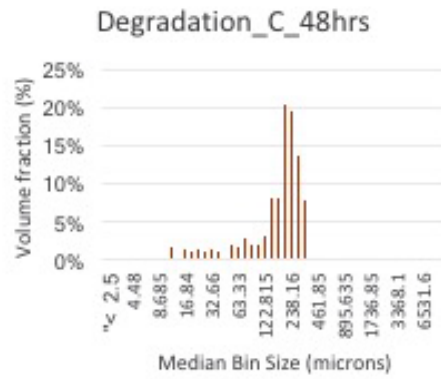
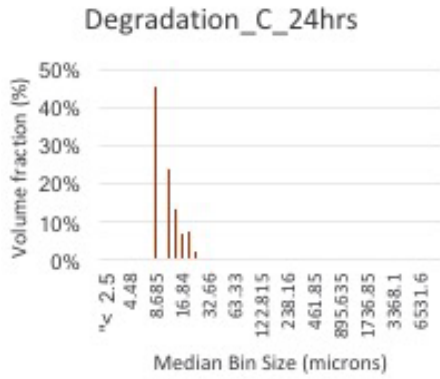
Droplet Size Distribution



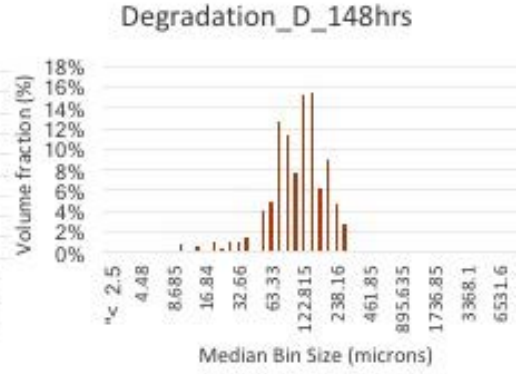
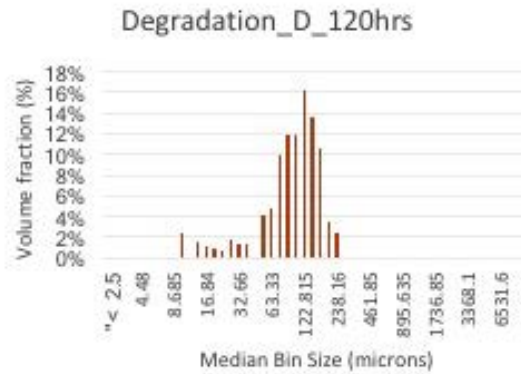
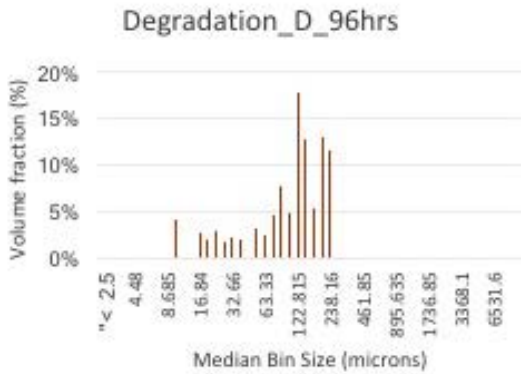
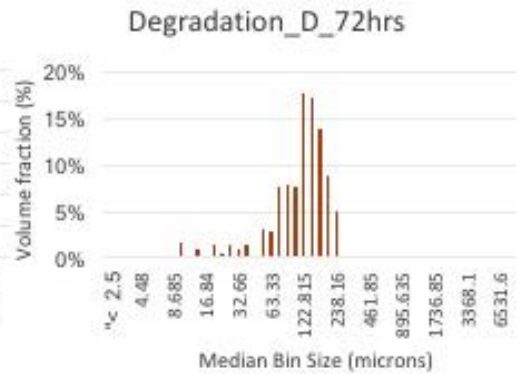
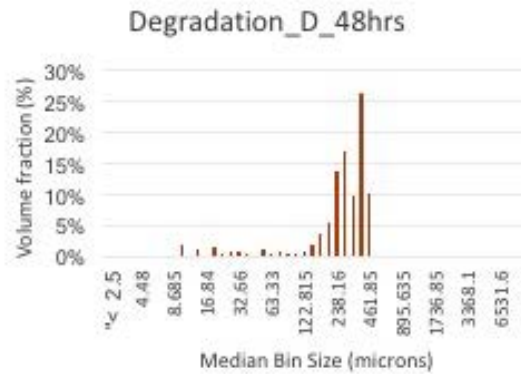
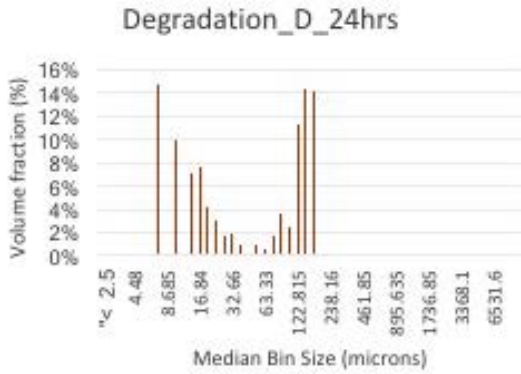
Bacteria; no dispersant



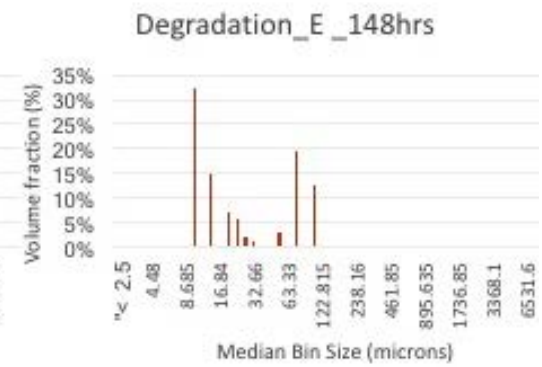
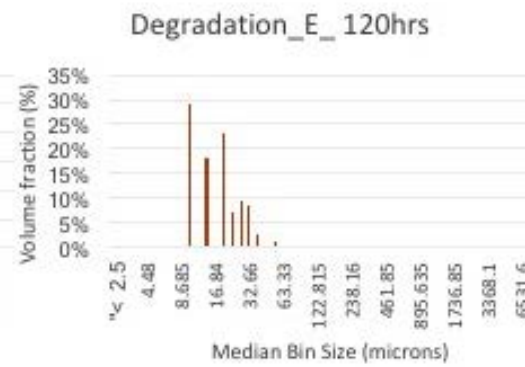
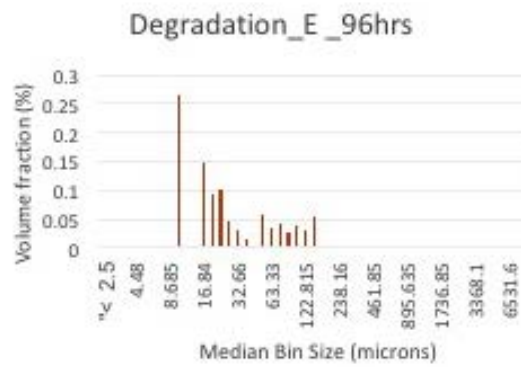
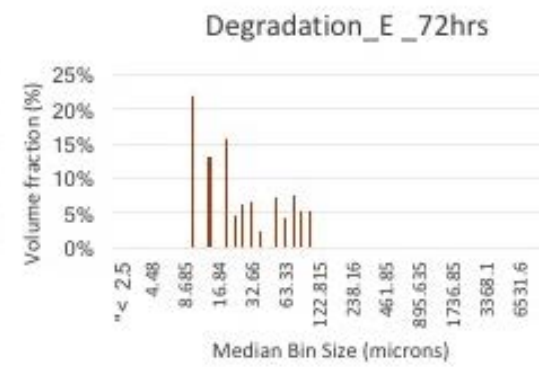
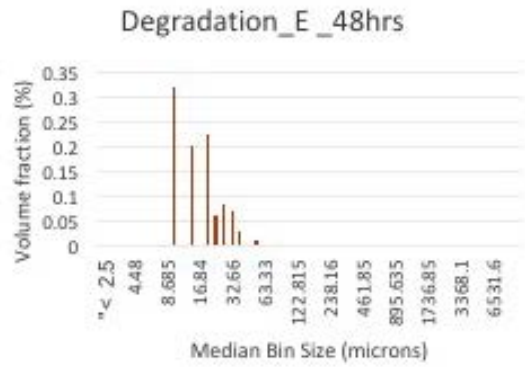
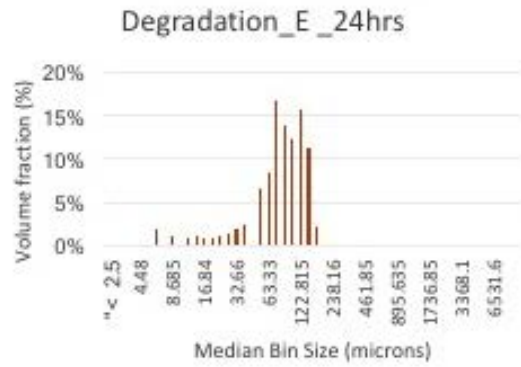
Bacteria; no dispersant



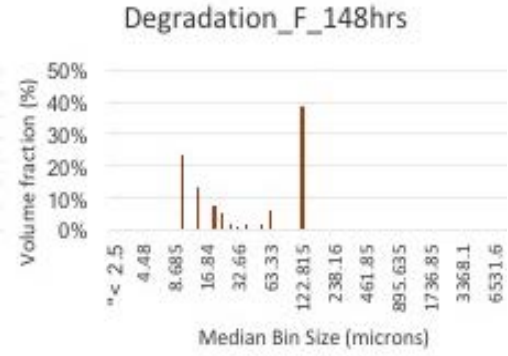
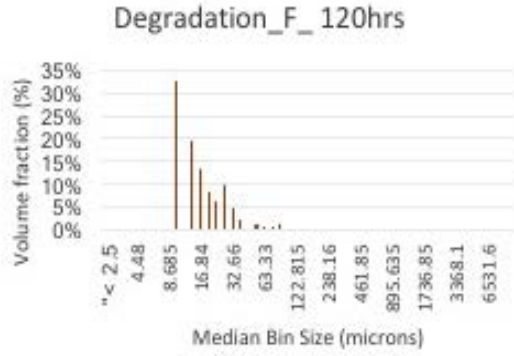
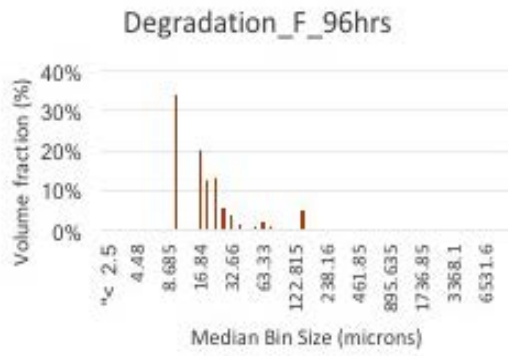
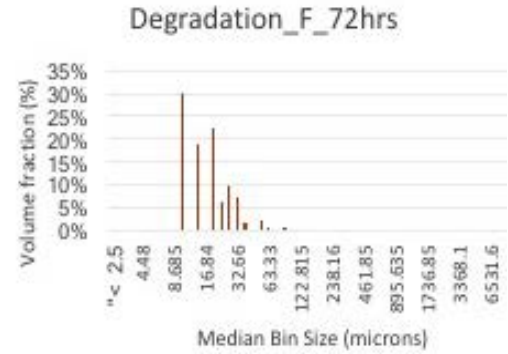
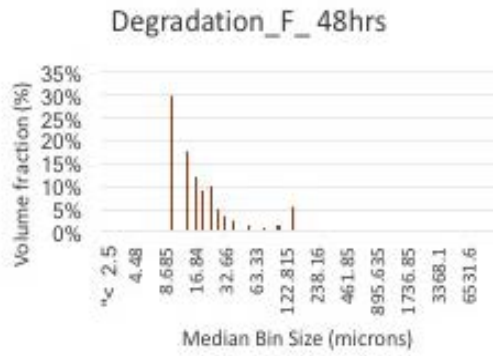
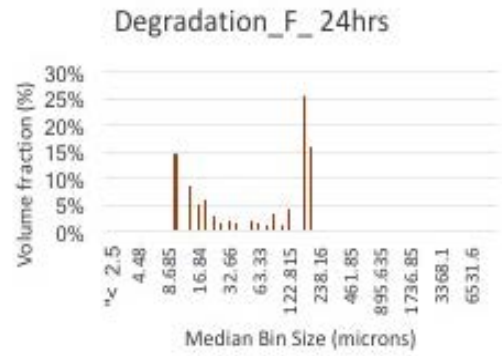
Bacteria; no dispersant



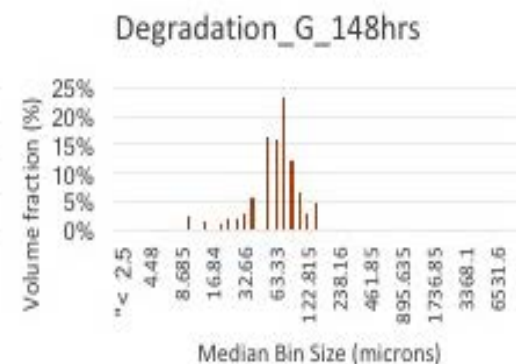
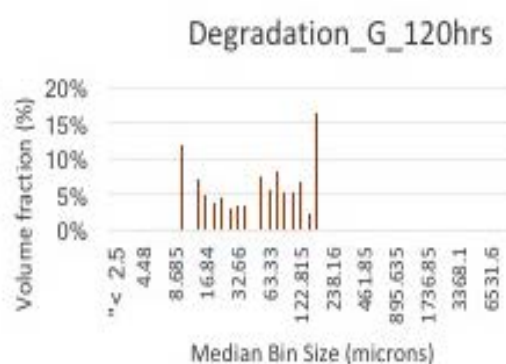
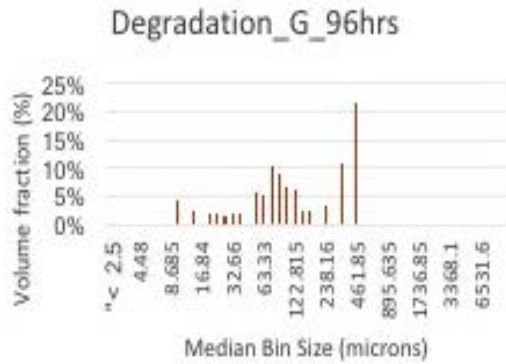
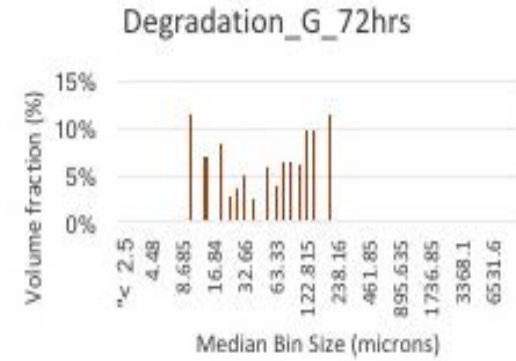
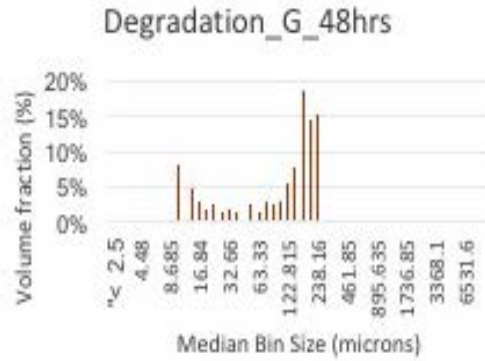
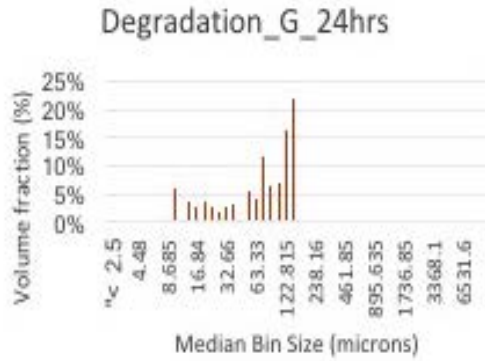
Bacteria; DOR = 1:100



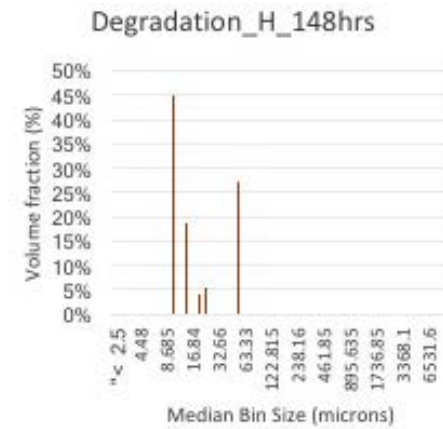
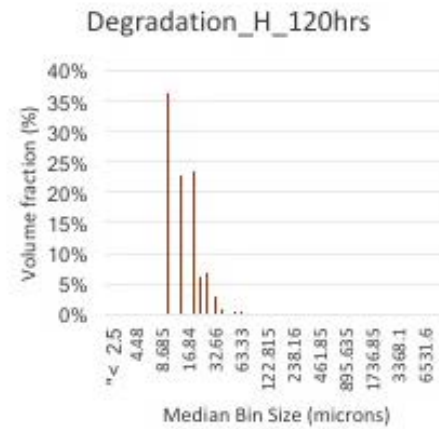
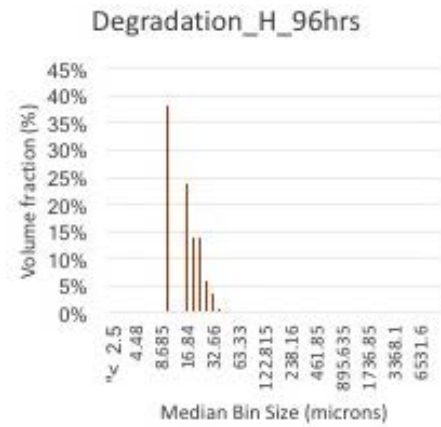
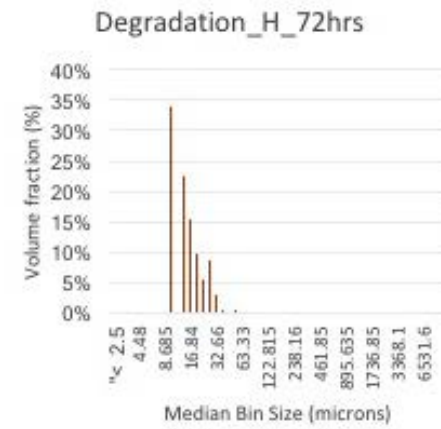
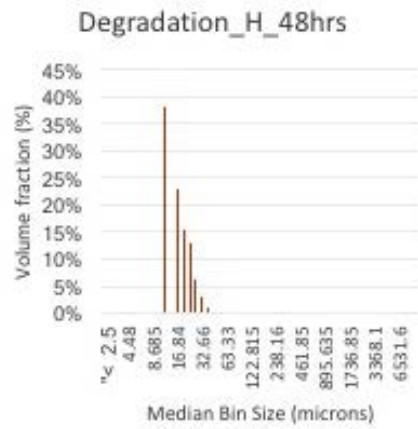
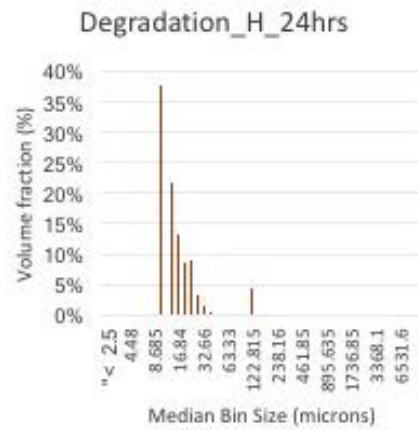
Bacteria; DOR = 1:40



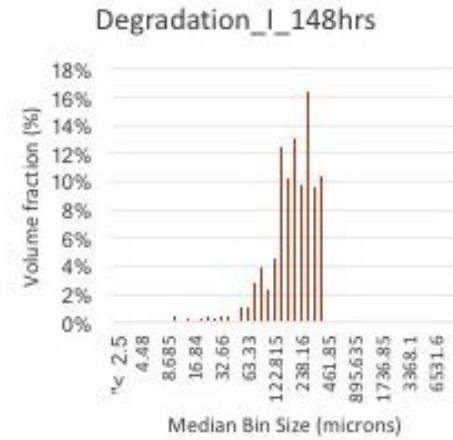
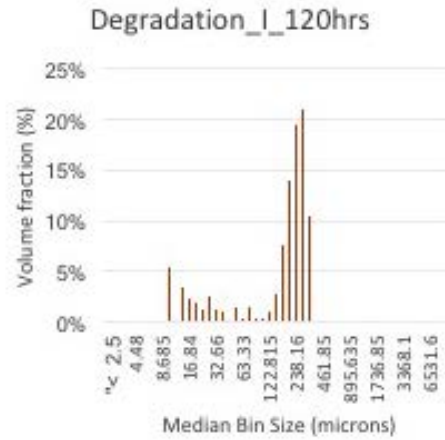
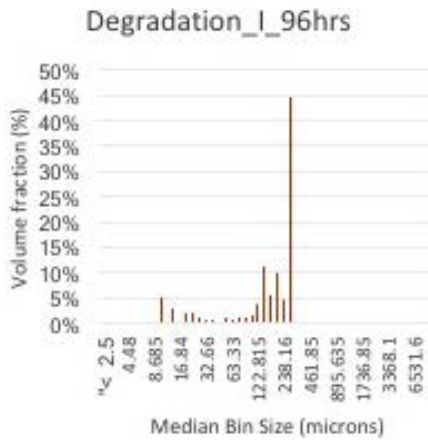
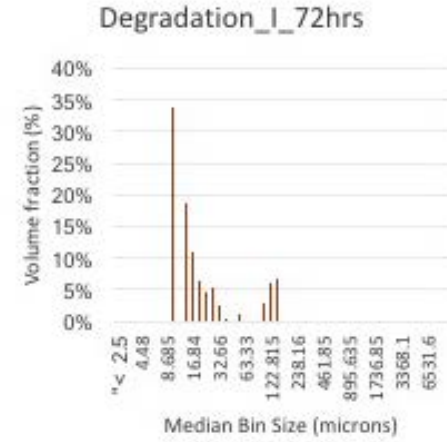
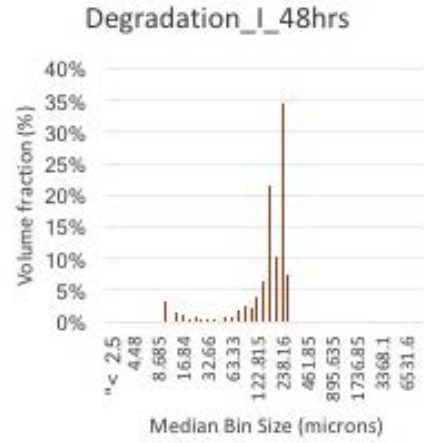
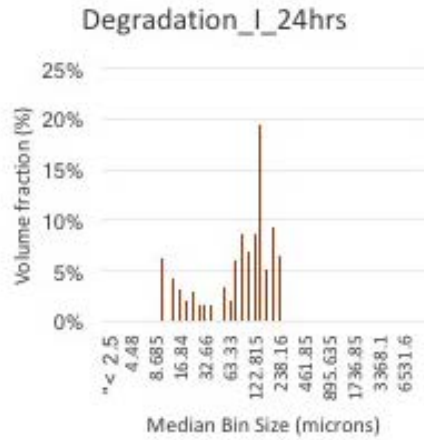
Bacteria; DOR = 1:20



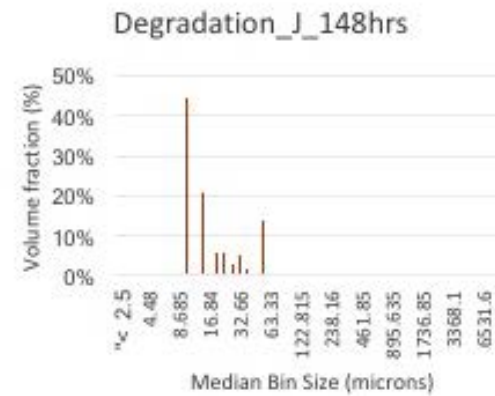
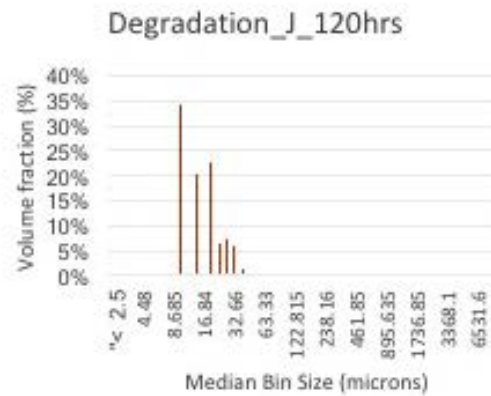
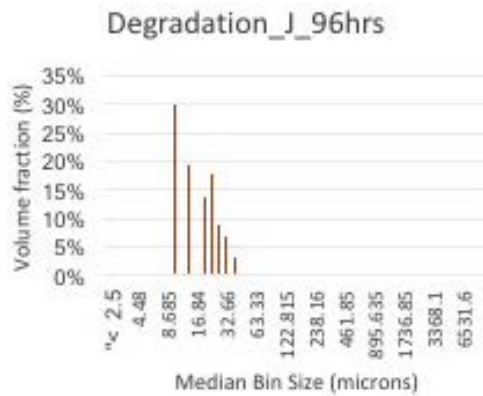
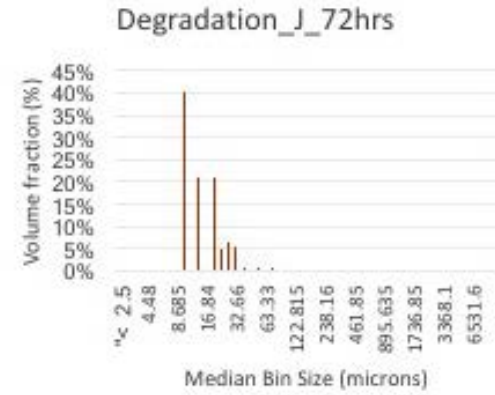
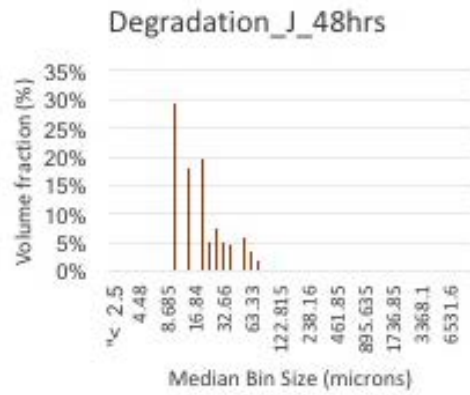
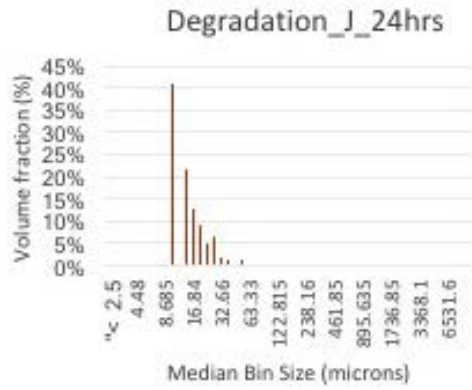
Bacteria; DOR = 1:10



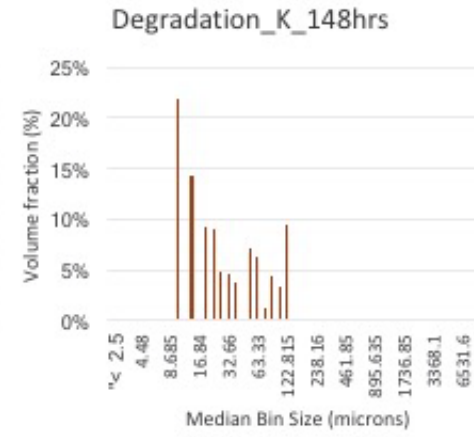
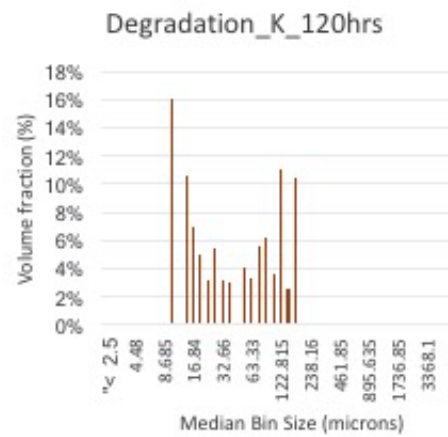
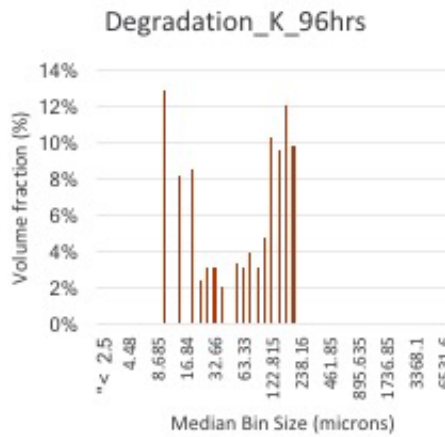
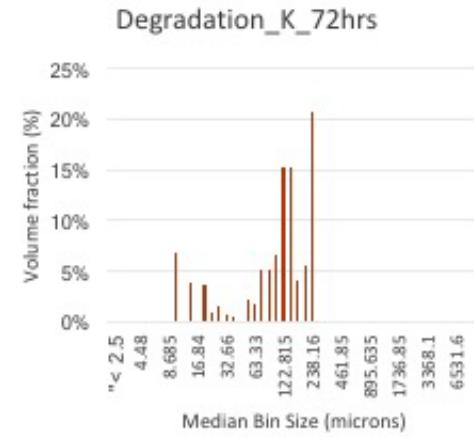
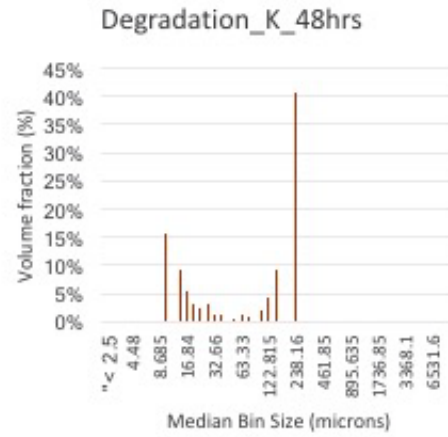
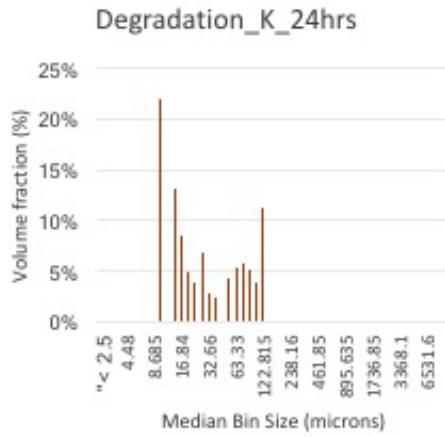
Fungi; No oil, no dispersant



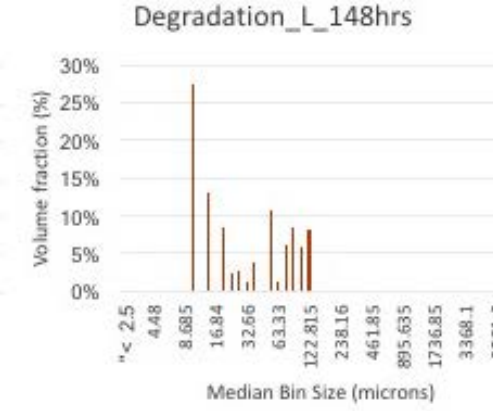
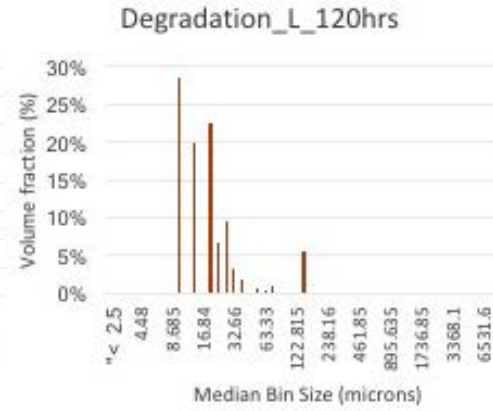
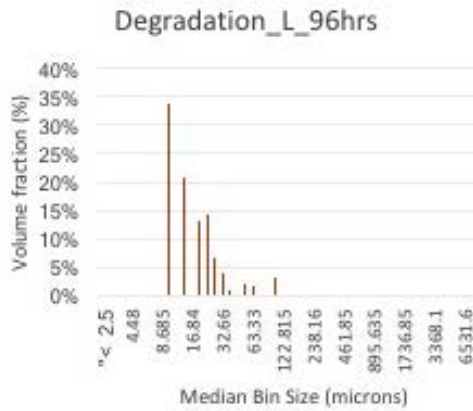
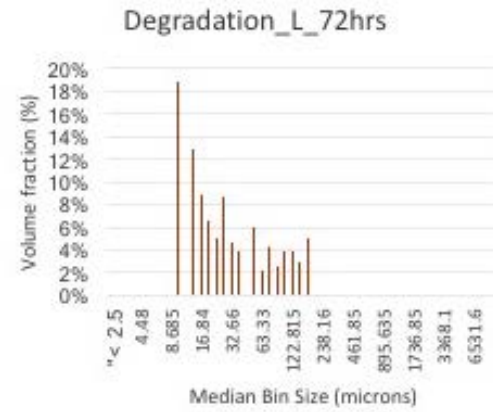
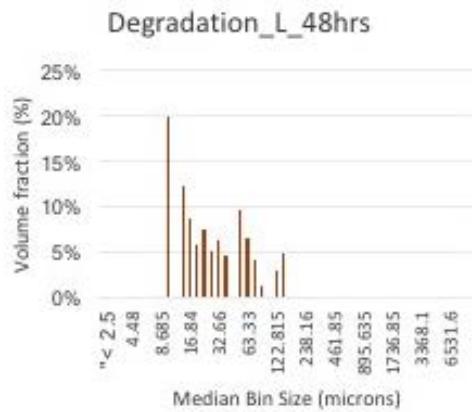
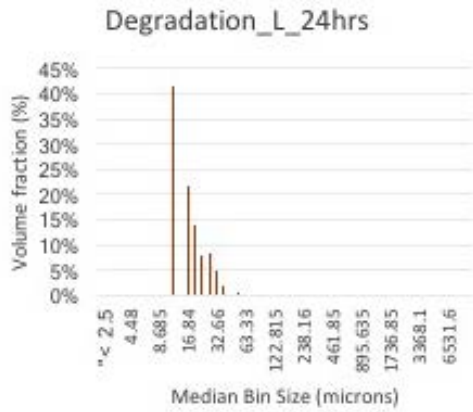
Fungi; No dispersant



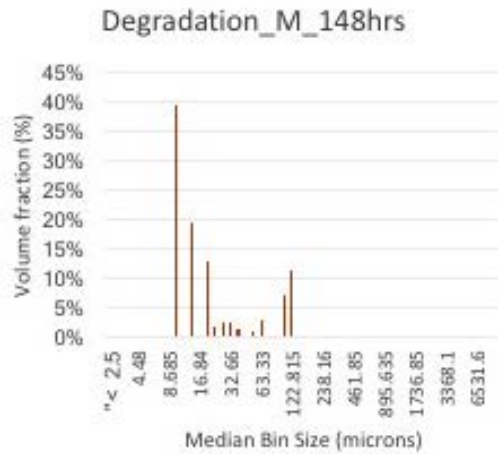
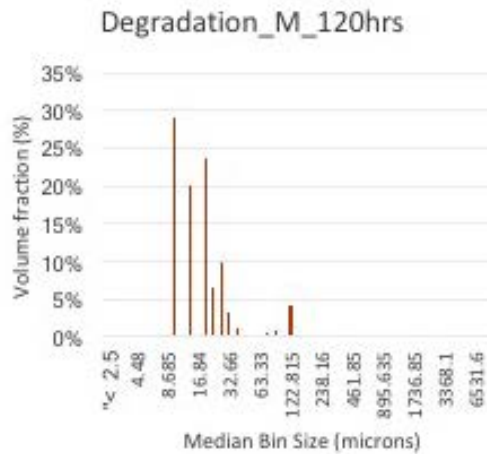
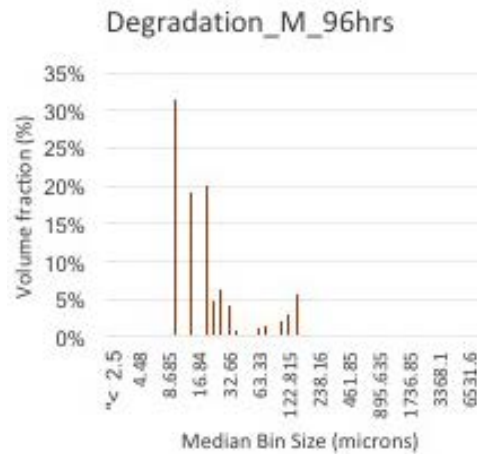
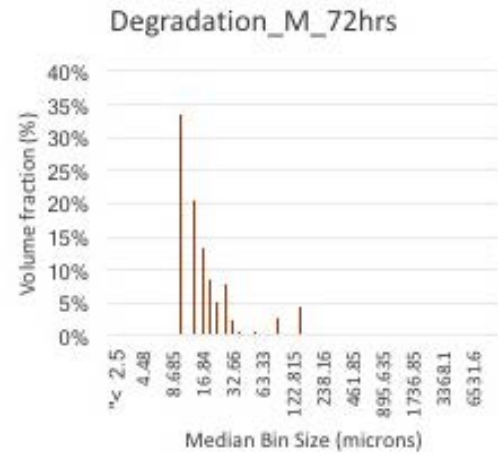
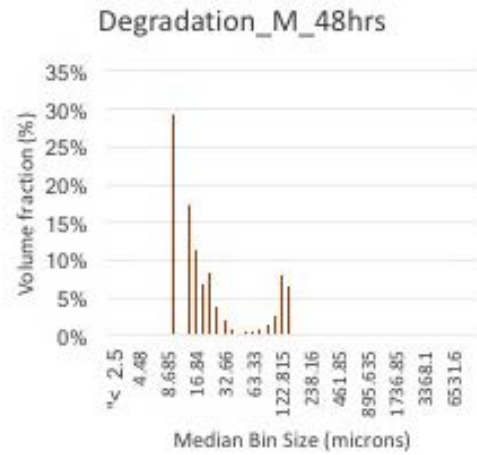
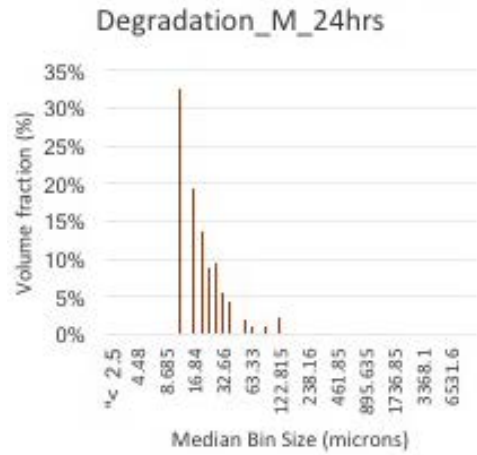
Fungi; DOR= 1:200



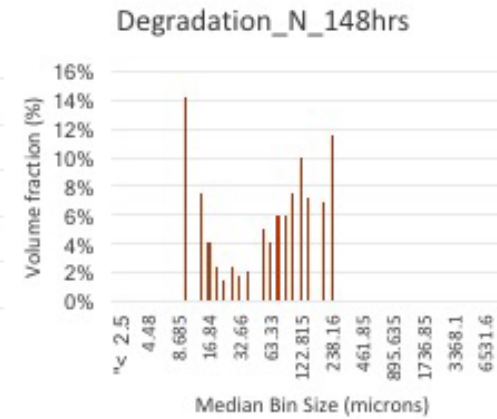
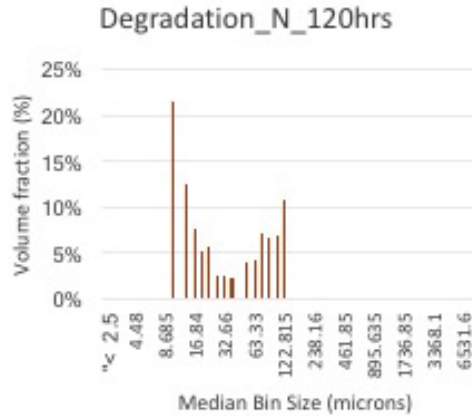
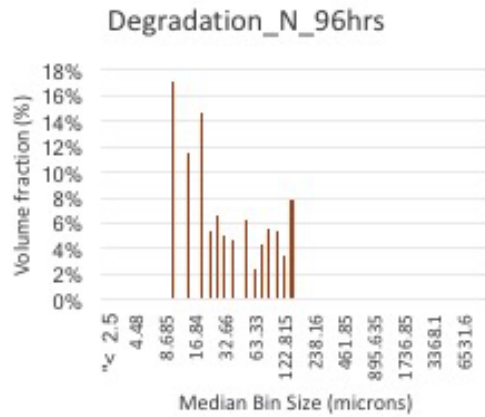
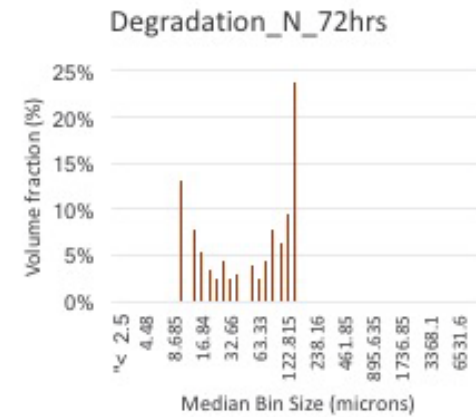
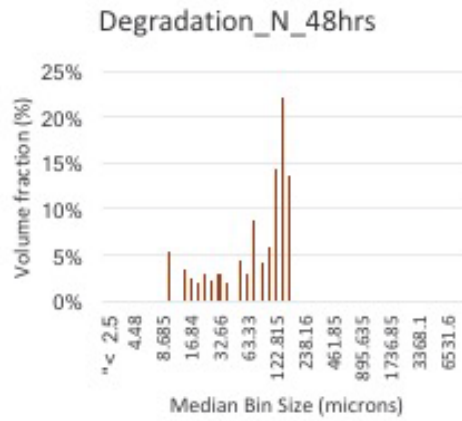
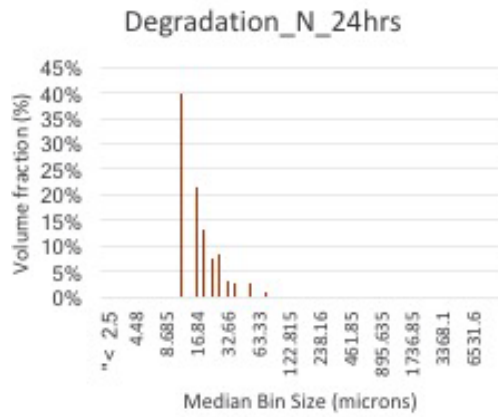
Fungi; DOR= 1:100



Fungi; DOR= 1:40



Fungi; DOR= 1:20



Fungi; DOR= 1:10

Appendix D

Determination of Oil, Dispersant, and Seawater Fluorescent Spectra

Appendix D

Determination of Oil, Dispersant, and Seawater Fluorescent Spectra

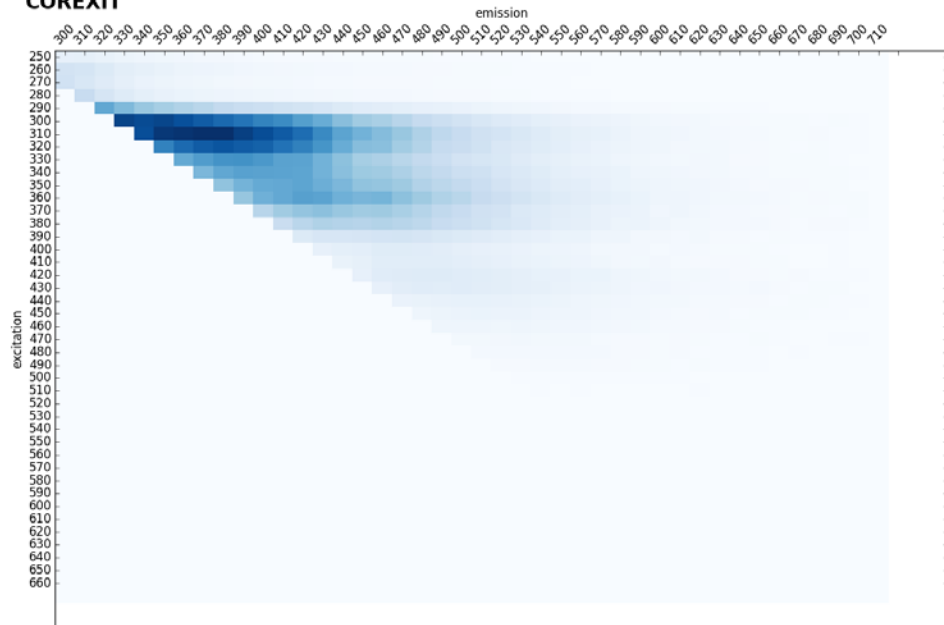
SEAWATER



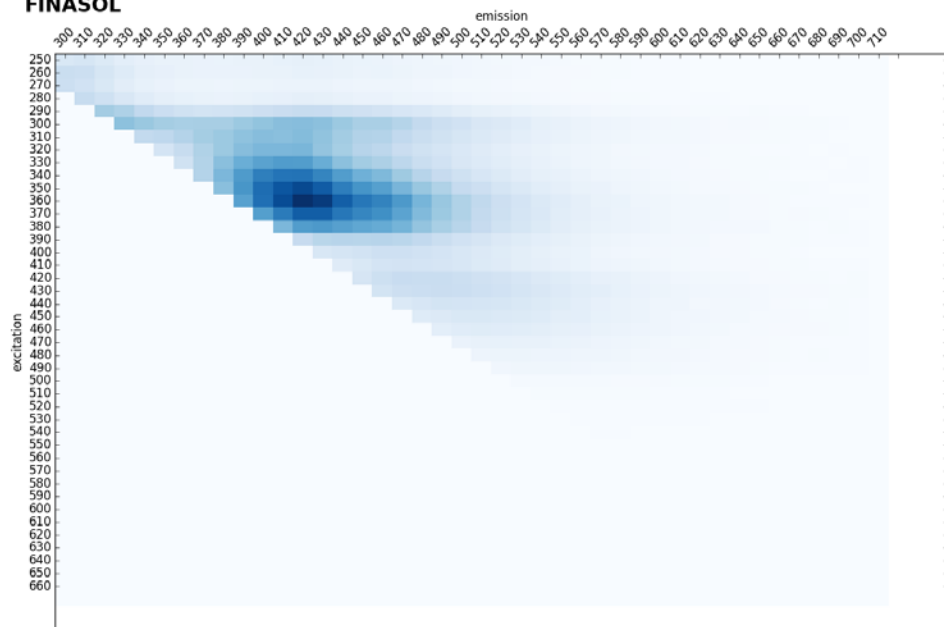
SEAWATER_0.22



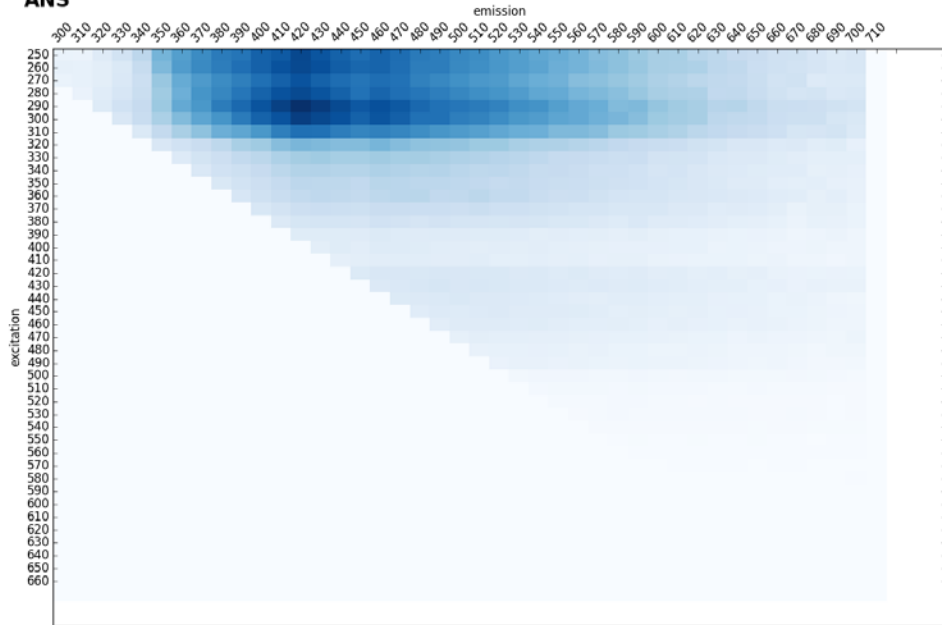
COREXIT



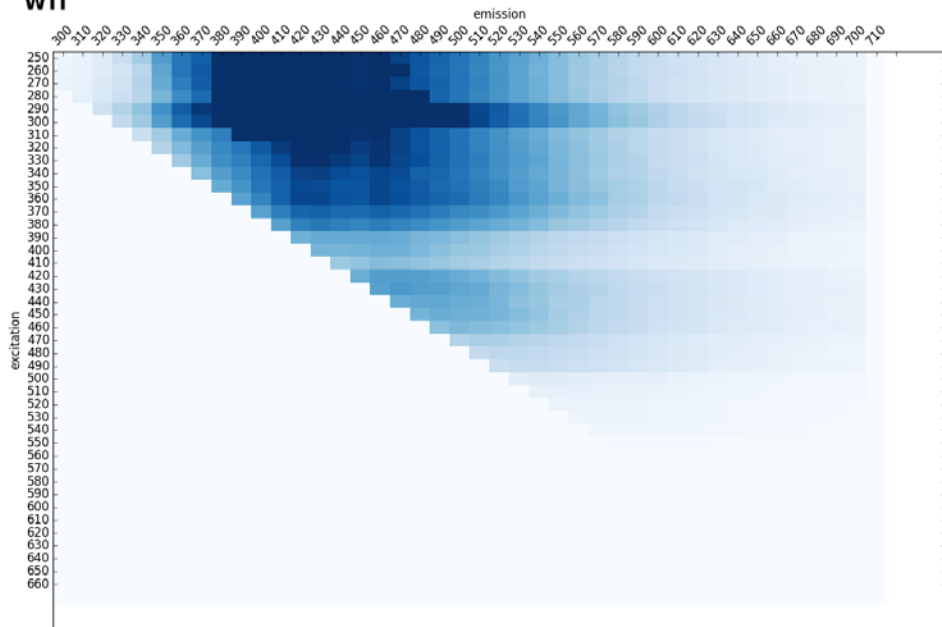
FINASOL



ANS



WTI



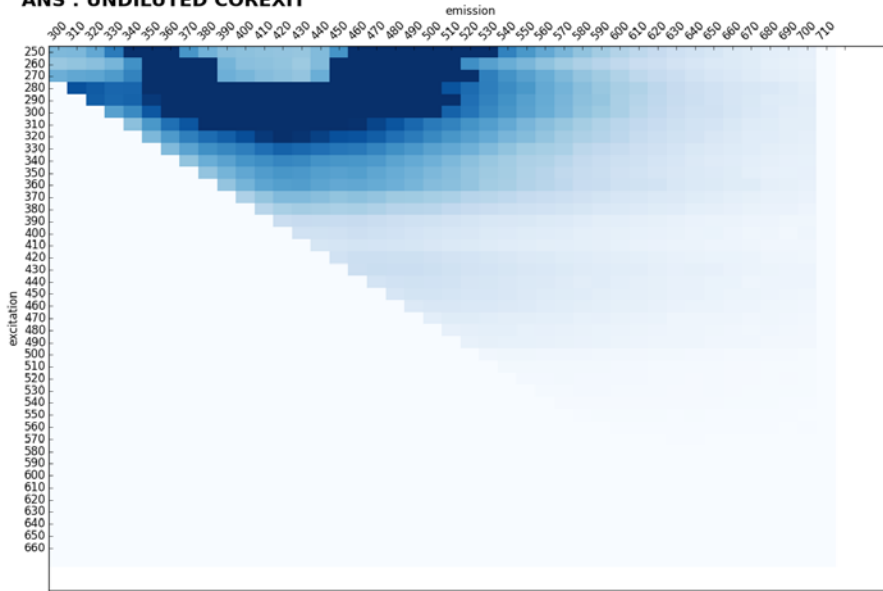
Appendix E

Determination of Oil, Dispersant, and Seawater Ratios Using Fluorescence

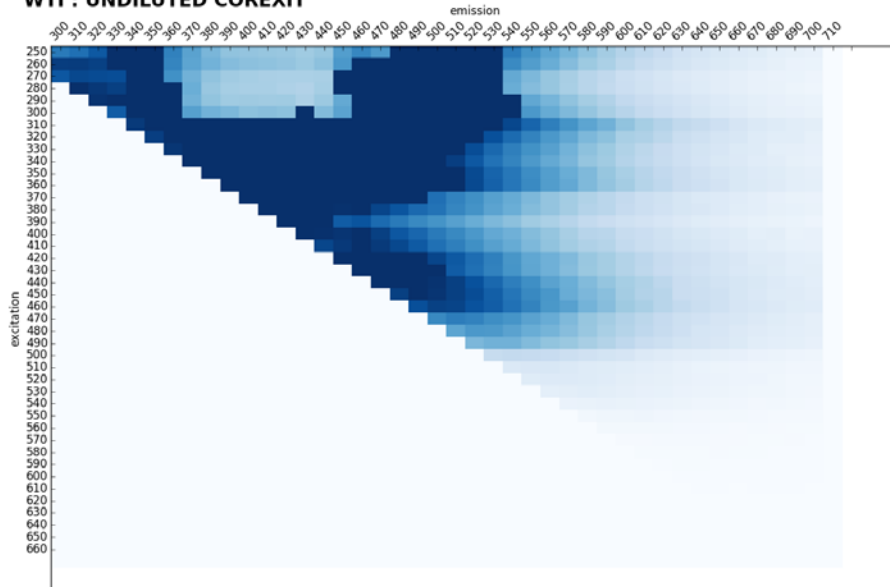
Appendix E

Determination of Oil, Dispersant, and Seawater Ratios Using Fluorescence

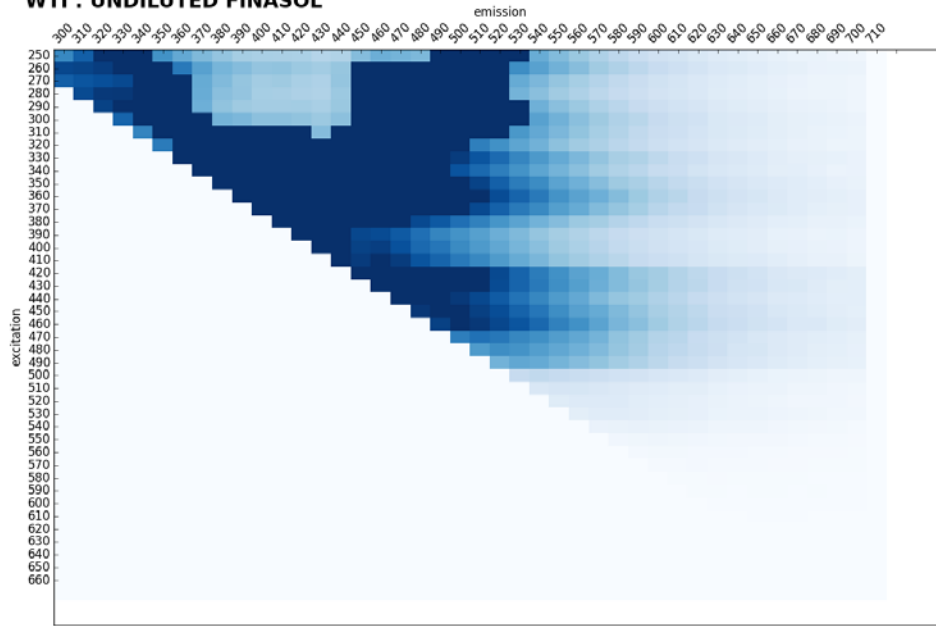
ANS : UNDILUTED COREXIT



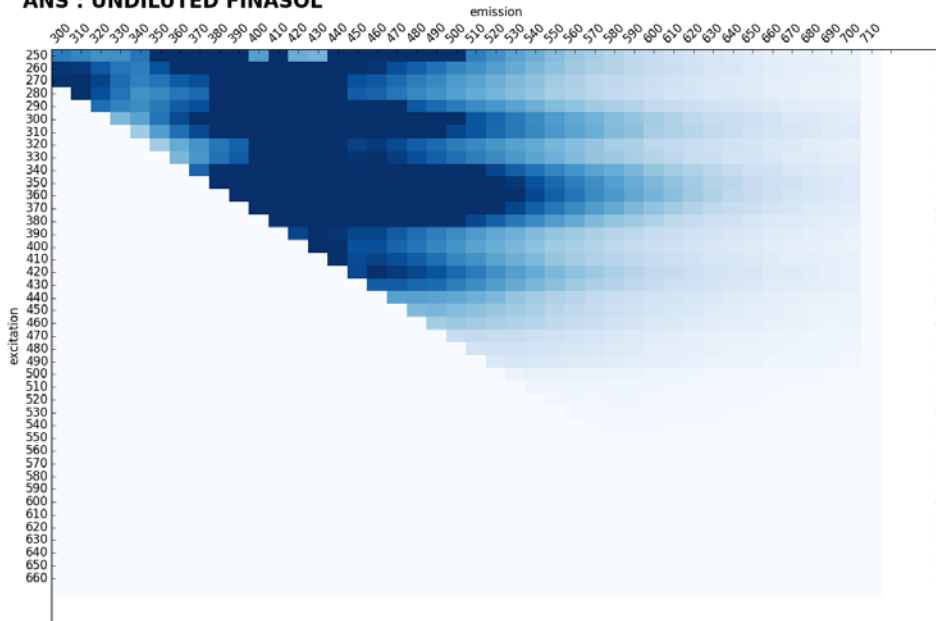
WTI : UNDILUTED COREXIT

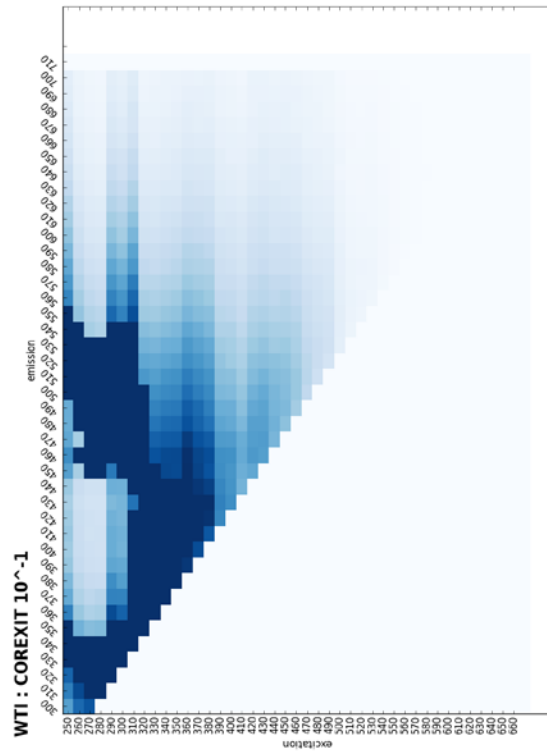
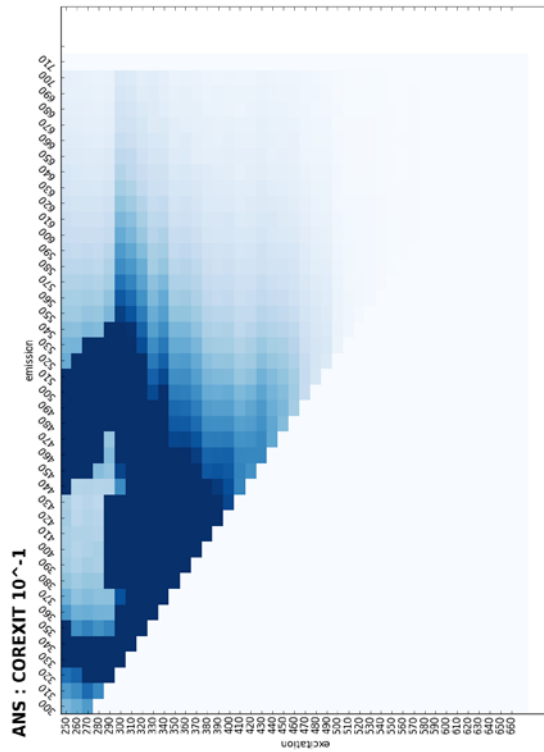
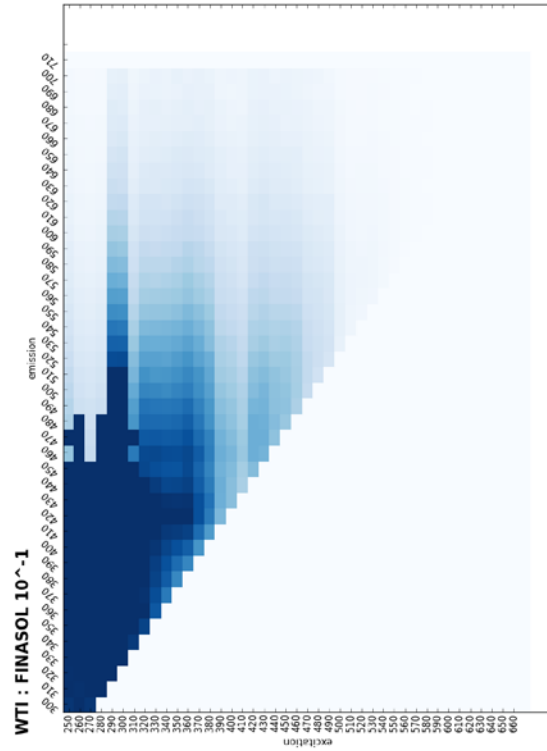
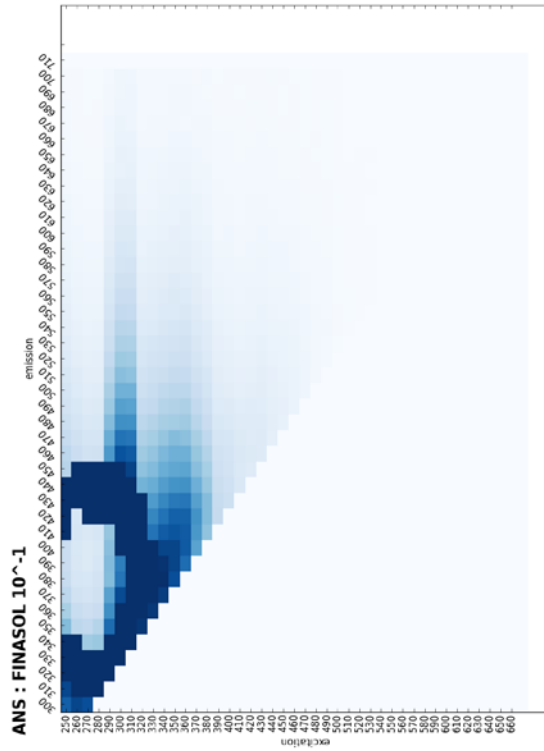


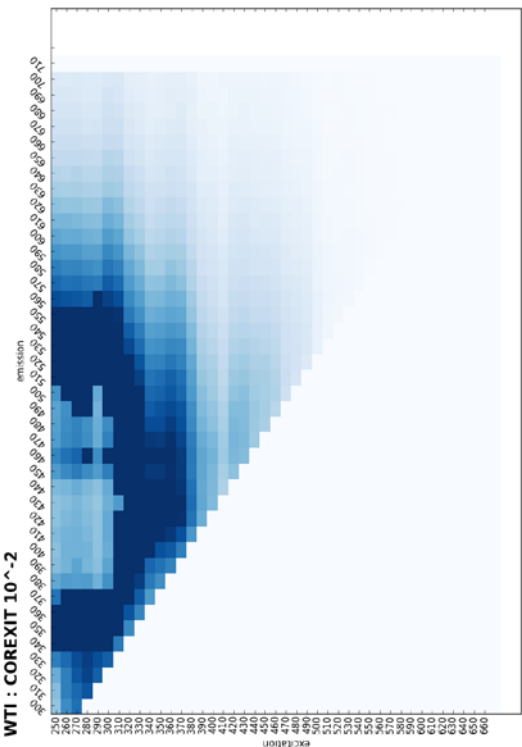
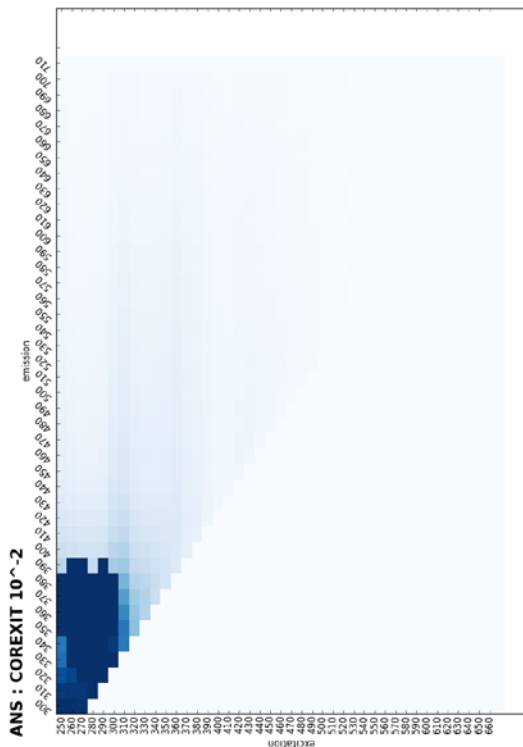
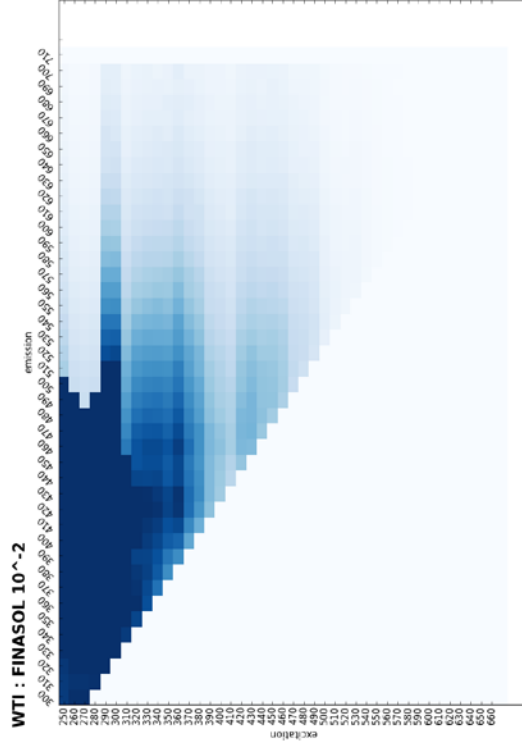
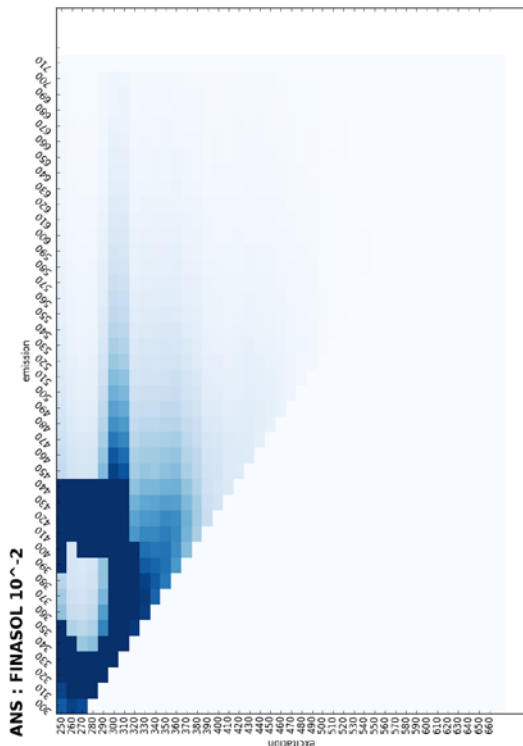
WTI : UNDILUTED FINASOL

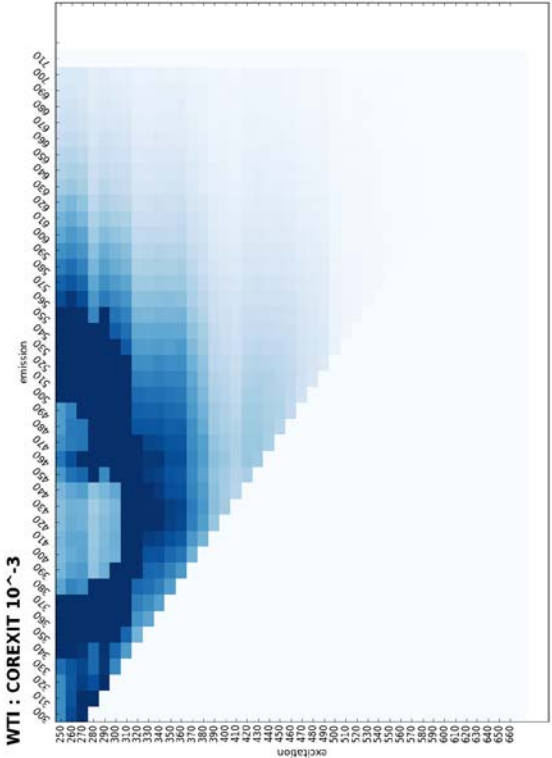
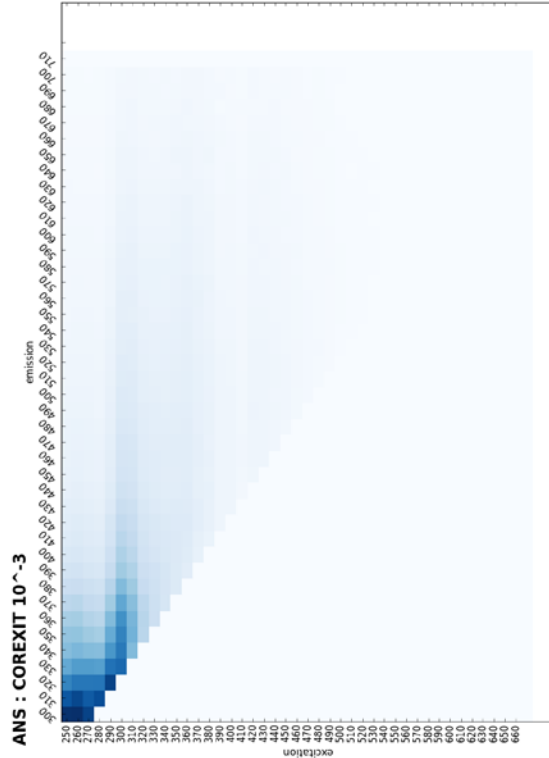
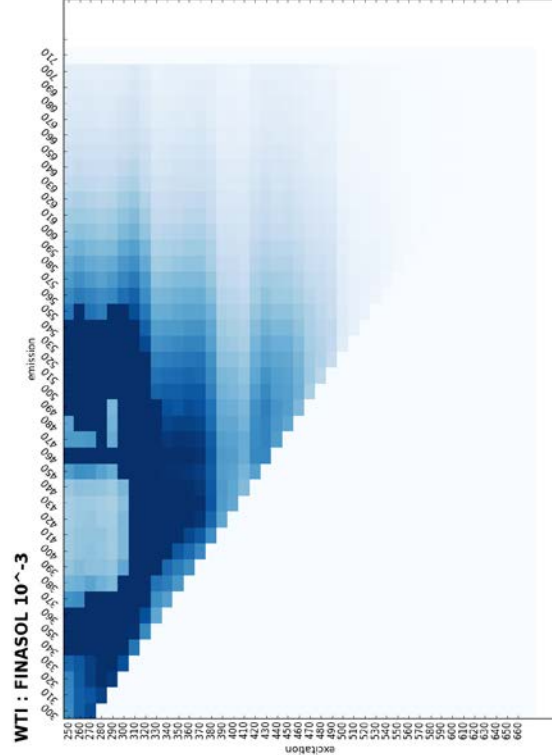
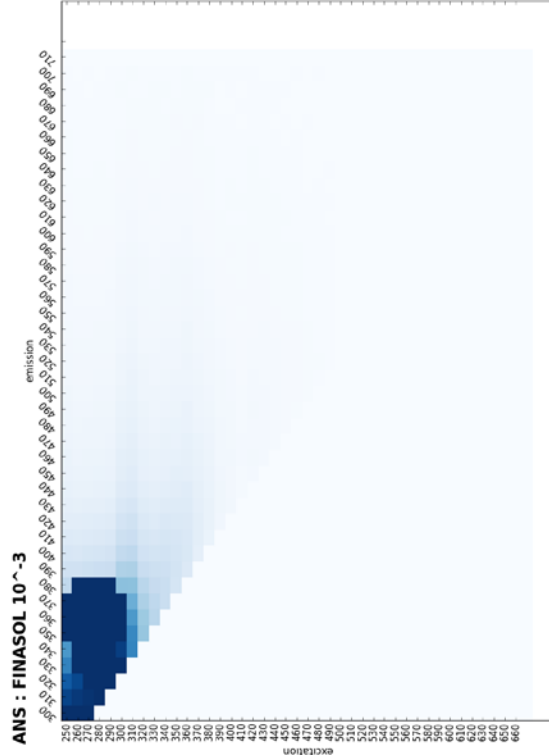


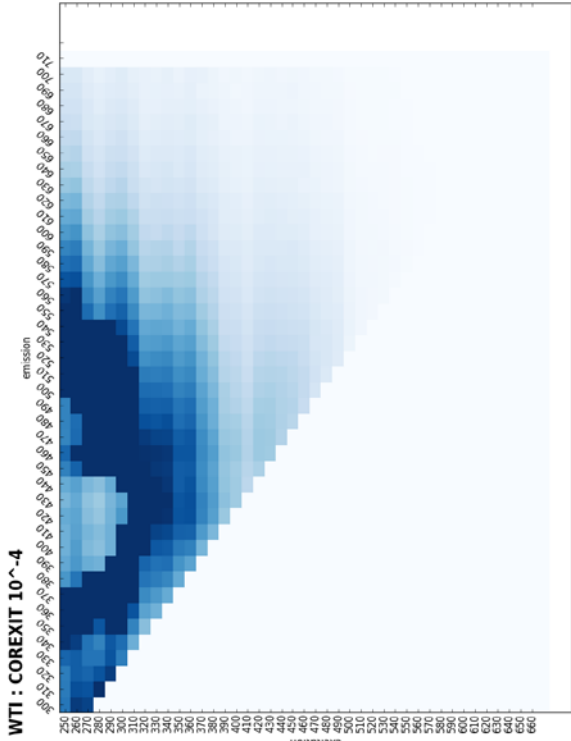
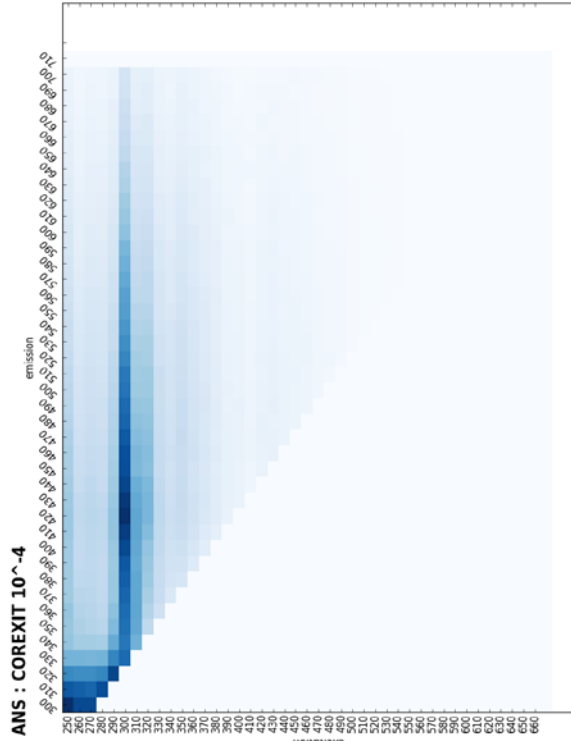
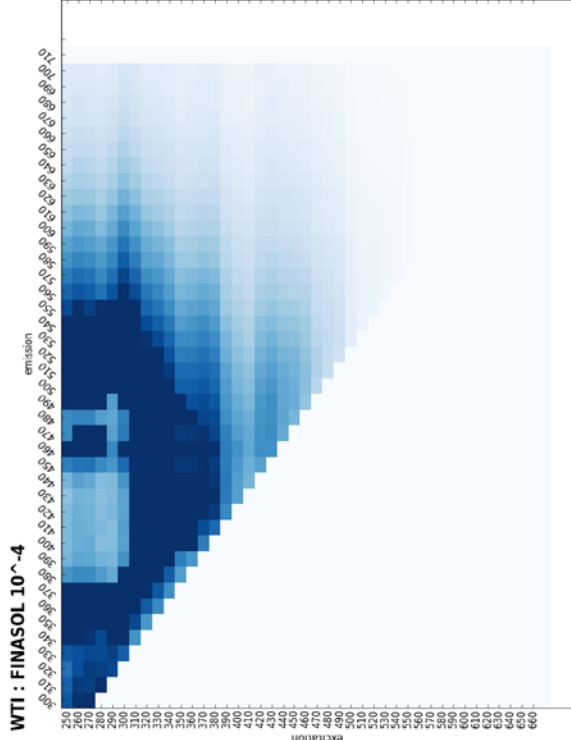
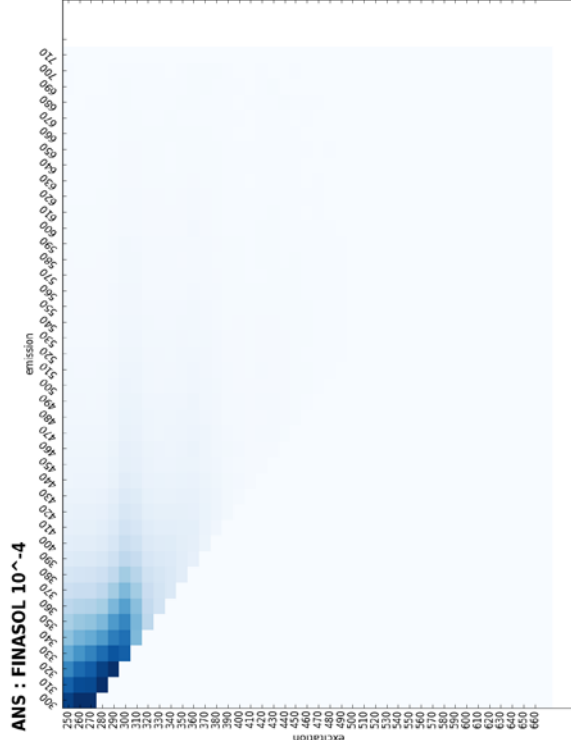
ANS : UNDILUTED FINASOL

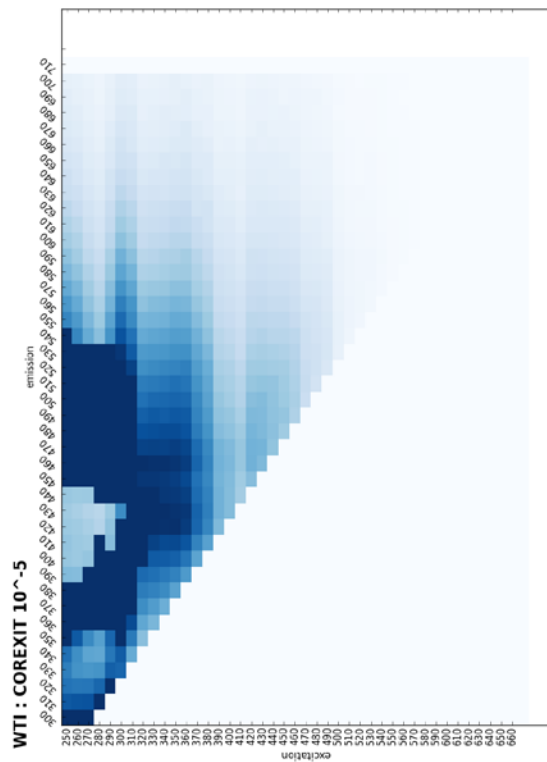
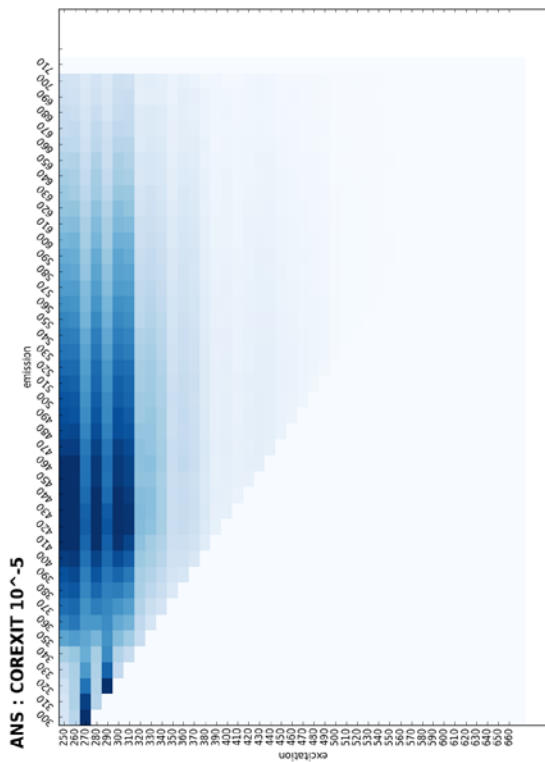
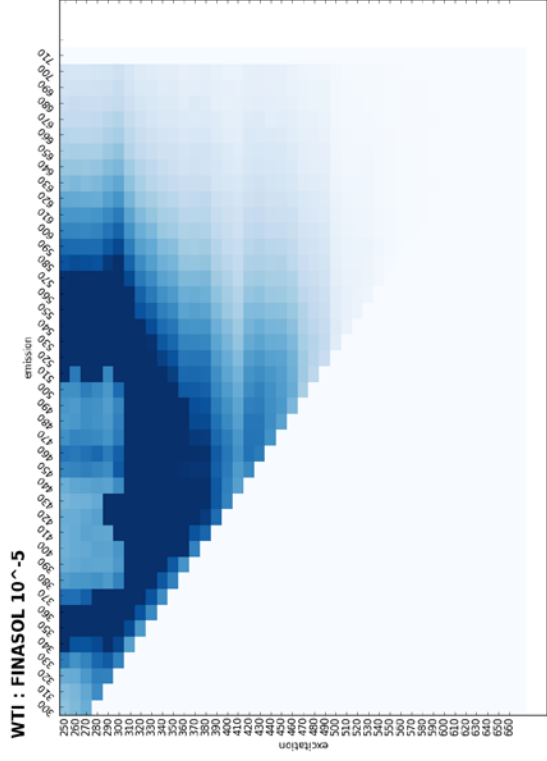
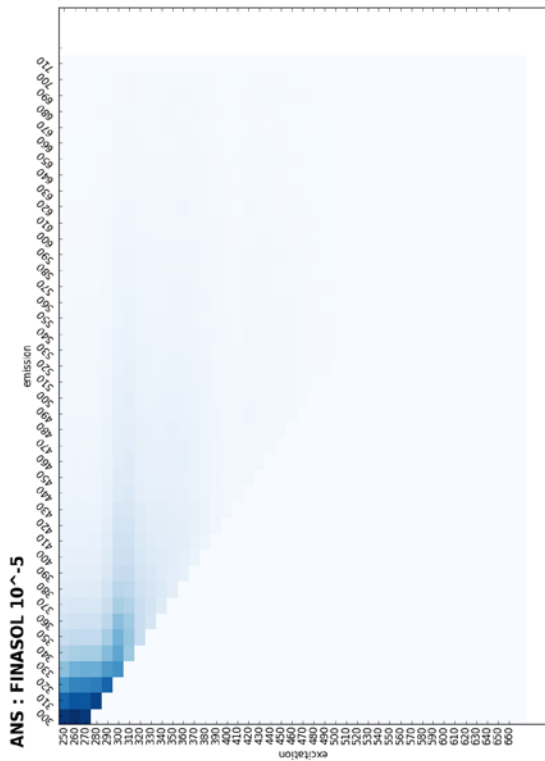


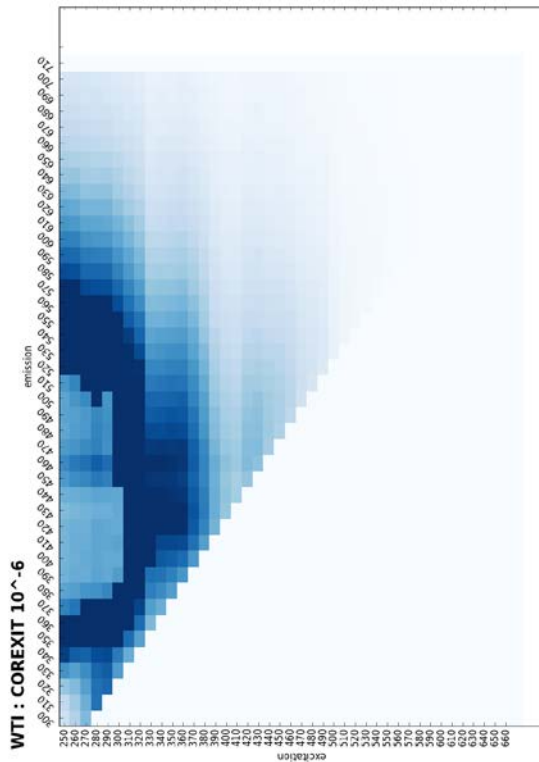
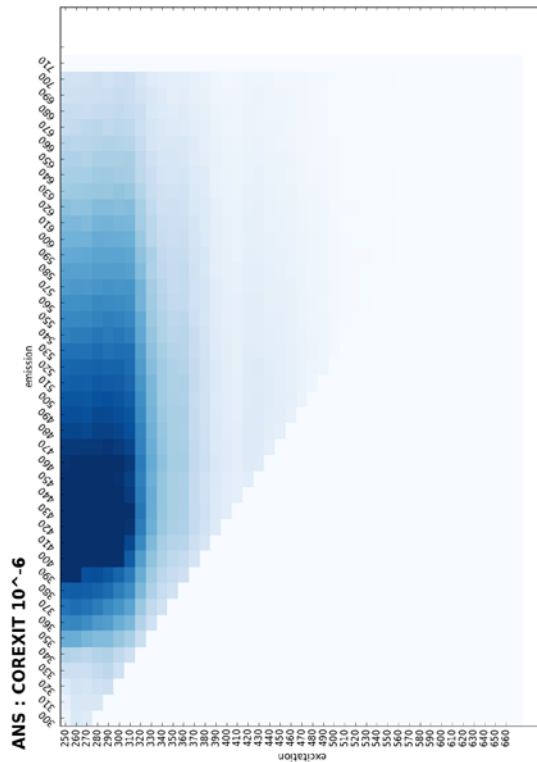
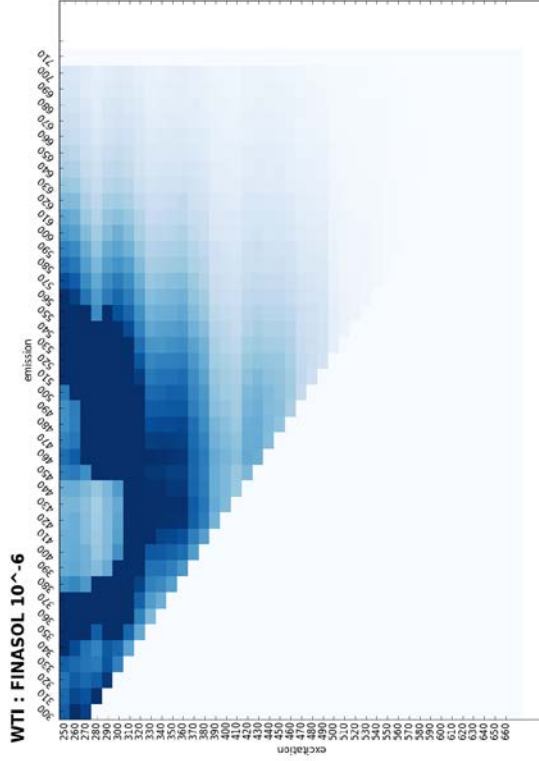
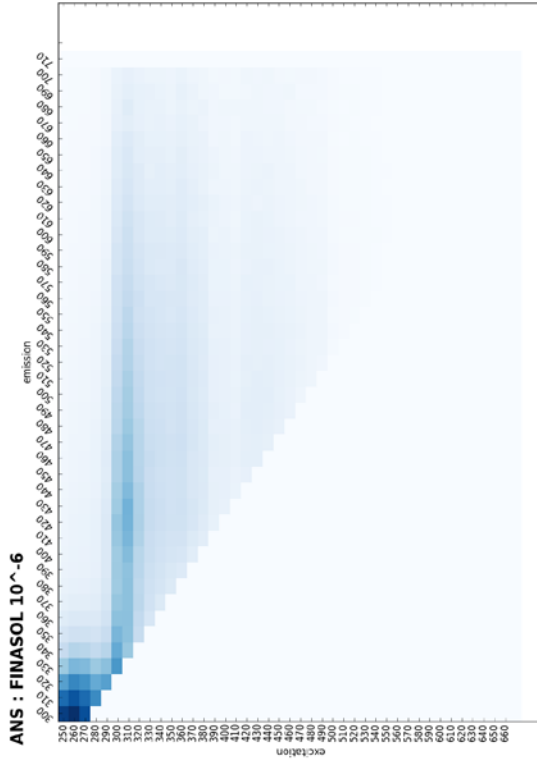












Distribution

**No. of
Copies**

**No. of
Copies**

Name
 Organization
 Address
 City, State and ZIP Code

Organization
 Address
 City, State and ZIP Code

Name
 Name
 Name
 Name
 Name (#)

Name
 Organization
 Address
 City, State and ZIP Code

Foreign Distribution

Name
 Organization
 Address
 Address line 2
 COUNTRY

Local Distribution

Pacific Northwest National Laboratory
 Name Mailstop
 Name Mailstop
 Name Mailstop
 Name Mailstop
 Name (PDF)



Pacific Northwest
NATIONAL LABORATORY

*Proudly Operated by **Battelle** Since 1965*

902 Battelle Boulevard
P.O. Box 999
Richland, WA 99352
1-888-375-PNNL (7665)

U.S. DEPARTMENT OF
ENERGY

www.pnnl.gov